DEVELOPMENT OF ELECTROCHEMICAL METHODS FOR THE DETECTION OF VITAMIN B_2, VITAMIN B_6, VITAMIN C, ALBUMIN, AND L-HYDROXYPROLINE

PHANUMAS YOMTHIANGTHAE

Graduate School Srinakharinwirot University

2022

การพัฒนาวิธีทางเคมีไฟฟ้าสำหรับการตรวจวัดวิตามินบี 2 วิตามินบี 6 วิตามินซี อัลบูมิน และแอล-ไฮดรอกซีโพรลีน

ภาณุมาศ ย่อมเที่ยงแท้

ปริญญานิพนธ์นี้เป็นส่วนหนึ่งของการศึกษาตามหลักสูตร
ปรัชญาดุษฎีบัณฑิต สาขาวิชาเคมีประยุกต์
คณะวิทยาศาสตร์ มหาวิทยาลัยศรีนครินทรวิโรฒ
ปีการศึกษา 2565

DEVELOPMENT OF ELECTROCHEMICAL METHODS FOR THE DETECTION OF VITAMIN B_2, VITAMIN B_6, VITAMIN C, ALBUMIN, AND L-HYDROXYPROLINE

PHANUMAS YOMTHIANGTHAE

A Dissertation Submitted in Partial Fulfillment of the Requirements

for the Degree of DOCTOR OF PHILOSOPHY

(Applied Chemistry)

Faculty of Science, Srinakharinwirot University

2022

THE DISSERTATION TITLED

DEVELOPMENT OF ELECTROCHEMICAL METHODS FOR THE DETECTION OF VITAMIN B_2, VITAMIN B_6, VITAMIN C, ALBUMIN, AND L-HYDROXYPROLINE

BY

PHANUMAS YOMTHIANGTHAE

HAS BEEN APPROVED BY THE GRADUATE SCHOOL IN PARTIAL FULFILLMENT OF THE REQUIREMENTS FOR THE DOCTOR OF PHILOSOPHY IN APPLIED CHEMISTRY AT SRINAKHARINWIROT UNIVERSITY

(Assoc. Prof. Dr. Chatchai Ekpanyaskul, MD.)
Dean of Graduate School

ORAL DEFENSE COMMITTEE

..... Major-advisor
(Assoc. Prof. Dr.Weena Siangproh)

..... Chair
(Prof. Dr.Orawon Chailapakul)

..... Committee
(Asst. Prof. Dr.Piyada Jittangprasert)

..... Committee
(Asst. Prof. Dr.Panarat Arunrattiyakorn)

..... Committee
(Asst. Prof. Dr.Mayuso Kuno)

Title	DEVELOPMENT OF ELECTROCHEMICAL METHODS FOR THE DETECTION OF VITAMIN B_2, VITAMIN B_6, VITAMIN C, ALBUMIN, AND L-HYDROXYPROLINE
Author	PHANUMAS YOMTHIANGTHAE
Degree	DOCTOR OF PHILOSOPHY
Academic Year	2022
Thesis Advisor	Associate Professor Dr. Weena Siangproh

This dissertation aims to develop simple and effective electrochemical methods for the detection of important analytes. The study was divided into two parts. The first part focused on the development of a simple electrochemical approach for the simultaneous detection of vitamin B_2, vitamin B_6, and vitamin C using a modifier-free screen-printed carbon electrode. This work emphasized the investigation of the effect of supporting electrolytes on the electrochemical behavior of each vitamin. The second part of this dissertation presented two subprojects that reported on the development of electrochemical methods for detecting biomarkers. The first subproject described the development of a simple and rapid approach for detecting urinary albumin on a paper-based analytical device using an electrochemical-chemical redox cycling process. This strategy highlighted the use of a unique combination of ferricyanide and methylene blue for signal amplification, without any electrode surface modification. The second subproject involved the development of a new sensing device for detecting L-hydroxyproline (Hyp) using a screen-printed graphene electrode (SPGE) coated with bismuth film (BiF) and poly(L-hydroxyproline) (Poly(Hyp)). This sensor (Poly(Hyp)/BiF/SPGE) can be fabricated by two simple modification processes: (1) the electrodeposition of BiF; and (2) the electropolymerization of Poly(Hyp). Therefore, all electrochemical methods presented in this dissertation were primarily based on simplicity and effectiveness with good analytical performance that can be applied to detect target analytes in various practical applications, such as food quality control and clinical diagnosis.

Keyword : Electrochemical detection, Vitamins, Albumin, L-hydroxyproline, Screen-printed electrode

ACKNOWLEDGEMENTS

First and foremost, I would like to express my sincere gratitude to my advisor, Associate Professor Dr. Weena Siangproh, for providing me with invaluable guidance, motivation, and encouragement throughout my Ph.D. period. She has been instrumental in helping me find solutions and providing valuable advice on various aspects of my research. Her unwavering support has been a source of great comfort to me during times of difficulty and concern. I am deeply grateful for the opportunity to pursue my Ph.D. under her expert guidance, and without her professional direction, this dissertation would not have been possible. It is an honor to have been under her supervision.

I would also like to acknowledge Professor Dr. Manel del Valle, a professor from the Department of Chemistry, Universitat Autònoma de Barcelona, for providing me with the opportunity to conduct research in Spain. I am appreciative to him for his guidance and support during my nearly one-year stay there. I am also grateful to the members of the Sensors and Biosensors group for their assistance from the very beginning of my time in the laboratory. Their kindness and camaraderie have left me with many cherished moments and memories.

I wish to extend a special thanks to Associate Professor Dr. Takeshi Kondo, who invited me to participate in the Sakura Science Project at the Tokyo University of Science in 2018. My time there, which was three weeks, was a valuable learning experience in both research and Japanese culture. I am deeply grateful to him for providing me with an opportunity that I will always treasure.

I would like to express my appreciation to all my fellow lab mates at the Electroanalytical and Imaging Sensor Research Group (EISRG) for their support and encouragement. The memories we shared are some of my most cherished, and I am grateful for their unwavering support. Additionally, I would like to thank the members of the Electrochemistry and Optical Spectroscopy Center of Excellence (EOSCE) at Chulalongkorn University, especially Professor Dr. Orawon Chailapakul, for their support with chemical and equipment resources throughout this dissertation.

I am also grateful to the National Research Council of Thailand (NRCT) for their financial support of my Ph.D. study through the Royal Golden Jubilee (RGJ) Ph.D. Program, as well as Thailand Science Research and Innovative (TSRI) through the Fundamental Fund. I would like to express my gratitude to the dissertation committee, Professor Dr. Orawon Chailapakul, Assistant

Professor Dr. Piyada Jittangprasert, Assistant Professor Dr. Panarat Arunrattiyakorn, and Assistant Professor Dr. Mayuso Kuno, for their invaluable feedback and recommendations.

Lastly, I would like to express my sincere gratitude to my family for their unconditional love and support. My parents have been a constant source of encouragement and have gone above and beyond to ensure my well-being throughout my study. My younger sisters have also been a great source of mental support and motivation, and I am grateful for their unwavering belief in me. I would also like to thank my friends and my partner for their support and for bringing joy to my life throughout my study period.

PHANUMAS YOMTHIANGTHAE

TABLE OF CONTENTS

Page

LIST OF TABLES

Page

LIST OF FIGURES

Page

CHAPTER 1
INTRODUCTION

1.1 Background

Over a period of more than ten years, it was clearly seen that the ongoing trend in analytical chemistry is to minimize the laboratory-scale equipment into portable devices, resulting in reduced consumption of hazardous substances and increased safety for end-users. Significant factors motivating the advancement of portable instruments include food and environmental concerns, the availability of cost-effective and uncomplicated devices, and the escalation of healthcare expenses. These factors led to the creation of portable devices for a variety of uses, including pharmaceutical analysis, environmental monitoring, clinical diagnosis, and food safety, by covering all analytical techniques, including thermal analysis, chromatography, spectroscopy, and electrochemistry. Among these developed techniques, electrochemical sensing devices have recently been proposed as alternative platforms for electroanalytical methods, offering advantages in terms of cost-effective instrumentation, simple fabrication, portability, and good analytical performance (Krejcova, Richtera, Hynek, Labuda, & Adam, 2017). This current movement allows for the development of various kinds of new electrochemical sensors that are effective and useful for various analytical aspects.

Vitamins play essential roles in various biological functions that impact the healthy and normal growth of the human body. For instance, vitamin B_2 (VB_2) is involved in energy metabolism, cellular respiration, and antibody production. Vitamin B_6 (VB_6) is related to macronutrient metabolism, neurotransmitter synthesis, and gene expression. Vitamin C (VC) serves as an antioxidant involved in tissue restoration, collagen formation, and enzymatic production of certain neurotransmitters. Abnormal levels of vitamins can lead to disorders or diseases, resulting in the malfunctioning of the human body. However, vitamins in biological fluids and some food products are present at low concentrations, making it difficult to measure their levels in real samples. Thus, a simple and low-cost

analytical platform is required to develop a powerful method for food and clinical applications.

Clinically-related molecules, including small-molecule substances and biomolecules, are another interesting group of substances that needed to be quantified to investigate their amount, form the basis to understand their functions in biological and physiological aspects and develop powerful clinical diagnoses (Labib, Sargent, & Kelley, 2016). These molecules perform a variety of vital biological functions, such as reserving and transferring genetic information, controlling biological activities, carrying small molecules, and catalyzing reactions. Furthermore, they can serve as biomarkers for diagnosing many diseases. For example, urinary albumin, which belongs to the family of globular proteins, is a well-established predictor of chronic kidney disease (CKD). Abnormal levels of urinary albumin may result in the gradual loss of kidney function, leading to glomerular and tubulointerstitial injury (Fassett et al., 2011). The prevalence of CKD at all stages in the adult Thai population is estimated to affect 10 million patients (C.-W. Yang et al., 2020), resulting in premature mortality, reduced quality of life, and increased healthcare spending (Srithongkul & Ungprasert, 2020). Thus, urinary albumin screening is highly necessary and recommended for patients who are at risk of expanding renal disorders to prevent the progression of CKD.

Amino acids are small-molecular substances that serve as the building blocks of proteins. They are crucial for cellular function and play diverse roles in nutrition and whole-body homeostasis, including metabolic regulation, reproduction, nucleic acid synthesis, cell signaling, and acid-base equilibrium. One notable example is L-hydroxyproline (Hyp), a derivative of L-proline. Hyp is an essential amino acid component of collagen and a few other extracellular animal proteins. It is necessary for the synthesis and stability of collagen, creating the triple-helical conformation (Kumar Srivastava, Khare, Kumar Nagar, Raghuwanshi, & Srivastava, 2016). Moreover, Hyp is a major substance in bone metabolism and can be released during the degradation process of bone collagen (Seibel, 2005). Abnormal levels of Hyp in blood or urine are associated with the breakdown of connective tissue, bone disorders, and vitamin C deficiency (Sahni, Zoltick,

McLean, & Hannan, 2010). Therefore, detecting Hyp in biological fluids enables the examination of bone-related diseases and collagen metabolism in the body, particularly the degree of collagen degradation.

Due to the importance of the mentioned target analytes and the requirement for the development of a detection method, electrochemical detection systems are particularly attractive as a method suitable for resource-limited applications due to their use of portable instruments and miniaturized devices. Their ability to analyze small sample volumes, provide rapid analysis times, and offer high analytical performance make them a cost-effective platform for electroanalytical purposes. The miniaturization of electrochemical equipment has motivated analytical chemists to develop a variety of devices with novel designs and broad applications. Disposable screen-printed electrodes (SPEs) are recognized as low-cost and miniaturized electrochemical sensors that offer high-volume production and high reproducibility (Wei Zhang, Wang, Luo, Wang, & Lin, 2020). The screen-printing technique, a cutting-edge technology, is used to fabricate SPEs, making them more suitable for various analytical purposes (Arduini, Cinti, Scognamiglio, Moscone, & Palleschi, 2017). The selection of materials used as inks for manufacturing SPEs on paper, plastic, or ceramic substrates is versatile and essential for detecting analytes of interest. Ordinary and modified carbon materials, including graphite, graphene, fullerene, and carbon nanotubes, are the most normally used for SPEs. Furthermore, the modification of the surface with nanomaterials, polymers, complexing agents, or enzymes has a significant impact on the sensing performance of SPEs (Syedmoradi et al., 2017). These modifiers enhance selectivity and amplify electrochemical signals to detect a variety of analytes, covering a broad range of electroanalysis in the fields of industry, food control, environmental monitoring, clinical diagnosis, or academic research (Antuña-Jiménez, González-García, Hernández-Santos, & Fanjul-Bolado, 2020).

Based on the aforementioned inspiration, this dissertation is divided into two primary parts, which present the electrochemical detection of water-soluble vitamins and biomarkers. The first part reported on the development of a straightforward

electrochemical approach for the simultaneous detection of VB_2, VB_6, and VC utilizing a modifier-free screen-printed carbon electrode. The effect of diverse supporting electrolytes on the electrochemical behavior of each vitamin was methodically investigated. The results indicated that a supporting electrolyte within the acid pH range was suitable for detecting all three vitamins. The quantification of VB_2, VB_6, and VC was performed using the square wave voltammetric technique, which exhibited excellent analytical performance. Furthermore, the measurement of these vitamins was conducted in juice and urine samples to demonstrate practical applications in the fields of food control and clinical analysis. To be highlighted here, this study offered an alternative methodology for the simultaneous detection of water-soluble vitamins without the requirement of complicated modified electrodes.

The second part of this dissertation is divided into two subprojects, that discussed the development of electrochemical methods for detecting biomarkers, namely albumin, and Hyp. The first subproject described the development of a simple and rapid detection approach for urinary albumin on a paper-based analytical device (PAD) using an electrochemical-chemical (EC) redox cycling process. This strategy utilized a unique combination of ferricyanide and methylene blue for signal amplification, without any electrode surface modification. In addition, PAD was preferably used as a disposable sensing platform, due to its advantages in terms of low cost, portability, and easy-to-use. The measurement of albumin was achieved through indirect detection by subtracting the signal current obtained from the EC process with and without albumin. This discovery obviated the need for creatinine correction, resulting in a powerful method for direct albumin quantification. Additionally, the proposed platform was applied to detect albumin in real urine samples, yielding satisfactory results. Given its potential in medical applications, the proposed strategy represents a promising tool for CKD screening and can be adapted to point-of-care testing in developing countries.

The second subproject involves the development of a new sensing device for detecting Hyp using a screen-printed graphene electrode (SPGE) coated with bismuth film (BiF) and poly(L-hydroxyproline) (Poly(Hyp)). The as-synthesized electrode

(Poly(Hyp)/BiF/SPGE) was fabricated by a two-step modification process. First, the electrodeposition of BiF was modified on a bare SPGE to generate BiF/SPGE. Subsequently, Hyp was utilized as a monomer to perform the electropolymerization at the same electrode surface, resulting in a Poly(Hyp)/BiF/SPGE. The proposed electrode surface had a porous thin film with uniform cavities, as confirmed by morphological characterization using scanning electron microscopy. The modified electrodes were subjected to electrochemical investigation using cyclic voltammetry and electrochemical impedance spectroscopy to confirm their higher catalytic activity, including electroactive surface area, compared to a bare electrode. The sensing efficiency of the proposed electrode for detecting Hyp was evaluated using differential pulse voltammetry, which provided good analytical performance. To demonstrate a practical application, the proposed assay was applied to measure Hyp in human urine samples, yielding satisfactory results. As a result, this enzyme-free electrode could serve as an alternative platform for Hyp measurement, with the potential to screen for the risk of bone-related diseases and collagen metabolism disorders.

1.2 Objectives of the research

The aim of this research comprised three specific goals, which are outlined below:

1. To develop a straightforward electrochemical method using an unmodified electrode to detect water-soluble vitamins, namely VB_2, VB_6, and VC, in food and biological samples.

2. To propose a novel electrochemical approach coupled with a paper-based device to measure albumin in human urine samples.

3. To develop a new enzyme-free Hyp biosensor based on a thin-film modified electrode as a potential alternative device for clinical applications.

1.3 Significance of the research

1. The originality of this research can be applied to detect various substances of interest in a wide range of applications, including food quality control and clinical diagnosis.

2. The proposed platforms present a new opportunity to use them as prototypes for alternative devices for electroanalytical purposes.

3. The materials used in this research can be fabricated through simple approaches, thus providing the potential to enhance their electrochemical sensing performances.

1.4 Scope of the research

This study focuses on the development of electrochemical methods for detecting water-soluble vitamins, specifically VB_2, VB_6, and VC, as well as particular biomarkers, namely albumin, and Hyp. Unmodified and modified SPEs were used as electrochemical sensing devices to measure the quantification of targeted analytes. To find the best detection platforms for different electroanalysis applications, the created platforms were constructed on a variety of substrates, including polymers and papers. Then, all parameters related to each developed work, such as the type of suitable supporting electrolyte and its pH, modifiers, and electrochemical parameters, were systematical examinations to obtain the optimal procedures. Followed by analytical performances, including linear concentration range, detection limit, interference study, accuracy, and precision, were investigated for each proposed research. Finally, the developed devices were applied to detect target analytes in food and biological samples, with the aim of proposing them as alternative tools for various analytical applications.

CHAPTER 2
THEORY AND LITERATURE REVIEWS

2.1 Electroanalytical chemistry

Electroanalytical chemistry represents one of the analytical techniques that rely on measuring the electrical properties occurring within an electrochemical cell. The electrical properties measured, such as current, potential, conductance, and resistance, are directly proportional to the number of relevant analytes in a sample. Electroanalytical methods are classified into different categories based on the type of electrochemical cells and the variety of measurable signals available, as follows:

Potentiometric method: an analysis involves measuring the potential difference between a reference electrode and an indicator electrode to provide essential information about the sample concentration. In this technique, changes in the concentration of a target analyte result in potential changes (vs. a reference electrode) at zero current. The electromotive force of a cell is dependent on the concentration of the analyte. Therefore, a direct calculation can be easily obtained from the Nernst equation (Equation (1)):

$$E_{cell} = E^0_{cell} - \left(\frac{RT}{nF}\right) ln\, Q \quad \text{.....Equation (1)}$$

where E_{cell} is the measured cell potential, E^0 is the standard cell potential, R is the universal gas constant, T is the temperature, n is the number of the transferred electron, F is the Faraday constant, and Q is the reaction quotient that represents the ratio of concentrations between the anode and the cathode.

Conductometric method: the technique is a bulk electroanalytical approach that is exclusively used for the analysis of ionic species and the monitoring of chemical reactions. This technique involves studying the electrolytic conductivity of the reacting species or resultant products (Shah, Arain, & Soylak, 2020). The conductance of an electrochemical cell is dependent on the ionic concentration of the species that are dissolved in an electrolyte. This electrical property cannot be attributed to the specific conductivity of a single ion or dissociated species in the solution, as every ion and some

species can be conductive. Direct measurement of conductance using only a conductivity meter is insufficient for quantification purposes. Therefore, conductometric titration is employed to measure the difference in conductance when adding the titrant, leading to the quantification of the interested ions or species. The equivalent point is then determined from the titration curve, resulting in the quantitative analysis of the target analytes.

Electrolytic method: applying current or potential to an electrolytic cell, to allow the electrochemical reaction of an analyte to occur, is the main concept of the analysis. This technique encompasses three sub-methods – electrogravimetry, coulometry, and voltammetry – that vary depending on the application. The electrogravimetric method studies the reduction of metal ions to metal using a constant potential, leading to the deposition of interested metal at the cathode, which is a solid metal electrode. The weight of the cathode before and after the plating step is measured, and the increase in weight corresponds to the metal concentration in the original solution. The coulometric method is based on the exhaustive electrolysis of an analyte, achieved by applying a constant potential or current to a working electrode surface relative to a reference electrode. Faraday's law governs the principle of this technique, stating that the total charge passing through the electrochemical cell is proportional to the absolute amount of analyte.

Voltammetric method: the technique involves the application of a constant or varied potential at the electrode surface to record the produced Faradaic current. Typically, interested analytes are measured using an easily-polarizable micro-electrode immersed in a static solution without stirring. Voltammetry can be categorized into two main sub-classes, namely polarography and amperometry, depending on the applied potential. Polarography involves the application of varied potentials over the surface of a dropping mercury electrode to allow chemical species to undergo oxidation or reduction. On the other hand, if the redox reactions of electroactive species are measured at a constant potential, the method is called amperometry. Voltammetry is widely used for quantification in several fields, including food quality control, environmental analysis, and biomedical diagnosis. Furthermore, this technique is crucial for understanding the

mechanisms and the kinetics of electrode reactions, as well as the electrochemical reactivity of an analyte.

Electrochemical impedance spectroscopy (EIS): EIS is a significant electrochemical approach for measuring the electrical resistance (impedance) of the electrode-electrolyte interface occurring in a circuit. It is an alternating current technique that applies multifrequency to an electrochemical system over a wide range, from less than 1 mHz to greater than 1 MHz. This technique has broad applicability since it can provide insight into the electrochemical mechanisms occurring at an electrode interface, including those involved in commercial battery operation, metal and alloy corrosion, and electrochemical biosensors. Furthermore, EIS can be used to study intrinsic material properties or specific processes that could influence the conductance, resistance, or capacitance of an electrochemical system.

Among the diverse range of electrochemical techniques, this dissertation explores the utilization of various voltammetric methods for analytical purposes, in combination with the EIS technique for electrochemical characterization of electrode surfaces.

2.1.1 Voltammetry

Voltammetry is a non-potentiometric technique that involves applying different potentials to a working electrode which has a small surface area of square millimeters, that is immersed in a static solution without stirring. This leads to a change in current due to the polarization at an electrode surface, which corresponds to the concentration of an electroactive analyte and enables quantitative analysis. The voltammetric measurement is performed in an electrolytic cell using an external power source as a potential generator to allow the electrochemical reaction to occur. This cell comprises a three-electrode system immersed in a supporting electrolyte. The three-electrode system consists of a working electrode where the electrochemical reaction occurs, a reference electrode whose potential remains constant and does not change upon passage of current, and a counter electrode that completes the circuit. After the

potential is applied to a cell, current flows between the working electrode and the counter electrode, which is proportional to the amount of analyte. The composition of an electrochemical cell used in voltammetry is shown in Figure 1 (Gomaa, Negm, & Abu-Qarn, 2018).

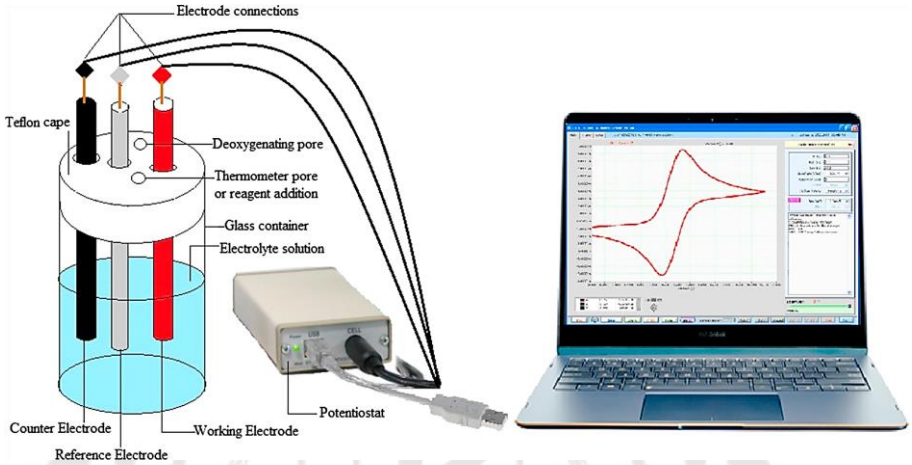

Figure 1 The typical composition of an electrochemical cell used in voltammetry.

Source: Gomaa, E. A., Negm, A., & Abu-Qarn, R. M. (2018). Cyclic voltammetry study of the electrochemical behavior of vanadyl sulfate in absence and presence of antibiotic. *Measurement, 125*, 645-650.

The initial period of this technique is known as polarography, which was discovered in 1920. Polarography utilizes a dropping mercury electrode (DME) to measure the interested compounds. The DME possesses renewable surfaces and can evaluate different metal ions by forming amalgams, resulting in excellent reproducibility and a large overpotential for hydrogen evolution. However, the toxicity of mercury and its propensity to oxidize at +0.4 V (vs a reference electrode) present significant challenges to polarography, necessitating the development of voltammetric techniques that use alternative working electrode materials, such as platinum, gold, and carbon-based electrodes. As a result, voltammetric methods with various sub-techniques, such as linear sweep voltammetry, cyclic voltammetry, pulse voltammetry, stripping voltammetry, and

chronoamperometry, can be applied for the qualitative and quantitative analysis of both inorganic and organic substances.

As previously mentioned, voltammetric measurements can be conducted using an electrolytic cell, wherein the potential is applied from an external power source. When the potential applied is insufficient to cause reduction or oxidation of the analyte, the charging current is generated due to the presence of solvated ions in the electrolyte. Upon the further application of potential, the analyte undergoes an electrochemical reaction at the electrode surface, which leads to a concentration difference between the electrode-solution interface and the bulk solution. This behavior results in the diffusion of the analyte in a concentration gradient from a high-concentration region to a low-concentration region, i.e., the electrode surface, and thereby generates a diffusion current (i_d). However, the current from the convection (i_c) and migration (i_m) processes may also occur in an electrochemical reaction, as shown in Equation (2).

$$i = i_d + i_c + i_m \quad \text{.....Equation (2)}$$

The primary objective of the voltammetric analysis is to investigate the diffusion current, and hence, any other forms of current should be minimized as much as possible. Solution stirring can induce a convection current, and to avoid this, analyte measurement should be conducted under static conditions without any perturbation. Similarly, the migration current results from the electrostatic attraction of targeted ions or molecules, leading to electrochemical reactions at the electrode surface. In this case, the cathode attracts cations while the anode attracts anions, resulting in the migration current. The addition of a supporting electrolyte to an electrochemical cell reduces the feasibility of such occurrences. By adding an electrolyte with inert properties, the ionic species present in the electrolyte will be attracted to the electrodes rather than the analyte. Consequently, the current of interest in a voltammetric method is derived exclusively from the diffusion process, which is related to the analyte concentration and diffusion rate according to Fick's law (Equation (3)):

$$\frac{\partial C}{\partial t} = D\frac{\partial^2 C}{\partial x^2} \quad \text{.....Equation (3)}$$

where *D* is the diffusion coefficient, *C* is an analyte concentration, *t* is time, and *x* is the distance of the analyte distributed onto an electrode surface. This relationship indicates that the diffusion rate is dependent on the concentration of the analyte, which means that the diffusion current is directly proportional to the analyte concentration as follows:

$$i_d \propto C$$
$$i_d = kC \quad \text{.....Equation (4)}$$

Voltammetry can be categorized into various sub-techniques based on the excitation signals that are applied to a working electrode. In this dissertation, cyclic voltammetry, differential pulse voltammetry, square wave voltammetry, and chronoamperometry were used for electrochemical measurements in the aspect of analyte detection, electrode modification, and characterization.

2.1.1.1 Cyclic voltammetry (CV)

CV is a powerful and widely used electrochemical technique that is commonly employed to investigate the redox processes of an analyte of interest. CV is a valuable method for studying the kinetics of electrode reactions, which are associated with the electron transfer process and chemical reaction. During CV operation, a potential is applied over time as a triangular potential-time waveform to a working electrode, as depicted in Figure 2A (Elgrishi et al., 2017). The resulting curve that is plotted between the obtained current and the applied potential is known as a cyclic voltammogram, as illustrated in Figure 2B. As the potential is scanned negatively from point A to point D, the concentration of ferrocenium (Fc^+) near the electrode surface is steadily reduced as it is converted to ferrocene (Fc). At point C, the peak cathodic current ($i_{p,c}$) is observed at a position of a peak cathodic potential ($E_{p,c}$), and the current is limited by the diffusion of Fc^+ from the bulk solution. This leads to a continuous increase in the Fc concentration at the electrode-solution interface, slowing down the mass transport of Fc^+ to the electrode surface. Consequently, as the potential is further negative, the diffusion rate of Fc^+ from the bulk solution to the electrode surface becomes slower, resulting in a decreasing

current as the scan continues (from point C to point D). Once the switching potential (D) is reached, the scan direction is reversed to apply the potential in a positive direction. Sweeping potential from point D to point G results in the oxidation of Fc to Fc^+, providing the peak anodic current ($i_{p,a}$) at a position of peak anodic potential ($E_{p,a}$) (point F). This process leads to an increasing Fc^+ concentration at the electrode-solution interface, hindering the mass transport of Fc to the electrode surface. Therefore, upon scanning to more positive potentials, the diffusion rate of Fc from the bulk solution to the electrode surface becomes slower, leading to a decreasing current as the scan continues (from point F to point G). At points B and E, the concentrations of Fc^+ and Fc at the electrode surface are equal, following the Nernst equation (Equation (1)), $E = E_{1/2}$. This relationship corresponds to the halfway potential between two observed peaks (C and F) and provides a straightforward approach to estimating the formal potential ($E^{0'}$) for a reversible electron transfer process.

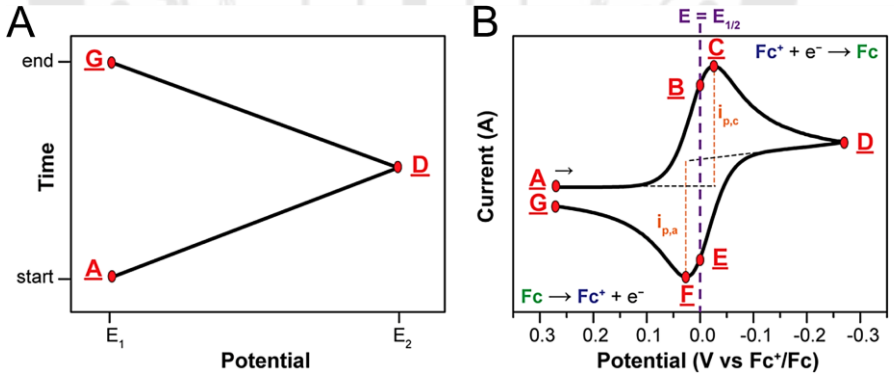

Figure 2 (A) Applied potential as a function of time for a general cyclic voltammetry experiment. (B) Cyclic voltammogram of the reversible reaction of a 1 mM Fc^+ solution.

Source: Elgrishi, N., Rountree, K. J., McCarthy, B. D., Rountree, E. S., Eisenhart, T. T., & Dempsey, J. L. (2017). A Practical Beginner's Guide to Cyclic Voltammetry. *Journal of Chemical Education*, *95(2)*, 197-206.

The scan rate in a CV experiment controls the speed at which the potential is applied. Increasing the scan rate leads to a reduction in the size of the diffusion layer and consequently results in higher observed currents. For electron transfer systems that involve freely diffusing redox species and are electrochemically reversible, Randles-Sevcik equation (Equation (5)) is used to describe the relationship between the peak current (i_p, A) and the square root of the scan rate (ν, V s^{-1}), where n is the number of electrons transferred in the redox event, A (cm^2) is the electrode surface area (generally used as the geometric surface area), D^0 (cm^2 s^{-1}) is the diffusion coefficient of the analyte, C^0 (mol cm^{-3}) is the bulk concentration of the analyte.

$$i_p = 0.446nFAC^0\left(\frac{nF\upsilon D_0}{RT}\right)^{1/2} \quad \text{.....Equation (5)}$$

The Randles-Sevcik equation provides indications on whether an analyte is freely diffusing in solution. According to equation 5, peak currents increase linearly with the square root of scan rates, resulting in a linear plot of i_p versus $\nu^{1/2}$. This behavior demonstrates that the electrochemical process taking place at the electrode-solution interface is diffusion-controlled. Conversely, the current response for electrode-adsorbed species is described by Equation (6), indicating that the plot of i_p as a function of ν is expected to be linear.

$$i_p = \frac{n^2F^2}{4RT}\nu A\Gamma^* \quad \text{.....Equation (6)}$$

Where Γ^* is the surface coverage of the adsorbed species (mol cm^{-2}). In addition to verifying that the analyte is freely diffusing, the Randles-Sevcik equation can be used to calculate the diffusion coefficient as well as the electroactive surface area.

2.1.1.2 Differential pulse voltammetry (DPV)

The CV technique is limited and not appropriate to detect an analyte within the concentration range of 10^{-2} to 10^{-6} M (Buffle & Tercier-Waeber, 2005) due to its low sensitivity and inability to distinguish peaks of two or more analytes. As a result, it is primarily suitable for qualitative analysis. To address this limitation, pulse-based voltammetric techniques have gained attention as means of quantitative measurement.

These techniques can be divided into several sub-methods depending on the applied potential-time waveform. DPV is an excellent technique for the quantification of organic and inorganic substances. This method involves the application of a constant pulse potential on a linear ramp potential, as shown in Figure 3A. The base potential value, at which no faradaic reaction occurs, is then applied to the electrode and is increased between pulses with equal increments (Simões & Xavier, 2017). The current is immediately measured before the pulse application (i_1) and at the end of the pulse (i_2), and the difference between them ($\Delta i = i_2 - i_1$) is recorded and plotted as a function of applied potential, known as the differential pulse voltammogram (Figure 3B) (González-Hernández, Alvarado-Gámez, Arroyo-Mora, & Barquero-Quirós, 2021). The peak height (Δi_p) is proportional to the analyte concentration in the solution.

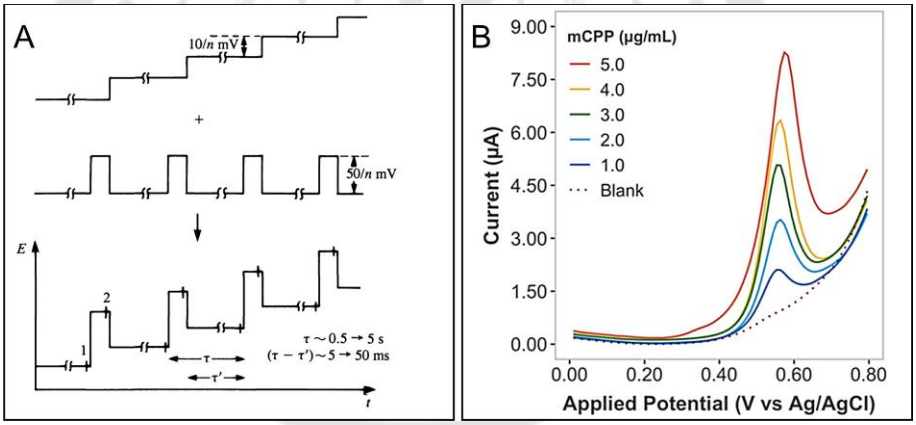

Figure 3 (A) Diagram of the application of pulse in DPV technique. (B) A typical response of differential pulse voltammogram.

Source: González-Hernández, J., Alvarado-Gámez, A. L., Arroyo-Mora, L. E., & Barquero-Quirós, M. (2021). Electrochemical determination of novel psychoactive substances by differential pulse voltammetry using a microcell for boron-doped diamond electrode and screen-printed electrodes based on carbon and platinum. *Journal of Electroanalytical Chemistry*, *882*.

2.1.1.3 Square wave voltammetry (SWV)

SWV is a highly sensitive and rapid pulse voltammetric technique utilized for quantification purposes. Analyzing the characteristic parameters of this technique enables the evaluation of the kinetics and mechanism of the electrode process under investigation. Figure 4A displays the potential-time waveform, which consists of a square wave superimposed on a staircase. The duration of one step in the staircase waveform corresponds to a full square wave cycle. The currents are measured at the end of the direct (i_1) and reverse (i_2) pulses, and the resulting differential current (Δi) is obtained as the signal intensity. Current-potential curves, known as square wave voltammograms, exhibit well-defined profiles and are typically symmetrical, as illustrated in Figure 4B (Simões & Xavier, 2017). This behavior is attributed to the measurement of all currents only at the end of each semiperiod, and the variations in the height and the width of the pulse potential remain constant for a specific potential range (Souza, Machado, & Avaca, 2003).

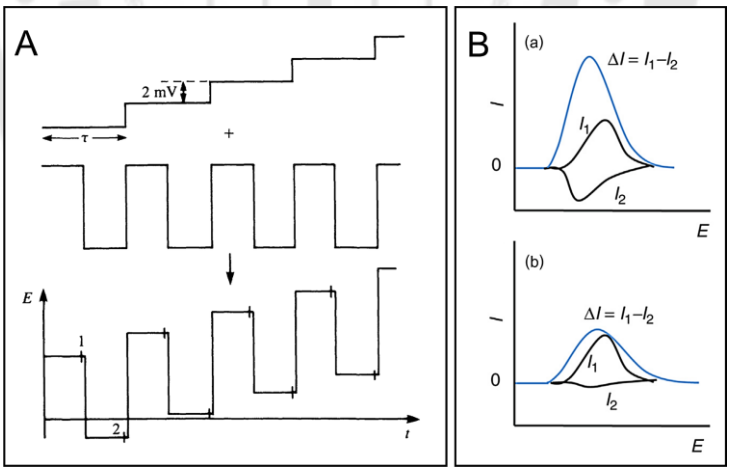

Figure 4 (A) Scheme of the potential-time waveform application consisting of a staircase and a square wave. (B) Square wave voltammograms, where (a) represents a redox process of a reversible system and (b) represents that of an irreversible system.

Source: Simões, F. R., & Xavier, M. G. (2017). Electrochemical Sensors. In *Nanoscience and its Applications* (pp. 155-178).

2.1.1.4 Chronoamperometry

Chronoamperometry involves the study of the variation of the current response with time under potentiostatic control. This technique measures the current flowing through the working electrode as a function of time as a constant potential is applied to the working electrode, as shown in Figure 5A. The current flow is correlated with the concentration of the oxidized or reduced species on the working electrode surface through the Cottrell equation (Equation (7)):

$$i(t) = \frac{nFAC^0D^{1/2}}{(\pi t)^{1/2}} \quad \text{.....Equation (7)}$$

where $i(t)$ is the current at time t (s), n is the number of electrons (eq. mol^{-1}), F is the Faraday's constant (96,485 C $eq.^{-1}$), A is the geometric area of the electrode (cm^2), C^0 is the analyte concentration (mol cm^{-3}), and D is the diffusion coefficient of the analyte (cm^2 s^{-1}).

In an unstirred cell, electroactive species will diffuse to the working electrode surface as a function of the potential applied. At the beginning of a potential step (E_1 to E_2), a large current arising from ion flux to the electrode surface to balance the charge in potential gives rise to a capacitive current (I_c), which decays rapidly. The concentration of electroactive species near the electrode interface decays with distance from the electrode and the arrival of species to the surface is diffusion-limited; therefore, faradaic current (I_d) near the electrode surface decays over time as the mass transport limit is reached. This behavior resulted in a normal exponential decay curve, as shown in Figure 5B (Inzelt, 2014).

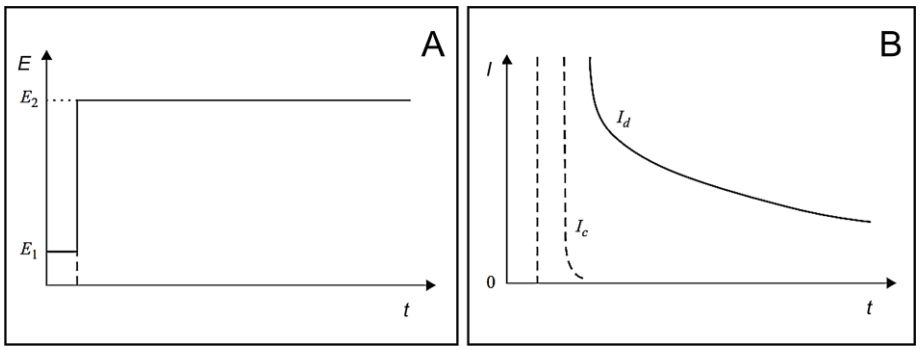

Figure 5 (A) Typical waveform of the potential step and (B) the chronoamperometric response.

Source: Inzelt, G. (2014). Chronoamperometry, Chronocoulometry, and Chronopotentiometry. In Encyclopedia of Applied Electrochemistry (pp. 207-214).

2.1.2 Electrochemical impedance spectroscopy (EIS)

2.1.2.1 Basic concept of EIS

EIS is an interfacial technique utilized to measure the electrical impedance of an electrochemical system as a function of frequency. It is a powerful tool used for characterizing the electrochemical behavior of materials and devices such as batteries, fuel cells, corrosion protection coatings, and sensors. The technique involves applying a small amplitude sinusoidal voltage to the system at a range of frequencies (Figure 6A) and measuring the resulting current response (Wang et al., 2021). Hence, the excitation signal is presented as a function of time, as illustrated in Equation (8):

$$E_t = E_0 \cdot \sin(\omega t) \quad \text{.....Equation (8)}$$

where E_t is the potential at the time, E_0 is the amplitude of the signal, and ω is the radial frequency.

The correlation between ω and the applied frequency (f) is calculated by Equation (9):

$$\omega = 2 \cdot \pi \cdot f \quad \text{.....Equation (9)}$$

In a linear system, the signal is shifted in phase (ϕ) and has a different amplitude than I_0 (Equation (10)):

$$I_t = I_0 \sin(\omega t + \Phi) \quad \text{.....Equation (10)}$$

Therefore, the impedance of the whole system can be obtained from Equation (11):

$$Z(\omega) = E(\omega)/I(\omega) = Z_0 exp(j\Phi) = Z_0(\cos\Phi + jsin\Phi) = Z_r + jZ_j \quad \text{.....Equation (11)}$$

where Z, E, I, ω, and ϕ are impedance, potential, current, frequency, and phase shift between E and I, respectively. Z_r and Z_j are real and imaginary parts of the impedance, while j is the imaginary number and is equal to $\sqrt{-1}$. The impedance can be expressed in terms of a magnitude (Z_0) and a phase shift. If the applied sinusoidal signal is plotted on the *X*-axis against the sinusoidal current response (I) on the *Y*-axis, the resulted curve is called as a “Lissajous Plot”, as shown in Figure 6B (Lvovich, 2014). On the other hand, by varying the frequency of the applied signal, a spectrum of impedance values, known as a “Nyquist Plot”, can be obtained, as depicted in Figure 6C.

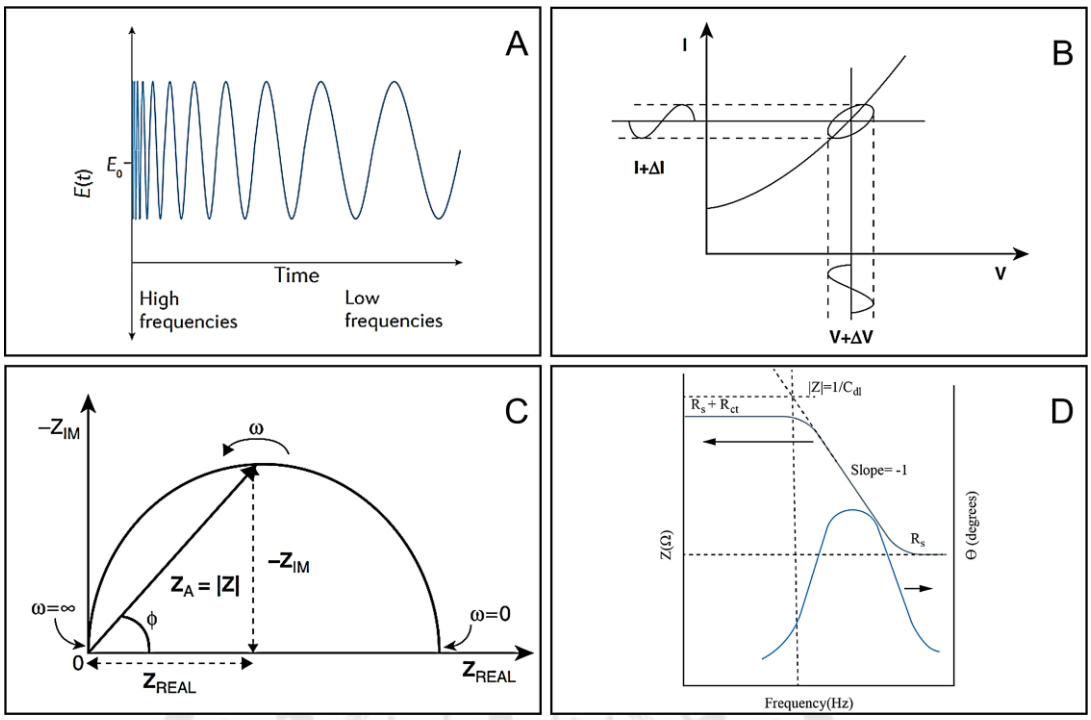

Figure 6 (A) A periodic perturbation signal with amplitude is applied from high to low frequencies. (B) The Lissajous plot and (C) the Nyquist plot with impedance vector. (D) The example of a Bode plot.

Source: Lvovich, V. F. (2014). Electrochemical Impedance Spectroscopy (EIS) Applications to Sensors and Diagnostics. In Encyclopedia of Applied Electrochemistry (pp. 485-507).

The impedance expression can be divided into two parts: a real part (Z_r or Z_{real} or Z')and an imaginary part (Z_j or Z_{imag} or Z''). As shown in Figure 6C, a Nyquist plot is obtained by constructing a relationship between the Z_{real} on the *X*-axis and the Z_{imag} on the *Y*-axis. Each point on the Nyquist plot represents an impedance value at a specific frequency. The left side of the plot on the *X*-axis indicates an impedance value at a high-frequency region, while the right side corresponds to an impedance value at a lower frequency. Furthermore, an impedance value can be represented by a vector (arrow) of length |*Z*|. The angle between this vector and the *X*-axis is known as the “phase angle”. Another way to present impedance results is to use a curve known as a “Bode plot” (see

Figure 6D), which consists of two types of logarithmic plots: magnitude versus frequency and phase versus frequency (Yavarinasab et al., 2021). This plot is useful to evaluate the capacitance of the electrochemical system, while the Nyquist plot is normally used to analyze the resistive processes.

In general, the overall resistance (R_{total}) of a whole circuit can be calculated by the summation of the resistances of each component. In that case, Ohm's law is used to calculate the overall resistance depending on a type of circuit as follows:

Series circuit: $$R_{total} = R_1 + R_2 + R_3 + \cdots + R_n$$ .....Equation (12)

Parallel circuit: $$\frac{1}{R_{total}} = \frac{1}{R_1} + \frac{1}{R_2} + \frac{1}{R_3} + \cdots + \frac{1}{R_n}$$ .....Equation (13)

However, the impedance does not obey Ohm's law due to its frequency-dependent property. The diffusion of electroactive species from the bulk solution to an electrode interface can generate an additional resistance, known as the Warburg impedance. The high-frequency region produces a small Warburg impedance because the reactant does not diffuse to an electrode surface. Conversely, applying lower frequencies creates a higher Warburg impedance since electroactive species are compelled to diffuse to an interface. This impedance can be determined from both the Nyquist plot and the Bode plot. A straight line with a slope of 45° on the Nyquist plot represents the infinite Warburg impedance, while a phase shift of 45° on the Bode plot reveals the Warburg effect (Magar, Hassan, & Mulchandani, 2021).

2.1.2.2 Equivalent circuits of EIS

An equivalent circuit involving electrical properties of resistance, capacitance, or inductance is created to simulate the electrochemical process of redox reactions occurring at an electrode-solution interface. This circuit is utilized to gain insight into the EIS system and evaluate the individual electrical components. In the Randles equivalent circuit, the electrical properties involved in an interfacial process include the solution resistance (R_s), the charge transfer resistance (R_{ct}), double-layer capacitance (C_{dl}), and Warburg impedance (Z_w), as illustrated in Figure 7 (Magar et al., 2021). After

fitting data to this circuit, a semicircle at a high-frequency domain with a straight line at a low-frequency region should be observed. The semicircle corresponds to the electron transfer process at the electrode-solution interface, while the straight line belongs to the diffusion process of electroactive species from the bulk solution to the electrode surface. The diameter of a semicircle corresponds to the R_{ct} value, which depends on the dielectric and insulating properties of each electrode-solution interface. A higher diameter of a semicircle indicates a higher electron transfer resistance. Hence, EIS is an effective technique to characterize the electrical properties of bare and modified electrodes.

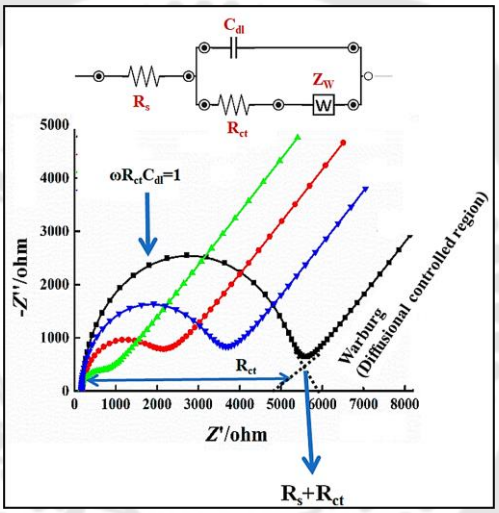

Figure 7 Impedance spectra showing a Randles equivalent circuit for an electrochemical system.

Source: Magar, H. S., Hassan, R. Y. A., & Mulchandani, A. (2021). Electrochemical Impedance Spectroscopy (EIS): Principles, Construction, and Biosensing Applications. *Sensors, 21*(19).

In the case of C_{dl}, the behavior of a perfect capacitor in an electrochemical system does not experimentally exist. Therefore, an additional electrical property known as a constant phase element (CPE) is introduced to account for the non-ideal

capacitance. This is caused by the roughness, non-homogeneity, or porosity of the electrode surface being investigated (Sun & Liu, 2019).

2.2 Miniaturized electrochemical devices

In the past decade, the application of miniaturized technology in analytical chemistry has significantly advanced analytical systems, addressing the limitations of traditional approaches. This progress has facilitated the scaling-down of instrumentation, apparatus, and devices, enabling measurements to be conducted outside of a laboratory setting. Moreover, the miniaturization of portable analytical systems offers substantial benefits, such as reduced production cost and decreased consumption of chemicals and solvents, resulting in decreased associated waste. These advantages make miniaturization a more environmentally sustainable approach than conventional methodologies (Pena-Pereira, 2014).

Among the various analytical techniques, electrochemical approaches are particularly well-suited for miniaturization due to the availability of fabrication for a small sensing platform with a compact potentiostat. Furthermore, their analytical performance is not compromised by the reduction in size, which enables sensitive detection of electroactive compounds in microliter sample volumes. As such, the continuous advancement of electrochemical detection using miniaturized devices remains a current focus.

In response to this trend, this dissertation focuses on the development of small-sized electrochemical devices, specifically a screen-printed electrode and a paper-based analytical device, for detecting various analytes.

2.2.1 Screen-printed electrode (SPE)

SPEs are a type of electrochemical sensor that is widely used in analytical chemistry and biosensing applications. They are typically created by screen-printing a conductive ink onto a non-conductive substrate, such as ceramic and polymer, in order to produce a pattern of working, counter, and reference electrodes, as illustrated in Figure 8 (Zensor R&D co., Ltd, 2016). The conductive ink used in the screen-printing process is

typically a carbon-based material, such as graphite, graphene, or carbon nanotubes, mixed with a binder, solvent, and other additives. Precise control of the ink deposition and pattern formation is achieved by depositing the ink onto the substrate through a fine mesh screen. Following the printing process, the electrodes are treated with a high-temperature curing process to remove any residual solvents and enhance the adhesion and conductivity of the ink. The resulting electrodes exhibit high sensitivity, stability, and reproducibility, making them an ideal choice for a wide range of electrochemical applications.

SPEs can be employed for various electrochemical measurements, including detection of small molecules, proteins, and nucleic acids. Additionally, they are frequently used in electroanalytical techniques, such as the voltammetric method, amperometry, and impedance spectroscopy. Compared to conventional bulk electrodes, SPEs have several advantages, including low cost, portability, and ease of use. They also require smaller sample volumes and can be readily integrated into other applications, such as microfluidic systems, for high-throughput analysis.

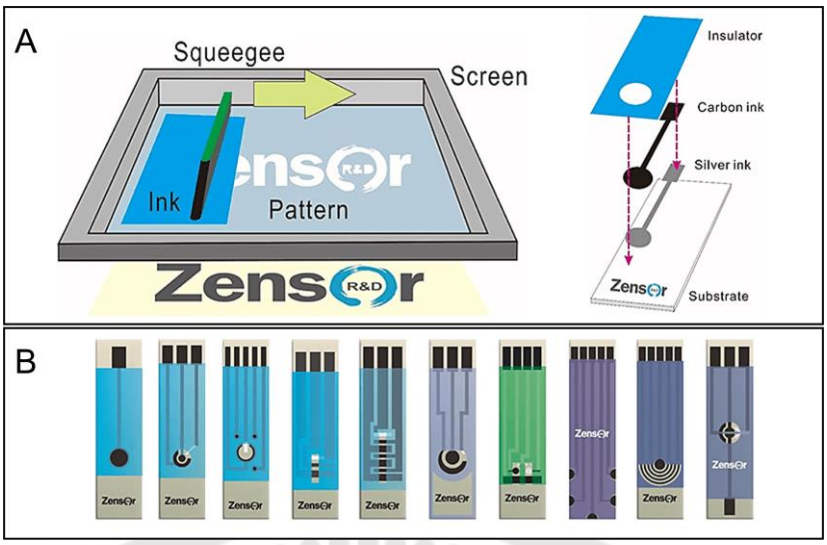

Figure 8 (A) The demonstration of a screen-printing process used for fabricating SPEs. (B) The availability of various SPE designs for wide practical applications.

Source: Zensor R&D co., L. (2016). Screen-printed carbon electrode. Retrieved from https://www.zensorrd.com/Article13.html

2.2.2 Paper-based analytical device (PAD)

The PAD is a type of diagnostic tool that employs paper as the primary substrate for conducting chemical or biological analyses. This low-cost, portable, and easy-to-use technology enables rapid detection and quantification of various analytes, including pathogens, toxins, and biomolecules. Typically, PADs are designed as small strips of paper, which can be fabricated using simple techniques such as printing, stamping, or cutting. They are compatible with various analytical purposes, including colorimetry, separation-related techniques, and electrochemistry. For colorimetric detection, the paper is functionalized with reagents that selectively interact with the target analyte, resulting in a visible color change or fluorescence signal that can be detected with the naked eye or a simple handheld device. Moreover, the paper can be fabricated as a microfluidic platform, known as a microfluidic paper-based analytical device (μPAD), allowing the separation of various analytes within the same single device. This feature

eliminates the need for external pumping equipment to enable fluid flow in the paper (Murphy et al., 2015). Furthermore, the paper-based device can be integrated with electrochemical detection by fabricating hydrophobic/hydrophilic barriers, followed by constructing a three-electrode system on a patterned paper. The resulting device is called an electrochemical paper-based analytical device (ePAD), providing the advantages of a low-cost and disposable paper-based platform with the high sensitivity and selectivity of an electrochemical approach (Primpray, Chailapakul, Tokeshi, Rojanarata, & Laiwattanapaisal, 2019). Figure 9 illustrates some examples of PADs used for analytical purposes (Pinyorospathum, Rattanarat, Chaiyo, Siangproh, & Chailapakul, 2019) (Khamcharoen, Henry, & Siangproh, 2022) (Placer, Lavilla, Pena-Pereira, & Bendicho, 2023).

PADs have numerous applications in healthcare, environmental monitoring, food safety, and forensic science. For instance, they can be used to detect infectious diseases in remote or resource-limited settings, monitor water quality in developing countries, and screen for drugs of abuse in forensic investigations. Thus, the simplicity, low cost, and versatility of PADs make them a promising tool for point-of-care diagnostics and field testing.

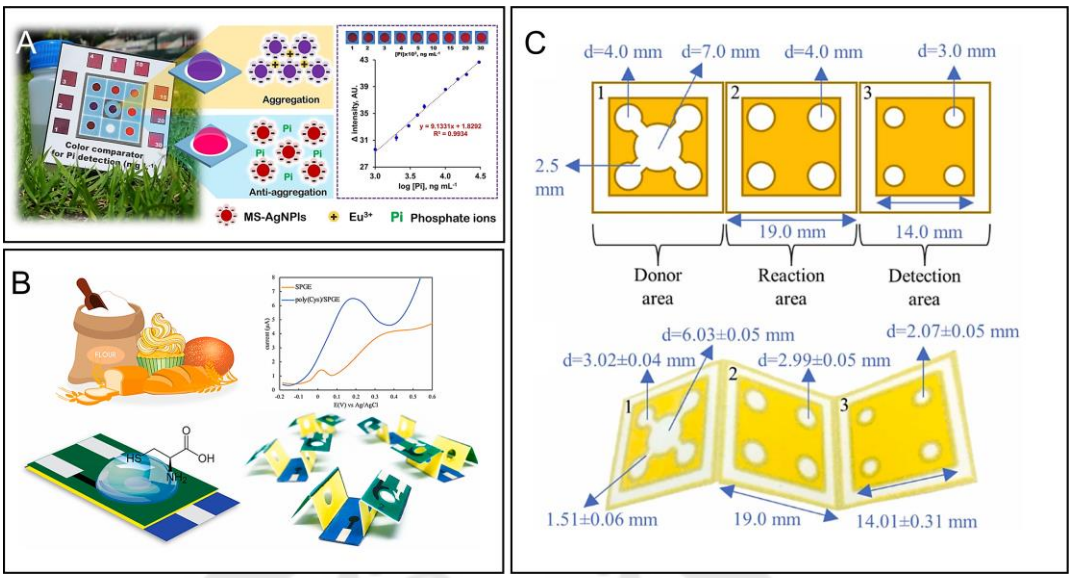

Figure 9 Some examples of PADs used for analytical purposes. (A) A colorimetric sensor for the detection of phosphate ions performed on PADs based on the anti-aggregation of 2-mercaptoethanesulfonate-modified silver nanoplates. (B) An all-in-one origami ePAD for the measurement of L-cysteine. (C) A 3D origami μPAD for the determination of iodide and iodate using colorimetric detection.

Source: (A) Pinyorospathum, C., Rattanarat, P., Chaiyo, S., Siangproh, W., & Chailapakul, O. (2019). Colorimetric sensor for determination of phosphate ions using anti-aggregation of 2-mercaptoethanesulfonate-modified silver nanoplates and europium ions. *Sensors and Actuators B: Chemical, 290*, 226-232., (B) Khamcharoen, W., Henry, C. S., & Siangproh, W. (2022). A novel l-cysteine sensor using in-situ electropolymerization of l-cysteine: Potential to simple and selective detection. *Talanta, 237*., and (C) Placer, L., Lavilla, I., Pena-Pereira, F., & Bendicho, C. (2023). A 3D microfluidic paper-based analytical device with smartphone-assisted colorimetric detection for iodine speciation in seaweed samples. *Sensors and Actuators B: Chemical, 377*.

2.3 Vitamins

Vitamins are organic compounds that play an essential role in maintaining normal physiological functions in the human body. These micronutrients are required in small

quantities and cannot be synthesized by the body; therefore they must be obtained from the diet or supplements. There are 13 recognized vitamins that are categorized into two groups: fat-soluble and water-soluble. Fat-soluble vitamins, including vitamins A, D, E, and K, are stored in the body's fat tissues and liver and are absorbed along with dietary fat. On the other hand, water-soluble vitamins such as vitamin C and the B-complex vitamins are not stored in the body to the same extent as fat-soluble vitamins and are excreted in the urine if taken in excess. Each vitamin has a specific function in the body, and deficiencies or excesses of certain vitamins can cause a range of health problems. For instance, vitamin A is crucial for vision and immune function, while vitamin C is necessary for collagen synthesis and wound healing. Table 1 summarizes the importance of each vitamin, showing appropriate intake levels, main functions in the body, food sources, and possible consequences of deficiencies and excesses (Y. Yang, Hu, Deng, & Yang, 2022).

Table 1 A summary of the importance of each vitamin.

Vitamin	Intake (mg/day)*	Main roles	Source	Possible consequence	
				Deficiency	Excess
A	0.7	Maintain normal function of human retina, bone growth	Retinol: animals; Carotenoids: fruits, vegetables	Blindness, decreased immune system efficiency, cancer	Severe headache, blurred vision, nausea, dizziness
B_1	1.2	Carbohydrate and amino acid metabolism	Rice, milk, eggs, meat	Metabolic diseases, beriberi, nervous system diseases	Excessive VB_1 is excreted in the urine
B_2	1.3	Promote cell growth and regeneration	Whole-grain products, eggs, liver	Inflammation of mouth corners and oral mucosa	Oxidative damage to DNA and liver
B_3	16	Main redox mediators in cell metabolism	Animal viscera, muscle tissues, fruits, egg yolks	Skin disease, digestive system symptoms, dementia	Flushing, hypotension
B_5	5	Amino acid catabolism, glycolysis and fatty acid metabolism	All types of animal and plant tissues	Fatigue, headache, nausea, vomiting, stomach pain	Mild diarrhea, gastrointestinal distress

Table 1 (Continued)

Vitamin	Intake (mg/day)*	Main roles	Source	Possible consequence	
				Deficiency	Excess
B_6	1.7	Cell growth and normal functional performance	Vegetables, protein-rich foods	Dermatitis, glossitis, anemia, numbness, weakened immune	Dermatological lesions; photosensitivity
B_7	0.03	Cofactor necessary for four important carboxylases	Meats, grains, vegetables	Skin diseases, nerve problems, growth retardation	-
B_9	0.3	Maintain and produce new cells, prevent DNA changes	Liver, dried beans, yolks, fruits, nuts, leafy vegetables	Neural tube defects, megaloblastic anemia, colon cancer	Impair the absorption of zinc and VB_{12}
B_{12}	0.0024	Nerve cell growth, red blood cell formation	Liver, kidney, meat, fish, clams, eggs, milk cheese	Neuropsychiatric, cardiovascular and hematological diseases	Renal failure, liver disease, neurotoxicity
C	100	Antioxidant; synthesis of collagen, carnitine, adrenaline	Fresh fruits and vegetables	Scurvy, anemia, infections, cardiovascular disease, cancer	Headache, difficulty sleeping, skin redness

Table 1 (Continued)

Vitamin	Intake (mg/day)*	Main roles	Source	Possible consequence	
				Deficiency	Excess
D	0.015	Promote the adsorption of calcium and phosphate in the intestine	Egg yolk, mushroom, cod, liver oil, fresh salmon	Osteomalacia in adults and rickets in children	Nausea, vomiting, muscle weakness, pain
E	13	Prevent the formation of reactive oxygen species	Fruits and vegetables, nuts, lean meat, milk, eggs	Circulatory disorders, fertility disorder, Alzheimer's disease	Hemorrhage and interrupt blood coagulation
K	0.12	Control calcium levels and synthesize proteins needed for blood coagulation	K_1: green vegetables; K_2: eggs, cheese, liver, meat	Decrease prothrombin and the tendency of excessive bleeding	-

*Dietary reference intake (DRI) for Thai adults (≥19 years old) (Bureau of Nutrition, 2020).

Source: Yang, Y., Hu, N., Deng, J., & Yang, J. (2022). Electrochemical Sensing for Vitamins. *Chemosensors, 10*(11).

2.3.1 Fat-soluble vitamins

Fat-soluble vitamins readily dissolve in organic solvents but have low solubility in water. These vitamins are essential nutrients necessary for maintaining human health. Each fat-soluble vitamin contains several active vitamers that perform specific functions. Among them, vitamin A (VA) is composed of retinol-based compounds, including retinoids derived from animals and carotenoids obtained from plants. VA is a crucial nutrient required for the biological activity involved in the synthesis of retinylidene chromophores and visual pigments.

Vitamin D (VD) is a critical determinant of bone and mineral metabolism. It is commonly referred to as the “sunshine vitamin” due to its production in the skin upon exposure to ultraviolet B (UVB) radiation from sunlight. This natural synthesis is the most effective means of obtaining VD (80-90%), with the remaining 10-20% obtained through dietary intake or supplements. VD is a vital hormone that plays a role in various metabolic pathways, including regulating the balance of calcium and phosphate in the bloodstream, and influencing bone mineralization. The two most commonly recognized forms of VD are ergocalciferol (D_2) and cholecalciferol (D_3). A notable VD_3 metabolite, 25-Hydroxyvitamin D (25-OHD), is an essential indicator of VD deficiency, and can be measured in human serum (Chauhan, Gupta, & Solanki, 2021).

Vitamin E (VE) is a group of substances that exhibit antioxidant activity similar to α-tocopherol, including all tocopherols and their derivatives. The liver absorbs various forms of VE, which are eventually secreted as the α-conformation (α-tocopherol). This particular form of VE provides significant biological benefits in the human body and acts as an antioxidant (Jashari et al., 2021). VE plays a crucial role in maintaining immune and neural health. Moreover, it impacts the proliferation and differentiation of smooth muscle cells, platelets, and monocytes and regulates the expansion of blood cells while also inhibiting platelet aggregation.

Vitamin K (VK) comprises 2-methyl-1,4-naphthoquinone and all of its derivatives, with phylloquinone (K_1) and menaquinone (K_2) being the most prevalent active forms. The primary function of VK is to act as a coenzyme for the synthesis of numerous

proteins associated with coagulation and bone metabolism. VK_1 is the predominant form of VK, serving as a redox mediator in photosynthesis. VK_2, on the other hand, is present in animals and is produced by bacteria in the intestine. It features a polyisoprenyl side chain that contains 6 to 13 units; hence it is also known as menaquinone-n (MK-n), with the value of n corresponding to the number of side chain units.

2.3.2 Water-soluble vitamins

Water-soluble vitamins are essential nutrients and are of great importance to human growth and development. These vitamins are comprised of various compounds and are widely present in several food sources. However, they cannot be stored in the human body for a long period and are rapidly excreted with urine, necessitating regular supplementation. Consuming an inadequate amount of these vitamins has negative impacts on human health, leading to numerous diseases. Therefore, it is crucial to detect vitamins in biological fluids and food samples to evaluate the risk of diseases and ensure the quality of food products.

Seven types of B vitamins, along with vitamin C, are essential nutrients that are classified as water-soluble vitamins. Vitamin B_1 (VB_1), also known as thiamine, can be utilized to synthesize pyrophosphate and thiamine diphosphate (Paudics et al., 2022), which are coenzymes involved in numerous metabolic processes, particularly in carbohydrate and branched-chain amino acid metabolisms. These substances are crucial for the normal metabolism of the human body, particularly for the nervous system.

Vitamin B_2 (VB_2), also referred to as riboflavin (RF), is a crucial constituent of flavoenzymes, which exist in active forms of flavin mononucleotide and flavin adenine dinucleotide. These substances serve as essential cofactors for regular respiration in tissues and facilitate the catabolism of carbohydrates, proteins, and fats to produce energy (Tesfaye, Negash, & Tessema, 2022). Moreover, RF possesses antioxidant properties that aid in preventing cataracts, and high dosages have been reported to be effective in the treatment of migraines (Namazi, Heshmati, & Tarighat-Esfanjani, 2015).

Vitamin B_3 (VB_3), also known as niacin, primarily comprises nicotinamide and nicotinic acid, and serves as the precursor to nicotinamide adenine dinucleotide (NAD). Niacin aids in the synthesis of sexual hormones, reduces cholesterol levels, regulates the functions of the brain and nervous system, and helps to maintain the health of the skin, tongue, and digestive system tissues. Furthermore, NAD-related compounds, along with its phosphorylated substances nicotinamide adenine dinucleotide phosphate (NADP) and their reduced forms NADH and NADPH, participate as major redox mediators in several metabolic processes within cells.

Vitamin B_5 (VB_5) primarily refers to D-pantothenic acid, which serves as a precursor for the formation of coenzyme A (CoA). VB_5 plays a crucial role in various biological activities, including energy metabolism and fatty acid oxidation (Bourgin, Kepp, & Kroemer, 2022). Additionally, this vitamin is involved in the synthesis of acetylcholine, red blood cells, and hormones secreted from the adrenal glands. Regarding the importance of CoA, it functions as the acetyl donor in acetylation reactions, playing a key role in the oxidation of fatty acids, pyruvate or α-ketoglutarate, as well as in the synthesis of fatty acids, cholesterols, and sterols, and biological acetylation.

Pyridoxine, pyridoxal, and pyridoxamine are classified as chemically related forms of vitamin B_6 (VB_6). Pyridoxine is the most stable form, which can be metabolized within the human body into biologically active forms, namely pyridoxal-5'-phosphate and pyridoxamine phosphate. These substances act as cofactors in catalyzing the reactions of more than 100 enzymes related to glycogen, amino acid, and lipid metabolisms (Porada, Fendrych, & Baś, 2021). VB_6 is involved in hemoglobin production and functioning, gene expression, and supports the nervous and immune systems. Additionally, VB_6 plays a vital role in promoting brain development during pregnancy and infancy.

Biotin, also known as vitamin B_7 (VB_7) or vitamin H, plays a crucial role as a coenzyme in the primary metabolic pathways in both mitochondria and cytoplasm. These pathways include amino acid catabolism, gluconeogenesis, and lipogenesis. In addition

to dietary intake, human intestinal bacteria can also synthesize biotin at a substantial rate, thus making biotin deficiency a rare occurrence in humans.

Vitamin B_9 (VB_9), also referred to as folic acid, plays a significant role in numerous synthetic biological reactions by serving as a coenzyme involved in nucleic acid synthesis and amino acid metabolism (Olmo, Rodriguez, Colina, & Heras, 2021). This crucial function encompasses the synthesis of purine and pyrimidine, as well as DNA fixation and methylation. Consequently, a deficiency of VB_9 can result in the malfunction of DNA replication, leading to abnormal cell division.

Vitamin B_{12} (VB_{12}), also known as cobalamin, is a coordination compound containing cobalt that plays a crucial role in the normal functioning of the nervous system and the maturation of red blood cells in the bone marrow (Guo, 2021). VB_{12} exists in several chemically related forms, including methylcobalamin, adenosylcobalamin, cyanocobalamin, and hydroxocobalamin. Of these, methylcobalamin and adenosylcobalamin are particularly significant to the human body, as they act as coenzymes for methionine synthase and methylmalonyl CoA mutase, respectively. These enzymes are involved in various metabolic processes, including the synthesis of nucleic acids and red blood cells, as well as the metabolism of carbohydrates, proteins, and lipids.

Vitamin C (VC), also known as L-ascorbic acid, is one of the most ubiquitous small biomolecules found in human blood. Its crucial role in protecting healthy cells from free radicals, harmful chemicals, cigarette smoke, and other pollutants makes it an essential component in resisting bacterial infections and preventing damage to our body cells. In addition to its protective functions, VC is involved in various human activities, including immune system function, wound healing, and the maintenance of cartilage, bone, and teeth. It acts as a cofactor of several enzymes, enhances intestinal iron absorption, participates in carnitine and collagen synthesis, as well as cell metabolism. Furthermore, VC serves as an ideal singlet oxygen scavenger and chelating agent (Tortolini, Tasca, Venneri, Marchese, & Antiochia, 2021).

As briefly mentioned earlier, this dissertation focuses on the development of an electroanalytical method to detect water-soluble vitamins. It is necessary to consume these vitamins daily at sufficient levels due to their inability to be stored in the body and rapid excretion with urine. Among various types of water-soluble vitamins, VB_2, VB_6, and VC have been selected as analytes of interest because of their availability in many food sources and their involvement in several important biological activities. For example, VB_2 and VB_6 play a role in cellular growth and development, while VC is associated with protection against common colds, scurvy, and cancer. This can be useful in evaluating clinical and food applications to indicate abnormalities or diseases and guarantee the quality of food products. Therefore, the importance of VB_2, VB_6, and VC, as well as their deficiency and dietary reference intake, are described in detail as follows.

2.3.3 Vitamin B_2 (VB_2)

VB_2 or riboflavin (RF) is a water-soluble vitamin categorized within the group of essential nutrients. It exists in a purified solid form as a stable yellow-orange crystalline powder stable at room temperature. However, it is unstable when exposed to sunlight. Upon consumption of RF, it undergoes conversion into two biologically active forms, namely flavin mononucleotide (FMN) and flavin adenine dinucleotide (FAD). These substances act as coenzymes, functioning as hydrogen receptors in the oxidation-reduction process within the body. The structures of RF, FMN, and FAD are illustrated in Figure 10.

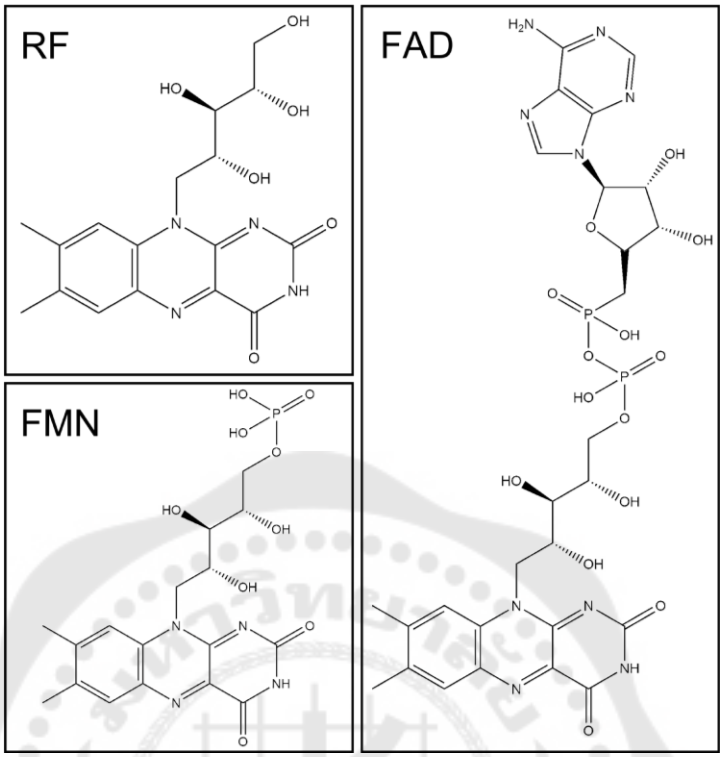

Figure 10 The chemical structures of RF, FMN, and FAD.

FMN and FAD act as coenzymes that participate in the metabolism of fatty acids and VB_6. FMN serves as a prosthetic group for various oxidoreductases, such as NADH dehydrogenase, and also functions as a cofactor in biological blue-light photoreceptors (Tsibris, McCormick, & Wright, 1966). FAD is involved in energy production and the synthesis of niacin from tryptophan. Moreover, it aids in the metabolism of carbohydrates, proteins, and lipids, which are essential for normal cell growth and development, and promotes the health of the nervous system, skin, and eyes.

The deficiency of VB_2 can be observed in various at-risk groups of the Thai population, including pregnant women, lactating women, infants, children, laborers, the elderly, and vegetarians (Songchitsomboon, Komindr, Kulapongse, Puchaiwatananon, & Udomsubpayakul, 1998). The signs and symptoms of VB_2 deficiency, known as ariboflavinosis, include inflammation of the throat, lips, and tongue, as well as a red and swollen tongue. Other symptoms include inflammation in the corners of the mouth (angular stomatitis), skin inflammation with the characteristics of redness, scaliness, itchiness, and

greasiness (seborrheic dermatitis), and normocytic anemia. Severe VB_2 deficiency can also lead to malfunctioning of VB_6, which is essential in synthesizing niacin from tryptophan. Additionally, some endocrine glands, such as the thyroid and adrenal glands, as well as certain medications, such as chlorpromazine, imipramine, and amitriptyline, chemotherapy drugs, such as doxorubicin and methotrexate, and antimalarial drugs like quinacrine, can cause VB_2 deficiency. Moreover, drinking alcoholic beverages can disrupt the digestion and absorption of RF in the intestine, thereby increasing the risk of VB_2 deficiency.

The dietary reference intake (DRI) of VB_2 for the Thai population is provided in Table 2, classified by groups, age, and gender (Bureau of Nutrition, 2020).

Table 2 The dietary reference intake (DRI) of VB_2 for the Thai population.

Groups	Age ranges	Reference intake of VB_2 (mg/day)
Infants	0 – 5 months old	0.2
	6 – 11 months old	0.4
Children	1 – 3 years old	0.5
	4 – 8 years old	0.6
Male adolescents	9 – 12 years old	0.9
	13 – 18 years old	1.3
Female adolescents	9 – 12 years old	0.9
	13 – 18 years old	1.0
Male adults	≥ 19 years old	1.3
Female adults	≥ 19 years old	1.1
Pregnant women	-	+ 0.3
Lactating women	-	+ 0.5

Source: Bureau of Nutrition, D. o. H., Ministry of Public Health. (2020). *DIETARY REFERENCE INTAKE FOR THAIS 2020*: A.V. PROGRESSIVE LTD., PART. (pp. 189).

2.3.4 Vitamin B_6 (VB_6)

VB_6, also known as pyridoxine (PN), is a water-soluble vitamin that has a slight solubility in organic solvents and lipids. It is easily degraded by UV radiation and alkaline solutions. Natural VB_6 can be found in three chemically related forms, as illustrated in Figure 11: pyridoxine, pyridoxal (PL), and pyridoxamine (PM). Each substance has a distinct substituent at the fourth position of the pyridine ring. PN contains a hydroxymethyl group, while PL and PM contain an aldehyde and an aminomethyl group, respectively. PN is heat-stable, but PL and PM rapidly decompose under high-temperature conditions.

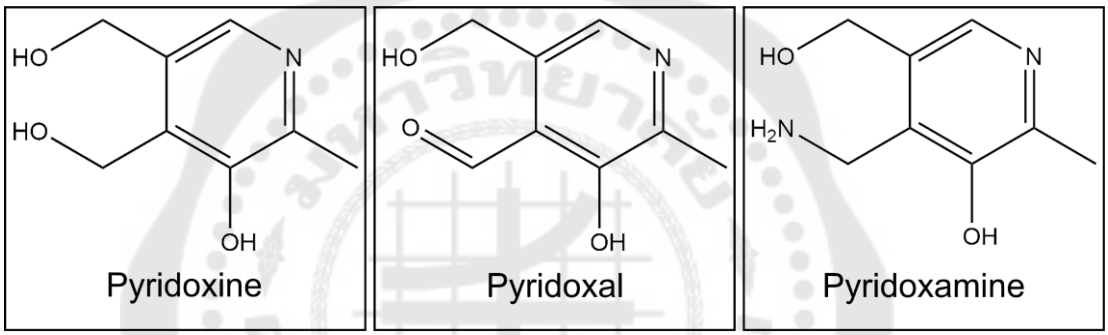

Figure 11 Chemically related forms of VB_6.

VB_6 nutrients are primarily found in food sources as phosphate-containing compounds. These derivatives are digested with enzymes in the stomach to release the phosphate group before absorption in the small intestine. They are then transported via the bloodstream to the liver to be converted into biologically active forms, namely pyridoxal-5'-phosphate and pyridoxamine phosphate. Finally, VB_6 is excreted in the urine as pyridoxic acid.

VB_6 plays a crucial role as a coenzyme in various biochemical reactions, including amino acid metabolism, glucose biosynthesis from glycogen breakdown in muscles, hemoglobin synthesis and function, niacin synthesis from tryptophan, and regulation of homocysteine levels in the blood. Additionally, VB_6 is involved in cognitive development by synthesizing various neurotransmitters such as serotonin, taurine, dopamine, norepinephrine, and gamma-aminobutyric acid. Furthermore, VB_6 is

associated with the immune system by promoting the synthesis of lymphocytes and interleukin 2.

As previously mentioned, VB_6 plays a critical role in maintaining optimal human health. The deficiency of this vitamin can have detrimental effects on the metabolism of amino acids, carbohydrates, and lipids. The signs and symptoms of VB_6 deficiency may include microcytic anemia resulting from impaired heme synthesis, skin inflammation (cheilosis and glossitis), weakened immunity, and neurological disorders such as depression, confusion, and somnolence. Additionally, VB_6 deficiency may be observed in patients with end-stage renal disease, renal dystrophy, and other kidney abnormalities. This condition includes absorption disorders, such as gastrointestinal diseases, chronic intestinal ulcers, and chronic alcoholism.

The dietary reference intake (DRI) of VB_6 for the Thai population is provided in Table 3, classified by groups, age, and gender (Bureau of Nutrition, 2020).

Table 3 The dietary reference intake (DRI) of VB_6 for the Thai population.

Groups	Age ranges	Reference intake of VB_6 (mg/day)
Infants	0 – 5 months old	0.1
	6 – 11 months old	0.3
Children	1 – 3 years old	0.5
	4 – 8 years old	0.6
Male adolescents	9 – 12 years old	1.0
	13 – 18 years old	1.3
Female adolescents	9 – 12 years old	1.0
	13 – 18 years old	1.2
Male adults	19 – 50 years old	1.3
	≥ 51 years old	1.7
Female adults	19 – 50 years old	1.3
	≥ 51 years old	1.5

Table 3 (Continued)

Groups	Age ranges	Reference intake of VB_6 (mg/day)
Pregnant women	-	+ 0.6
Lactating women	-	+ 0.7

Source: Bureau of Nutrition, D. o. H., Ministry of Public Health. (2020). *DIETARY REFERENCE INTAKE FOR THAIS 2020*: A.V. PROGRESSIVE LTD., PART. (pp. 211).

2.3.5 Vitamin C (VC)

VC or ascorbic acid is a water-soluble vitamin that is naturally found in the L-isomer form as the biologically active compound. Its chemical formula is $C_6H_8O_6$, and its molar mass is 176.13 g mol^{-1}. The solid form of VC appears as a white crystalline stable powder, but it is easily oxidized when dissolved in water or heated under high-temperature conditions. Upon the oxidation process, ascorbic acid is converted into dehydroascorbic acid, which undergoes hydrolysis to form diketogulonic acid. Further oxidation of this substance results in the formation of oxalic acid, threonic acid, and other by-products. These compounds, including ascorbic acid, are finally excreted in the urine. Figure 12 displays the chemical structure of ascorbic acid, major metabolites, and degradation products (Zempleni, Suttie, Gregory Iii, & Stover, 2013).

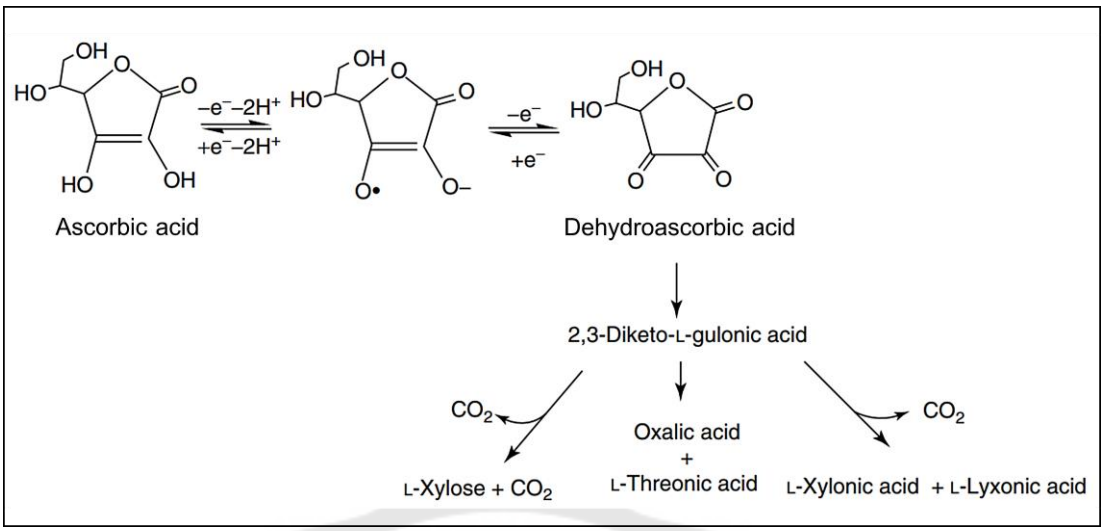

Figure 12 The chemical structure of ascorbic acid, major metabolites, and degradation products.

Source: Zempleni, J., Suttie, J. W., Gregory Iii, J. F., & Stover, P. J. (2013). *Handbook of Vitamins*.

The absorption of VC in the intestine is dependent on the level of VC consumption. A low intake of VC, ranging from 30 – 180 mg/day, results in high absorption rates (80 – 90%) within the human body through active transport mechanisms that require energy (ATP). However, high levels of VC consumption exceeding 1,000 mg/day lead to decreasing absorption rates (75%) due to simple diffusion. Once absorbed, VC is transported in the form of free acid and does not bind to proteins. It subsequently reaches various cells such as leucocytes and red blood cells, where it is metabolized.

VC functions as a vital substance in numerous enzymatic reactions involved in essential biological activities. One example is collagen, a crucial fibrous protein that contributes to the formation of bones, ligaments, muscles, teeth, connective tissues, and skin. Collagen is synthesized from glycine, proline, hydroxyproline, and other related amino acids, with proline hydroxylase and lysine hydroxylase acting as catalysts. The completion of this process requires VC as a cofactor. Thus, a deficiency of VC leads to changes in the structure of collagen, resulting in abnormal wound healing, connective

tissue disorders, bone-related diseases, and scurvy. Additionally, VC plays a role in the synthesis of carnitine, acting as a cofactor in the hydroxylation of trimethyllysine and gamma-butyrobetaine. It also contributes to catecholamine synthesis, which helps to prevent depression and unstable emotions.

VC functions as an antioxidant, eliminating free radicals both inside and outside cells. This vital role includes protecting cells and preventing tissue deterioration, as well as inhibiting peroxidation of unsaturated fatty acids. VC further aids the immune system by promoting lymphocyte function and phagocytic activity of neutrophils, which eliminates pathogens in the body. By inhibiting histamine secretion in response to allergen exposure, VC can help to reduce irritation of the respiratory mucosa, relieve sneezing, runny nose, redness, and skin rash. Additionally, VC prevents the formation of nitrosamines, a type of carcinogen, by blocking the reaction of nitrites and secondary amines. VC also enhances the absorption of non-heme iron in the intestine, increasing its bioavailability.

The dietary reference intake (DRI) of VC for the Thai population is provided in Table 4, classified by groups, age, and gender (Bureau of Nutrition, 2020).

Table 4 The dietary reference intake (DRI) of VC for the Thai population.

Groups	Age ranges	Reference intake of VC (mg/day)
Infants	0 – 5 months old	40
	6 – 11 months old	50
Children	1 – 3 years old	25
	4 – 5 years old	30
	6 – 8 years old	40
Male adolescents	9 – 12 years old	60
	13 – 15 years old	85
	16 – 18 years old	100

Table 4 (Continued)

Groups	Age ranges	Reference intake of VC (mg/day)
Female adolescents	9 – 12 years old	60
	13 – 18 years old	80
Male adults	≥ 19 years old	100
Female adults	≥ 19 years old	85
Pregnant women	-	+ 10
Lactating women	-	+ 60

Source: Bureau of Nutrition, D. o. H., Ministry of Public Health. (2020). *DIETARY REFERENCE INTAKE FOR THAIS 2020*: A.V. PROGRESSIVE LTD., PART. (pp. 253).

2.3.6 Literature reviews

Currently, liquid chromatography (LC) is considered as a reliable method for detecting water-soluble vitamins due to its sensitivity, selectivity, and capability for simultaneous measurement (Khaksari, Mazzoleni, Ruan, Kennedy, & Minerick, 2017) (Vállez-Gomis, Peris-Pastor, Benedé, Chisvert, & Salvador, 2021) (Gliszczyńska-Świgło & Rybicka, 2014). This technique is suitable for routine analysis in wide-ranging applications of clinical diagnosis, cosmetic products, as well as food and pharmaceutical industries (Abano & Godbless Dadzie, 2014). However, despite its advantages, the LC technique still suffers from certain limitations that are unavoidable, including costly instrumentation, long analysis time, the need for a large volume of solution, and multiple sample preparation steps. These limitations have prompted the development of other analytical methods that can offer valuable alternative options for detecting water-soluble vitamins.

The electroanalytical method is an effective choice for the detection of analytes of interest due to its simplicity, cost-effectiveness, and ease of miniaturization. This technique can be used to detect most of the water-soluble vitamins owing to their

electrochemical reactivity (Huang, Tian, Zhao, Liu, & Guo, 2021). Consequently, an electrochemical mapping of water-soluble vitamins, as depicted in Figure 13, has been constructed to indicate the potential axis of each vitamin (Lovander et al., 2018). This mapping has revealed that each vitamin possesses a unique potential value, thereby allowing for simultaneous detection. For instance, VB_2 has a potential value of -0.22 V (versus NHE); whereas VC and VB_6 have potential values of +0.39 V and +1.00 V (versus NHE), respectively. As these values are widely spaced apart, simultaneous detection should be achievable since the electrochemical signals would not overlap.

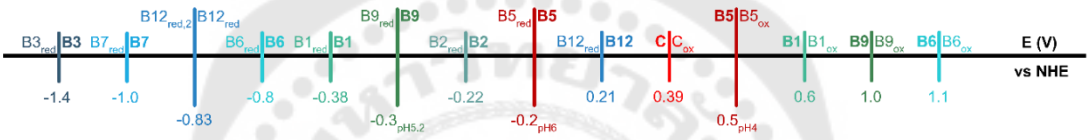

Figure 13 An electrochemical mapping of water-soluble vitamins drawing by the IUPAC convention of positive (oxidation) on the right. All vitamin potentials (versus a normal hydrogen electrode (NHE)) are at pH 7.0 unless indicated by a subscript for $E_{1/2}$.

Source: Lovander, M. D., Lyon, J. D., Parr, D. L., Wang, J., Parke, B., & Leddy, J. (2018). Critical Review—Electrochemical Properties of 13 Vitamins: A Critical Review and Assessment. *Journal of The Electrochemical Society, 165*(2), G18-G49.

Therefore, this dissertation focuses on the development of the electroanalytical method for simultaneous detection of VB_2, VB_6, and VC. This section will present a review of the literature related to this work, which will describe the electrode materials and electroanalytical techniques utilized for detection.

In 2007, the first report on the simultaneous detection of VB_2, VB_6, and VC was proposed (Gu, Yu, & Chen, 2007). This work described the use of electrochemical methods to pretreat a glassy carbon electrode (GCE), enhancing its electrical properties and overcoming slow electrode kinetics. The pretreatment process of a GCE was achieved in phosphate media through anodic oxidation at +1.8 V (vs SCE) and potential

cycling ranging from -0.8 V to +1.0 V. The results showed that pretreating a GCE under suitable conditions is necessary for the accurate determination of vitamins, resulting in good electrochemical behaviors obtained. DPV measurements showed that the linear ranges of each vitamin were 5.0 nM to 0.10 mM for VB_2, 2.5 μM to 7.5 mM for VB_6, and 75 μM to 75 mM for VC. The real sample analysis was accomplished by detecting these vitamins in multivitamin tablets with satisfactory results.

In 2013, the second report on the simultaneous detection of VB_2, VB_6, and VC was described (Nie et al., 2013). This work proposed the preparation of functionalized poly(3,4-ethylenedioxythiophene) (PEDOT) films by incorporating two electroactive species, ferrocenecarboxylic acid and ferricyanide, during the electropolymerization of PEDOT at a GCE surface. The resulting nanostructured films combine the advantages of high conductivity and stability of PEDOT with the good electrochemical activity of the electroactive species. The synthesized sensors were characterized using both morphological and electrochemical techniques, exhibiting excellent electrocatalytic activity toward the oxidation of vitamins. The performance of the sensors, obtained from DPV measurements, showed that the linear ranges of each vitamin were 1.0 μM to 300.0 μM for VB_2, 15.0 μM to 1,000.0 μM for VB_6, and 20.0 μM to 1,500.0 μM for VC. In addition, the sensors possessed high selectivity with no interference from other potential competing species and have been successfully employed for the simultaneous determination of vitamins in orange juice samples with satisfactory results.

In 2014, the third report on the simultaneous detection of VB_2, VB_6, and VC was presented (Nie, Zhang, Xu, Lu, & Bai, 2014). This study involved the development of a novel electrode material, called poly(3,4-ethylene-dioxythiophene)/Zirconia nanoparticles (PEDOT/ZrO_2NPs) nanocomposite. The researchers used a simple one-step electrodeposition method to synthesize this material on a GCE surface. The resulting material exhibited a large specific area, high conductivity, and rapid redox properties, making it an excellent sensing platform for detecting vitamins. By employing DPV as a quantitative method, the detection limits for VB_2, VB_6, and VC were found to be 0.012 μM, 0.20 μM, and 0.45 μM, respectively. Moreover, the modified electrode demonstrated good

reproducibility, long-term stability, and high selectivity. The proposed sensor was successfully applied to perform the simultaneous detection of vitamins in honey samples, yielding satisfactory results. Therefore, this research could lead to the development of low-cost and effective electrochemical sensors, making them attractive candidates for practical applications.

In 2015, the fourth report on the simultaneous detection of VB_2, VB_6, and VC was proposed (G. Liu, Wang, & Sun, 2015). This work described an alternative electrochemical method for detecting these vitamins using a modified electrode constructed by electropolymerization of silver-doped poly(L-arginine) on a GCE. The electrochemical properties of the fabricated sensor were studied using CV and EIS techniques, demonstrating good electrocatalytic activity of the modified electrode for the oxidation of the three vitamins. Under optimal conditions, the linear ranges, obtained from linear sweep voltammetry (LSV), for the detection of vitamins were determined to be 0.1 μM to 23.0 μM for VB_2, 10.0 μM to 3.0 mM for VB_6, and 5.0 μM to 4.0 mM for VC, with corresponding detection limits of 0.08 μM, 5.0 μM, and 3.0 μM. The developed sensing platform was successfully applied to the simultaneous detection of these three vitamins in multivitamin tablets with satisfactory results.

In 2017, the fifth and latest report on the simultaneous detection of VB_2, VB_6, and VC was described (Puangjan, Chaiyasith, Taweeporngitgul, & Keawtep, 2017). This study proposed the fabrication of a new electrochemical sensor that employs a combination of chemically functionalized multiwall carbon nanotubes, cuprous oxide, and silver oxide composite on a copper substrate. The modified electrode exhibited excellent electrochemical catalytic activity towards the oxidation of selected vitamins. The performance of the proposed electrode was superior to that of a simple copper substrate due to its robust structure, excellent conductivity, and large surface area. DPV was used as a quantitative technique in this work, and the linear ranges were found to be 0.05 – 1,752.65 μM for VB_2, 0.02 – 1,056.12 μM for VB_6, and 0.05 – 1,628.54 μM for VC, with detection limits of 14 nM, 8 nM, and 11 nM, respectively. The results indicated that the developed electrode could facilitate better discrimination between species, making it

suitable for the simultaneous determination of these vitamins in various real samples such as honey, orange juice, and human urine. Therefore, the sensor offers a practical approach for the detection of vitamins and has the potential to be further developed for the measurement of other biochemical compounds.

As mentioned in the literature reviews, previous reports use GCEs that were modified with various metallic nanomaterials and conductive polymers. The resulting sensors exhibited high sensitivity and selectivity towards the simultaneous detection of VB_2, VB_6, and VC. However, the major limitation of previous works was the use of a conventional GCE to perform electrochemical measurement. This necessitated the use of a large solution volume, resulting in a large volume of liquid waste. To address this issue, a miniaturized electrochemical device can be used as an alternative platform. As a result, this dissertation presents the first work to develop a miniaturized device for the simultaneous detection of VB_2, VB_6, and VC. The unmodified screen-printed carbon electrode was used as a low-cost and disposable sensor, eliminating the need for the synthesis of complex materials. Under optimized conditions, the proposed electrode offers good sensitivity and selectivity, making it suitable for analyzing real juice and urine samples.

2.4 Albumin

Albumin is a family of globular proteins that is highly water-soluble and moderately soluble in concentrated salt (Hutapea et al., 2023). This macromolecule is present in various parts of animals, such as in blood plasma or serum, muscle, egg white, and milk, as well as in many plant tissues and fluids. Albumin consists of more than 500 amino acids, with an approximate molecular weight of 67 kDa for human serum albumin (HSA), 69 kDa for bovine serum albumin, and 47 kDa for ovalbumin (Elzoghby, Samy, & Elgindy, 2012). HSA contains a repeating series of six helical subdomains as shown in Figure 14 (Sugio, Kashima, Mochizuki, Noda, & Kobayashi, 1999), with α-helices of 67%, turns of 10%, random coil of 23%, and no-β sheets (Mishra & Heath, 2021). As a plasma protein in human blood, albumin has an average half-life of 19 days and exhibits stability

within a pH range of 4 – 9 (Kratz, 2008). Critical factors affecting the coagulation of albumin include heating, pH conditions close to the isoelectric point, and the concentration of salt (Jun et al., 2011). In adults, albumin is synthesized daily in the liver at a rate of 12 g before being released to other organs in the human body (Bujacz, 2012). The normal albumin level in healthy adults is 3.4 – 4.7 g dL^{-1}, which is calculated as 60% of total plasma protein (Vincent, 2009). Albumin in the bloodstream functions in maintaining osmotic pressure by preventing fluid from leaking out of blood vessels into other tissues. Additionally, albumin acts as a guardian of the acid-base equilibrium due to its abundance of electrically negative charges. It can also function as an antioxidant, inhibiting the production of free radicals (Hosseini, Pirsa, & Farzi, 2021). Another vital function of albumin is to assist in the metabolism and transportation of other biological substances, such as fatty acids, hormones, ions, minerals, and drugs, throughout the body.

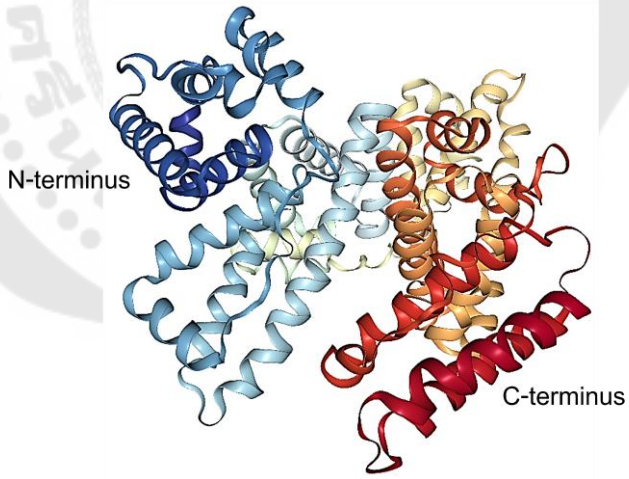

Figure 14 The 3D crystal structure of HSA, generated by NGL Viewer (PDB ID: 1AO6). Six helical subdomains are differentiated by colors.

Source: Sugio, S., Kashima, A., Mochizuki, S., Noda, M., & Kobayashi, K. (1999). Crystal structure of human serum albumin at 2.5 Å resolution. *Protein Engineering, Design and Selection, 12*(6), 439-446.

2.4.1 Urinary albumin and the risk of relevant diseases

In general, albumin is filtered through the glomerulus within the kidney before being released with urine. Thus, detecting urinary albumin levels can indicate the kidney status in relation to protein metabolism. Dysfunction of albumin reabsorption may imply microalbuminuria in the early stage of diabetes (Tojo & Kinugasa, 2012). Untreated this abnormality can lead to the gradual loss of kidney function and progress to end-stage renal disease (Pattanaprateep, Ingsathit, McEvoy, Attia, & Thakkinstian, 2018). This condition is categorized as chronic kidney disease (CKD), which is a significant global health problem (Srithongkul & Ungprasert, 2020). CKD can cause premature mortality, decreased life quality, and high spending on medical care. The prevalence of CKD at stages three to five in Caucasians and Asians showed a similar trend, affecting approximately 10% of each population (Anothaisintawee, Rattanasiri, Ingsathit, Attia, & Thakkinstian, 2009). In the same way, a cross-sectional survey of Thai citizen in 2010 reported a 9% prevalence of CKD at all stages, indicating that 6.2 million patients suffered from this disease (Ingsathit et al., 2009). Previous study has indicated that individuals with CKD and diabetes mellitus may progress to renal failure at twice the rate of those with CKD but without diabetes ("KDOQI Clinical Practice Guideline for Diabetes and CKD: 2012 Update," 2012). Furthermore, cardiovascular disease (CVD) is widely recognized as a significant risk factor for those with CKD, thereby increasing the possibility of mortality from CVD-related complications (M. Liu et al., 2014).

The prevalence of patients with CKD and relevant diseases is currently increasing, leading to a significant public health problem in Thailand. Therefore, early detection of albuminuria, coupled with appropriate medical treatment, has been shown to prevent the progression of kidney diseases, as well as reduce the risk of CVD and diabetes, particularly among high-risk groups such as the elderly (Keane & Eknoyan, 1999). The standard method for accurate quantifying albumin excretion is through a 24-hour urine collection (Polkinghorne, 2006). Several factors affecting this analysis include the activity of the patient, psychological state, amount of protein intake, body temperature, and blood pressure (Kamińska, Dymicka-Piekarska, Tomaszewska, Matowicka-Karna, &

Koper-Lenkiewicz, 2020). A normal albumin excretion condition is found at a urinary albumin concentration of fewer than 30 mg/24 h (Lambers Heerspink et al., 2008). An increased urinary albumin concentration in the range of 30 – 300 mg/24 h indicates microalbuminuria, which is a warning sign of diabetic nephropathy and CVD (Mogensen, 1984). Failure to treat this abnormality can lead to macroalbuminuria, characterized by a high concentration of urinary albumin more than 300 mg/24 h, which increases the risk of irreversible CKD (Ansar, ShahrokhiRad, & Lebady, 2016). The major limitation of a 24-h urine collection is that it is inconvenient for critical patients, resulting in a delay in the report by at least one week. Nonetheless, it remains a reliable diagnosis due to the low incidence of false-positive results in elderly patients, making it a good indicator for quantitative albumin excretion. As a result, a 24-h urine collection strategy has been considered a suitable approach for albumin measurement to accurately indicate a risk of renal failure.

2.4.2 Literature reviews

The conventional albumin screening test can be conducted in the resource-limited laboratory using a semiquantitative dye-binding dipstick. This simple test involves wetting a chemically impregnated test strip with urine and interpreting the albumin concentration by observing the color change, making it suitable for self-testing. Immunologically-based assays, such as immunonephelometry, immunoturbidimetry, and radioimmunoassay, have been proposed as traditional laboratory methods for confirming and quantitatively measuring albumin (Comper & Osicka, 2005). These techniques utilize the basis of antigen-antibody interaction, providing high selectivity with low false-positive results. More recently, the LC technique has been proposed as another standard method for albumin detection to reduce false-negative results because the dye-binding test and immunochemical-based assays cannot analyze all intact albumin in urine, including albumin peptide fragments and non-immunoreactive intact albumin. Thus, using a column containing size-selective gel materials to separate albumin from other proteins based on its size could enhance the reliability of this technique.

Until now, the electroanalytical method has emerged as a favorable option for clinical diagnostic applications owing to its remarkable sensitivity, operational simplicity, and cost-effective instrumentation. These advantages have propelled the extensive development of portable and miniaturized biosensors. Accordingly, the focus of this dissertation is the development of the electroanalytical method for the detection of albumin using a small sensing device. In this section, a literature review will be presented, outlining the progress of miniaturized devices and detection strategies employed for albumin measurement.

In 2010, the first report regarding the electrochemical detection of albumin using SPE was presented (Pinwattana et al., 2010). The sensor employed an immunoassay strategy to detect phosphorylated bovine serum albumin (BSA-OP) by using CdSe/ZnS quantum dots (QDs) as labels. The QDs were conjugated with an anti-phosphoserine antibody and used in a sandwich immunoassay to amplify the electrochemical signals. BSA-OP was introduced to primary BSA antibody-coated microwells, and the QD-labeled anti-phosphoserine antibody was subsequently added to achieve immunorecognition. Finally, the bound QD was dissolved in an acid-dissolution step and detected via square-wave stripping analysis. This study proposed indirect detection by measuring the cadmium solution using an *in situ* plated mercury film deposited on the SPE. Under optimal SWV conditions, the measured current responses were proportional to the concentration of BSA-OP. The method exhibited good reproducibility and a detection limit of 0.5 ng mL^{-1}. This QD-based electrochemical immunoassay offered a simple and cost-effective way to analyze protein biomarkers.

In 2016, the second report was published regarding the electrochemical detection of albumin using SPE (Tsai et al., 2016). This study described the development of a simple and sensitive electrochemical immunosensor for detecting urinary albumin in the range of microalbuminuria. The immunosensor was based on a carboxyl-enriched porous screen-printed carbon electrode, which increased the detection sensitivity due to the enlarged surface area for electrochemical detections. The sensor surface was functionalized with antihuman albumin antibodies via covalent immobilization.

Chronoamperometric measurement was employed for quantitative analysis by detecting $K_3[Fe(CN)_6]$ as a redox probe, which enabled this immunosensor to detect urinary albumin in a wide range from 10 μg mL^{-1} to 300 μg mL^{-1} with a detection limit of 9.7 μg mL^{-1}. Moreover, this sensor demonstrated high specificity and selectivity towards albumin detection by performing the measurement with possible interfering compounds commonly found in urine. Thus, the biosensor proposed herein was easy to prepare and can be used for low-cost, rapid, and sensitive screening of microalbuminuria. This approach provided a promising platform for developing clinical point-of-care diagnostic applications.

In the same year, the third report on the electrochemical detection of bovine serum albumin (BSA) using a modified screen-printed gold electrode was proposed (Kukkar, Sharma, Kumar, Kim, & Deep, 2016). The sensor was fabricated using a new material, namely molybdenum disulfide (MoS_2) nanoflakes, which were then bioconjugated with anti-BSA antibodies. The detection strategy employed the CV technique in the presence of a $K_3[Fe(CN)_6]/K_4[Fe(CN)_6]$ redox probe, which resulted in the specific formation of a BSA-iron complex. The sensor's response was found to be directly proportional to the concentration of BSA over a wide range of 0.01 ng mL^{-1} to 10 ng mL^{-1}, with a low detection limit of 6 pg mL^{-1}. This study demonstrated the improved sensitivity of a sensing system without the need for cross-linkers between the sensory material (MoS_2) and biorecognition molecule (antibody). Moreover, this simple approach can be extended to detect other iron-binding protein molecules, such as HSA, transferrin, lactoferrin, and ferritin.

In 2020, the fourth report on the electrochemical detection of HSA through a modified screen-printed carbon electrode was presented (Choosang, Thavarungkul, Kanatharana, & Numnuam, 2020). This study demonstrated the development of a novel type of immunosensor capable of detecting HSA in urine and human serum without the requirement of labels. The immunosensor was fabricated through the modification of an electrode surface with a nanocomposite of ferrocene (Fc) and poly(3,4-ethylenedioxythiophene):poly(styrenesulfonate) (PEDOT:PSS), which was subsequently coated with poly(*para*-phenylenediamine) (P*p*PD) and functionalized with gold

nanoparticles (AuNPs). Anti-HSA antibodies were then chemisorbed onto the AuNPs/P*p*PD layer. When HSA was present, it bound to the immobilized antibodies, resulting in a change in the electrochemical signal of the Fc oxidation. The sensor exhibited high sensitivity under optimal DPV conditions, with a detection limit of 0.54 pg L^{-1}. Additionally, the sensor demonstrated good reusability, stability, reproducibility, and specificity. The performance of the immunosensor was validated by comparing its results to those obtained from a standard immunoturbidimetric method. In conclusion, this developed immunosensor has the potential to serve as a valuable diagnostic tool for the detection of HSA levels in urine and human serum.

In 2021, the fifth report on the electrochemical detection of microalbuminuria using a microchip platform was proposed (Tseng et al., 2021). The research presented a novel method for detecting microalbuminuria levels in human urine samples using an electrochemical biosensor. The microchip was designed with screen-printed electrodes and a double-layer reagent paper that was impregnated with amaranth. The amaranth molecule was absorbed onto the electrode surface through a redox reaction after dropping $K_3[Fe(CN)_6]$ solution on the paper, and then the urine sample was introduced onto the device. This led to an interaction between the modified surface and the microalbuminuria content, resulting in the formation of an electrically-inert amaranth-albumin complex that hindered the transfer of electrons, causing a decreasing peak current. The microalbuminuria concentration was then determined by the CV technique within the range of 0.1 mg dL^{-1} to 40 mg dL^{-1}. The results of the microalbuminuria concentration measurements were in good agreement with the official method, indicating that the proposed platform provides a reliable and convenient approach for performing sensitive point-of-care testing. This could be useful for the rapid and accurate detection of microalbuminuria status in patients with CKD.

In 2022, the sixth and latest report on the electrochemical detection of urinary albumin/creatinine ratio (ACR) using a small sensing device was presented (Jia et al., 2022). This study detailed the development of a wireless and flexible electrochemical tag for the *in-situ* quantification of ACR. The tag integrates a flexible circuit electrochemical

board with chronoamperometry and DPV to detect creatinine and albumin, respectively. A near-field communication (NFC) module was utilized for wireless power and data transmission. A disposable screen-printed carbon electrode array was connected to the circuit board, which included a non-enzymatic sensor with the modification of nano copper for creatinine detection and an electrochemical immunosensor with the treatment of an electrode surface for albumin detection. Within an effective working distance of 1 ~ 2 cm, the ACR sensing platform could be powered wirelessly by the NFC-enabled smartphone via electromagnetic coupling, performing real-time urine ACR detection and data transmission. The tag exhibited high consistency with clinical laboratory methods for several synthetic urine samples. Consequently, this battery-free platform provides a rapid and convenient method for the detection of urinary biochemical substances such as ACR, with broad prospects in mobile health and point-of-care testing.

As mentioned in the literature reviews, previous reports have utilized SPEs as miniature sensing devices that were modified with various nanomaterials and conductive polymers to enhance their sensitivity. The selectivity of these sensors can be improved through the use of immunoassay principles, whereby antibodies are immobilized onto the electrode surface, followed by the binding of antigens, leading to the specific recognition of albumins. Some immunosensors require a labeling component to conjugate with the desired antibody or antigen, while others do not, resulting in diverse detection strategies that facilitate albumin measurements. In the case of the label-free approach, indirect detection using Fe^{2+}/Fe^{3+} from $K_3[Fe(CN)_6]$ as a redox probe is a popular strategy for measuring albumin concentrations due to its non-electroactivity. However, using only this redox substance may not be adequate for sensitive detection of very low analyte concentrations, necessitating a high concentration of $K_3[Fe(CN)_6]$ (the maximum concentration being 0.1 M $K_3[Fe(CN)_6]$). Therefore, a lower concentration of this chemical should be used for an electrochemical immunoassay.

To address the aforementioned issue, a novel electrochemical-chemical (EC) redox cycling process has been proposed for the detection of *Plasmodium falciparum* histidine-rich protein 2, a malaria biomarker, using a label-free immunoassay (Dutta &

Lillehoj, 2018). The proposed detection scheme enhances the electrochemical signal without requiring electrode surface modification. The system utilizes a combination of 1 mM hexaammineruthenium (III) ($[Ru(NH_3)_6]^{3+}$) as an electron mediator and 50 µM methylene blue (MB) as a mediator substrate. The process begins with the reduction of $[Ru(NH_3)_6]^{3+}$ to $[Ru(NH_3)_6]^{2+}$ via a normal electrochemical reaction at the gold electrode interface, followed by the oxidation of $[Ru(NH_3)_6]^{2+}$ back to $[Ru(NH_3)_6]^{3+}$ due to the chemical reaction of MB, which converts MB_{ox} to MB_{red}. This process occurs continuously, leading to the simultaneous regeneration of $[Ru(NH_3)_6]^{3+}$, and a large electrochemical response is obtained. Protein quantification is achieved by observing the reduction in the detection signal, which is inversely proportional to the amount of antigen bound to the electrode surface corresponding to its concentration in the sample. This EC system offers rapid electrokinetics due to the similar formal potential of MB_{ox}/MB_{red} and $[Ru(NH_3)_6]^{3+}/[Ru(NH_3)_6]^{2+}$ couples, enabling fast electron transfer between these two couples. Additionally, these substances exhibit excellent stability at room temperature, eliminating the need for refrigeration. However, the primary limitation of this method is the high cost of the chemical $[Ru(NH_3)_6]Cl_3$ as the substrate, making it scarce in general laboratories. Hence, alternative electroactive species should be proposed to reduce the cost of measurement.

As a result, this dissertation presents the development of the EC redox cycling process for detecting urinary albumin. Instead of employing $[Ru(NH_3)_6]^{3+}/[Ru(NH_3)_6]^{2+}$, readily available $[Fe(CN)_6]^{3+}/[Fe(CN)_6]^{2+}$ were used as a redox couple, in combination with MB. The proof-of-concept BSA measurement was performed through an indirect detection strategy, using a disposable ePAD as the detection platform. The quantification was achieved by observing the decrease in the detection signal, which is inversely proportional to the amount of BSA that hindered the electron transfer of the redox probe to the electrode surface, indicative of its concentration in the sample. Under optimized conditions, the proposed strategy offered a wide concentration range that covered the risk status of kidney disease, making it suitable for the albumin analysis of real urine samples in CKD patients.

2.5 L-Hydroxyproline (Hyp)

Hyp is a non-proteinogenic amino acid that is not involved in the primary structure of proteins but rather appears as a result of a post-translational modification. It is produced through the hydroxylation of the amino acid proline, which results in the addition of a hydroxyl group to the beta- or gamma-carbon atom in the proline molecule, as shown in Figure 15. Hyp is particularly abundant in collagen, a fibrous protein that provides structural support to various tissues in the body, such as skin, bones, tendons, and cartilage, making it valuable to be a collagen biomarker and its related metabolism (Piez, Eigner, & Lewis, 2002). Its presence in collagen is vital for the stability and strength of collagen fibers, as it enables the formation of the triple-helical conformation and strong cross-links with neighboring molecules. The biosynthesis of Hyp involves the activity of prolyl hydroxylase, which requires vitamin C as a cofactor. A deficiency in vitamin C can impair collagen synthesis and lead to the development of scurvy, a condition characterized by weakness, bleeding gums, and poor wound healing.

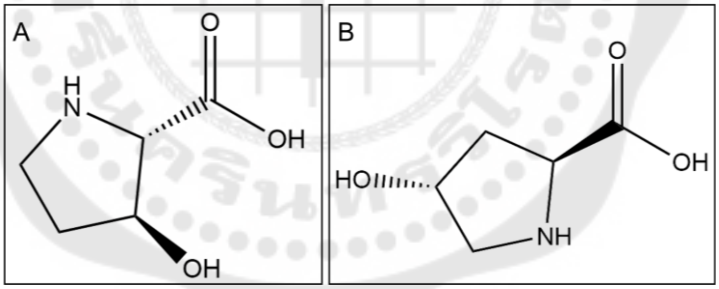

Figure 15 The chemical structure of Hyp with two isomeric forms: (A) *trans*-3-hydroxy-L-proline and (B) *trans*-4-hydroxy-L-proline.

In living organisms, two isomeric forms of Hyp have been identified in animals, predominantly in collagen and a few other extracellular proteins that contain a collagen-like sequence of amino acids. These two forms are *trans*-3-hydroxy-L-proline (3-Hyp) and *trans*-4-hydroxy-L-proline (4-Hyp). 3-Hyp is present in type I collagen, which is a component of skin, tendon, vascular ligature, and bones. 4-Hyp is found in type IV collagen, which makes up the basal lamina and epithelial layer of the basement

membrane. Both of these amino acids are synthesized through co-translational and post-translational modifications by the hydroxylation of proline residues with the help of two separate enzymes, prolyl-3-hydroxylase and prolyl-4-hydroxylase. Prolyl-3-hydroxylase is only found in animal sources, while prolyl-4-hydroxylase is broadly distributed in nature and has been recognized in several vertebrates, invertebrates, and plants. The latter enzyme plays a vital role in the folding mechanism of newly synthesized procollagen polypeptide chains into triple helix collagen. Another crucial function of 4-Hyp in collagen is its potential to serve as a target for pharmaceutical modulation of increased collagen synthesis observed in patients with various fibrous disorders.

2.5.1 Role of Hyp in the pathogenesis of different diseases

As previously mentioned, collagen serves as a critical structural component in all organs, providing essential stability and supporting organ growth. Collagen-related diseases, resulting from Hyp abnormality, can lead to severe pathological conditions and even mortality. Genetic abnormalities in collagen encoding genes or abnormal degradation and cross-linking can cause a range of heritable diseases, including Ehlers-Danlos syndrome, epidermolysis bullosa, and osteogenesis imperfecta, as well as non-heritable diseases, such as scurvy, diabetes, and arthritis (Bruckner-Tuderman & Bruckner, 1998). Therefore, utilizing Hyp as a biomarker can offer valuable insights into the pathogenesis and treatment strategies of several collagen-related diseases. This approach is of immense value for both biomedical research and drug development.

Urinary Hyp is historically important as a marker of bone resorption (Cremers, Garnero, & Seibel, 2008). This process occurs naturally and is a vital part of the bone metabolism process in which specialized cells called osteoclasts break down old or damaged bone tissue, followed by the liberation of minerals (calcium and phosphorous) into the blood circulating system. Bone resorption also results in the degradation of bone collagen, releasing Hyp into the bloodstream possibly in protein-bound, peptide-bound, and free forms (Cundy, Reid, & Grey, 2014). After this process, Hyp is transported to the liver to be oxidized, but its small portion (~10%) is excreted in the urine. Normal values of

free Hyp in adults are 0.70 – 1.55 μg/mL for serum and 0.35 – 1.15 mg/24 hours for urine. When bone resorption increases, urinary Hyp excretion rises due to the increased catabolism rate of type I bone collagen. Therefore, measuring Hyp in a biological fluid would be the simplest approach to rapidly detect the early stage of bone-related diseases.

Hyp can be the end product of non-enzymatic hydroxylation of proline, which is catalyzed by free radicals and reactive oxygen species. It serves as an essential biochemical marker of collagen damage during vitiligo, a common depigmentary disorder characterized by white patches on the skin. Some cases of vitiligo are characterized by chronic and progressive destruction of cutaneous melanocytes in the skin, hair, and mucosal surfaces, which is the key factor in the pathogenesis of this complex and multifactorial disorder. This involves both genetic and non-genetic factors, affecting approximately 1% of the worldwide population in both genders (Picardo & Taïeb, 2010). Given that the degradation of collagen in vitiligo is primarily caused by free radicals and reactive oxygen species, it is possible that elevated levels of plasma Hyp in vitiligo patients are associated with the non-enzymatic oxidation of proline. Therefore, measuring increased Hyp levels in a blood sample could potentially prevent the progression of vitiligo and protect against serious psychosocial impacts affecting normal life.

A deficiency in protein during wound healing can reduce the effectiveness of new capillary treatment, fibroblast proliferation, collagen synthesis, and proteoglycans synthesis. This can also impact the remodeling and contraction of the wound, and in some cases, lead to a suppression of the immune system. A normal and stable cellular structure of the extracellular matrix is indicative of a complete wound-healing process after a tissue injury, as it generates new collagen to repair damaged tissues. The breakdown of collagen releases free Hyp and its peptide-bound form, making Hyp a valuable biochemical marker during wound healing. Hyp is widely used to assess tissue collagen content and serves as an indicator of collagen turnover after wound healing (Kumar, Katoch, & Sharma, 2006). An increased Hyp content in granulation tissue indicates better maturation and proliferation of collagen during wound healing, which implies better

healing progress (Veis & Anesey, 1965). Therefore, measuring the amount of Hyp in a wound can provide valuable information on the rate of collagen synthesis and the effectiveness of wound healing. This information can guide treatment decisions and ensure that the wound heals properly.

Psoriasis is a chronic inflammatory skin disease characterized by an abnormal buildup of skin cells that results in silvery white scaly patches (Christophers, 2001). Patients with psoriasis have been observed to have altered collagen metabolism, which can lead to skin damage and contribute to the disease. Hyp has been found to play a role in psoriasis by influencing collagen synthesis and degradation in the skin. The expression of enzymes that break down collagen, such as matrix metalloproteinases (MMPs), is increased in psoriatic skin, which can contribute to skin damage and thickening. Moreover, Hyp levels in the skin of patients with psoriasis are decreased when compared to healthy individuals, resulting in a decrease in collagen synthesis. This, in turn, can contribute to abnormal skin cell proliferation and skin damage seen in psoriasis. Therefore, Hyp could serve as a vital diagnostic biochemical marker in the early assessment of severe psoriasis.

2.5.2 Literature reviews

Several analytical techniques have been developed for the measurement of Hyp in serum and urine to investigate bone resorption rates and collagen metabolism. Colorimetric assays with specific reagents are simple and practical methods for quantifying Hyp (Woessner, 1961) (Bergman & Loxley, 1970) (Jamall, Finelli, & Que Hee, 1981). The detection procedure involves oxidizing hydrolyzed Hyp, followed by adding a reagent to produce a chromophore. However, this strategy has the main advantages in terms of a time-consuming process and difficulty controlling the oxidation of Hyp and color formation reactions. Chromatographic methods with various columns and detectors have been developed to enhance separation performance, making them conventional approaches for routine analysis (Mazzi, Fioravanzo, & Burti, 1996) (Inoue, Iguch, Kouno, & Tsuruta, 2001) (Delport, Maas, van der Merwe, & Laurens, 2004) (Hušek, Pohlídal, &

Slabík, 2002). Nevertheless, the major limitation of these techniques is the requirement of expensive instruments that are costly to maintain. The electrochemical method has recently received attention as an alternative analytical technique for Hyp measurement due to its simplicity, rapidity, and portability. Therefore, this dissertation aims to develop an electroanalytical method for detecting Hyp. This section provides a literature review related to this work, describing the electrode materials and electroanalytical techniques used for detection.

In 2015, the first report on the construction of a novel biosensor for electrochemically detecting Hyp was proposed (Sakamoto et al., 2015). The biosensor utilized two enzymes, namely L-hydroxyproline epimerase and D-hydroxyproline dehydrogenase, to convert L-Hyp to D-Hyp and then oxidize D-Hyp with the aid of ferrocene. The measurement was conducted by chronoamperometry using the SPCE. Tris-HCl buffer or Hyp solution was dropped onto an electrode surface, and a constant potential of 0.25 V was applied to the working electrode. Upon current reaching stability, 1 µL of each enzyme solution was added to complete the reaction. The current response was determined as the difference before and after the addition of a drop of L-Hyp. The sensor can detect L-Hyp concentrations ranging from 10 – 100 µM with high selectivity over other amino acids, making it suitable for implementation in bio-industrial applications.

In 2020, the second report on the electrochemical detection of Hyp was presented (Durairaj, Sidhureddy, & Chen, 2020). This research described a new method for measuring Hyp using gold nanoparticles (AuNPs) that were electrochemically deposited on a GCE. The electrochemical behavior of the AuNPs/GCE for the oxidation of Hyp was examined using CV, which showed higher electrocatalytic activity compared to a bare GCE and a bulk Au electrode. DPV was used to investigate the electrochemical sensing performance of the AuNPs, which exhibited a low limit of detection (26 µM) and high sensitivity. The interference of other amino acids present in collagen and urine was also tested, demonstrating high selectivity and good reproducibility. Furthermore, the real sample analysis was performed using bovine Achilles tendon collagen type I and human urine, further confirming that the proposed electrode has the potential to be a promising

sensor for the effective detection of Hyp in various real samples. Thus, this study provided a new and easy-to-use electrochemical method for detecting Hyp, which could be useful for diagnosing diseases and monitoring treatments related to collagen metabolism.

In 2022, the third and latest report regarding the electrochemical detection of Hyp was proposed (Jesadabundit, Jampasa, Patarakul, Siangproh, & Chailapakul, 2021). This study described the development of an enzyme-free biosensor for the detection of Hyp. The biosensor was based on molecularly imprinted polymers (MIPs) created using a mixture of monomers containing 3-aminophenylboronic acid (3-APBA) and o-phenylenediamine (OPD) in the presence of L-Hyp. The MIPs are co-electropolymerized onto a SPCE using CV. The proposed biosensor operated by measuring the change in charge transfer resistance (R_{ct}) of a mediator that was obstructed by L-Hyp molecules that were bound to the imprinted surface. The calibration curve was obtained within a range of 0.4 to 25 μg mL^{-1} with a limit of detection and quantification of 0.13 and 0.42 μg mL^{-1}, respectively. The biosensor demonstrated high selectivity and sensitivity, and it was successfully employed to detect L-Hyp in human serum samples. Therefore, this fabricated L-Hyp biosensor has great potential for clinical applications as an alternative tool for accessing the risk of developing bone diseases and tracking symptoms.

As mentioned in the literature reviews, previous studies propose different kinds of electrochemical sensors for Hyp determination, encompassing both enzymatic and nonenzymatic systems. The bienzymatic sensor exhibited high selectivity, it lacked simplicity, stability under severe conditions, and long-term storage. The AuNPs/GCE demonstrated high sensing performance for Hyp detection, indicating its good electrocatalytic activity. However, the formation of Au-oxide at a similar potential to Hyp oxidation was a major limitation, making it impossible to measure Hyp at low concentrations. The MIPs-based sensor, while providing long-term stability and eliminating the need for sample pretreatment, still involved complicated and time-consuming procedures during its fabrication. To address these limitations, the primary objective of this dissertation is to develop a Hyp sensing platform with high sensitivity and selectivity using a simple fabrication process.

Therefore, the development of a screen-printed graphene electrode (SPGE) that was coated with bismuth film (BiF) and poly(L-hydroxyproline) (Poly(Hyp)) was proposed as a sensor for measuring Hyp. BiF is used to modify the electrodes to reduce the formation of metal-oxide at an electrode surface, thereby limiting oxygen interference. This modification results in low background current and good chemical stability. Poly(amino acids) (PAAs) have been widely used in sensing applications to enhance sensitivity (Kaewjua & Siangproh, 2022) (Thanh et al., 2022) (Assaf, Shamroukh, Rabie, & Khodari, 2023). PAAs are alternative polymers that can improve the electrochemical response, ensuring good stability and strong adherence to the electrode surface (Kordasht, Hasanzadeh, Seidi, & Alizadeh, 2021). Thus, a Poly(Hyp)-based electrode was developed as a sensing material for electroanalytical purposes. The suitably modified electrode was fabricated by a two-step modification process: (1) the electrodeposition of BiF and (2) the electropolymerization of Poly(Hyp), resulting in a Poly(Hyp)/BiF/SPGE. Good analytical performance was achieved with a wide linear range and low limit of detection at the micromolar level. With this platform, the practical measurement of Hyp was successfully conducted in human urine samples without a complicated pretreatment step. As a result, the proposed sensor has great potential to use as an alternative tool for screening the risk of collagen metabolism, bone diseases, and other related disorders.

CHAPTER 3
Methodology

This chapter presents the experimentations that exhibit stages of development in the electrochemical detection of water-soluble vitamins and biomarkers. The methodology was divided into two parts depending on the target analytes. The first part focuses on the development of a simple electrochemical approach for the simultaneous detection of vitamin B_2, vitamin B_6, and vitamin C using a modifier-free screen-printed carbon electrode. The second part is the development of electrochemical methods for detecting biomarkers, namely albumin and L-hydroxyproline (Hyp), leading to the distribution of two subprojects. The first subproject is the development of a simple and rapid detection approach for urinary albumin on a disposable paper-based analytical device using an electrochemical-chemical redox cycling process. The second subproject involves the development of a new sensing device for detecting Hyp using a screen-printed graphene electrode coated with bismuth film and poly(L-hydroxyproline). Each project comprises detailed information on chemicals, instruments, fabrication procedures for each sensing device, and electrochemical measurements.

3.1 The development of a simple electrochemical approach for the simultaneous detection of vitamin B_2, vitamin B_6, and vitamin C using a modifier-free screen-printed carbon electrode

The content presented in this section is derived from the original research article, see Appendix 1 for the complete article.

3.1.1 Chemicals and reagents

All chemicals were used as received without further purification. Carbon paste (C2130307D1) and silver/silver chloride paste (C2130809D5) were purchased from Gwent Group (Torfaen, United Kingdom). Riboflavin (vitamin B_2, VB_2) and L-ascorbic acid (vitamin C, VC) were purchased from Sigma-Aldrich (St. Louis, MO, USA). Pyridoxine

hydrochloride (vitamin B_6, VB_6) was purchased from Hi-Media Laboratories Pvt., Ltd. (India). Sodium dihydrogen orthophosphate ($NaH_2PO_4.2H_2O$) and di-Sodium hydrogen orthophosphate ($Na_2HPO_4.2H_2O$) were acquired from Ajax Finechem Pty., Ltd. (New South Wales, Australia). Ethanol and ortho-phosphoric acid (H_3PO_4, 85% purity) were acquired from Merck (Darmstadt, Germany). Acetone (commercial grade) was purchased from CaHC (Thailand) Co., Ltd. (Bangkok, Thailand).

All solutions were prepared using Milli-Q water from a Millipore water purification system (R = 18.2 MΩ cm at 25°C). All of the stock standard solutions (1 mM) were weekly prepared in water and kept in the dark at -20°C. As for working standard solutions preparation, the stock standard solution was diluted with supporting electrolyte and mixed using a vortex mixer. Phosphate buffer solution (PBS), which was served as a supporting electrolyte, was prepared by mixing 0.1 M NaH_2PO_4 and 0.1 M Na_2HPO_4 and adjusted to the desired pH with 0.1 M H_3PO_4. Britton-Robinson buffer solution (BRBS) was prepared by mixing equal volumes of 0.04 M CH_3COOH, 0.04 M H_3BO_3, and 0.04 M H_3PO_4 that has been adjusted to the desired pH with 0.2 M NaOH. Acetate buffer solution (ABS) was also prepared by mixing 0.1 M CH_3COOH and 0.1 M CH_3COONa and adjusting to the desired pH with 0.1 M HCl or 0.1 M NaOH.

3.1.2 Fabrication of a sensing device

The electrode pattern was designed using Adobe Illustrator CC 2018. To obtain the electrode templates for screening, the designed patterns were built by Chaiyaboon Brothers Co., Ltd. (Bangkok, Thailand). Screen-printed electrodes were fabricated by using a manual screen-printing method on the transparent sheet as a substrate which was described in the previous report (Nantaphol, Jesadabundit, Chailapakul, & Siangproh, 2019). Briefly, the cleaned transparent sheet was screened with carbon paste to obtain working electrodes and counter electrodes. Then, these electrodes were placed in an oven at a temperature of 55°C for 30 min to remove the solvent and to dry the electrodes. Next, silver/silver chloride (Ag/AgCl) paste was screened on the same transparent sheet to obtain reference electrodes and the

conductive pads. After that, they were placed in an oven at a temperature of 55°C for 30 min. Finally, the common screen-printed carbon electrodes (SPCE) were obtained and ready to use for an experiment. The realistic picture of the obtained electrode, called an electrochemical transparent-film based analytical device (eTFAD), was shown in Figure 16.

Figure 16 A realistic picture of an electrochemical transparent film-based analytical device (eTFAD) consisting of screen-printed working (middle), reference (left), and counter (right) electrodes.

3.1.3 Electrochemical measurement

The electrochemical experiments were performed by a potentiostat/galvanostat PGSTAT128N from Metrohm-Autolab (Switzerland) with the NOVA 1.10 software (Kanaalweg 29-G 3526 KM Utrecht, The Netherlands). A three-electrode system was fabricated on a transparent sheet which was employed throughout the experiment. The geometric area of a working electrode was 0.126 cm^2 (calculated from circular area = πr^2; r = 0.2 cm). For the electrochemical measurement, 100 µL aliquot of a standard or a sample solution was thoroughly dropped covering all three electrodes

onto the detection zone. After that, electrochemical techniques including cyclic voltammetry (CV) or square wave voltammetry (SWV) were conducted. For CV measurement, the potential was applied over the range from -1.1 V to 1.3 V with a scan rate of 100 mV/s. Similarly, SWV measurement was also performed for the simultaneously quantitative determination by applying the potential from -1.0 V to 1.3 V with a step potential of 5 mV, an amplitude of 25 mV, and a frequency of 5 Hz.

3.1.4 Sample preparation

To demonstrate the practicality of the proposed electrode for application, two types of samples including mixed vegetable and fruit juice and artificial urine were investigated for the simultaneous determination of water-soluble vitamins.

The mixed vegetable and fruit juice were purchased from a convenience store in Thailand. 5 mL of juice sample was added into a test tube. Then, the sample was centrifuged for 15 minutes at 2500 rpm followed by filtration through a filter paper and kept in a dark container at 4°C. After that, samples were spiked at various concentrations of standard vitamins, and the spiked solution was diluted 10-fold with PBS pH 3.5 (a suitable dilution order) and measured the quantity using the SWV technique as followed by topic 3.1.3. Then, the average recovery percentage was calculated.

Artificial urine was purchased from Carolina Biological Supply Company (Burlington, USA). For the sample preparation, the artificial urine and spiked artificial urine were merely diluted 1000-fold with PBS pH 3.5 which is a suitable dilution order for this sample. After that, the samples and spiked samples were quantitively measured by using the same procedure to the juice sample.

3.2 The development of a simple and rapid detection approach for urinary albumin on a disposable paper-based analytical device using an electrochemical-chemical redox cycling process

The content presented in this section is derived from the original research article, see Appendix 2 for the complete article.

3.2.1 Chemicals and reagents

All chemicals were used exactly as they were received, with no further purification. The graphene paste (ZP-1838) was purchased from Serve Science Co., Ltd (Bangkok, Thailand). Silver/silver chloride paste (Ag/AgCl, C2130809D5) was purchased from Gwent Group (Torfaen, United Kingdom). Bovine serum albumin (BSA, A3311), methylene blue (MB, M9140), L-ascorbic acid, D(+)-glucose monohydrate, urea, uric acid, dopamine hydrochloride, and creatinine were acquired by Sigma-Aldrich (St. Louis, MO, USA). Potassium ferricyanide ($K_3[Fe(CN)_6]$, AJA393), sodium chloride (NaCl), potassium chloride (KCl), ammonium chloride (NH_4Cl), magnesium chloride ($MgCl_2$), calcium chloride ($CaCl_2$), di-sodium hydrogen orthophosphate dihydrate ($Na_2HPO_4.2H_2O$) and sodium hydroxide pellets (NaOH) were supplied from Ajax Finechem Pty., Ltd (New South Wales, Australia). Potassium dihydrogen phosphate (KH_2PO_4) was obtained from Quality Reagent Chemical (Selangor, Malaysia). Sodium sulphate (Na_2SO_4) was provided from BDH Laboratory Supplies (London, UK). The acetone (commercial grade) was purchased from CaHC (Thailand) Co., Ltd (Bangkok, Thailand).

All solutions were prepared with Milli-Q water (R = 18.2 MΩ cm^{-1} at 25°C) obtained from a Millipore water purification system. Throughout this study, a phosphate-buffered saline (PBS) solution was used as a supporting electrolyte. This solution consisted of 137 mM NaCl, 2.7 mM KCl, 10 mM Na_2HPO_4, and 1.8 mM KH_2PO_4. The pH of this electrolyte was then adjusted to 7.4 with 0.1 M NaOH. Subsequently, all working solutions, including interferences and samples, were prepared in PBS (pH 7.4).

3.2.2 Manufacturing process of a sensing device

With a variety of paper designs, a foldable electrochemical paper-based device (ePAD) was specifically designed to propose an alternative style for a simple detection of urinary albumin. Figure 17 presents the pattern of paper devices created using Adobe Illustrator CC 2018. The ePAD had two main components, namely a gray side (left) serving as a counter electrode (CE) and a reference electrode (RE) on the hydrophilic area, and an orange side (right) serving as a working electrode (WE) (1.5 cm x 3.0 cm in size) on the hydrophobic area. To fabricate the ePAD, the device pattern was

first printed on filter paper (Whatman no. 4) employing the wax-printing technique using Fuji Xerox ColorQube 8580. The printed device was then placed on a hot plate at 175°C for 50 s to allow the wax to dissolve into the paper. At this point, the ePAD was made up of both hydrophobic and hydrophilic areas in the same device. Subsequently, a three-electrode system was created on the patterned paper using the manual screen-printing method described in the previous report (Boonkaew et al., 2020). In brief, graphene paste was directly screen-printed onto a paper device to produce both WE and CE. WE had a geometric area of 0.126 cm^2 (calculated using circular area = πr^2; r = 0.2 cm). Then, to create RE and conductive pads, Ag/AgCl paste was screen-printed onto the same device. Following each screen-printing process, the device was heated in an oven at 55°C for 30 min to allow the solvent in the pastes to evaporate and the electrodes to dry. After that, a transparent tape was applied on the back side of the orange paper to prevent solution leakage during electrochemical measurement. Before use, the middle hydrophilic area of the gray side was punctured to create a sample reservoir (5 mm in diameter). A double-sided adhesive tape was used to attach the upper and lower parts of the paper device on the gray side. Then, the paper device was folded by folding a gray side attached to an orange side, which allowed the solution to flow directly to cover electrode surfaces. Besides, after connecting the paper device with electrical wires from a potentiostat, a transparent tape was used to attach the paper device to the smooth surface of a lab bench, making both sides of the paper attach more firmly with no leaking of the solution. The ePAD is now ready to be used for the detection of albumin in the next step.

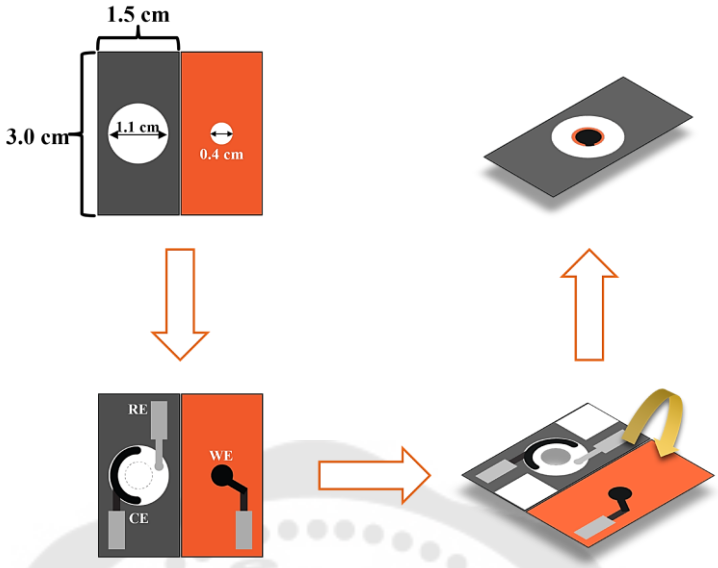

Figure 17 The design and composition of ePAD that was used in this work.

3.2.3 Electrochemical measurement

The ECAS100 potentiostat from Zensor Research & Development Corporation (Taiwan) was used for the electrochemical experiments. As a redox cycling process, the mixture solution containing 4 mM of $[Fe(CN)_6]^{3-}$ and 0.05 mM of MB in PBS (pH 7.4) was used for this study, and a blue-green color solution was obtained. This solution was prepared in a microcentrifuge tube and labeled as in the absence of albumin. In the presence of albumin, a redox cycling solution and BSA standard solution were mixed in the same tube. For detection, 100 µL of a pure redox cycling solution or that mixed with BSA standard solution was thoroughly dropped onto an ePAD sample reservoir, covering all three electrodes. Subsequently, electrochemical techniques, such as cyclic voltammetry (CV) and differential pulse voltammetry (DPV), were performed. The potential was applied over a range of +0.6 to -0.6 V, with a scan rate of 100 mV s^{-1} for CV measurements. DPV measurements were used for quantitative analysis using potentials ranging from +0.5 to -0.2 V, with an increment potential of 10 mV, an amplitude of 50 mV, a pulse width of 200 ms, a sample width of 100 ms, and a pulse period of 500 ms. To quantify albumin concentration, the signal current of the redox cycling solution with BSA

standard solution was measured and compared with the signal current of the redox cycling solution without BSA standard solution. The analysis can be conducted for 1 min, as presented in Figure 18.

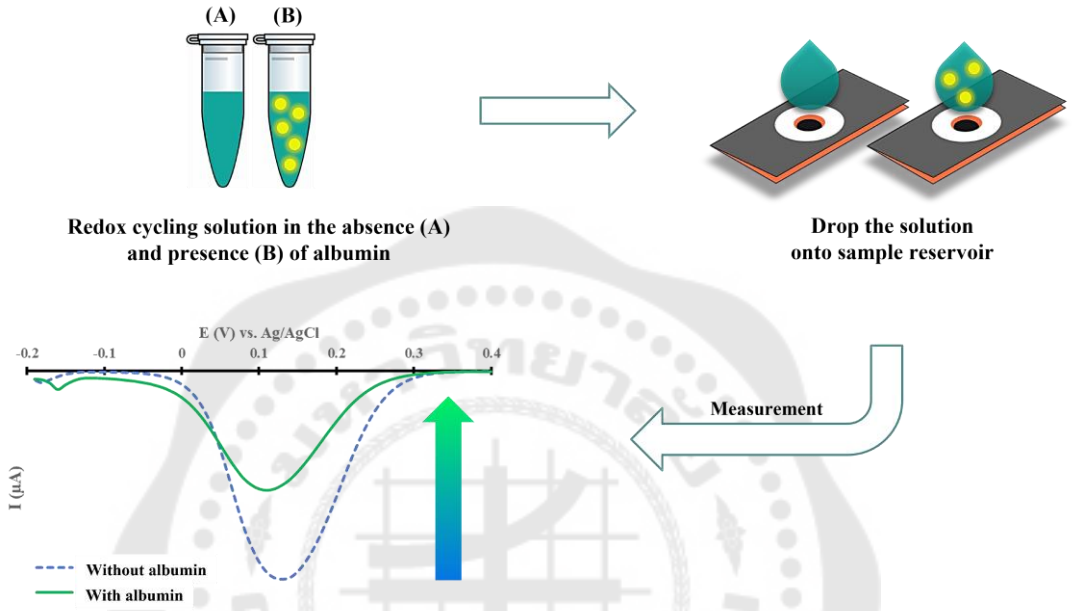

Figure 18 Schematic illustration of the overall detection process for the measurement of albumin by mixing BSA standard solution with a redox cycling solution.

3.2.4 Sample preparation

Urine samples were examined for albumin detection to demonstrate the real-world application of the proposed method. Urine samples were collected from healthy human volunteers in our laboratory and immediately refrigerated at 4°C. All volunteers were informed about what would happen to the human subjects in a trial. Urine samples were filtered through a Whatman no. 1 filter paper to remove small particles before being diluted 50-fold with PBS pH 7.4. Subsequently, the diluted samples were mixed with 4 mM $[Fe(CN)_6]^{3-}$ and 0.05 mM MB. These solutions were then measured using the DPV technique as described in Section 3.2.3, to detect the concentration of albumin in urine

samples. The Bradford assay was employed to confirm the accuracy of the proposed method (Bradford, 1976).

3.3 The development of a new sensing device for detecting L-hydroxyproline using a screen-printed graphene electrode coated with bismuth film and poly(L-hydroxyproline)

3.3.1 Chemicals and reagents

Graphene paste (ZP-1838) was purchased from Serve Science Co., Ltd. (Bangkok, Thailand). Silver/silver chloride paste (Ag/AgCl, C2130809D5) was purchased from the Gwent Group (Torfaen, United Kingdom). *trans*-4-Hydroxy-L-proline (99%) was acquired from Thermo Fisher GmbH (Kandel, Germany). Bismuth standard solution (1,000 mg L^{-1} from $Bi(NO_3)_3$ in 0.5 M HNO_3), disodium hydrogen phosphate (Na_2HPO_4), sodium dihydrogen phosphate dihydrate ($NaH_2PO_4{\cdot}2H_2O$), potassium ferricyanide ($K_3[Fe(CN)_6]$) and potassium ferrocyanide ($K_4[Fe(CN)_6]$) were supplied by Merck KGaA (Darmstadt, Germany). D(+)-Glucose monohydrate, urea, creatinine, proline, L-ascorbic acid, uric acid, dopamine hydrochloride, and bovine serum albumin were obtained from Sigma-Aldrich (St. Louis, MO, USA). Sodium chloride and sodium bicarbonate were obtained from Ajax Finechem Pty., Ltd. (New South Wales, Australia). Acetone (commercial grade) was purchased from Siam Iwata Co., Ltd. (Bangkok, Thailand). All materials and chemicals were used exactly as they were received, without further purification.

All solutions were prepared using deionized (DI) water (R = 18.2 MΩ cm^{-1}) obtained using the Millipore Milli-Q water purification system. This study used 0.1 M phosphate buffer solution (PBS) pH 7.0 as a supporting electrolyte composing the mixture of Na_2HPO_4 and $NaH_2PO_4{\cdot}2H_2O$. Then, the pH of this electrolyte was adjusted to the desired value using 1 M HCl or 1 M NaOH. Afterward, all stock solutions of Hyp, including interfering substances and samples, were prepared daily in PBS pH 7.0 to reduce day-to-day variability.

3.3.2 Apparatus

Voltammetric measurements were performed using a multichannel potentiostat/galvanostat/impedance analyzer MultiPalmSens4 (PalmSens, Houten, The Netherlands) controlled by the MultiTrace software. Electrochemical impedance spectroscopy (EIS) was conducted on an Autolab PGSTAT30 (Eco Chemie, Utrecht, The Netherlands) equipped with a Frequency Response Analysis module. This work used the SPGE as a sensing platform with graphene and Ag/AgCl pastes fabricated as working electrodes (WE), counter electrodes (CE), reference electrodes (RE), and conductive pads. The electrode templates for graphene and Ag/AgCl pastes were designed using Adobe Illustrator CC 2018 and separately constructed by Chaiyaboon Co., Ltd. (Bangkok, Thailand). The surface morphologies of bare and modified electrodes were verified by a field emission gun-scanning electron microscope (FEG-SEM) equipped with an energy dispersive X-ray (EDX) analysis (MERLIN SM0087, Zeiss, Jena, Germany).

3.3.3 Fabrication of a screen-printed graphene electrode (SPGE)

A three-electrode system was generated on a PVC substrate (with a thickness of 0.15 mm) using the manual screen-printing technique described in previous work (Yomthiangthae, Kondo, Chailapakul, & Siangproh, 2020). Briefly, graphene paste was directly screen-printed through a template onto a substrate to produce both the WE and CE. The WE had a geometric area of 0.126 cm^2 (calculated using circular area = πr^2, where r = 0.2 cm). Ag/AgCl paste was screen-printed through another template onto the same substrate to create both the RE and conductive pads. Following each fabrication process, the electrodes were heated in an oven at 55°C for 30 min to evaporate the solvent in the paste and dry the electrodes. Each electrode template was thoroughly rinsed with acetone before storage in a dry place. The completed SPGE, as well as the design and composition of the electrodes, is shown in Figure 19A.

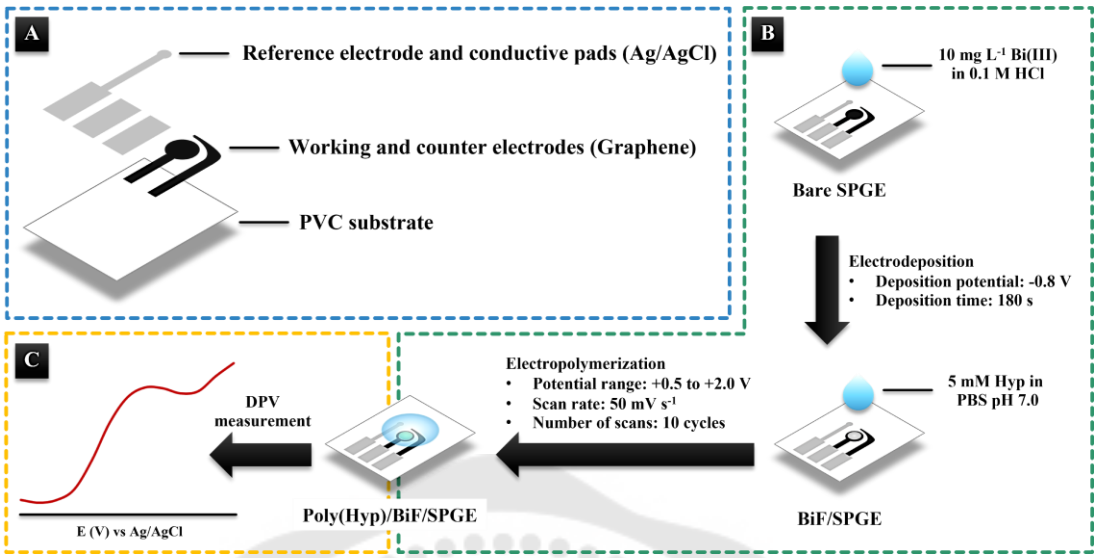

Figure 19 (A) The design and composition of SPGE. (B) The synthesis process of BiF and Poly(Hyp). (C) The DPV measurement of Hyp.

3.3.4 Synthesis of BiF and Poly(Hyp) onto the electrode surface

The two-step synthesis of BiF and Poly(Hyp) is sequentially illustrated in Figure 19B. First, BiF was produced via an electrodeposition process by dropping 100 µL of 10 mg L^{-1} Bi(III) in 0.1 M HCl onto the bare SPGE. Then, the electrochemical reduction was conducted at a constant potential of -0.8 V for 180 s, resulting in the SPGE being modified with the reduced BiF (BiF/SPGE). Subsequently, the electropolymerization process was performed to synthesize Poly(Hyp) by dropping 100 µL of 5 mM Hyp in PBS pH 7.0 onto BiF/SPGE. Afterward, cyclic voltammetry (CV) was conducted by applying the potential range of +0.50 to +2.0 V for 10 cycles at a scan rate of 50 mV s^{-1}, enabling the modification of Poly(Hyp) on BiF/SPGE surface (Poly(Hyp)/BiF/SPGE). After each modification process, the obtained electrode was rinsed with DI water to eliminate unreacted substances that could remain on the electrode surface.

3.3.5 Electrochemical measurements

Electrochemical measurements were all conducted at room temperature (22°C ± 2°C). Electrochemical characterizations of bare and modified SPGEs were performed via CV and EIS with the mixture solution of 5 mM $K_3[Fe(CN)_6]/K_4[Fe(CN)_6]$ (1:1) in 0.1 M KCl. CV measurements were performed in the potential range of -0.5 V to +0.9 V at a scan rate of 50 mV s^{-1}. For EIS study, impedance spectra were recorded in the frequency range of 100 kHz to 0.1 Hz with a fixed AC amplitude of 10 mV and an applied potential of +0.25 V. For the analysis of impedance spectra, the data were fitted to the Randles equivalent circuit, consisting of the solution resistance (R_s), the charge transfer resistance between the solution and the electrode surface (R_{ct}), the Warburg impedance (Z_w, related to the diffusion of electroactive species from the solution and the electrode surface), and the constant phase element (CPE, the capacitive element associated with the behavior of a double-layer).

For Hyp electrochemical analysis, CV and differential pulse voltammetry (DPV) were the selected techniques. To study the electrochemical behavior of Hyp, CV measurements were conducted by applying potentials ranging from +0.5 V to +2.0 V at a scan rate of 50 mV s^{-1}. DPV measurements (Figure 19C) were used for quantification by scanning potentials ranging from +0.2 V to +1.4 V with a step potential of 0.025 V, a pulse potential of 0.2 V, and a pulse time of 0.15 s. To access the selectivity, stability, and reproducibility of the proposed electrode, chronoamperometric measurements were performed by applying a constant potential of +0.8 V for 300 s.

3.3.6 Sample preparation

Urine samples were collected from six healthy human volunteers (three men and three women) and immediately refrigerated at 4°C. All of the human subjects were informed about what would happen in the trial, and they agreed to the description. Samples were used without any purification process. Before analysis, aliquots of each sample (100 µL) were spiked with known Hyp concentrations and then diluted with PBS pH 7.0 to the final volume of 1,000 µL. Afterward, 100 µL of the prepared samples was

dropped onto the proposed electrodes and DPV measurement was performed, as described in Section 3.3.5, to quantify Hyp in urine.

CHAPTER 4
Results and discussion

This chapter illustrates the results and discussion regarding the development of electrochemical detection of water-soluble vitamins and biomarkers. The chapter is divided into three projects, each following the proposed methodology presented in Chapter 3.

4.1 The development of a simple electrochemical approach for the simultaneous detection of vitamin B_2, vitamin B_6, and vitamin C using a modifier-free screen-printed carbon electrode

The content presented in this section is derived from the original research article, see Appendix 1 for the complete article.

4.1.1 Electrochemical behavior for the simultaneous detection of VB_2, VB_6, and VC

Cyclic voltammetry was initially used to investigate the electrochemical properties and the possibility of simultaneous detection of VB_2, VB_6, and VC. To examine the oxidation or reduction mechanism of selected vitamins on a common SPCE surface, cyclic voltammograms of VB_2, VB_6, and VC in Britton-Robinson buffer solution (BRBS) at pH 7 were preliminary recorded at a scan rate of 100 mV/s. The obtained voltammograms from both individual and simultaneous detection were shown in Figure 20. The cyclic voltammogram of VB_2 shown in Figure 20A exhibited a pair of sharp and well-behaved redox peaks at -0.60 V and -0.75 V for anodic and cathodic peaks, respectively. This result revealed that VB_2 could display a reversible property because the ratio between anodic and cathodic current is around 1.0. However, the separation of anodic and cathodic peak potential is around 0.15 V which is greater than $0.059/n$ V of the reversible process (n is the number of electron transfers). The result might be attributed to the fact that VB_2 provided a slow rate for the electron transfer reaction (Sá, da Silva, Jost, &

Spinelli, 2015). The cyclic voltammogram of VC depicted in Figure 20B displayed a sharp and strong oxidation peak at 0.35 V with a peak current of 27.65 μA. This result indicated that VC occurs in an irreversible process at an electrode surface. Similarly, VB_6 also occurs in an irreversible process due to the presence of a small and broad oxidation peak at 0.82 V as demonstrated in Figure 20C. From these results, it could be concluded that the possibility for the simultaneous detection of VB_2, VB_6, and VC can be performed on the proposed analytical electrode because of the explicit distinction of peak potential position.

Subsequently, the simultaneous detection of VB_2, VC, and VB_6 was also investigated as shown in Figure 20D. From the voltammogram, VB_2 exhibited a pair of outstanding redox peaks at -0.48 V and -0.61 V for anodic and cathodic peaks, respectively. Meanwhile, VC and VB_6 provided a broad anodic peak at 0.41 V and 0.90 V, respectively. The obtained voltammogram confirmed that the simultaneous detection of VB_2, VC, and VB_6 in oxidative direction is possible owing to the distinction of peak potential position as same as anticipated results obtained from the individual detection. The discovered results are in good agreement with the previous critical review of all vitamins (Lovander et al., 2018), therefore, the simultaneous detection of VB_2, VC, and VB_6 can be performed using a common SPCE.

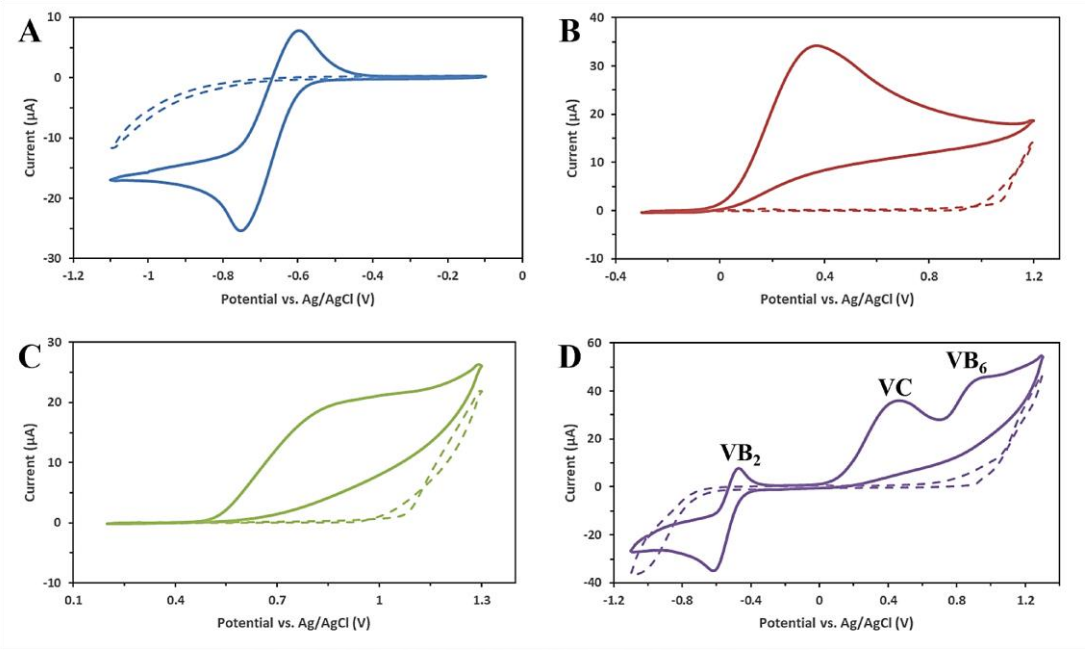

Figure 20 Cyclic voltammograms obtained from common SPCEs in the absence (dash line) and presence (solid line) of 1 mM VB_2 (A), 1 mM VC (B), 1 mM VB_6 (C), and the mixture solution of 1 mM VB_2, 1 mM VC, and 1 mM VB_6 (D). BRBS pH 7 served as a supporting electrolyte. All cyclic voltammograms were recorded at a scan rate of 100 mV/s.

4.1.2 Influence of pH and supporting electrolyte on the electrooxidation of VB_2, VC, and VB_6

The effects of adjusting the pH values of supporting electrolytes on the oxidative behavior of VB_2, VC, and VB_6 disclose significant information about the mechanisms of electrochemical reactions at a common SPCE. Therefore, the influences of pH and supporting electrolytes on the electrooxidation of VB_2, VC, and VB_6 were carefully investigated by square wave voltammetry. The suitable pH conditions were preliminarily studied using BRBS at pH 5, 7, and 9 as a representative of acidic, neutral, and basic buffer electrolytes, respectively. The obtained voltammograms from the simultaneous detection were shown in Figure 21A. With increasing pH value, the anodic currents of VB_2, VC, and VB_6 were decreased obviously. In this case, the acidic supporting

electrolyte would strongly affect a higher current. By considering the pK_a values of each vitamin, the results might be attributed to the fact that ionic forms of target analytes affect the electrooxidation processes at the electrode surface. According to data obtained from the literature (Swain, 2012), the pK_a values of each vitamin are the following: VB_2 = -0.2 and 6.0, VC = 4.2, and VB_6 = 5.6 and 9.4. These values indicated that the three compounds can exist in their ionic forms in aqueous solutions. Figure 22 shows the charge versus pH curves (CurTiPot software) for VB_2, VC, and VB_6 molecules (Gutz, 2021). As can be observed, VB_2 and VB_6 are amphoteric molecules (pI = 2.9 and 7.5, respectively) that can exist in cationic, anionic, and neutral forms. On the contrary, VC presents a weak acid character and is predominantly negatively charged in solutions with a pH higher than 6.5. As the result shown in Figure 21A, vitamins in BRBS pH 5 which is in the acidic range provided the highest anodic currents. It could be reasoned that VB_2, VC, and VB_6 exist predominantly in neutral, anionic, and cationic forms, respectively. These ionic forms easily occur electrons transfer at an electrode surface. On the other hand, anodic currents decreased when vitamins dissolved in BRBS pH 7 and 9, which is in neutral and alkaline range, because VB_2 and VB_6 exist predominantly in cationic and neutral forms, respectively. Meanwhile, VC exists completely in anionic forms. These ionic forms in neutral and basic supporting electrolytes hardly occur electron transfer at an electrode surface. From these results, it can be concluded that an acidic supporting electrolyte is a suitable electrolyte for the detection of VB_2, VC, and VB_6.

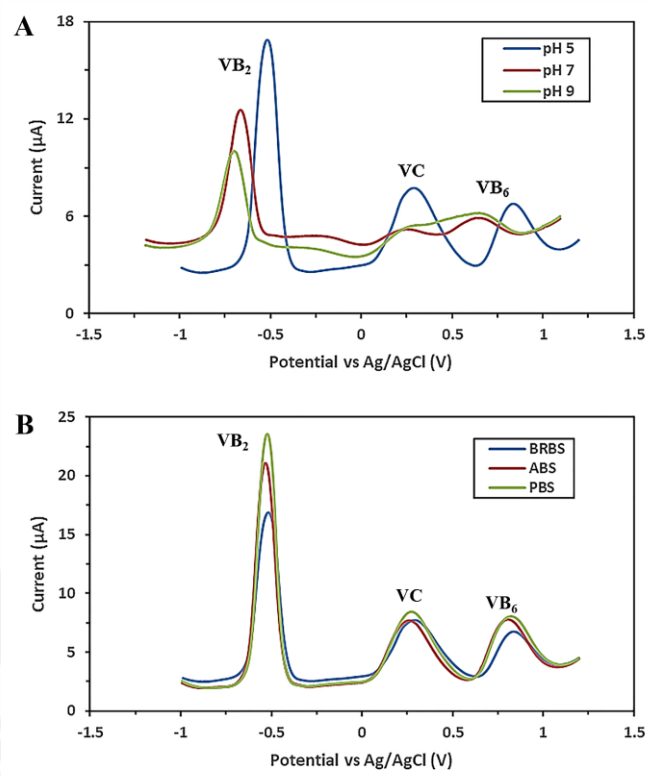

Figure 21 Square wave voltammograms of a mixture of vitamins solution (0.1 mM VB_2, 0.4 mM VC, and 0.4 mM VB_6) in BRBS at pH 5, 7, and 9 (A) and in BRBS, ABS, and PBS at pH 5 (B) obtained from common SPCEs. All square wave voltammograms were recorded at a step potential of 5 mV, an amplitude of 25 mV, and a frequency of 5 Hz.

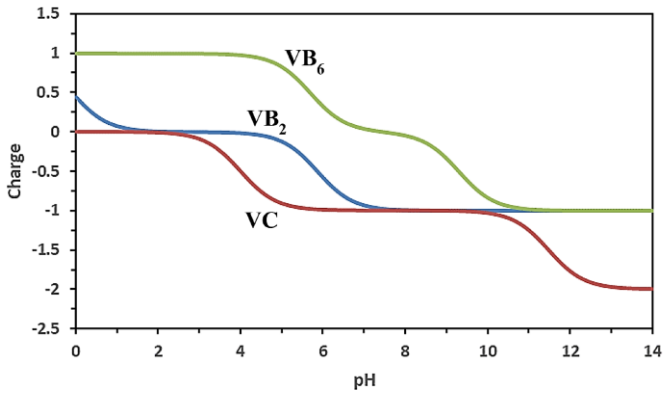

Figure 22 Charge versus pH curves (CurTiPot software) for VB_2 (blue line), VC (red line), and VB_6 (green line).

Afterward, the type of supporting electrolytes was investigated at fixed pH 5 that corresponded to the previous step to obtain the appropriate electrolyte for the detection of VB_2, VC, and VB_6. As mentioned previously, based on electrochemical works, buffer systems were universally served as supporting electrolytes due to the ability of pH regulation. In this study, buffer systems at pH 5 consisting of Britton-Robinson buffer solution (BRBS), acetate buffer solution (ABS), and phosphate buffer solution (PBS) were studied by square wave voltammetry for the selection of appropriate supporting electrolyte. Figure 21B shows square wave voltammograms of a mixture solution in various buffer systems at pH 5. By considering anodic currents, PBS at pH 5 provided the highest responses. In this case, the buffer property in terms of electrical conductivity would get involved in the oxidation of these vitamins. Consequently, the electrical conductivity of species containing in the proposed buffer system was discussed as reported in previous works (Ho & Palmer, 1995) (Weast, 1988). To deeply consider, PBS at pH 5 consisted of H_3PO_4, NaH_2PO_4, and Na_2HPO_4 which each provided the specific conductance (20°C) of 5.5, 2.2, and 4.6 mS/cm, respectively. These values were higher than other species contained in other buffer systems. For example, ABS at pH 5 containing CH_3COOH and CH_3COONa provided the specific conductance (20°C) of 0.3 and 3.9 mS/cm, respectively. Similarly, BRBS at pH 5 containing H_3PO_4, CH_3COOH, and H_3BO_3 provided

the specific conductance (25°C) of boric acid of 0.008 mS/cm. It could be ascribed that the more specific conductance was better electrical conductivity. As a result, the resistance of the electrochemical cell could decrease and eliminate the electromigration effects which were desired in controlled-potential experiments. Accordingly, it can be concluded that PBS in acidic pH value is a suitable electrolyte for the detection of VB_2, VC, and VB_6.

To confirm the effect of acidic electrolyte, the influence of solution pH on the electrochemical behavior of VB_2, VC, and VB_6 in PBS using a common SPCE was studied in specific pH ranges from 3.5 to 6.5. Figure 23A shows the anodic peak potentials (E_{pa}) for these vitamins and their linear regression equations: E_{pa} (V) = -0.0533*pH*-0.295 (r^2 = 0.9929) for VB_2; E_{pa} (V) = 0.0556*pH*+0.0334 (r^2 = 0.9901) for VC; and E_{pa} (V) = -0.054*pH*+1.0377 (r^2 = 0.9925) for VB_6. According to the derived Nernst equation (Equation (14)), which explains the relationship between E_{pa} and *pH*, where *n* and *m* represent the numbers of electrons and protons involved in the reaction, and *a* and *b* are coefficients of oxidant and reductant in the reaction (Thomas et al., 2014).

$$E_{pa}=E^0+\left(\frac{0.0591}{n}\right)\log\left[\frac{(OX)^a}{(R)^b}\right]-\left(0.0591\frac{m}{n}\right)pH \quad \text{.....Equation (14)}$$

All of the slopes between E_{pa} and *pH* of each vitamin were very imminent to 59 mV/pH at 25°C, indicating that the overall electrochemical process at the proposed electrode was proton-dependent-the electron transfer which was regulated by a transfer of an equal number of protons and electrons.

Furthermore, the anodic peak currents (I_{pa}) as a function of pHs were also investigated as presented in Figure 23B. The anodic currents of VB_2, VC, and VB_6 do not have a significant distinction with increasing pH value until it reaches 6.5. Consequently, the difference in anodic peak potential between VC and VB_6 was primary considered to select the appropriate pH value. The difference of anodic peak potential between these two vitamins decreases with increasing pH value, leading to the overlapping of anodic peaks. PBS at pH 3.5 provided the highest difference of anodic peak potential, therefore, it was chosen as an appropriate pH value for the simultaneous detection of VB_2, VC, and VB_6. This can be supposed that due to these vitamins dissolved in the acidic solution (pH

3.5) in which VB_2 and VC predominantly exist in neutral forms, meanwhile, VB_6 is positively charged because of the protonation of nitrogen in the pyridine ring. These molecules and ionized forms can be oxidized at differently applied potential using a common SPCE.

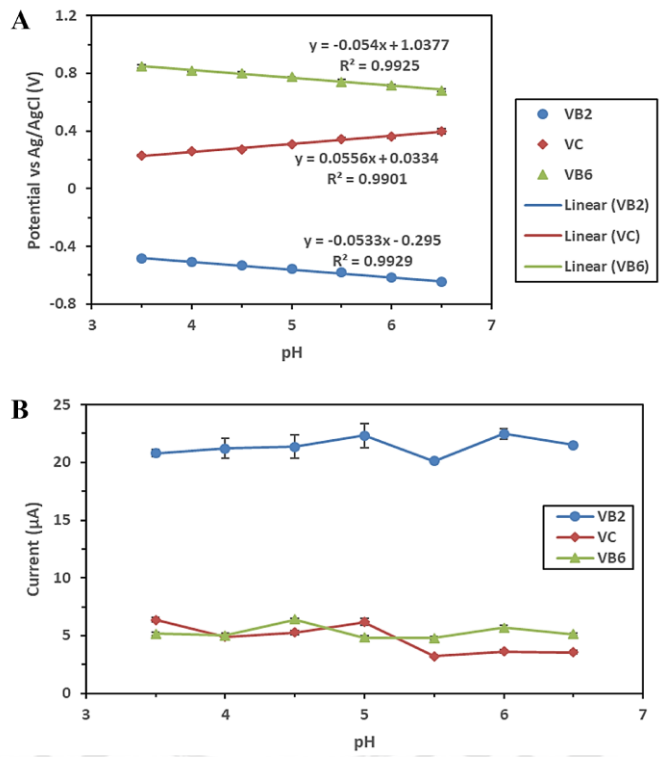

Figure 23 Influences of solution pH on anodic peak potentials (A) and peak currents (B) for the oxidation of 100 μM VB_2, 400 μM VC, and 400 μM VB_6 in various pH values of PBS at a common SPCE.

4.1.3 The effect of scan rate on the electrooxidation of VB_2, VC, and VB_6

To elucidate whether the mass transfer of the analyte toward the electrode surface is diffusion or adsorption controlled, the effect of scan rate on the electrooxidation of VB_2, VC, and VB_6 was investigated by cyclic voltammetry. Figure 24A shows cyclic voltammograms of VB_2, VC, and VB_6 at a common SPCE using different scan rates. The results presented that the redox peak currents for VB_2 increased with increasing the scan rate, while their redox peak potentials remained the same values, suggesting the electron

transfer process was reversible. On the other hand, the anodic peak currents for VC and VB_6 increased with increasing the scan rate, however, their anodic peak potentials gradually shifted to positive values, introducing the electron transfer processes were irreversible. The linear dependence of the anodic peak current of all three vitamins versus the square root of the scan rate was observed as displayed in Figure 24B. These behaviors demonstrate that the electrochemical oxidations of all three vitamins at a common SPCE are diffusion-controlled processes (Jiang et al., 2015).

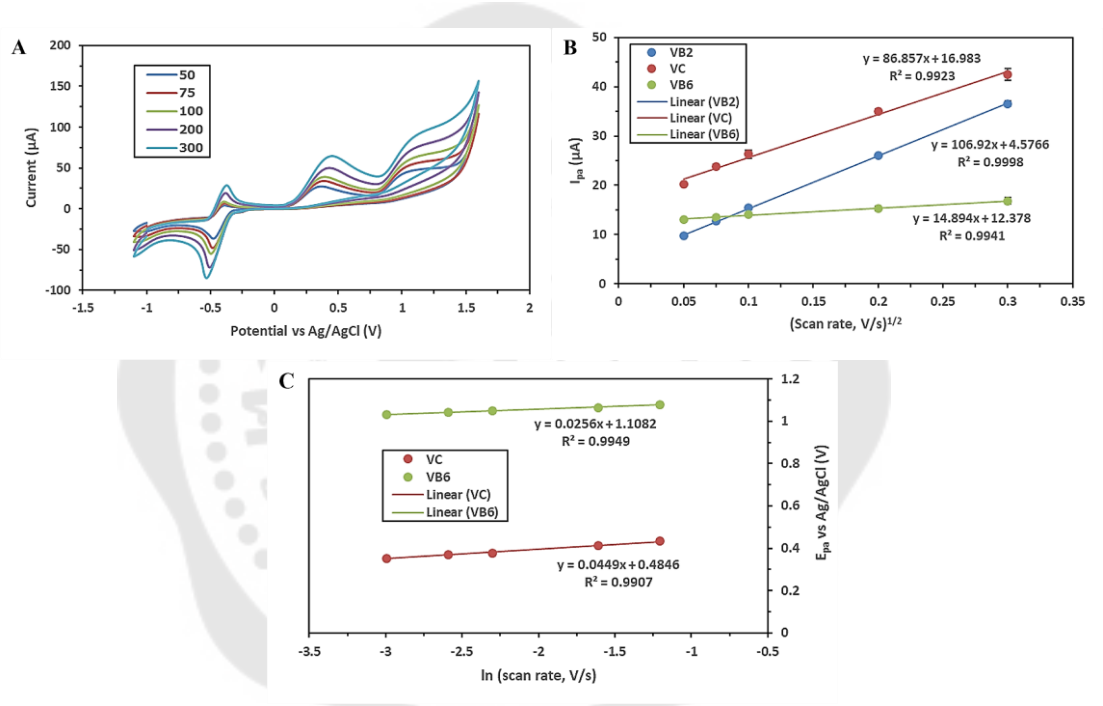

Figure 24 (A) Cyclic voltammograms for 1 mM VB_2, 1 mM VC, and 1 mM VB_6 in PBS pH 3.5 at the common SPCE using a series of scan rates (50, 75, 100, 200, and 300 mV/s). (B) The relationship between the anodic peak currents (I_{pa}) and the square root of scan rates. (C) The variation of anodic peak potential (E_{pa}) and the natural logarithm of scan rates (ln ν) from 50 to 300 mV/s.

Using the information received from the linear regression of the relationship between anodic peak currents (I_{pa}) and the square root of scan rates ($\nu^{1/2}$), the relationship

as shown in Equation (15) was applied to estimate the diffusion coefficients (D_0) of all three vitamins (Boni, Wong, Dutra, & Sotomayor, 2011).

$$I_{pa} = 0.496FAC_s{D_0}^{1/2}\left(\frac{F}{RT}\right)^{1/2}\nu^{1/2} \quad \text{.....Equation (15)}$$

When F is the Faraday constant, A is a geometric area of the working electrode (0.126 cm^2), C_s is the concentration of vitamins (1 x 10^{-6} mol/cm^3), D_0 is the diffusion coefficient of vitamins, R is a gas constant (8.31447 J/mol/K), and T is a temperature (298 K). The calculated D_0 values of VB_2, VC, and VB_6 were found to be 8.07 x 10^{-6}, 5.32 x 10^{-6}, and 1.57 x 10^{-7} cm^2/s, respectively. Then, the number of electrons (n) involved in the electrooxidation of VB_2 was determined by the derived Randles-Sevcik relationship for a reversible process (Equation (16)).

$$I_{pa} = (2.69\ x\ 10^5)n^{3/2}AC_s{D_0}^{1/2}v^{1/2} \quad \text{.....Equation (16)}$$

Using Equation (16) and the previously estimated D_0 of VB_2, the number of electrons involved in the electrooxidation of VB_2 can be calculated and was found to be n = 1.07 (n ~ 1). Next, the number of electrons involved in the electrooxidation of VC and VB_6 was determined by the derived Randles-Sevcik relationship for the irreversible process (Equation (17)).

$$I_{pa} = (2.99\ x\ 10^5)n[(1-\alpha)n_\alpha]^{1/2}AC_s{D_o}^{1/2}\nu^{1/2} \quad \text{.....Equation (17)}$$

To calculate the n value, it is unavoidable to solve initially the factor of $(1\text{-}\alpha)n_\alpha$. Using the Laviron theory for oxidative reaction (Equation (18)) (Laviron, 1979), the calculation is based on the linear relationship between anodic peak potential (E_{pa}) and the natural logarithm of scan rates (ln ν), as shown in Figure 24C. Depended on Equation (18) and the slopes received from the linear relationship between the E_{pa} an ln ν, the factors of $(1\text{-}\alpha)n_\alpha$ for VC and VB_6 were found to be 0.572 and 1.00, respectively.

$$E_{pa} = E^0 + \frac{RT}{(1-\alpha)nF}ln\frac{RTk_s}{(1-\alpha)nF} + \frac{RT}{(1-\alpha)nF}ln\,\nu \quad \text{.....Equation (18)}$$

After calculating the factors of $(1\text{-}\alpha)n_\alpha$, using Equation (17) and the formerly estimated D_0 of VC and VB_6, the number of electrons involved in the electrooxidation of

VC and VB_6 can be calculated and were found to be n = 1.32 (n ~ 2) and n = 0.998 (n ~ 1), respectively.

4.1.4 Analytical performance for the detection of VB_2, VC, and VB_6

Square wave voltammetry was selected for the simultaneous determination of VB_2, VC, and VB_6 in mixture solutions due to its better resolution and higher sensitivity than cyclic voltammetry. Under the optimized experimental conditions (a step potential of 5 mV, an amplitude of 25 mV, and a frequency of 5 Hz), square wave voltammograms for the electrooxidation of different concentrations of VB_2, VC, and VB_6 mixture at a common SPCE were obtained, as shown in Figure 25A. The results presented that the well-defined anodic peaks of all three vitamins are separated sufficiently to discriminate and measure the current. Besides, the increment in the peak currents of all three vitamins can be observed with increasing their concentrations at the same time. Figure 25B displays the calibration curves of all three vitamins, indicating that the anodic peak currents for the electrooxidation of all three vitamins increased proportionally with their corresponding concentrations. From these results, the linear ranges for the simultaneous determination of VB_2, VC, and VB_6 were found to be 1-60 μM, 10-400 μM, and 10-400 μM with the detection limit (calculated as the 3σ value of the blank) of 0.37 μM, 5.07 μM, and 3.32 μM, respectively. Comparison of the analytical performance to previous works and this work was shown in Table 5. Even though, detection limits and linear ranges of the proposed system are not as low as those received by other modified electrodes. However, this work was first proposed the simultaneous determination of VB_2, VC, and VB_6 using a common SPCE by systematically studied all experimental parameters that affected peak separation and sensitivity. Our proposed methodology provided various advantages, such as a low-cost sensor, the modification-free electrode, and requires a small sample volume for analysis. Moreover, this proposed system is easy to apply for commercialization of the electrode in the future.

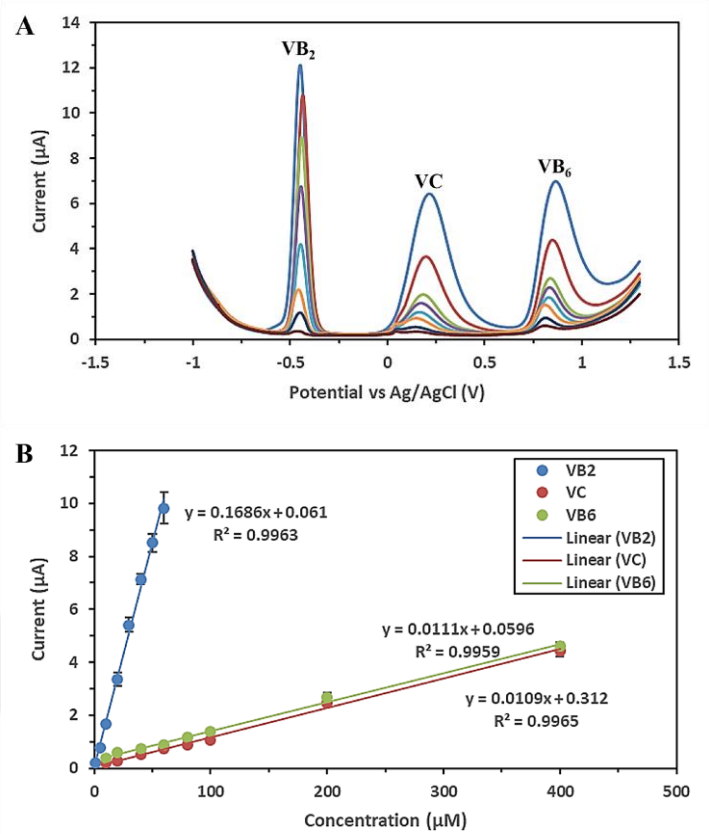

Figure 25 (A) Square wave voltammograms of VB_2, VC, and VB_6 in concentration ranges of 1-60 µM, 10-400 µM, and 10-400 µM, respectively, in PBS pH 3.5 at common SPCEs. (B) Calibration plots between anodic peak currents of each vitamin versus concentration.

Table 5 Comparison of the analytical performance between this study and previous works for the simultaneous detection of VB_2, VC, and VB_6.

Working electrode	Modification time*	Detection technique	Detection limit (μM)			Linear range (μM)			Ref.
			VB_2	VC	VB_6	VB_2	VC	VB_6	
PGCE	15 min	DPV	0.001	-	0.8	0.005-100	75-75,000	2.5-7,500	(Gu et al., 2007)
PEDOT/Fc^-/GCE	5 min	DPV	0.05	0.7	0.1	0.1-300	1.5-2,000	0.5-1,500	(Nie et al., 2013)
PEDOT/$Fe(CN)_6^{4-}$/GCE			0.02	0.5	0.3	0.04-200	1-2,000	0.7-1,500	
PEDOT/ZrO_2NPs/GCE	10 min	DPV	0.012	0.45	0.2	0.05-300	1-1,500	0.5-1,000	(Nie et al., 2014)
Ag-PLA/GCE	10 min	LSV	0.08	3	5	0.1-23	5-4,000	10-3,000	(G. Liu et al., 2015)
f-MWCNT-Cu_2O-Ag_2O composite/copper substrate	> 1 day	DPV	0.014	0.011	0.008	0.05-1,752	0.05-1,626	0.02-1,056	(Puangjan et al., 2017)
Modification-free SPCE	-	SWV	0.37	5.07	3.32	1-60	10-400	10-400	This work

*Estimated modification time (1 electrode). All modification steps were included. PGCE: Pretreated glassy carbon electrode; MWCNT: Multi-wall carbon nanotubes; PEDOT: Poly(3,4-ethylenedioxythiophene); Fc^-: Ferrocenecarboxylic acid; $Fe(CN)_6^{4-}$: Ferricyanide; ZrO_2NPs: Zirconia nanoparticles; Ag-PLA: Silver doped poly(L-arginine); *f*-MWCNT-Cu_2O-Ag_2O: Functionalized multi-walled carbon nanotubes supporting Cu_2O and Ag_2O composite.

To investigate the practicality of a common SPCE for the simultaneous determination of VB_2, VC, and VB_6, the individual determination of each vitamin was performed by varying the concentration of one analyte while those of the others have remained constant. The results in Figure 26A display that the anodic peak currents of VB_2 increased with concentration while the anodic peak currents of VC and VB_6 were equally unaltered at these concentrations as shown in Figure 26B. In the same way, as can be seen in Figure 26C and 26D, the anodic peak currents of VC increased linearly with increasing the concentrations. Similarly, Figure 26E and 26F show that the anodic peak current signals for VB_6 also increased with increasing the concentrations. By comparison between anodic peak currents and concentrations from individual and simultaneous determinations, the slopes of each vitamin were virtually unchanged. It could be emphasized that the electrooxidation processes of each vitamin are independent, therefore, the simultaneous determinations of these vitamins are feasible without any interference from their presence together.

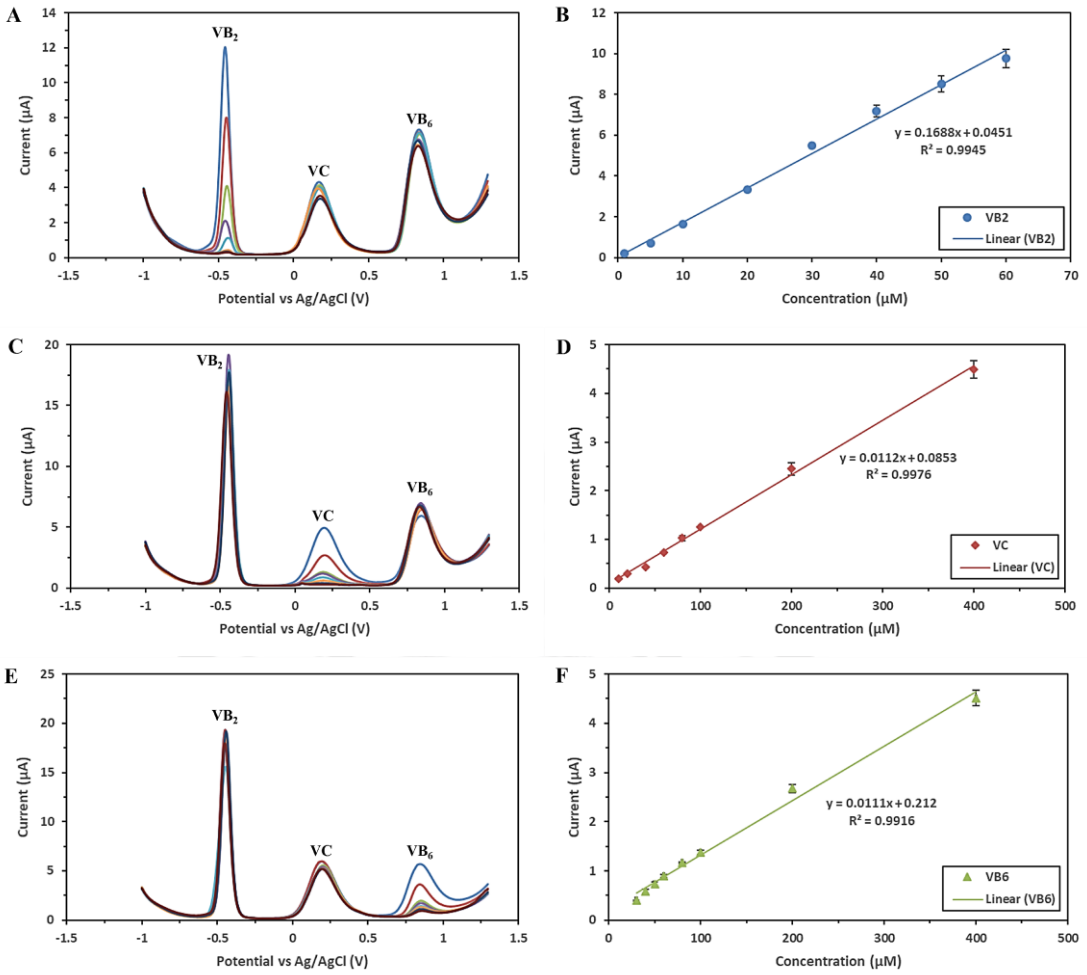

Figure 26 Square wave voltammograms obtained from common SPCEs of (A) VB_2, (C) VC, and (E) VB_6 in PBS pH 3.5 at different concentrations in the range of 1-60 μM, 10-400 μM, and 10-400 μM, respectively. Each vitamin was detected by varying the concentration of one analyte while those of the others remained constant. Calibration plots of their anodic peak currents versus concentrations for (B) VB_2, (D) VC, and (F) VB_6.

The reproducibility of all three vitamins at various concentrations was calculated in the term of relative standard deviation (RSD) by using seven different electrodes (n = 7). The value was lower than 6.5%, which can be acceptable (AOAC International., 1995). As shown in Table 6, indicated that this electrode can be

successfully employed for the simultaneous determination of water-soluble vitamins with excellent reproducibility.

Table 6 The reproducibility (calculated as relative standard deviation) of VB_2, VC, and VB_6 at different concentrations obtained from common SPCEs.

Vitamin	Concentration (μM)	RSD (%, *n* = 7)
VB_2	1	4.90
	20	2.78
	60	2.34
VC	10	6.43
	60	4.95
	400	3.70
VB_6	10	6.27
	60	4.24
	400	2.44

4.1.5 Interference study

To investigate the selectivity of the proposed electrode and developed method, the influence of various foreign species on the simultaneous determination of 20 μM VB_2, 60 μM VC, and 60 μM VB_6 in PBS pH 3.5 was evaluated. The tolerance limit was calculated to be lower than 5% of a relative error. The results revealed that 3,000-fold and 1,000-fold concentration ratios of Na^+, K^+, Mg^{2+}, Ca^{2+}, Al^{3+}, Cl^-, HCO_3^-, SO_4^{2-}, and PO_4^{3-}, 300-fold and 100-fold concentration ratios of VB_1, VB_3, VB_5, glucose, fructose, citrate, L-lysine, L-cysteine, and L-methionine; 30-fold and 10-fold concentration ratios of Fe^{2+}, Cu^{2+}, VB_9, and oxalate; 15-fold and 5-fold concentration ratios of VB_{12} and uric acid, and 5-fold concentration ratios of albumin and globulin did not interfere the measurement of VB_2, VC, and VB_6 (Table 7). No change significantly in the current signal was observed. Thus, the proposed electrodes were good selectivity towards the simultaneous determination of these three vitamins.

Table 7 Tolerance ratio of foreign species in the simultaneous determination of 20 μM VB_2, 60 μM VC, and 60 μM VB_6 on the common SPCEs.

Foreign species	Tolerance ratio ($C_{species}/C_{target\ vitamin}$)		
	VB_2	VC	VB_6
Na^+, K^+, Mg^{2+}, Ca^{2+}, Al^{3+}, Cl^-, HCO_3^-, SO_4^{2-}, PO_4^{3-}	3,000	1,000	1,000
VB_1, VB_3, VB_5, glucose, fructose, citrate, L-lysine, L-cysteine, L-methionine	300	100	100
Fe^{2+}, Cu^{2+}, VB_9, oxalate	30	10	10
VB_{12}, uric acid	15	5	5
Albumin, globulin	5	5	5

4.1.6 Application in real samples

To examine the practicality and reliability of the proposed method, the simultaneous determinations of VB_2, VC, and VB_6 at a common SPCE were performed in mixed vegetable and fruit juice and artificial urine sample. The concentrations of these vitamins were determined by square wave voltammetry using the standard addition method to prevent any matrix influence. Recovery studies were carried out by spiking VB_2, VC, and VB_6 to the samples at various concentration levels. The experimental results revealed in Table 8 and Table 9 display that the recovery values were in the range of 83.91 -109.10%, which can be acceptable. Furthermore, to confirm the accuracy of the proposed method, the concentrations of VB_2, VC, and VB_6 in these samples were also determined by HPLC-DAD. The paired *t*-test between two methods disclosed that the results were in good agreement because the calculated t-value (2.15) was less than the critical value (2.31) for a two-tailed comparison. Therefore, a common SPCE can be successfully performed for the simultaneous determination of VB_2, VC, and VB_6 in real applications.

Table 8 The determination of VB_2, VC, and VB_6 in mixed vegetable and fruit juice by SWV and HPLC (n = 3).

Analyte	Add (μM)	Found (μM)	Recovery (%)	RSD (%)	HPLC (μM)
VB_2	0	ND	-	-	ND
	10	9.92 ± 0.07	99.19	4.30	10.02 ± 0.09
	30	27.59 ± 0.07	91.96	1.68	29.09 ± 0.12
	50	46.81 ± 0.22	93.63	2.98	47.82 ± 0.12
VC	0	17.59 ± 0.02	-	6.37	ND
	40	50.06 ± 0.07	86.92	5.88	41.39 ± 0.07
	80	81.89 ± 0.11	83.91	6.10	82.07 ± 0.11
	200	209.06 ± 0.16	96.08	3.92	203.48 ± 0.16
VB_6	0	ND	-	-	ND
	40	42.90 ± 0.05	107.25	4.90	42.10 ± 0.15
	80	87.23 ± 0.06	109.04	3.01	84.83 ± 0.21
	200	207.04 ± 0.19	103.52	4.86	211.04 ± 0.22

ND = Not detectable

Table 9 The determination of VB_2, VC, and VB_6 in artificial urine by SWV and HPLC (n = 3).

Analyte	Add (μM)	Found (μM)	Recovery (%)	RSD (%)	HPLC (μM)
VB_2	0	ND	-	-	ND
	10	10.80 ± 0.13	107.96	6.92	10.53 ± 0.23
	30	32.92 ± 0.33	109.10	6.14	32.15 ± 0.33
	50	52.30 ± 0.25	104.59	2.91	51.85 ± 0.15
VC	0	ND	-	-	ND
	40	37.12 ± 0.03	92.79	7.17	38.40 ± 0.03
	80	72.89 ± 0.01	91.11	1.52	75.29 ± 0.01
	200	192.90 ± 0.9	96.45	4.51	193.10 ± 0.09
VB_6	0	ND	-	-	ND
	40	36.73 ± 0.03	91.82	6.64	38.33 ± 0.03
	80	70.92 ± 0.04	88.65	4.05	74.12 ± 0.04
	200	198.85 ± 0.10	99.43	4.62	200.60 ± 0.10

ND = Not detectable

4.2 The development of a simple and rapid detection approach for urinary albumin on a disposable paper-based analytical device using an electrochemical-chemical redox cycling process

The content presented in this section is derived from the original research article, see Appendix 2 for the complete article.

4.2.1 Preliminary study of EC redox cycling process

Prior to performing the albumin detection, an electrochemical investigation of EC redox cycling system was first conducted to demonstrate the potential of each proposed process to support the expected results. Cyclic voltammograms of buffer solutions containing only $[Fe(CN)_6]^{3-}$, MB, and the mixture of $[Fe(CN)_6]^{3-}$ and MB were obtained using ePADs, as presented in Figure 27A. The CV curve of a solution containing only $[Fe(CN)_6]^{3-}$ revealed a pair of redox peaks at +0.36 and -0.15 V, with anodic and cathodic peak currents of +10.64 and -10.67 μA, respectively. Because of the high peak separation (0.51 V) and low peak currents, the electrochemical reaction of $[Fe(CN)_6]^{3-}$ proceeds at a slow rate. Similarly, the solution containing only MB produced a pair of redox peaks at -0.21 and -0.30 V, with anodic and cathodic peak currents of +6.21 and -4.05 μA, respectively. This can be assumed that MB (MB_{ox}) directly obtains two electrons and one proton to form leucomethylene blue (LMB, MB_{red}), and that LMB is then oxidized back to MB by losing two electrons and one proton (Ju, Zhou, Cai, & Chen, 1995). According to the findings, MB can also provide a reversible process at the bare graphene electrode surface. On the other hand, the CV curve of a solution containing both $[Fe(CN)_6]^{3-}$ and MB showed high peak currents for $[Fe(CN)_6]^{3-/4-}$ redox couple of +30.90 and -29.01 μA at peak potentials of +0.21 and +0.05 V (peak separation of 0.16 V) for anodic and cathodic directions, respectively. Another pair of redox peaks for $MB_{ox/red}$ was observed at -0.23 and -0.31 V, with anodic and cathodic peak currents of +4.97 and -2.61 μA, respectively. In comparison with a solution containing only $[Fe(CN)_6]^{3-}$, the redox couple of $[Fe(CN)_6]^{3-/4-}$ in mixture solution generated 3 times higher peak currents and 3.2 times lower peak separation. The findings indicated that the EC redox cycling process

can increase electron transfer efficiency across the interface. In contrast, the anodic-cathodic peak current of MB obtained from the mixture solution was lower than that obtained from the solution containing only MB. This possibly was the signal of MB molecules that remained after the redox cycling system proceeded, and thus, a low electrochemical signal was obtained. To explain a unique EC redox cycling process, $[Fe(CN)_6]^{3-}$ is reduced to $[Fe(CN)_6]^{4-}$ via an electrochemical reaction at the bare graphene electrode, which is then re-oxidized by MB via a chemical reaction, as presented in Figure 27B. Due to the simultaneous regeneration of $[Fe(CN)_6]^{3-}$, this redox cycling process continuously occurs, resulting in a large electrochemical signal. Based on these findings, it can be concluded that the EC redox cycling process between $[Fe(CN)_6]^{3-}$ and MB was effective for amplifying the detection signal when using an unmodified electrode.

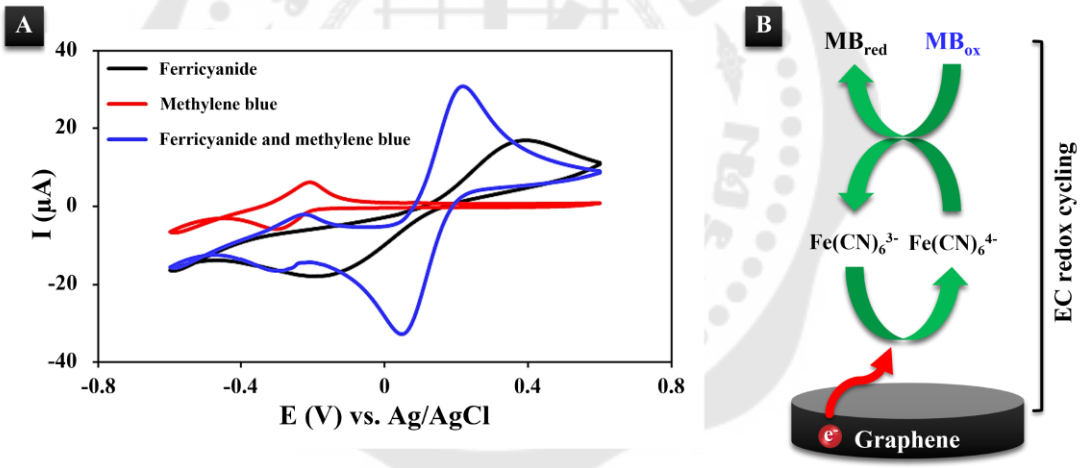

Figure 27 (A) Cyclic voltammograms of PBS (pH 7.4) containing only 1 mM $[Fe(CN)_6]^{3-}$ (black line), 0.05 mM MB (red line), and the mixture of 1 mM $[Fe(CN)_6]^{3-}$ and 0.05 mM MB (blue line). (B) Schematic illustration of EC redox cycling process using $[Fe(CN)_6]^{3-}$ and MB.

Furthermore, the DPV technique was used to confirm this EC redox cycling process. In this work, an electrochemical measurement in the reductive direction was selected to avoid some interferences observed in the sample, such as ascorbic acid, uric

acid, and dopamine, which provide the signal in the oxidative direction (Wenjing Zhang et al., 2018). As a result, DPV measurements were performed using potentials ranging from +0.5 to -0.5 V. The solution containing only $[Fe(CN)_6]^{3-}$ exhibited a broad voltammogram at a cathodic potential of +0.01 V with a cathodic current of -3.76 µA, as presented in Figure 28. Meanwhile, the DPV curve of a solution containing only MB revealed a well-defined cathodic peak at -0.23 V with a current of -11.30 µA. The mixture solution of $[Fe(CN)_6]^{3-}$ and MB, on the other hand, generated a sharp and symmetrical peak of $[Fe(CN)_6]^{3-}$ at a cathodic potential of +0.14 V with a cathodic current of -34.90 µA. Another peak was a cathodic peak of MB at a potential of -0.25 V with a current of -8.76 µA. The signal of $[Fe(CN)_6]^{3-}$ obtained from a mixture solution generated 9.3-fold higher cathodic current with a higher positive potential than the signal obtained from a solution containing only $[Fe(CN)_6]^{3-}$. For the MB peak, the signal current of MB obtained from the mixture solution was lower than that of the MB single solution. The results of this additional investigation were in good agreement with those of the CV study, indicating that the proposed EC redox cycling process has a high catalytic capability for the electrochemical reduction of $[Fe(CN)_6]^{3-}$. As a result, without any modifications to the working electrode, a high sensitivity for albumin detection can be obtained.

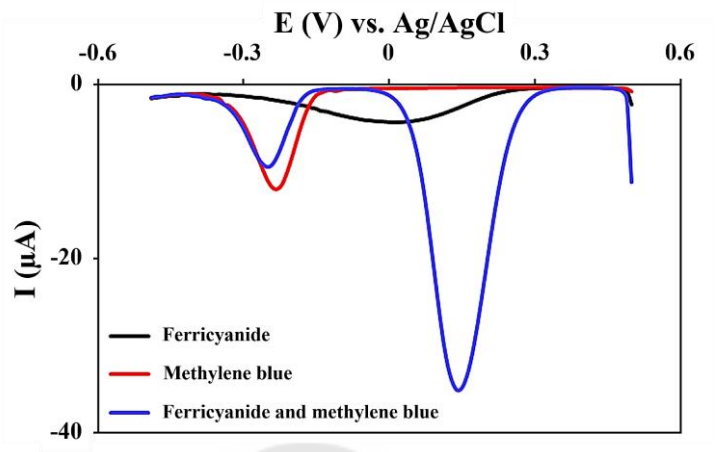

Figure 28 Differential pulse voltammograms of PBS (pH 7.4) containing only 1 mM $[Fe(CN)_6]^{3-}$ (black line), 0.05 mM MB (red line), and the mixture of 1 mM $[Fe(CN)_6]^{3-}$ and 0.05 mM MB (blue line). All DPV curves were recorded using the potentials ranging from +0.5 to -0.5 V, with an increment potential of 10 mV, an amplitude of 50 mV, a pulse width of 200 ms, a sample width of 100 ms, and a pulse period of 500 ms.

4.2.2 Optimization of EC redox cycling process

Important parameters of the EC redox cycling process were evaluated sequentially using the DPV technique to achieve the highest sensitivity for albumin detection. The concentrations of $[Fe(CN)_6]^{3-}$ and MB were optimized using ready-to-use ePADs without electrode pretreatment. The effect of $[Fe(CN)_6]^{3-}$ concentration was first investigated in the range of 0.1 – 5 mM with a constant concentration of 0.05 mM MB. The cathodic currents of $[Fe(CN)_6]^{3-}$ clearly increased with increasing concentrations, as presented in Figure 29A. Until 4 mM of $[Fe(CN)_6]^{3-}$ was applied, this response became constant. The cathodic currents of MB, on the other hand, gradually decreased with increasing $[Fe(CN)_6]^{3-}$ concentrations and then reached a constant response at 2 mM of $[Fe(CN)_6]^{3-}$. This can be suggested that the EC redox cycling process prefers high concentrations of $[Fe(CN)_6]^{3-}$ for electrochemical reduction, resulting in high production of $[Fe(CN)_6]^{4-}$. Subsequently, the large amount of $[Fe(CN)_6]^{4-}$ will be re-oxidized by MB back to $[Fe(CN)_6]^{3-}$, as previously described in Section 4.2.1; thus, the high cathodic response

of $[Fe(CN)_6]^{3-}$ was obtained. Based on the results obtained, it can be concluded that 4 mM of $[Fe(CN)_6]^{3-}$ was an appropriate concentration to use for further investigation. The concentration of MB was then optimized in the range of 0.01 – 0.1 mM with a constant concentration of 4 mM $[Fe(CN)_6]^{3-}$. The cathodic current of $[Fe(CN)_6]^{3-}$ increased with increasing MB concentration, as presented in Figure 29B; however, the response decreased after 0.05 mM of MB was applied. Meanwhile, the cathodic current of MB slightly increased with increasing MB concentrations. These results showed that increasing the MB concentration above 0.05 mM did not improve the efficiency of $[Fe(CN)_6]^{3-}$ detection; thus, 0.05 mM of MB was chosen as an optimal concentration for this parameter.

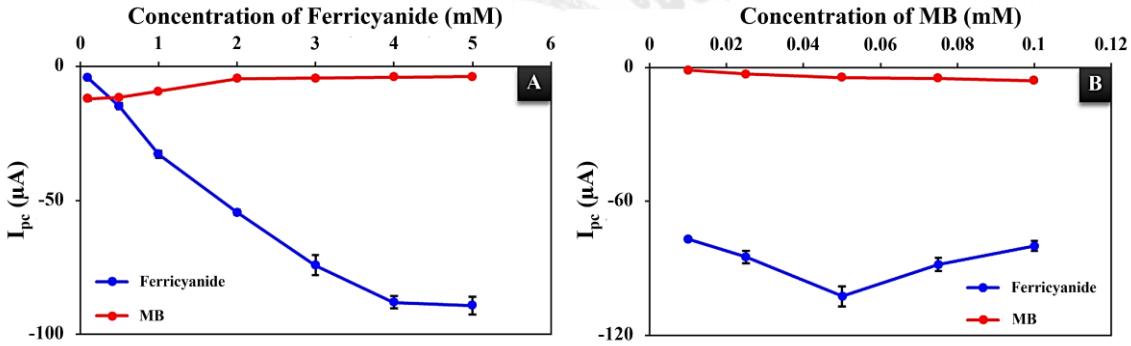

Figure 29 Optimization for the concentration of (A) $[Fe(CN)_6]^{3-}$ (from 0.1 – 5 mM) and (B) MB (from 0.01 – 0.1 mM) obtained from the DPV technique using ePADs (n = 3).

4.2.3 Albumin detection using EC redox cycling process

The albumin detection was performed using the DPV technique under optimized experimental conditions, as presented in Figure 30A. A differential pulse voltammogram of a buffer solution containing only 400 mg dL^{-1} BSA standard solution revealed no cathodic peak, indicating that BSA is a non-electroactive macromolecule that cannot occur in the reduction process on an unmodified graphene electrode. As a result, the EC redox cycling process was applied to provide a high current response. A cathodic

peak of $[Fe(CN)_6]^{3-}$ at +0.13 V with a peak current of -79.17 µA was observed on the DPV curve of a redox solution containing 4 mM $[Fe(CN)_6]^{3-}$ and 0.05 mM MB. The results indicated that the redox cycling process produced a high signal current of $[Fe(CN)_6]^{3-}$, expecting a high sensitivity for albumin detection without further electrode modification. Subsequently, a cathodic peak of $[Fe(CN)_6]^{3-}$ at +0.11 V with a peak current of -43.73 µA was observed in a mixture solution of 4 mM $[Fe(CN)_6]^{3-}$, 0.05 mM MB, and 400 mg dL^{-1} BSA standard solution. In comparison with a redox solution containing both $[Fe(CN)_6]^{3-}$ and MB, the lower cathodic peak potential was obtained, and the difference in the cathodic peak current (ΔI_{pc}) was equal to -35.44 µA, indicating that BSA hinders the electron-transfer process of the EC redox cycling system, as shown in Figure 30B. This behavior may be the obstruction of negatively charged BSA (pI = 4.7) (Vlasova & Saletsky, 2009) at the electrode surface, leading to the blocking of the reduction process for $[Fe(CN)_6]^{3-}$ to accept electrons from a working electrode. This circumstance resulted in a diminishing current response because $[Fe(CN)_6]^{3-}$ is hardly reduced to $[Fe(CN)_6]^{4-}$, which is then slightly re-oxidized by MB. Aside from detecting albumin by mixing a BSA standard with a redox cycling solution, another method, which is the dropping and drying of the BSA standard solution on the working electrode, was also proposed as shown in Figure 31. The cathodic peak of $[Fe(CN)_6]^{3-}$ at +0.13 V with a peak current of -79.17 µA obtained from a redox cycling solution on a bare working electrode is presented in Figure 32. In contrast, a redox cycling solution on a working electrode covered with BSA, labeled as BSA/Graphene, generated a cathodic peak of $[Fe(CN)_6]^{3-}$ at +0.11 V with a peak current of -48.10 µA. The lower cathodic peak potential was obtained, and the ΔI_{pc} was equal to -31.07 µA when compared with the signal current in the absence of BSA. The results indicated that the BSA molecule blocks the electroactive sites on the graphene surface, resulting in a lower cathodic response of a redox cycling solution. This finding was compatible with albumin detection by mixing a BSA standard solution with a redox cycling solution; however, it was not suitable for a rapid detection, which was the ultimate goal, due to the time-consuming process of drying BSA on the working electrode. Based on these findings, the detection method by mixing all solutions in the same microcentrifuge

tube was selected to measure albumin simply and rapidly. As a result, in the following investigation, BSA will be quantified using a mixture of BSA standard solution and a redox cycling solution.

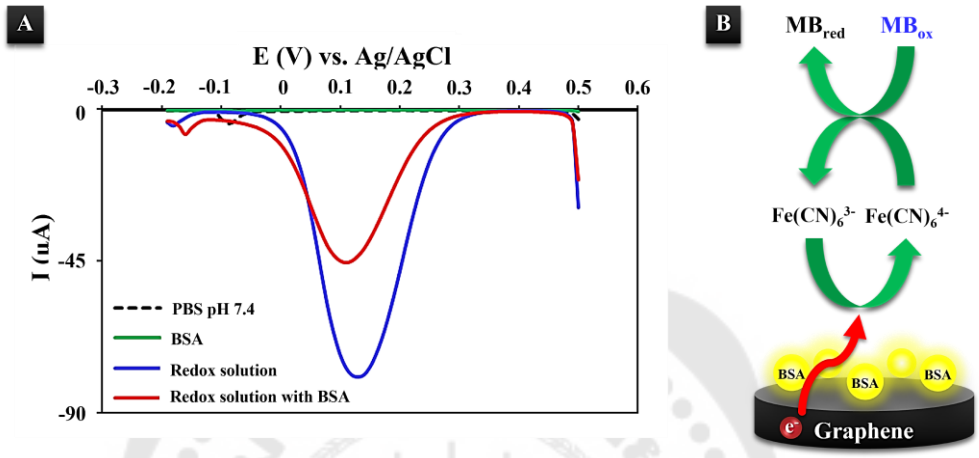

Figure 30 (A) Differential pulse voltammograms of PBS (pH 7.4) (black dash line) containing only 400 mg dL^{-1} BSA standard solution (green line), the mixture of 4 mM $[Fe(CN)_6]^{3-}$ and 0.05 mM MB (blue line), and the mixture of 4 mM $[Fe(CN)_6]^{3-}$, 0.05 mM MB, and 400 mg dL^{-1} BSA standard solution (red line). (B) Schematic illustration of the EC redox cycling process in the presence of BSA.

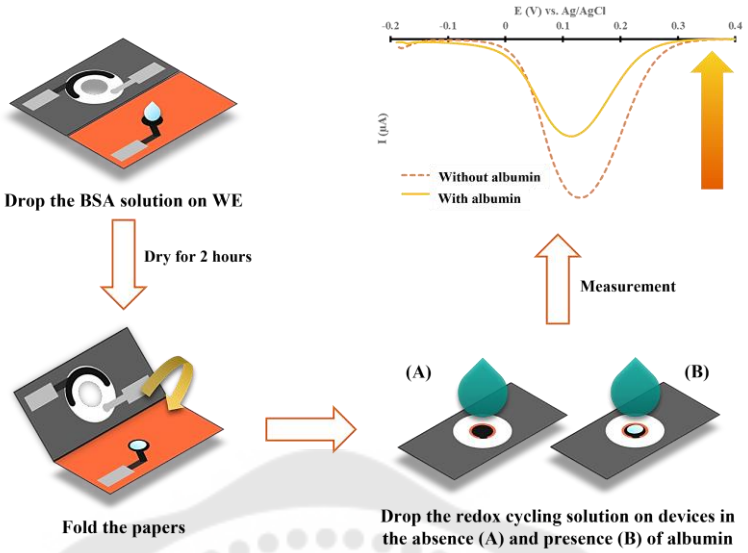

Figure 31 Schematic illustration of the detection procedure for measuring albumin by dropping and drying BSA standard solution on the working electrode surface. First, 10 μL of 400 mg dL^{-1} BSA standard solution was applied to the working electrode and allowed to dry for 2 hours at room temperature. Subsequently, 100 μL of a redox cycling solution was dropped on the paper device, and DPV measurements were performed under the same conditions as described in Section 3.2.3.

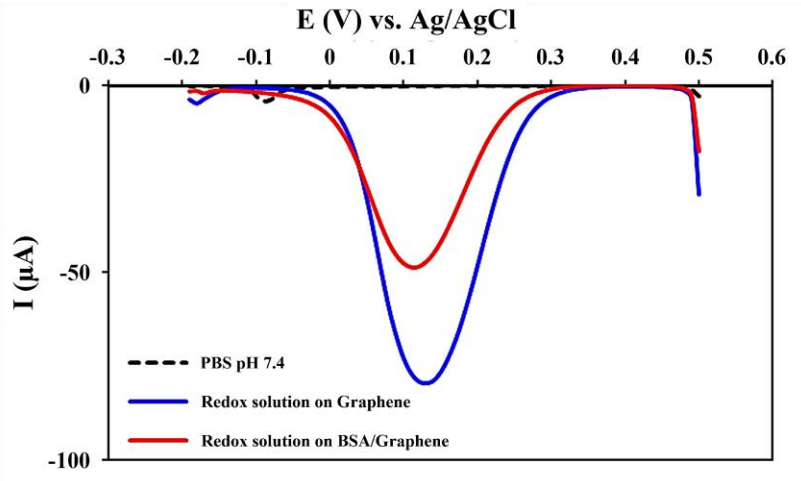

Figure 32 Differential pulse voltammograms of PBS (pH 7.4) (black dash line) and a redox cycling solution containing 4 mM $[Fe(CN)_6]^{3-}$ and 0.05 mM MB in the absence (blue line) and presence (red line) of 400 mg dL^{-1} BSA obtained from dropping and drying BSA standard solution on the working electrode.

4.2.4 Analytical performance

Following the presentation of the albumin detection strategy in Section 4.2.3, the analytical performance of albumin was evaluated by combining the optimal redox cycling solution (4 mM $[Fe(CN)_6]^{3-}$ and 0.05 mM MB) with various concentrations of BSA standard solution. As presented in Figure 33A, the peak currents decreased as a function of BSA concentration. Figure 33B presents the relationship between different BSA concentrations and ΔI_{pc} values. The results indicated that the change in the ΔI_{pc} responses has a non-linear relationship with the BSA concentrations. The logarithmic value of the BSA concentrations was plotted against the ΔI_{pc} values to obtain the linear relationship, as presented in the inset of Figure 33B. This discovery revealed that the calibration curve was obtained in the range of 1 – 500 mg dL^{-1} (y = -20.199x + 0.7704 with a correlation coefficient (r^2) of 0.9904). The limit of detection ($3SD_{blank}/slope$) and the limit of quantification ($10SD_{blank}/slope$) from a calculation were found to be 0.072 and 0.24 mg dL^{-1}, respectively. These findings demonstrated that the EC redox cycling process can

achieve highly sensitive and quantitative detection of BSA over a wide linear range. Table 10 presents the comparison of the analytical performance between the proposed method and those of some previous reports for albumin detection found in the literature. According to this information, our assay proposed the detection of BSA using non-modified graphene electrodes fabricated on a paper substrate for the first time, which have the advantages of cost-effectiveness, simple disposability, and uncomplicated operation. Furthermore, the proposed method was very compelling for rapid detection in clinical applications, so that the performance of this proposed sensor would be sufficient for the detection of BSA in real urine samples.

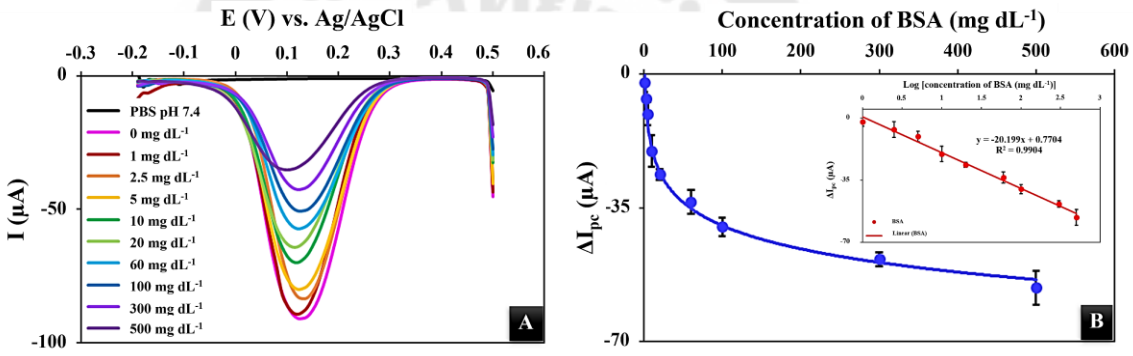

Figure 33 (A) Differential pulse voltammograms for different BSA concentrations mixed with 4 mM $[Fe(CN)_6]^{3-}$ and 0.05 mM MB in PBS (pH 7.4). (B) The ΔI_{pc} of BSA on ePADs at different concentrations (1 to 500 mg dL^{-1}). Inset: Calibration curve plotted on a logarithmic scale. BSA concentrations: 1, 2.5, 5, 10, 20, 60, 100, 300, and 500 mg dL^{-1}.

Table 10 Comparison of the analytical performance between the proposed method and other reports based on electrochemical techniques for the detection of albumin.

Biosensor	Measured solution	Detected technique	Detection limit (mg dL^{-1})	Linear range (mg dL^{-1})	Ref.
In situ Hg film/SPCE	Cd^{2+} releasing from CdSe/ZnS QDs labeled antibody	SWSV	5.0×10^{-6}	5.0×10^{-6} – 5.0×10^{-3}	(Pinwattana et al., 2010)
Anti-HSA/COOH-P-SPCE	0.1 M $[Fe(CN)_6]^{3-}$	CA	0.097	0.1 – 3.0	(Tsai et al., 2016)
Anti-BSA/MoS_2/SPAuE	5 mM $[Fe(CN)_6]^{3-/4-}$	CV	6.0×10^{-8}	1.0×10^{-7} – 1.0×10^{-4}	(Kukkar et al., 2016)
Anti-HSA/AuNPs/P*p*PD/PEDOT:PSS-Fc/SPCE	HSA	DPV	5.4×10^{-12}	1.0×10^{-11} – 1.0×10^{-4}	(Choosang et al., 2020)
Amaranth/SPCE	4 mM $[Fe(CN)_6]^{3-}$	CV	0.1	0.1 – 40	(Tseng et al., 2021)
Anti-HSA/COOH-P-SPCE	10 mM $[Fe(CN)_6]^{3-/4-}$	DPV	0.63	0.1 – 3.0	(Jia et al., 2022)
ePAD (unmodified graphene as WE)	4 mM $[Fe(CN)_6]^{3-}$ and 0.05 MB	DPV	0.072	1 – 500	This work

COOH-P-SPCE: Carboxyl porous screen-printed carbon electrode; SPAuE: Screen-printed gold electrode; P*p*PD: Poly(*para*-phenylenediamine); PEDOT: Poly(3,4-ethylenedioxythiophene); PSS: Poly(styrenesulfonate); Fc: Ferrocene

The reproducibility of this device was also investigated using three different concentrations of BSA standard solution (10, 80, and 400 mg dL^{-1}) mixed with 4 mM $[Fe(CN)_6]^{3-}$ and 0.05 mM MB in PBS (pH 7.4). For each mixture solution, nine sensors (*n* = 9) were examined, and the electrochemical measurements were then performed using the DPV technique. The relative standard deviations were found to be in the range of 3.38% – 6.26%, indicating that good device-to-device reproducibility with low variation was obtained for BSA detection.

4.2.5 Interference study

The influence of some possible interfering substances found in urine samples on the detection of BSA using the EC redox cycling process was investigated using the DPV technique under optimal conditions to elucidate the selectivity of the proposed assay. The redox cycling solution (4 mM $[Fe(CN)_6]^{3-}$ and 0.05 mM MB) containing 50 mg dL^{-1} BSA standard solution was detected via DPV measurement using ePADs, in which the signal current was set to 100%. The freshly prepared mixture solutions containing the redox cycling solution, 50 mg dL^{-1} BSA standard solution, and some foreign substances were successively detected under the same DPV conditions. The interfering substances used for this study were 400 µg dL^{-1} dopamine, 30 mg dL^{-1} ascorbic acid, 85 mg dL^{-1} uric acid, 500 mg dL^{-1} Na^+, K^+, NH_4^+, Mg^{2+}, Ca^{2+}, SO_4^{2-}, glucose, creatinine, and 2000 mg dL^{-1} urea, which are the maximum concentrations found in the samples (Krieg, Gunsser, Steinhagen-Thiessen, & Becker, 1986) (Roe & Hall, 1939) (Pagana & Pagana, 2007). The cathodic response of solution in the absence of foreign species was used to normalize the signal currents of solutions containing interferences. Figure 34 shows that the changes in the cathodic current of BSA containing interferences were less than ±5%, indicating that foreign species had no significant effect on the signal current of the redox cycling solution containing BSA. These findings confirmed the good selectivity of developed redox probes for albumin detection in the presence of various possibly interfering substances.

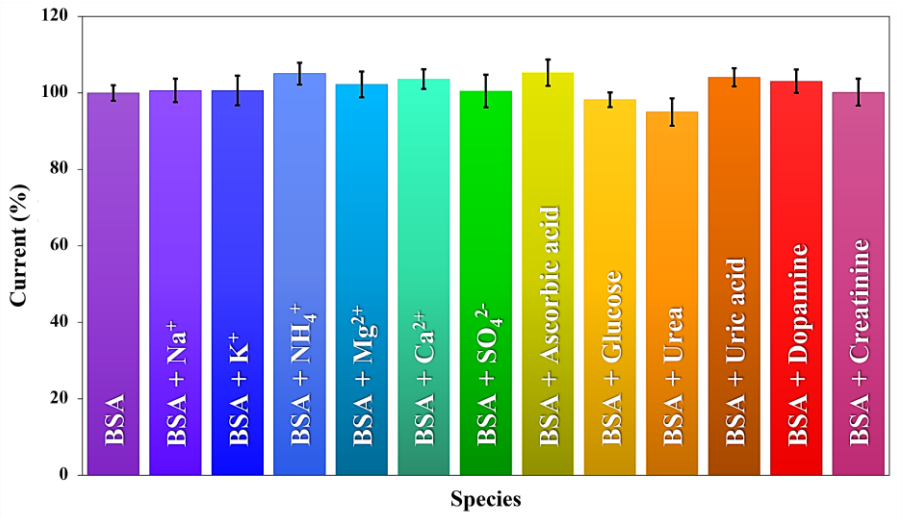

Figure 34 Effect of some interfering substances on the detection of 50 mg dL^{-1} BSA standard solution mixed with 4 mM $[Fe(CN)_6]^{3-}$ and 0.05 mM MB (n = 3).

4.2.6 Dilution effect

Because urine contains a highly variable matrix that may affect albumin detection, the influence of dilution effect was investigated to ensure accurate quantification. Various dilution ratios of a real urine sample containing 50 mg dL^{-1} BSA standard solution with redox cycling solution (4 mM $[Fe(CN)_6]^{3-}$ and 0.05 mM MB) were examined for recovery tests. We selected PBS (pH 7.4) as a diluent solution for BSA detection in this experiment. Table 11 presents that a dilution of at least 50-fold resulted in a good recovery, indicating that interferences in urine would be eliminated during albumin detection. This discovery suggested that a 50-fold dilution using PBS (pH 7.4) could avoid a variety of interferences and dilution effects in urine samples. As a result, urine samples are diluted at 50-fold with PBS (pH 7.4) before analysis.

Table 11 Recovery values of 50 mg dL^{-1} BSA detection in a real urine sample using different dilution factors (n = 3).

Dilution factor	Recovery (%)
0	128.95 ± 1.94
10	111.84 ± 3.98
25	106.86 ± 2.70
50	100.54 ± 4.83
100	100.90 ± 4.31

4.2.7 Matrix effect

A matrix-matched calibration was performed using a 50-fold diluted urine sample (where no albumins were present by precipitation with 0.1 M $CuSO_4$) to assess the matrix effect for this proposed method. The matrix effect (Sang et al., 2019) was calculated by the following relationship (Equation (19)):

$$Matrix\ effect = \left(\frac{A}{B} - 1\right) \times 100\% \quad \text{.....Equation (19)}$$

where *A* denoted the slope of calibration curve in matrix (diluted urine) and *B* denoted the slope of calibration curve in solvent (PBS pH 7.4).

In this study, BSA concentrations ranging from 1 to 500 mg dL^{-1} were spiked directly into diluted urine samples. The solutions were then mixed with 4 mM $[Fe(CN)_6]^{3-}$ and 0.05 mM MB. DPV measurements were used to detect the signal currents of these mixture solutions. Because of the different batch of fabricated ePADs, normalized currents ($I_{normalized}$) of cathodic responses were then calculated using the following relationship (Equation (20)):

$$I_{normalized} = \frac{I - I_{min}}{I_{max} - I_{min}} \quad \text{.....Equation (20)}$$

where *I* was the cathodic peak current of a solution containing different concentrations of BSA. The maximum and minimum cathodic peak currents obtained from each calibration data set were denoted by I_{max} and I_{min}, respectively.

Subsequently, $I_{normalized}$ values were plotted against the same logarithmic value of BSA concentrations as used for the external calibration curve. As presented in Figure 35, the matrix effect was found to be -15.17%, indicating that the proposed sample dilution is capable of removing interferences in urine due to a matrix effect value of approximately |15%| (Wan et al., 2018). This finding demonstrated that the matrix effect was negligible, implying that the matrix-matched calibration would not be required because the 50-fold dilution of urine not only eliminated interfering substances but also decreased the matrix in the sample. A sample matrix had no significant effect on the detection of BSA in a real sample; thus, the redox cycling solution can be used to accurately detect albumin in complex biological samples.

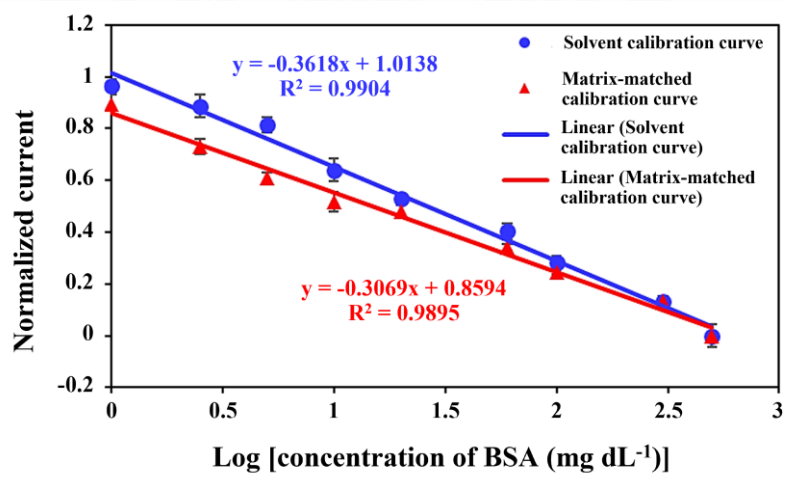

Figure 35 Comparison of a solvent calibration curve with a matrix-matched calibration curve for BSA detection (n = 3).

4.2.8 Application in real urine samples

The detection of albumin in 13 urine samples obtained from healthy volunteers was evaluated to demonstrate the practical application of this developed assay. All samples were diluted 50-fold in PBS (pH 7.4) before being mixed with 4 mM $[Fe(CN)_6]^{3-}$ and 0.05 mM MB. These solutions were then performed by DPV measurement

using ePADs, and the amount of albumin in the samples was calculated using the linear equation of the standard calibration curve. The recovery study was investigated to verify the accuracy and reliability by adding the known concentration of 50 mg dL^{-1} BSA standard solution into diluted samples. The results summarized in Table 12 indicate that good recovery values were obtained in the range of 96.04% – 104.60%. Moreover, the results obtained using the proposed method were validated by comparing them with the standard Bradford assay. The calculated *t*-value (0.86) was less than the critical *t*-value (2.18) for a two-tailed comparison; the results revealed that the albumin concentrations obtained using this method and those using the standard method were not significantly different. These results indicated the accuracy and reliability of albumin detection in urine samples without creatinine correction. As a result, albumin detection using a mixture solution of $[Fe(CN)_6]^{3-}$ and MB as a redox probe could be a powerful alternative tool for point-of-care testing of urinary albumin in the early stages of kidney disease.

Table 12 Recovery values of albumin detection in real urine samples obtained using the proposed method and the standard method (n = 3).

Sample	Added (mg dL^{-1})	Proposed method			Found from standard method (mg dL^{-1})*
		Found (mg dL^{-1})	Recovery (%)	RSD (%)	
Urine 1	0	< LOD	-	-	0.45 ± 0.020
	50	50.85 ± 1.74	101.70	2.98	50.54 ± 0.039
Urine 2	0	< LOD	-	-	3.18 ± 0.040
	50	50.78 ± 1.06	101.56	1.83	52.63 ± 0.035
Urine 3	0	< LOD	-	-	2.82 ± 0.06
	50	48.02 ± 2.20	96.04	3.78	50.82 ± 0.73
Urine 4	0	< LOD	-	-	0.59 ± 0.0052
	50	50.88 ± 0.15	101.77	0.37	50.05 ± 0.016
Urine 5	0	< LOD	-	-	2.92 ± 0.013
	50	49.30 ± 2.40	98.60	4.45	50.45 ± 0.013
Urine 6	0	< LOD	-	-	0.13 ± 0.014
	50	50.63 ± 1.00	101.27	1.92	48.46 ± 0.0062
Urine 7	0	< LOD	-	-	2.59 ± 0.0025
	50	50.88 ± 2.62	101.77	4.90	50.87 ± 0.011
Urine 8	0	< LOD	-	-	0.80 ± 0.0042
	50	49.46 ± 0.78	98.91	1.51	48.76 ± 0.025

Table 12 (Continued)

Sample	Added (mg dL^{-1})	Proposed method			Found from standard method (mg dL^{-1})*
		Found (mg dL^{-1})	Recovery (%)	RSD (%)	
Urine 9	0	< LOD	-	-	1.16 ± 0.0018
	50	48.26 ± 1.25	96.51	2.86	50.30 ± 0.010
Urine 10	0	< LOD	-	-	0.44 ± 0.0021
	50	49.06 ± 1.54	98.11	3.14	50.51 ± 0.0046
Urine 11	0	< LOD	-	-	0.72 ± 0.0067
	50	49.41 ± 1.70	98.82	3.41	50.95 ± 0.014
Urine 12	0	< LOD	-	-	0.99 ± 0.0042
	50	52.30 ± 1.66	104.60	3.22	50.05 ± 0.017
Urine 13	0	< LOD	-	-	0.49 ± 0.0017
	50	51.01 ± 2.31	102.02	5.18	51.39 ± 0.0053

*Bradford assay was used as the standard method

4.3 The development of a new sensing device for detecting L-hydroxyproline using a screen-printed graphene electrode coated with bismuth film and poly(L-hydroxyproline)

4.3.1 Characterization of bare and modified electrodes

4.3.1.1 Morphological characterization

Bare (without Poly(Hyp)/BiF) and modified (with Poly(Hyp)/BiF) electrodes were characterized by FEG-SEM to investigate their surface morphology, as presented in Figure 36. The low magnification (5,000X) of SEM images of the modified electrodes showed a rough and crumbling graphene sheet, indicating that BiF and Poly(Hyp) successfully covered the graphene surface. To explain the features of each modifier, a high magnification (50,000X) was applied to reveal more details of the electrode surface. Results showed that the sensor modified only BiF and Poly(Hyp) generated thin films over the graphene electrode (Figures 36D and 36F). Moreover, the modification of both BiF and Poly(Hyp) created cavities of porous structure (Figures 36H and 36J), indicating a high surface-to-volume ratio (Bollella, 2020). In this case, the as-synthesized Poly(Hyp)/BiF/SPGE (Figure 36J) produced a thin layer with uniform sponge-like cavities; meanwhile, BiF/Poly(Hyp)/SPGE (Figure 36H) produced a disordered and heterogeneous porous surface. These results indicated that the modification order affected the electrode morphology, possibly resulting in the difference in the electrochemical signal of each modified electrode.

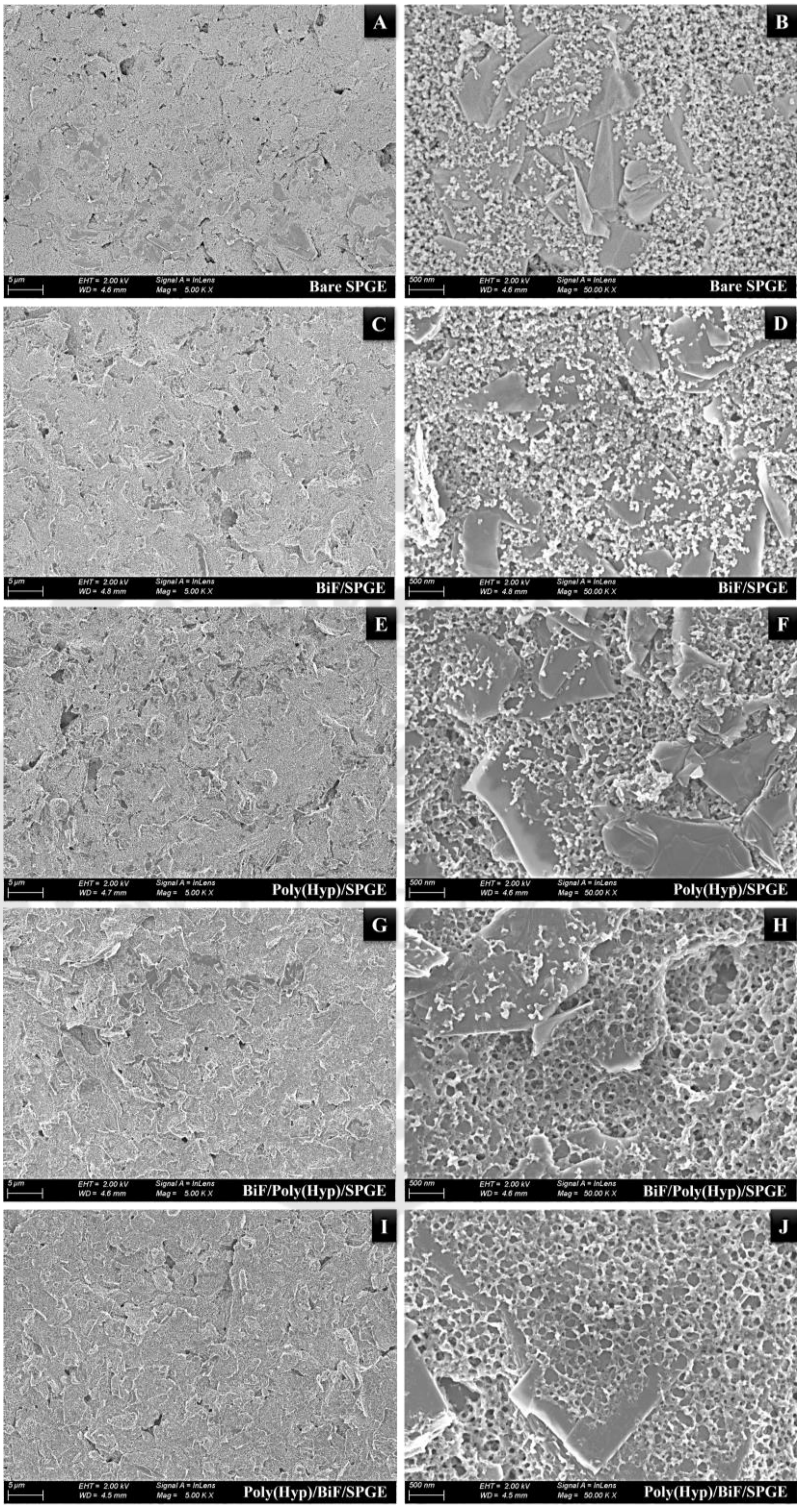

Figure 36 FEG-SEM images of the surface of bare and modified SPGEs at low (A, C, E, G, I) and high (B, D, F, H, J) magnification. Specific modification is annotated on each image.

To confirm the presence of BiF and Poly(Hyp) on the electrode surface, we employed EDX analysis and Fourier-transform infrared (FTIR) spectroscopy, as displayed in Figure 37. The elemental analysis of the Poly(Hyp)/BiF/SPGE was investigated by EDX spectroscopy (Figure 37A), which showed significant intensities of carbon (C), nitrogen (N), oxygen (O), and bismuth (Bi). The results indicated that the Bi intensity was caused by the formation of BiF (Bartlett et al., 2013), while the intensities obtained for C, N, and O belonged to the L-Hyp molecule, which was used as a monomer to synthesize Poly(Hyp). These findings suggest that a layer of BiF and Poly(Hyp) was produced on the graphene surface.

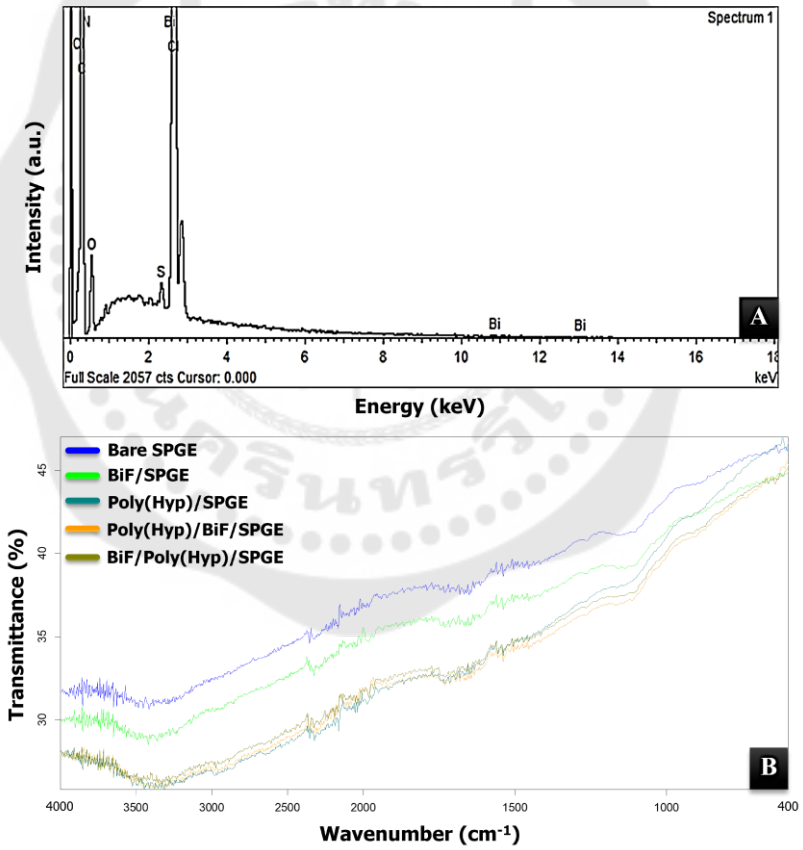

Figure 37 (A) The EDX analysis of the Poly(Hyp)/BiF/SPGE. (B) FTIR spectra obtained from bare and modified electrodes.

To predict the functional groups present on each electrode surface, we further investigated FTIR analysis, as depicted in Figure 37B. The results indicated that the spectra of with and without Poly(Hyp)/BiF onto electrode surfaces showed the same peaks in every frequency range, suggesting that the results may not differ significantly. The layer of BiF and Poly(Hyp) was formed as a thin film covering the graphene surface, making it difficult to clearly observe characteristic peaks or bands. Therefore, the intensity of each spectrum was considered to identify each electrode surface.

All spectra showed broad peaks at the wavenumber 3,600 – 3,100 cm^{-1}, which belonged to the O-H stretching vibrations. Compared to the bare electrode and BiF/SPGE, an increased intensity of Poly(Hyp)-based sensors was also observed, which was supposed to be hydroxyl groups of L-Hyp residues of the polymer. Further confirmation of Poly(Hyp) was observed at wavenumbers of 3,000 – 2,500 cm^{-1} and 1,700 – 1,600 cm^{-1}. The first frequency range is attributed to the ammonium salt structure due to the protonated form of L-Hyp molecules at pH 7.0, while the latter possibly belonged to amide functional groups of the polymer (Puska, Yli-Urpo, Vallittu, & Airola, 2016). For the BiF investigation, the increased intensity of BiF-based electrodes at the wavenumber 700 – 400 cm^{-1} was assumed to be the vibration of bismuth and other atoms, such as Bi-O (Astuti et al., 2016). These EDX and FTIR results confirm the formation of BiF and Poly(Hyp) deposited on the graphene surface.

The explanation for the formation mechanism of BiF and Poly(Hyp) was discussed as follows. First, the BiF was electrodeposited using 10 mg L^{-1} Bi(III) solution in 0.1 M HCl by applying a constant potential of -0.8 V for 180 s, as the I-t curve shown in Figure 38A. This step causes Bi(III) to be rapidly reduced to Bi(0), which will deposit on an electrode surface. This reaction generated a thin layer covering the SPGE surface, resulting in the BiF/SPGE. After that, the Poly(Hyp) was electropolymerized using 5 mM L-Hyp solution in PBS pH 7.0 by cycling a potential range of +0.5 to +2.0 V (vs. Ag/AgCl) at a scan rate of 50 mV s^{-1} for 10 cycles. The smooth and thin film was observed on BiF/SPGE surface (Figures 36I and 36J), indicating the successful electrode modification of Poly(Hyp). None of the previous reports described the modification of Poly(Hyp) on the

electrode surface. Therefore, the mechanism of Poly(Hyp) growth may be explained by the basis of poly(proline) (Poly(Pro)) because Hyp is one of the derivatives of Pro (Arslan & Çakır, 2014). The cyclic voltammogram of L-Hyp electropolymerization on BiF/SPGE was shown in Figure 38B. None of the peaks were obtained in the first cycle, which means L-Hyp possibly did not occur in an electrochemical reaction. The second cycle provided an oxidation peak at +1.27 V, relating to the free radical of L-Hyp (Yu & Chen, 2006) (Pushpanjali, Manjunatha, & Srinivas, 2020). Then, the produced radical was attached to BiF/SPGE surface, possibly by forming the bismuth-oxygen linkage. After that, the attached molecule interacts with another L-Hyp molecule by forming the peptide bond with the removal of the water molecule, and this process continues. After finishing cycle scanning, Poly(Hyp) was obtained by coating on BiF/SPGE. When the number of cycles increased, the current of the oxidation peak at +1.27 V decreased and maintained constant at the fifth cycle, indicating the formation of polymer film at the electrode surface.

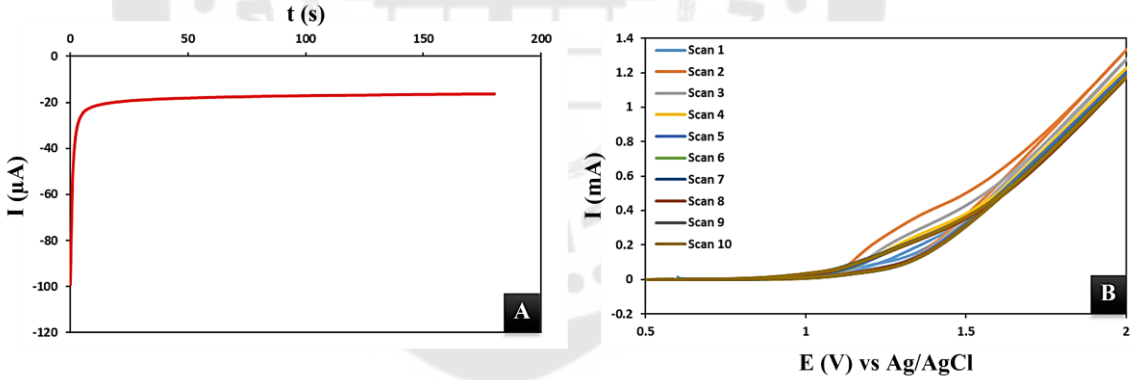

Figure 38 (A) The I-t curve for the electrodeposition of BiF at SPGE. (B) Cyclic voltammograms for the electropolymerization of Poly(Hyp) at BiF/SPGE.

4.3.1.2 Electrochemical characterization

Cyclic voltammograms of 0.1 M KCl containing 5 mM $[Fe(CN)_6]^{3-/4-}$ as electroactive species recorded at bare and modified electrodes are presented in Figure 39A. The redox couple exhibited a peak potential separation (ΔE_p) of 0.54, 0.39, 0.30,

0.28, and 0.34 V at bare SPGE, BiF/SPGE, Poly(Hyp)/SPGE, Poly(Hyp)/BiF/SPGE, and BiF/Poly(Hyp)/SPGE, respectively. Regarding the peak current (I_p), the redox species detected from modified electrodes exhibited higher currents than those detected from the bare electrode. The decreasing ΔE_p and increasing I_p indicated that the performance of Poly(Hyp)/BiF/SPGE was better than that of other electrodes for the oxidation/reduction of the $[Fe(CN)_6]^{3-/4-}$ probe. Furthermore, the calculation of the electroactive surface area of bare and modified electrodes is presented as follows. The Randles-Sevcik equation (Equation (16)) was used to calculate the electroactive surface area of bare and modified electrodes using $[Fe(CN)_6]^{3-/4-}$ as the redox species.

$$I_p = (2.69 \times 10^5) n^3 A D_0^{1/2} \nu^{1/2} C_0^* \quad \text{.....Equation (16)}$$

where I_p is the peak current obtained from the CV curves (A), n is the number of electrons transferred during the redox event (n = 1), A is the electroactive surface area (cm^2), D_0 is the diffusion coefficient of $[Fe(CN)_6]^{3-/4-}$ (7.6×10^{-6} cm^2 s^{-1}), ν is the scan rate (V s^{-1}), and C_0^* is the concentration of $[Fe(CN)_6]^{3-/4-}$ (5.0×10^{-6} mol cm^{-3}). The relationship between I_p and $\nu^{1/2}$ on each electrode was plotted to obtain the slope.

Based on the known parameters, the calculated electroactive surface area of each electrode was as follows: 0.116 cm^2 for bare SPGE, 0.136 cm^2 for BiF/SPGE, 0.189 cm^2 for Poly(Hyp)/SPGE, 0.191 cm^2 for Poly(Hyp)/BiF/SPGE, and 0.171 cm^2 for BiF/Poly(Hyp)/SPGE. The results showed that modified electrodes provided larger electroactive surface areas than the bare electrode, indicating that BiF and Poly(Hyp) can improve the electron transfer process. The SPGE modified with BiF and Poly(Hyp) to obtain Poly(Hyp)/BiF/SPGE provides the largest electroactive surface area of 0.191 cm^2, indicating its capability to be a candidate sensor for Hyp detection.

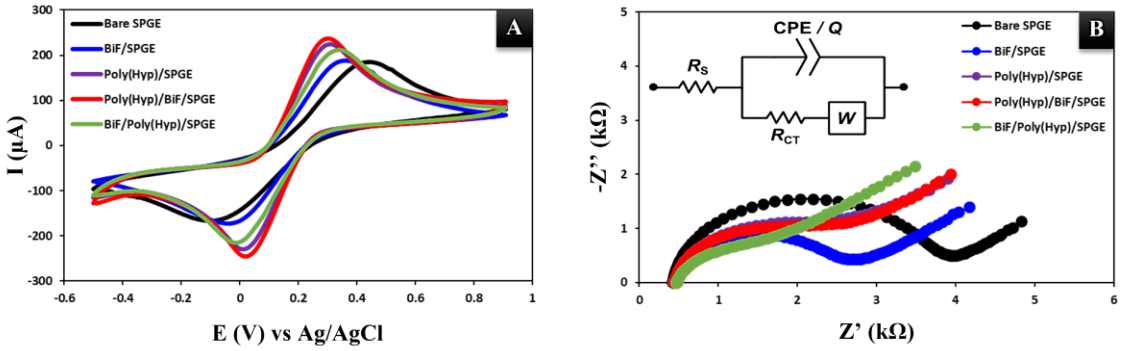

Figure 39 (A) Cyclic voltammograms of 5 mM $[Fe(CN)_6]^{3-/4-}$ in 0.1 M KCl recorded at bare and modified SPGEs. (B) Nyquist plots of bare and modified SPGEs.

To confirm the successful formation of BiF and Poly(Hyp), EIS is a powerful technique for studying the electrochemical properties on the electrode surface. Figure 39B shows the Nyquist plots obtained from the EIS study of bare and modified electrodes using 0.1 M KCl containing 5 mM $[Fe(CN)_6]^{3-/4-}$ as the redox species. The Nyquist plots contain a semicircular section and a linear section. The semicircular section observed at a higher frequency domain corresponds to the electron transfer process, and the linear section observed at a lower frequency domain corresponds to the diffusion process. The diameter of the semicircle equals the charge transfer resistance (R_{ct}) of the electrode surface, and this value depends on the dielectric and insulating properties of the electrode/electrolyte solution interface (Li, Xie, & Li, 2011). The semicircles obtained from modified electrodes are smaller than that of the bare electrode, indicating that the bare electrode has a higher R_{ct} value than modified electrodes. By fitting the data to the equivalent circuit, the R_{ct} values were obtained as shown in Table 13. The results indicated that bare SPGE has a higher electron transfer resistance than modified electrodes. The capacitances in terms of the CPE (Q_{dl}) of all electrodes were also recorded by the EIS software, as shown in Table 13. The electronic properties of the interface may not be sufficiently described by the ideal capacitive element, particularly when the electrode surface has a roughness or porosity. Then, CPE (Q_{dl}), non-ideal capacitance, has to be introduced instead of the ideal electrical double layer capacitance (C_{dl}) (Zheng,

Goonetilleke, Pettit, & Roy, 2010). Table 13 shows that modified electrodes have higher CPE values than bare SPGE possibly because of the increase in the dielectric constant, conductivity, and porosity. This finding can be attributed to the grafting of charged polymer and metal-based material onto the electrode surface (Hafaid et al., 2009). These results could be another criterion to support the performance of Poly(Hyp)/BiF/SPGE in enhancing the oxidation current of Hyp detection.

Table 13 Charge transfer resistances (R_{ct}) and component phase elements (CPE) of bare and modified electrodes.

Electrodes	R_{ct} (kΩ)	CPE (μF)
Bare SPGE	3.76	2.71
BiF/SPGE	2.39	3.48
Poly(Hyp)/SPGE	3.54	50.60
Poly(Hyp)/BiF/SPGE	3.42	84.35
BiF/Poly(Hyp)/SPGE	3.14	43.48

4.3.2 Optimization of BiF and Poly(Hyp) formation

4.3.2.1 BiF optimization

Given the modification of BiF on bare SPGE using the electrodeposition method, the accumulation of the Bi(III) precursor on the electrode surface depended on the Bi(III) concentration, deposition potential, and deposition time. Therefore, the parameters for detecting Hyp on Poly(Hyp)/BiF/SPGE were optimized. During the optimization process, the conditions for the electropolymerization of Poly(Hyp) were constant, whereas those for the formation of BiF were varied. To obtain the highest response for Hyp detection, the optimized parameters for DPV measurements were considered, as shown in Figure 40. The results indicated that suitable BiF growth was

accomplished using a 10 mg L^{-1} Bi(III) solution in 0.1 M HCl at a fixed potential of -0.8 V for 180 s.

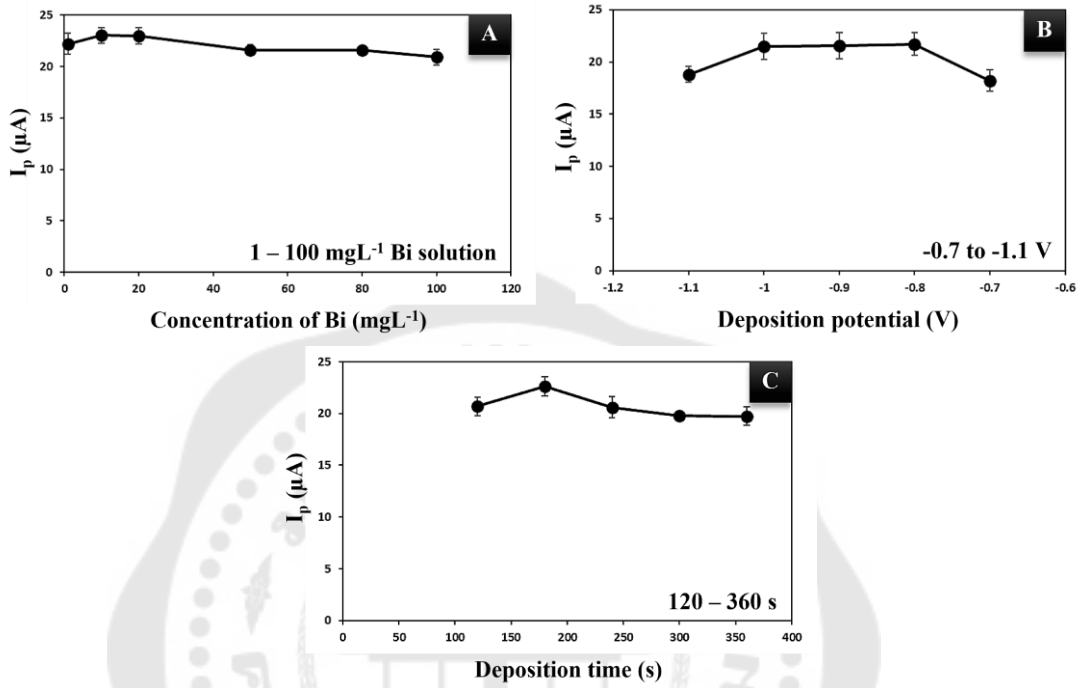

Figure 40 The effect of (A) Bi(III) concentration, (B) deposition potential, and (C) deposition time for 10 mM Hyp detection on Poly(Hyp)/BiF/SPGE sensors (*n* = 3).

4.3.2.2 Poly(Hyp) optimization

The CV technique was used to perform the electropolymerization of Poly(Hyp) onto the BiF/SPGE surface. Thus, the parameters related to polymer film formation were also investigated because they would affect the current response of the target analyte. So that the conditions, namely the concentration of Hyp as a monomer, applied potential range, scan rate, and number of scans, were optimized by detecting Hyp on Poly(Hyp)/BiF/SPGE. The conditions for the electrodeposition of BiF were constant, whereas those for the formation of Poly(Hyp) formation were varied. Then, the prepared sensors were applied to measure the DPV responses of Hyp, as depicted in Figure 41. The results indicated that the appropriate Poly(Hyp) growth was accomplished

using 5 mM Hyp in PBS pH 7.0 with a potential range of +0.5 to +2.0 V at a scan rate of 50 mVs^{-1} for 10 polymerization cycles.

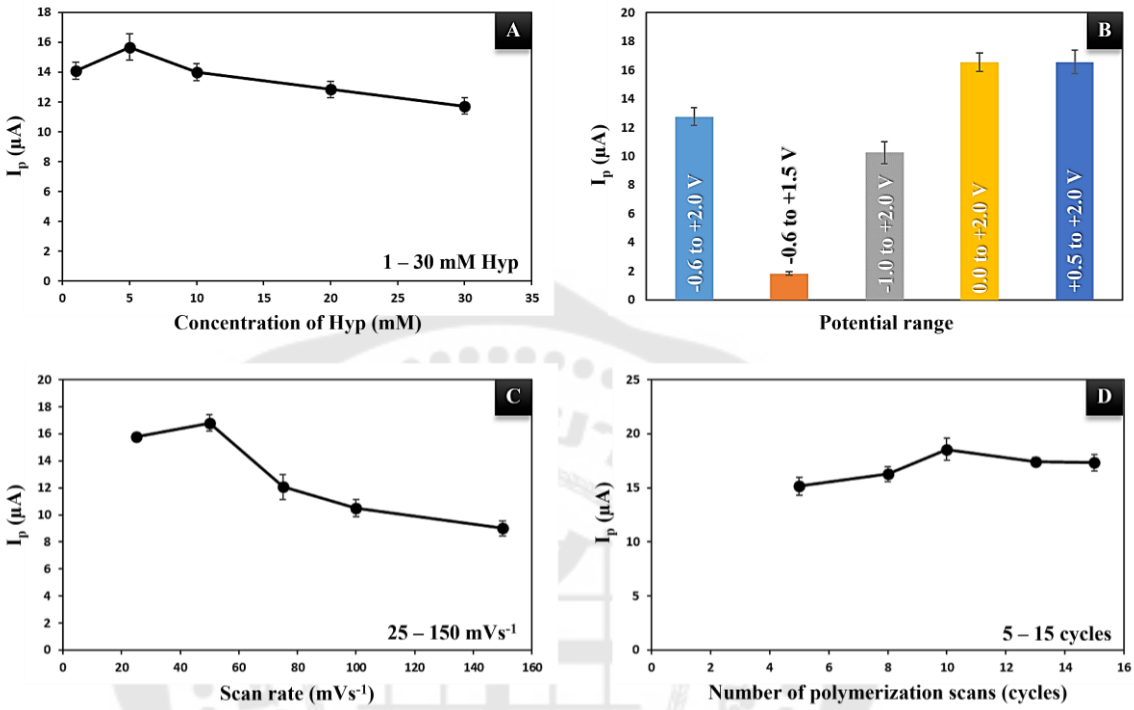

Figure 41 The effect of (A) Hyp monomer concentration, (B) applied potential range, (C) scan rate, and (D) number of polymerization cycles for 10 mM Hyp detection on Poly(Hyp)/BiF/SPGE sensors (n = 3).

4.3.3 Electrochemical behavior of Hyp on different electrodes

The electrochemical responses obtained from Hyp detection on bare and modified electrodes were investigated using the CV and DPV techniques. Modified electrodes were fabricated under optimized conditions. Figure 42A presents the CV curves of Hyp on different SPGEs. The results showed that the oxidation peaks varied in the potential range of +1.2 to +1.5 V, depending on the electrodes. The bare SPGE and BiF/SPGE exhibited low anodic peaks at the potentials of +1.46 and +1.45 V, respectively. By contrast, Poly(Hyp)-based electrodes exhibited high oxidation peaks with less positive

potentials of +1.25 V for Poly(Hyp)/SPGE, +1.24 V for Poly(Hyp)/BiF/SPGE, and +1.21 V for BiF/Poly(Hyp)/SPGE. The results obtained from DPV measurements corresponded to those obtained from CV. As shown in Figure 42B, the oxidation potential of each electrode shifted negatively in the following order: +1.20 V for bare SPGE, +1.10 V for BiF/SPGE, +0.90 V for Poly(Hyp)/SPGE, +0.87 V for Poly(Hyp)/BiF/SPGE, and +0.90 V for BiF/Poly(Hyp)/SPGE. The low anodic peak potential can confirm that BiF and Poly(Hyp) could act as electrocatalysts for Hyp detection. The difference in anodic peak current (ΔI_{pa}) measured in the Hyp solution subtracted from that measured in the PBS solution was also investigated. The ΔI_{pa} values obtained from modified electrodes were higher than that obtained from the bare electrode, indicating that BiF and Poly(Hyp) can improve the electron transfer efficiency. However, the modification order of BiF and Poly(Hyp) also significantly affected the Hyp response. BiF/Poly(Hyp)/SPGE exhibited a lower ΔI_{pa} value than Poly(Hyp)/BiF/SPGE because of its higher background current. This can be supposed that the BiF layer might hinder the electrical conductivity of Poly(Hyp) toward Hyp detection, resulting in low sensitivity. Thus, Poly(Hyp)/BiF/SPGE is a suitable electrode for Hyp detection and will be used for further measurements.

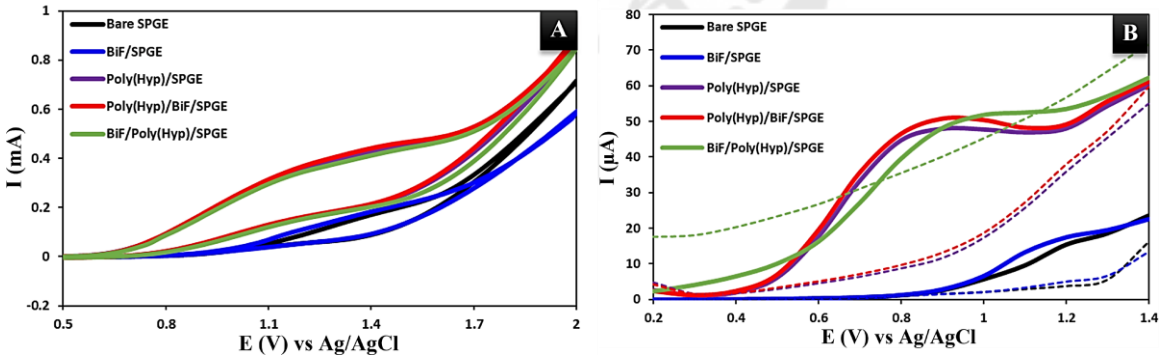

Figure 42 (A) CV curves of 20 mM Hyp and (B) DPV curves of PBS pH 7.0 in the absence (dash line) and presence (solid line) of 10 mM Hyp obtained from bare and modified SPGEs.

4.3.4 Electrochemical behavior of Hyp on Poly(Hyp)/BiF/SPGE

Hyp oxidation on Poly(Hyp)/BiF/SPGE was further investigated using the CV technique with different scan rates, as illustrated in Figure 43A. The results showed that the anodic peak current increases with the increase in scan rates. Furthermore, the anodic peak potential shifted to a positive direction, indicating the irreversible process of Hyp on the proposed electrode. To study the mass transfer kinetics of Hyp at the electrode interface, the slope value of the logarithmic plots of the difference in anodic peak current (Log ΔI_{pa}) vs. the scan rate (Log v) was obtained, as shown in the inset of Figure 43A. The slope value was determined to be 0.49, which is close to the anticipated value of 0.5, confirming that the oxidation process of Hyp on Poly(Hyp)/BiF/SPGE was diffusion-controlled. Moreover, Andrieux and Savèant's theoretical model (Equation (15)) was used to calculate the diffusion coefficient (D_0) of Hyp by plotting the square root of the scan rates ($v^{1/2}$) against the difference in anodic peak current (ΔI_{pa}), as shown in Figure 43B.

$$\Delta I_{pa} = 0.496FAC_sD_0^{1/2}\left(\frac{F}{RT}\right)^{1/2}v^{1/2} \quad \text{.....Equation (15)}$$

where F is Faraday's constant (96,485.339 C mol^{-1}), A is the electroactive surface area (0.191 cm^2), C_s is the Hyp concentration (20 × 10^{-6} mol cm^{-3}), R is the gas constant (8.31447 J K^{-1} mol^{-1}), and T is the temperature (295.15 K). Using the slope of this relationship, the D_0 value of Hyp was determined to be 1.32 × 10^{-6} cm^2 s^{-1}. Afterward, the number of electrons transferred at the electrode interface (n) was calculated using Equation (17).

$$\Delta I_{pa} = (2.99\ x\ 10^5)n[(1-\alpha)n_\alpha]^{1/2}AC_sD_0^{1/2}v^{1/2} \quad \text{.....Equation (17)}$$

The factor (1-α)n_α was calculated based on Laviron's theory by plotting the relationship between the natural logarithm of the scan rates (Ln. v) and the anodic peak potentials (E_{pa}) (y = 0.0722x + 1.5308). Using the slope of this relationship, the factor (1-α)n_α was determined to be 0.352. Then, the number of transferred electrons can be estimated to be 1.69 or ~2.

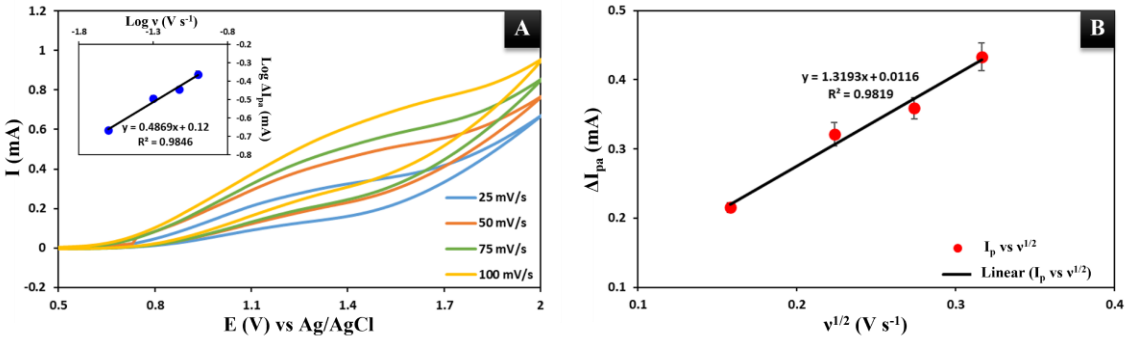

Figure 43 (A) CV curves of 20 mM Hyp in PBS pH 7.0 at Poly(Hyp)/BiF/SPGE using different scan rates (the inset exhibits the logarithmic plots between the different anodic peak current and the scan rate). (B) The relationship between $v^{1/2}$ and ΔI_{pa} values (n = 3).

The influence of pH on Hyp oxidation was also investigated using PBS with different pH values. This study calculated the number of protons involved on the electrode surface. Figure 44A depicts the CV responses of Hyp on Poly(Hyp)/BiF/SPGE in the pH range of 5.0 to 9.0, showing that the E_{pa} value decreased with the increase in pH value. Then, this relationship was plotted, as shown in Figure 44B (blue square dots), following the Nernst equation (Equation (21)) (Dai, Crawford, Song, Fisher, & Lawrence, 2015):

$$E_{pa} = E^{0}_{formal} - 2.303\left(\frac{mRT}{nF}\right)pH \quad \text{.....Equation (21)}$$

where m and n are the numbers of protons and electrons involved on the electrode interface, respectively. Using the slope obtained from this relationship, the number of protons can be calculated as 0.86 or ~1. Hence, the mechanism of Hyp oxidized on Poly(Hyp)/BiF/SPGE involves two electrons and one proton. Figure 45 presents the possible reaction of Hyp oxidation on the proposed electrode.

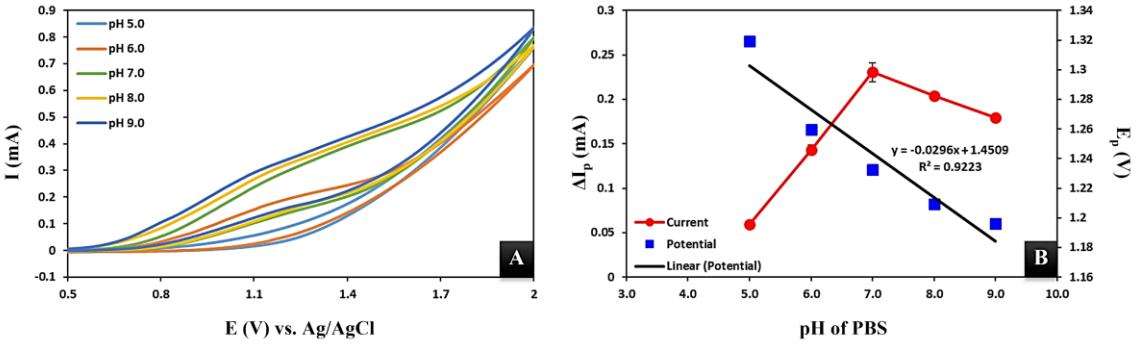

Figure 44 (A) CV curves of 20 mM Hyp in different pH values. (B) The relationship of ΔI_{pa} and E_{pa} of 20 mM Hyp in different pH values (n = 3).

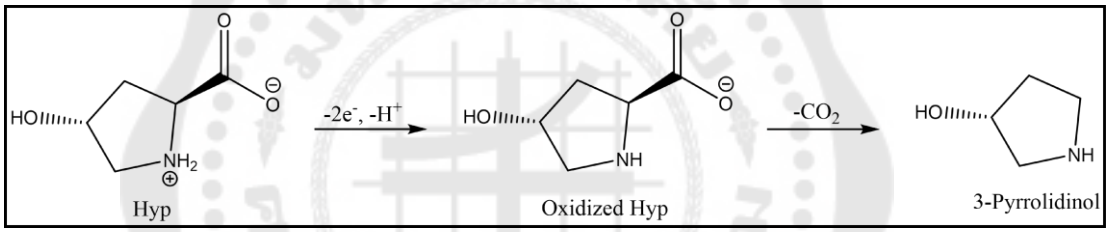

Figure 45 The possible reaction of Hyp oxidation in PBS pH 7.0 at the Poly(Hyp)/BiF/SPGE.

Furthermore, the ΔI_{pa} values were plotted against the pH values of PBS, as presented in Figure 44B (the red curve), indicating that the highest ΔI_{pa} value was observed at pH 7.0. The results indicated that the signal first increased from acidic (pH 5.0 and 6.0) to neutral (pH 7.0) pH and then decreased when Hyp dissolved in basic electrolytes (pH 8.0 and 9.0). This behavior explained that the Hyp structure contains carboxyl and amino functional groups. When the pH value was changed from 5.0 to 7.0, we believed the deprotonation of Hyp occurred, facilitating the oxidation process. Thus, the peak current increased. Further adjusting the pH to an alkaline value affected the decreasing responses because of the formation of the conjugate base. Therefore, Hyp

quantification should be performed under physiological pH conditions, making it suitable for the analysis of body fluids, such as blood, saliva, and urine.

4.3.5 Optimization of DPV conditions

DPV was performed as a detection technique for the quantitative analysis of Hyp. DPV parameters, such as step potential, pulse potential, and pulse time, were optimized because they affected the analytical performance of the proposed sensor. While the optimization of the investigated parameter was performed, the other parameters were kept constant. The step potential, pulse potential, and pulse time were studied in the range of 0.025 to 0.2 V, 0.05 to 0.25 V, and 0.05 to 0.25 s, respectively. As shown in Figure 46, the results indicated that a step potential of 0.025 V, a pulse potential of 0.2 V, and a pulse time of 0.15 s were suitable conditions depending on the highest ΔI_{pa} value. After that, these parameters were used to detect 1 mM Hyp, and the obtained results were compared to those before optimization. The results in Figure 46D showed that the optimized parameters used for Hyp detection provided a 5.66-fold higher ΔI_{pa} value, indicating that a higher sensitivity should be obtained. Therefore, the DPV quantification and the application of real sample analysis were studied under these optimal conditions.

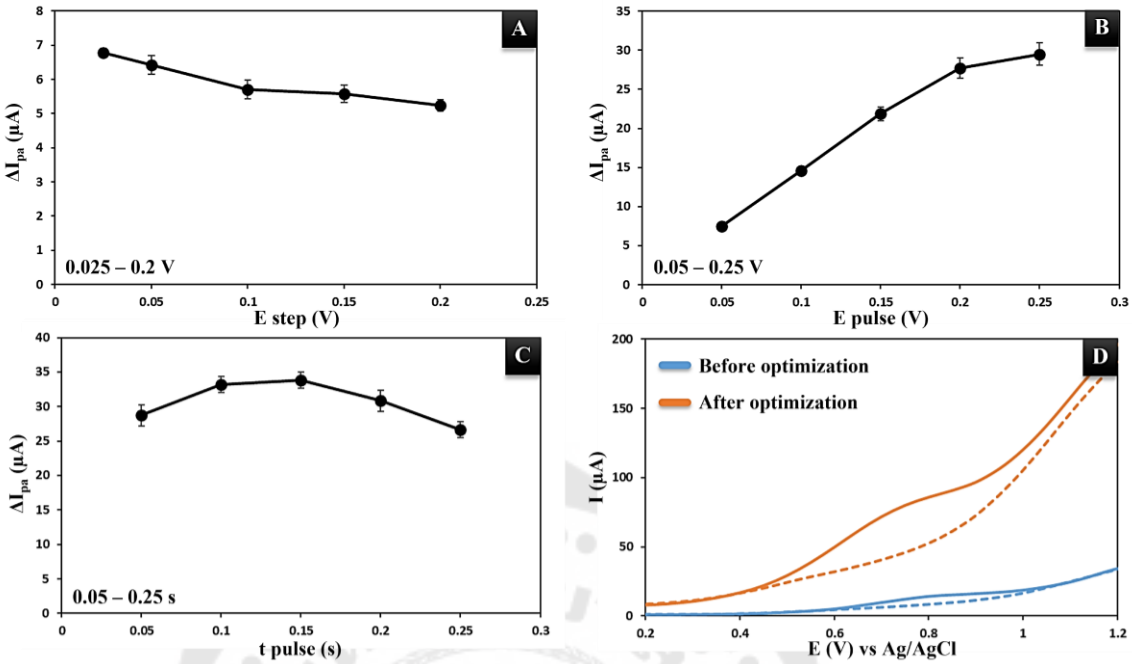

Figure 46 The optimization of DPV parameters, such as (A) step potential, (B) pulse potential, and (C) pulse time, from the detection of 1 mM Hyp on Poly(Hyp)/BiF/SPGE (*n* = 3). (D) DP voltammograms of PBS pH 7.0 in the presence (solid line) and absence (dash line) of 1 mM Hyp before (blue curve) and after (orange curve) DPV optimization.

4.3.6 Analytical performance

The differential pulse voltammograms of different Hyp concentrations prepared in PBS pH 7.0 are displayed in Figure 47A, showing that the peak current increased with the increase in concentration. A linear curve was obtained by plotting the ΔI_{pa} values and the known Hyp concentrations. As shown in Figure 47B, a good linear relationship was detected in the range of 0.01 to 5.0 mM with a linear regression (r^2) of 0.9974. The LOD value for Hyp detection was determined to be 9.21 μM, calculated from $3SD_{blank}/slope$. The obtained analytical performance was compared with that of previous works, as shown in Table 14. The data showed that the LOD value of the proposed electrode was not the lowest. However, the wide linear range covered the low and high Hyp contents in biological samples, being the major advantage of this work. Moreover, the proposed nonenzymatic sensor can be simply fabricated by two-step modification

within 13 min, resulting in a stable and controllable composite on the electrode surface. The as-synthesized composite does not require any pretreatment step before use. Thus, these outstanding features lead to the possibility of being a valuable and practical Hyp sensor for real applications.

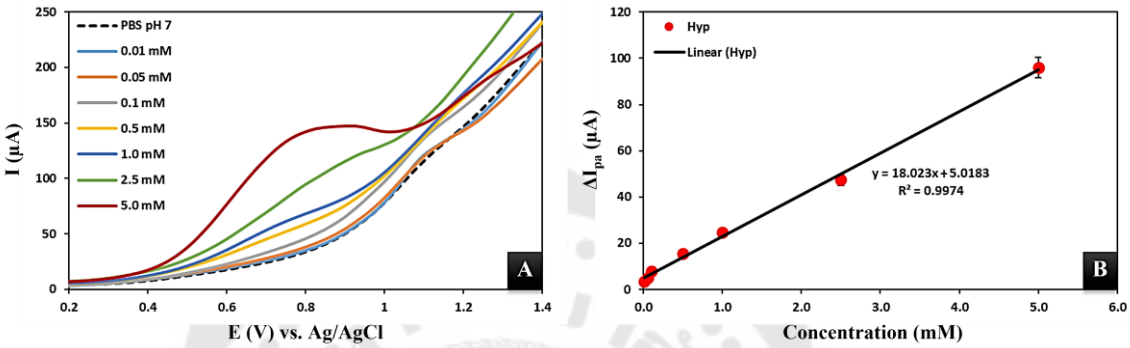

Figure 47 (A) Differential pulse voltammograms obtained from Poly(Hyp)/BiF/SPGEs recorded in the absence (dash curve) and presence (solid curve) of 0.01 – 5.0 mM Hyp in PBS pH 7.0. (B) The linear relationship between ΔI_{pa} values and various Hyp concentrations.

Table 14 Comparison of the analytical performance between the proposed sensor and previous reported sensors based on electrochemical Hyp detection.

Method	Sensor	Linear range	LOD	Ref.
CA	L-HypE and D-HypDH/SPCE*	10 – 100 µM	2.4 µM	(Sakamoto et al., 2015)
DPV	AuNPs/GCE	1 – 100 mM	0.28 mM	(Durairaj et al., 2020)
EIS	MIP/SPCE	3.05 – 190.65 µM	0.99 µM	(Jesadabundit et al., 2021)
DPV	Poly(Hyp)/BiF/SPGE (This work)	0.01 – 5.0 mM	9.21 µM	This work

*Screen-printed carbon electrode modified with L-hydroxyproline epimerase and D-hydroxyproline dehydrogenase

Reproducibility and stability were also investigated. The relative standard deviation (RSD) values for Hyp detection at concentrations of 0.1, 0.5, and 1.0 mM using 10 different electrodes were reported as reproducibility. The results revealed good reproducibility with RSD values of 4.88%, 4.06%, and 3.78%. Furthermore, the stability of the proposed sensor was examined after storing the prepared modified electrodes at room temperature. As shown in Figure 48, the ΔI_{pa} value was stable within 12 days, with the percentage of the decreased signal less than 3.02%. The results showed that good stability was obtained even though the sensors were kept under normal conditions. Hence, the proposed electrode can be an alternative sensor for Hyp detection in real-world applications.

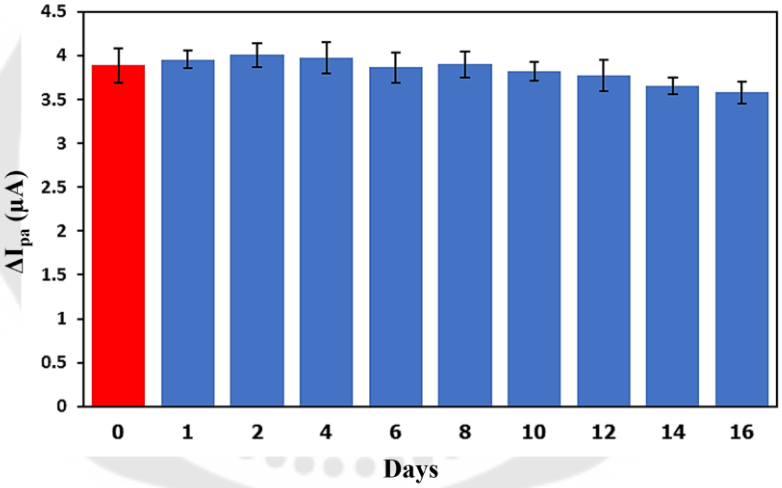

Figure 48 CA responses of 0.5 mM Hyp obtained from Poly(Hyp)/BiF/SPGE sensors (*n* = 4) that were stored within 0 – 16 days.

4.3.7 Interference study

To evaluate the selectivity toward Hyp detection, the effect of interferences was investigated by measuring 0.5 mM Hyp in the presence of some possible interfering substances detected in urine, possibly providing the electrochemical signal in the oxidative direction. In this case, the interfering compounds were 0.025 mM dopamine,

0.05 mM proline, 0.1 mM uric acid, 0.25 mM ascorbic acid, 0.5 mM NaCl, 5 mM $NaHCO_3$, 5 mM urea, 5 mM creatinine, 5 mM glucose, and 300 mg L^{-1} albumin, which are the maximum concentrations detected in the urine of normal human subjects (Yomthiangthae, Chailapakul, & Siangproh, 2022) (Wenjing Zhang et al., 2018). Figure 49 presents the effect of foreign substances of interest on the Poly(Hyp)/BiF/SPGE sensor, showing no significant changes in the ΔI_{pa} values (less than ±5%). The results indicated that interfering substances did not affect Hyp detection. As a result, the proposed platform provided good selectivity and could be further applied for practical use.

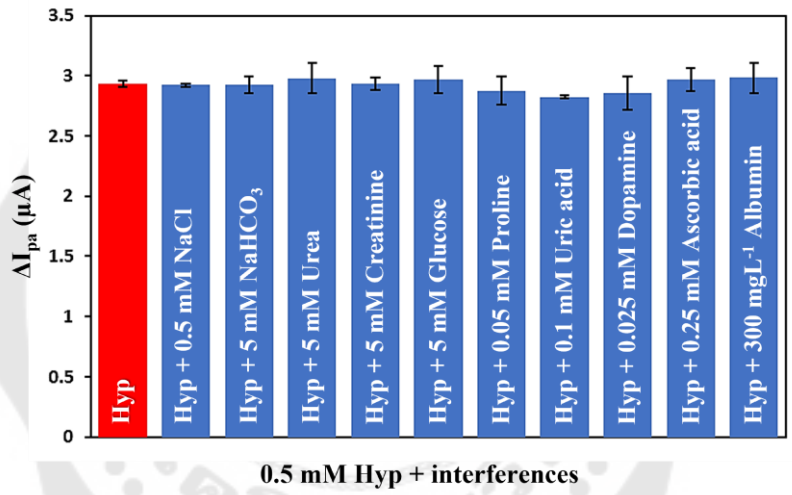

Figure 49 The interference study of the proposed sensor for the Hyp detection (0.5 mM) in the presence of some possible interfering substances (n = 3).

4.3.8 Application in real samples

To verify the practicality of Poly(Hyp)/BiF/SPGE, Hyp detection in real human urine was conducted. The standard addition method was used to measure the Hyp concentration in samples by spiking different known concentrations, as shown in Table 15. The recovery and RSD values were calculated to evaluate the accuracy and precision, obtaining acceptable values from 96.20% to 102.68% with a deviation of less than 4.4%. These results confirmed that the fabricated Poly(Hyp)/BiF/SPGE could be used as an

alternative platform for Hyp analysis without any enzymes or complex modification protocols.

Table 15 The practical application of the Poly(Hyp)/BiF/SPGE for the Hyp detection in human urine samples (n = 3).

Gender	Sample	Added (mM)	Found (mM)*	Recovery (%)	RSD (%)
Male	Urine 1	0	-	-	-
		0.05	0.048 ± 0.18	96.20	3.42
		1	1.02 ± 0.81	101.85	3.24
	Urine 2	0	-	-	-
		0.05	0.051 ± 0.20	102.67	3.77
		1	0.99 ± 0.99	99.29	4.33
	Urine 3	0	-	-	-
		0.05	0.048 ± 0.29	96.94	4.13
		1	0.98 ± 0.32	98.01	1.40
Female	Urine 4	0	-	-	-
		0.05	0.050 ± 0.27	100.54	3.72
		1	1.00 ± 0.26	99.70	1.11
	Urine 5	0	-	-	-
		0.05	0.050 ± 0.28	100.54	3.91
		1	0.98 ± 0.25	97.61	1.11
	Urine 6	0	-	-	-
		0.05	0.050 ± 0.21	99.61	2.92
		1	1.03 ± 0.33	102.68	1.39

*Found concentration ± SD.

CHAPTER 5
Conclusions and future works

5.1 Conclusions

This dissertation presented the development of electroanalytical methods used for the application of food quality control and clinical diagnosis. In particular, the focus was on miniaturized electrochemical devices as sensing platforms for detecting analytes of interest. The downsizing of bulky devices, along with simple fabrication procedures and the use of low-cost materials, had led them to be easy-to-use sensors with economic benefits. The compatibility of these devices with portable instrumentation can significantly reduce the need for laboratory-scale equipment, making them suitable for field analysis and resource-limited settings. This development serves as a driving force behind the creation of effective sensors for various electroanalytical applications. For the specific conclusion, it can be summarized as follows:

5.1.1 The development of a simple electrochemical approach for the simultaneous detection of vitamin B_2, vitamin B_6, and vitamin C using a modifier-free screen-printed carbon electrode

A simple and cost-effective SPCE was developed for the simultaneous detection of water-soluble vitamins, namely VB_2, VC, and VB_6. The measurement of these vitamins at a modifier-free SPCE was performed for the first time. The proposed electrode offered several advantages over conventional modified electrodes such as disposability, simple fabrication, elimination of electrode maintenance, and low solution volume requirement. The effect of various supporting electrolytes was systematically studied to elucidate the electrochemical behavior of the vitamins. Under optimal conditions, using PBS pH 3.5 as a suitable supporting electrolyte, the SPCE exhibited good sensitivity, selectivity, and reproducibility for the simultaneous detection of VB_2, VC, and VB_6 in the oxidative direction. Finally, the proposed procedure was applied for the simultaneous detection of these vitamins in mixed vegetable fruit juice as well as artificial urine, yielding

satisfactory results. Therefore, this proposed assay can be considered a promising and attractive choice for the simultaneous detection of water-soluble vitamins in food and clinical samples.

5.1.2 The development of a simple and rapid detection approach for urinary albumin on a disposable paper-based analytical device using an electrochemical-chemical redox cycling process

A disposable paper-based device was successfully developed to detect urinary albumin using a powerful EC redox cycling process for the first time. This process involved the use of a mixture of two electroactive species, namely $[Fe(CN)_6]^{3-}$ and MB, which generated a large electrochemical signal without requiring any modification to the working electrode. The albumin detection strategy was based on the indirect detection method, which involved the decrement of cathodic current in the presence of the target analyte. Under optimized conditions, the calibration curve showed a linear relationship between the difference in the cathodic peak current (ΔI_{pc}) and the logarithmic concentration of BSA standard solution within a wide range of 1 to 500 mg dL^{-1}. The detection and quantification limits were determined to be 0.072 and 0.24 mg dL^{-1}, respectively, and the method demonstrated good reproducibility for detection with the RSDs lower than 6.3%. Moreover, the developed method exhibited good selectivity for albumin detection in an environment of interferences; thus, it was successfully applied to detect albumin in real urine samples without creatinine correction, yielding desirable results. The simplicity of operation, cost-effectiveness of paper-based devices, and a short measurement time of 1 min were the major advantages of this procedure. Therefore, this redox cycling process offered a promising system for point-of-care testing and can be adapted in the future for the simple and highly sensitive detection of other biomolecules.

5.1.3 The development of a new sensing device for detecting L-hydroxyproline using a screen-printed graphene electrode coated with bismuth film and poly(L-hydroxyproline)

A concept for fabricating a novel material that served as a sensing platform for Hyp analysis in biological fluids was developed. The material was made by combining BiF and Poly(Hyp) on the SPGE surface. Among the various modification combinations, the Poly(Hyp)/BiF/SPGE sensor was fabricated using a two-step process: (1) the electrodeposition of BiF using a Bi(III) solution and (2) the electropolymerization of Poly(Hyp) using a L-Hyp solution. The morphology of the synthesized material was found to be a sponge-like thin film with a uniform distribution of electroactive cavities on the graphene surface. This structure provided a large area for interaction with the substance of interest, leading to enhanced sensitivity in detection. Electrochemical characterization confirmed that the proposed electrode had a larger electroactive surface area than the electrode without modifiers, facilitating the electrochemical reaction. The analytical performance of the proposed sensor was investigated by DPV, revealing a wide linear range with a low limit of detection. This sensing platform also demonstrated good reproducibility, stability, and selectivity for Hyp detection. In practical applications, the developed sensor was used to quantify Hyp in human urine samples, yielding satisfactory results. Therefore, this facilely synthesized material can lead to the development of an enzyme-free biosensor that could serve as a valuable sensing platform for Hyp detection in the clinical field. This could enable the screening and detection of collagen metabolism abnormalities, bone disorders, and other related diseases.

5.2 Future works

Although the electrochemical detections presented in this dissertation are simple, rapid, and effective, certain limitations in analytical performance must be addressed. For example, the sensitivity of the sensor can be enhanced by modifying the electrode surface with conductive materials, such as nanomaterials, metal alloys, and polymers. Such an effort could result in a new and powerful sensing device for the

sensitive detection of analytes of interest. The selectivity of the method can also be improved by using specific recognition between target analytes and certain substances such as reagents and antibodies. Moreover, the separation of analytes on a single miniaturized device is a promising strategy to improve selectivity, as it reduces the influence of unpredictable interferences that may be present in the sample. This solution has the potential to eliminate sample preparation steps, making analytical methods more convenient and powerful. Thus, these motivations provide new challenges for a wide range of electroanalytical applications in the future.

REFERENCES

Abano, E. E., & Godbless Dadzie, R. (2014). Simultaneous detection of water-soluble vitamins using the High Performance Liquid Chromatography (HPLC) - a review. *Croatian Journal of Food Science and Technology, 6*(2), 116-123. doi:10.17508/cjfst.2014.6.2.08

Anothaisintawee, T., Rattanasiri, S., Ingsathit, A., Attia, J., & Thakkinstian, A. (2009). Prevalence of chronic kidney disease: a systematic review and meta-analysis. *Clinical Nephrology, 71*(03), 244-254. doi:10.5414/cnp71244

Ansar, M. M., ShahrokhiRad, R., & Lebady, M. K. (2016). Risk Factors of Microalbuminuria and Macroalbuminuria in Type 2 Diabetic Patients in North of Iran - Rasht. *Nephro-Urology Monthly, 9*(1). doi:10.5812/numonthly.40031

Antuña-Jiménez, D., González-García, M. B., Hernández-Santos, D., & Fanjul-Bolado, P. (2020). Screen-Printed Electrodes Modified with Metal Nanoparticles for Small Molecule Sensing. *Biosensors, 10*(2). doi:10.3390/bios10020009

AOAC International. (1995). Official methods of analysis of AOAC International. In (pp. volumes (loose-leaf)). Arlington, Va.: AOAC International.

Arduini, F., Cinti, S., Scognamiglio, V., Moscone, D., & Palleschi, G. (2017). How cutting-edge technologies impact the design of electrochemical (bio)sensors for environmental analysis. A review. *Analytica Chimica Acta, 959*, 15-42. doi:10.1016/j.aca.2016.12.035

Arslan, E., & Çakır, S. (2014). A novel palladium nanoparticles-polyproline-modified graphite electrode and its application for determination of curcumin. *Journal of Solid State Electrochemistry, 18*(6), 1611-1620. doi:10.1007/s10008-014-2382-6

Assaf, H. F., Shamroukh, A. A., Rabie, E. M., & Khodari, M. (2023). Green synthesis of CaO nanoparticles conjugated with l-Methionine polymer film to modify carbon paste electrode for the sensitive detection of levofloxacin antibiotic. *Materials Chemistry and Physics, 294*. doi:10.1016/j.matchemphys.2022.127054

Astuti, Y., Fauziyah, A., Nurhayati, S., Wulansari, A. D., Andianingrum, R., Hakim, A. R., & Bhaduri, G. (2016). Synthesis of α-Bismuth oxide using solution combustion method and its photocatalytic properties. *IOP Conference Series: Materials Science and Engineering, 107*. doi:10.1088/1757-899x/107/1/012006

Bartlett, P. N., Cook, D., de Groot, C. H., Hector, A. L., Huang, R., Jolleys, A., . . . Reid, G. (2013). Non-aqueous electrodeposition of p-block metals and metalloids from halometallate salts. *RSC Advances, 3*(36). doi:10.1039/c3ra40739j

Bergman, I., & Loxley, R. (1970). The determination of hydroxyproline in urine hydrolysates. *Clinica Chimica Acta, 27*(2), 347-349. doi:10.1016/0009-8981(70)90355-4

Bollella, P. (2020). Porous Gold: A New Frontier for Enzyme-Based Electrodes. *Nanomaterials, 10*(4). doi:10.3390/nano10040722

Boni, A. C., Wong, A., Dutra, R. A. F., & Sotomayor, M. D. P. T. (2011). Cobalt phthalocyanine as a biomimetic catalyst in the amperometric quantification of dipyrone using FIA. *Talanta, 85*(4), 2067-2073. doi:10.1016/j.talanta.2011.07.038

Boonkaew, S., Teengam, P., Jampasa, S., Rengpipat, S., Siangproh, W., & Chailapakul, O. (2020). Cost-effective paper-based electrochemical immunosensor using a label-free assay for sensitive detection of ferritin. *The Analyst, 145*(14), 5019-5026. doi:10.1039/d0an00564a

Bourgin, M., Kepp, O., & Kroemer, G. (2022). Immunostimulatory effects of vitamin B5 improve anticancer immunotherapy. *OncoImmunology, 11*(1). doi:10.1080/2162402x.2022.2031500

Bradford, M. M. (1976). A rapid and sensitive method for the quantitation of microgram quantities of protein utilizing the principle of protein-dye binding. *Analytical Biochemistry, 72*(1-2), 248-254. doi:10.1016/0003-2697(76)90527-3

Bruckner-Tuderman, L., & Bruckner, P. (1998). Genetic diseases of the extracellular matrix: more than just connective tissue disorders. *Journal of Molecular Medicine, 76*(3-4), 226-237. doi:10.1007/s001090050213

Buffle, J., & Tercier-Waeber, M. L. (2005). Voltammetric environmental trace-metal analysis and speciation: from laboratory to in situ measurements. *TrAC Trends in Analytical Chemistry, 24*(3), 172-191. doi:10.1016/j.trac.2004.11.013

Bujacz, A. (2012). Structures of bovine, equine and leporine serum albumin. *Acta Crystallographica Section D Biological Crystallography, 68*(10), 1278-1289. doi:10.1107/s0907444912027047

Bureau of Nutrition, D. o. H., Ministry of Public Health. (2020). *DIETARY REFERENCE INTAKE FOR THAIS 2020*: A.V. PROGRESSIVE LTD., PART.

Chauhan, D., Gupta, P. K., & Solanki, P. R. (2021). Amine Functionalized Noble Metal: Metal Oxide Nanohybrid for Efficient Electrochemical Determination of 25-Hydroxy Vitamin-D3 in Human Serum. *Journal of The Electrochemical Society, 168*(11). doi:10.1149/1945-7111/ac3116

Choosang, J., Thavarungkul, P., Kanatharana, P., & Numnuam, A. (2020). AuNPs/PpPD/PEDOT:PSS-Fc modified screen-printed carbon electrode label-free immunosensor for sensitive and selective determination of human serum albumin. *Microchemical Journal, 155*. doi:10.1016/j.microc.2020.104709

Christophers, E. (2001). Psoriasis – epidemiology and clinical spectrum. *Clinical and Experimental Dermatology, 26*(4), 314-320. doi:10.1046/j.1365-2230.2001.00832.x

Comper, W. D., & Osicka, T. M. (2005). Detection of urinary albumin. *Advances in Chronic Kidney Disease, 12*(2), 170-176. doi:10.1053/j.ackd.2005.01.012

Cremers, S., Garnero, P., & Seibel, M. J. (2008). Biochemical Markers of Bone Metabolism. In *Principles of Bone Biology* (pp. 1857-1881).

Cundy, T., Reid, I. R., & Grey, A. (2014). Metabolic bone disease. In *Clinical Biochemistry: Metabolic and Clinical Aspects* (pp. 604-635).

Dai, C., Crawford, L. P., Song, P., Fisher, A. C., & Lawrence, N. S. (2015). A novel sensor based on electropolymerized substituted-phenols for pH detection in unbuffered systems. *RSC Advances, 5*(126), 104048-104053. doi:10.1039/c5ra22595g

Delport, M., Maas, S., van der Merwe, S. W., & Laurens, J. B. (2004). Quantitation of hydroxyproline in bone by gas chromatography–mass spectrometry. *Journal of Chromatography B, 804*(2), 345-351. doi:10.1016/j.jchromb.2004.01.039

Durairaj, S., Sidhureddy, B., & Chen, A. (2020). Sensitive Electrochemical Analysis of Hydroxyproline in Achilles Tendon Collagen and Human Urine. *Journal of The Electrochemical Society, 167*(16). doi:10.1149/1945-7111/abcbb6

Dutta, G., & Lillehoj, P. B. (2018). Wash-free, label-free immunoassay for rapid electrochemical detection of PfHRP2 in whole blood samples. *Scientific Reports, 8*(1). doi:10.1038/s41598-018-35471-8

Elgrishi, N., Rountree, K. J., McCarthy, B. D., Rountree, E. S., Eisenhart, T. T., & Dempsey, J. L. (2017). A Practical Beginner's Guide to Cyclic Voltammetry. *Journal of Chemical Education, 95*(2), 197-206. doi:10.1021/acs.jchemed.7b00361

Elzoghby, A. O., Samy, W. M., & Elgindy, N. A. (2012). Albumin-based nanoparticles as potential controlled release drug delivery systems. *Journal of Controlled Release, 157*(2), 168-182. doi:10.1016/j.jconrel.2011.07.031

Fassett, R. G., Venuthurupalli, S. K., Gobe, G. C., Coombes, J. S., Cooper, M. A., & Hoy, W. E. (2011). Biomarkers in chronic kidney disease: a review. *Kidney International, 80*(8), 806-821. doi:10.1038/ki.2011.198

Gliszczyńska-Świgło, A., & Rybicka, I. (2014). Simultaneous Determination of Caffeine and Water-Soluble Vitamins in Energy Drinks by HPLC with Photodiode Array and Fluorescence Detection. *Food Analytical Methods, 8*(1), 139-146. doi:10.1007/s12161-014-9880-0

Gomaa, E. A., Negm, A., & Abu-Qarn, R. M. (2018). Cyclic voltammetry study of the electrochemical behavior of vanadyl sulfate in absence and presence of antibiotic. *Measurement, 125*, 645-650. doi:10.1016/j.measurement.2018.05.046

González-Hernández, J., Alvarado-Gámez, A. L., Arroyo-Mora, L. E., & Barquero-Quirós, M. (2021). Electrochemical determination of novel psychoactive substances by differential pulse voltammetry using a microcell for boron-doped diamond

electrode and screen-printed electrodes based on carbon and platinum. *Journal of Electroanalytical Chemistry, 882*. doi:10.1016/j.jelechem.2021.114994

Gu, H.-Y., Yu, A.-M., & Chen, H.-Y. (2007). Electrochemical Behavior and Simultaneous Determination of Vitamin B2, B6, and C at Electrochemically Pretreated Glassy Carbon Electrode. *Analytical Letters, 34*(13), 2361-2374. doi:10.1081/al-100107301

Guo, L. (2021). Electrochemical sensors based on Au-PPy NPs@f-CNTs nanocomposite modified glassy carbon electrode for determination of Vitamin B12 as a key agent in human motion coordination. *International Journal of Electrochemical Science*. doi:10.20964/2021.10.31

Gutz, I. G. R. (2021). CurTiPot – pH and Acid–Base Titration Curves: Analysis and Simulation freeware, version 4.3.1. Retrieved from http://www.iq.usp.br/gutz/Curtipot_.html

Hafaid, I., Gallouz, A., Mohamed Hassen, W., Abdelghani, A., Sassi, Z., Bessueille, F., & Jaffrezic-Renault, N. (2009). Sensitivity Improvement of an Impedimetric Immunosensor Using Functionalized Iron Oxide Nanoparticles. *Journal of Sensors, 2009*, 1-12. doi:10.1155/2009/746548

Ho, P. C., & Palmer, D. A. (1995). *Electrical conductivity measurements of aqueous boric acid at 25--350{degree}C at saturation vapor pressure. Final report.* Retrieved from United States:

Hosseini, S. N., Pirsa, S., & Farzi, J. (2021). Biodegradable nano composite film based on modified starch-albumin/MgO; antibacterial, antioxidant and structural properties. *Polymer Testing, 97*. doi:10.1016/j.polymertesting.2021.107182

Huang, L., Tian, S., Zhao, W., Liu, K., & Guo, J. (2021). Electrochemical vitamin sensors: A critical review. *Talanta, 222*. doi:10.1016/j.talanta.2020.121645

Hušek, P., Pohlıdal, A. n., & Slabık, D. (2002). Rapid screening of urinary proline–hydroxyproline dipeptide in bone turnover studies. *Journal of Chromatography B, 767*(1), 169-174. doi:10.1016/s0378-4347(01)00558-8

Hutapea, T. P. H., Madurani, K. A., Syahputra, M. Y., Hudha, M. N., Asriana, A. N., Suprapto, & Kurniawan, F. (2023). Albumin: Source, preparation, determination, applications, and prospects. *Journal of Science: Advanced Materials and Devices, 8*(2). doi:10.1016/j.jsamd.2023.100549

Ingsathit, A., Thakkinstian, A., Chaiprasert, A., Sangthawan, P., Gojaseni, P., Kiattisunthorn, K., . . . Singh, A. K. (2009). Prevalence and risk factors of chronic kidney disease in the Thai adult population: Thai SEEK study. *Nephrology Dialysis Transplantation, 25*(5), 1567-1575. doi:10.1093/ndt/gfp669

Inoue, H., Iguch, H., Kouno, A., & Tsuruta, Y. (2001). Fluorometric determination of N-terminal prolyl dipeptides, proline and hydroxyproline in human serum by pre-column high-performance liquid chromatography using 4-(5,6-dimethoxy-2-phthalimidinyl)-2-methoxyphenylsulfonyl chloride. *Journal of Chromatography B: Biomedical Sciences and Applications, 757*(2), 369-373. doi:10.1016/s0378-4347(01)00162-1

Inzelt, G. (2014). Chronoamperometry, Chronocoulometry, and Chronopotentiometry. In *Encyclopedia of Applied Electrochemistry* (pp. 207-214).

Jamall, I. S., Finelli, V. N., & Que Hee, S. S. (1981). A simple method to determine nanogram levels of 4-hydroxyproline in biological tissues. *Analytical Biochemistry, 112*(1), 70-75. doi:10.1016/0003-2697(81)90261-x

Jashari, G., Kastrati, G., Korecká, L., Metelka, R., Sýs, M., & Ashrafi, A. M. (2021). Electrochemical Behaviour of Tocopherols: Possibilities of Their Simultaneous Voltammetric Detection. *Applied Sciences, 11*(17). doi:10.3390/app11178095

Jesadabundit, W., Jampasa, S., Patarakul, K., Siangproh, W., & Chailapakul, O. (2021). Enzyme-free impedimetric biosensor-based molecularly imprinted polymer for selective determination of L-hydroxyproline. *Biosensors and Bioelectronics, 191*. doi:10.1016/j.bios.2021.113387

Jia, Y., Liu, G., Xu, G., Li, X., Shi, Z., Cheng, C., . . . Liu, Q. (2022). Battery-free and wireless tag for in situ sensing of urinary albumin/creatinine ratio (ACR) for the

assessment of albuminuria. *Sensors and Actuators B: Chemical, 367*. doi:10.1016/j.snb.2022.132050

Jiang, G., Gu, X., Jiang, G., Chen, T., Zhan, W., & Tian, S. (2015). Application of a mercapto-terminated binuclear Cu(II) complex modified Au electrode to improve the sensitivity and selectivity for dopamine detection. *Sensors and Actuators B: Chemical, 209*, 122-130. doi:10.1016/j.snb.2014.11.109

Ju, H., Zhou, J., Cai, C., & Chen, H. (1995). The electrochemical behavior of methylene blue at a microcylinder carbon fiber electrode. *Electroanalysis, 7*(12), 1165-1170. doi:10.1002/elan.1140071213

Jun, J. Y., Nguyen, H. H., Paik, S.-Y.-R., Chun, H. S., Kang, B.-C., & Ko, S. (2011). Preparation of size-controlled bovine serum albumin (BSA) nanoparticles by a modified desolvation method. *Food Chemistry, 127*(4), 1892-1898. doi:10.1016/j.foodchem.2011.02.040

Kaewjua, K., & Siangproh, W. (2022). A novel tyramine sensing-based polymeric L-histidine film-coated screen-printed graphene electrode: Capability for practical applications. *Electrochimica Acta, 419*. doi:10.1016/j.electacta.2022.140388

Kamiński, J., Dymicka-Piekarska, V., Tomaszewska, J., Matowicka-Karna, J., & Koper-Lenkiewicz, O. M. (2020). Diagnostic utility of protein to creatinine ratio (P/C ratio) in spot urine sample within routine clinical practice. *Critical Reviews in Clinical Laboratory Sciences, 57*(5), 345-364. doi:10.1080/10408363.2020.1723487

KDOQI Clinical Practice Guideline for Diabetes and CKD: 2012 Update. (2012). *American Journal of Kidney Diseases, 60*(5), 850-886. doi:10.1053/j.ajkd.2012.07.005

Keane, W. F., & Eknoyan, G. (1999). Proteinuria, albuminuria, risk, assessment, detection, elimination (PARADE): A position paper of the National Kidney Foundation. *American Journal of Kidney Diseases, 33*(5), 1004-1010. doi:10.1016/s0272-6386(99)70442-7

Khaksari, M., Mazzoleni, L. R., Ruan, C., Kennedy, R. T., & Minerick, A. R. (2017). Data representing two separate LC-MS methods for detection and quantification of

water-soluble and fat-soluble vitamins in tears and blood serum. *Data in Brief, 11*, 316-330. doi:10.1016/j.dib.2017.02.033

Khamcharoen, W., Henry, C. S., & Siangproh, W. (2022). A novel l-cysteine sensor using in-situ electropolymerization of l-cysteine: Potential to simple and selective detection. *Talanta, 237*. doi:10.1016/j.talanta.2021.122983

Kordasht, H. K., Hasanzadeh, M., Seidi, F., & Alizadeh, P. M. (2021). Poly (amino acids) towards sensing: Recent progress and challenges. *TrAC Trends in Analytical Chemistry, 140*. doi:10.1016/j.trac.2021.116279

Kratz, F. (2008). Albumin as a drug carrier: Design of prodrugs, drug conjugates and nanoparticles. *Journal of Controlled Release, 132*(3), 171-183. doi:10.1016/j.jconrel.2008.05.010

Krejcova, L., Richtera, L., Hynek, D., Labuda, J., & Adam, V. (2017). Current trends in electrochemical sensing and biosensing of DNA methylation. *Biosensors and Bioelectronics, 97*, 384-399. doi:10.1016/j.bios.2017.06.004

Krieg, M., Gunsser, K. J., Steinhagen-Thiessen, E., & Becker, H. (1986). [Comparative quantitative clinico-chemical analysis of the characteristics of 24-hour urine and morning urine]. *J Clin Chem Clin Biochem, 24*(11), 863-869.

Kukkar, M., Sharma, A., Kumar, P., Kim, K.-H., & Deep, A. (2016). Application of MoS2 modified screen-printed electrodes for highly sensitive detection of bovine serum albumin. *Analytica Chimica Acta, 939*, 101-107. doi:10.1016/j.aca.2016.08.010

Kumar, R., Katoch, S. S., & Sharma, S. (2006). Beta-adrenoceptor agonist treatment reverses denervation atrophy with augmentation of collagen proliferation in denervated mice gastrocnemius muscle. *Indian J Exp Biol, 44*(5), 371-376.

Kumar Srivastava, A., Khare, P., Kumar Nagar, H., Raghuwanshi, N., & Srivastava, R. (2016). Hydroxyproline: A Potential Biochemical Marker and Its Role in the Pathogenesis of Different Diseases. *Current Protein & Peptide Science, 17*(6), 596-602. doi:10.2174/1389203717666151201192247

Labib, M., Sargent, E. H., & Kelley, S. O. (2016). Electrochemical Methods for the Analysis of Clinically Relevant Biomolecules. *Chemical Reviews, 116*(16), 9001-9090. doi:10.1021/acs.chemrev.6b00220

Lambers Heerspink, H. J., Brantsma, A. H., de Zeeuw, D., Bakker, S. J. L., de Jong, P. E., & Gansevoort, R. T. (2008). Albuminuria Assessed From First-Morning-Void Urine Samples Versus 24-Hour Urine Collections as a Predictor of Cardiovascular Morbidity and Mortality. *American Journal of Epidemiology, 168*(8), 897-905. doi:10.1093/aje/kwn209

Laviron, E. (1979). General expression of the linear potential sweep voltammogram in the case of diffusionless electrochemical systems. *Journal of Electroanalytical Chemistry and Interfacial Electrochemistry, 101*(1), 19-28. doi:10.1016/s0022-0728(79)80075-3

Li, J., Xie, H., & Li, Y. (2011). Fabrication of gold nanoparticles/polypyrrole composite-modified electrode for sensitive hydroxylamine sensor design. *Journal of Solid State Electrochemistry, 16*(2), 795-802. doi:10.1007/s10008-011-1431-7

Liu, G., Wang, Y. M., & Sun, D. M. (2015). Simultaneous determination of vitamins B2, B6 and C using silver-doped poly(L-arginine)-modified glassy carbon electrode. *Journal of Analytical Chemistry, 71*(1), 102-109. doi:10.1134/s1061934815120114

Liu, M., Li, X. C., Lu, L., Cao, Y., Sun, R. R., Chen, S., & Zhang, P. Y. (2014). Cardiovascular disease and its relationship with chronic kidney disease. *Eur Rev Med Pharmacol Sci, 18*(19), 2918-2926.

Lovander, M. D., Lyon, J. D., Parr, D. L., Wang, J., Parke, B., & Leddy, J. (2018). Critical Review—Electrochemical Properties of 13 Vitamins: A Critical Review and Assessment. *Journal of The Electrochemical Society, 165*(2), G18-G49. doi:10.1149/2.1471714jes

Lvovich, V. F. (2014). Electrochemical Impedance Spectroscopy (EIS) Applications to Sensors and Diagnostics. In *Encyclopedia of Applied Electrochemistry* (pp. 485-507).

Magar, H. S., Hassan, R. Y. A., & Mulchandani, A. (2021). Electrochemical Impedance Spectroscopy (EIS): Principles, Construction, and Biosensing Applications. *Sensors, 21*(19). doi:10.3390/s21196578

Mazzi, G., Fioravanzo, F., & Burti, E. (1996). New marker of bone resorption: hydroxyproline-containing peptide High-performance liquid chromatographic assay without hydrolysis as an alternative to hydroxyproline determination: a preliminary report. *Journal of Chromatography B: Biomedical Sciences and Applications, 678*(2), 165-172. doi:10.1016/0378-4347(95)00473-4

Mishra, V., & Heath, R. J. (2021). Structural and Biochemical Features of Human Serum Albumin Essential for Eukaryotic Cell Culture. *International Journal of Molecular Sciences, 22*(16). doi:10.3390/ijms22168411

Mogensen, C. E. (1984). Microalbuminuria Predicts Clinical Proteinuria and Early Mortality in Maturity-Onset Diabetes. *New England Journal of Medicine, 310*(6), 356-360. doi:10.1056/nejm198402093100605

Murphy, A., Gorey, B., de Guzman, K., Kelly, N., Nesterenko, E. P., & Morrin, A. (2015). Microfluidic paper analytical device for the chromatographic separation of ascorbic acid and dopamine. *RSC Advances, 5*(113), 93162-93169. doi:10.1039/c5ra16272f

Namazi, N., Heshmati, J., & Tarighat-Esfanjani, A. (2015). Supplementation with Riboflavin (Vitamin B2) for Migraine Prophylaxis in Adults and Children: A Review. *International Journal for Vitamin and Nutrition Research, 85*(1-2), 79-87. doi:10.1024/0300-9831/a000225

Nantaphol, S., Jesadabundit, W., Chailapakul, O., & Siangproh, W. (2019). A new electrochemical paper platform for detection of 8-hydroxyquinoline in cosmetics using a cobalt phthalocyanine-modified screen-printed carbon electrode. *Journal of Electroanalytical Chemistry, 832*, 480-485. doi:10.1016/j.jelechem.2018.11.055

Nie, T., Xu, J.-K., Lu, L.-M., Zhang, K.-X., Bai, L., & Wen, Y.-P. (2013). Electroactive species-doped poly(3,4-ethylenedioxythiophene) films: Enhanced sensitivity for

electrochemical simultaneous determination of vitamins B2, B6 and C. *Biosensors and Bioelectronics, 50*, 244-250. doi:10.1016/j.bios.2013.06.057

Nie, T., Zhang, K., Xu, J., Lu, L., & Bai, L. (2014). A facile one-pot strategy for the electrochemical synthesis of poly(3,4-ethylenedioxythiophene)/Zirconia nanocomposite as an effective sensing platform for vitamins B2, B6 and C. *Journal of Electroanalytical Chemistry, 717-718*, 1-9. doi:10.1016/j.jelechem.2014.01.006

Olmo, F., Rodriguez, A., Colina, A., & Heras, A. (2021). UV/Vis absorption spectroelectrochemistry of folic acid. *Journal of Solid State Electrochemistry, 26*(1), 29-37. doi:10.1007/s10008-021-05026-5

Pagana, K. D., & Pagana, T. J. (2007). *Mosby's diagnostic and laboratory test reference* (8th ed.). St. Louis, Mo.: Mosby Elsevier.

Pattanaprateep, O., Ingsathit, A., McEvoy, M., Attia, J., & Thakkinstian, A. (2018). Cost-Effectiveness Analysis of Renin-Angiotensin Aldosterone System Blockade in Progression of Chronic Kidney Disease. *Value in Health Regional Issues, 15*, 155-160. doi:10.1016/j.vhri.2017.12.011

Paudics, A., Hessz, D., Bojtár, M., Bitter, I., Horváth, V., Kállay, M., & Kubinyi, M. (2022). A pillararene-based indicator displacement assay for the fluorescence detection of vitamin B1. *Sensors and Actuators B: Chemical, 369*. doi:10.1016/j.snb.2022.132364

Pena-Pereira, F. (2014). From Conventional to Miniaturized Analytical Systems. In *Miniaturization in Sample Preparation* (pp. 1-28).

Picardo, M., & Taïeb, A. (2010). *Vitiligo*.

Piez, K. A., Eigner, E. A., & Lewis, M. S. (2002). The Chromatographic Separation and Amino Acid Composition of the Subunits of Several Collagens*. *Biochemistry, 2*(1), 58-66. doi:10.1021/bi00901a012

Pinwattana, K., Wang, J., Lin, C.-T., Wu, H., Du, D., Lin, Y., & Chailapakul, O. (2010). CdSe/ZnS quantum dots based electrochemical immunoassay for the detection of phosphorylated bovine serum albumin. *Biosensors and Bioelectronics, 26*(3), 1109-1113. doi:10.1016/j.bios.2010.08.021

Pinyorospathum, C., Rattanarat, P., Chaiyo, S., Siangproh, W., & Chailapakul, O. (2019). Colorimetric sensor for determination of phosphate ions using anti-aggregation of 2-mercaptoethanesulfonate-modified silver nanoplates and europium ions. *Sensors and Actuators B: Chemical, 290*, 226-232. doi:10.1016/j.snb.2019.03.059

Placer, L., Lavilla, I., Pena-Pereira, F., & Bendicho, C. (2023). A 3D microfluidic paper-based analytical device with smartphone-assisted colorimetric detection for iodine speciation in seaweed samples. *Sensors and Actuators B: Chemical, 377*. doi:10.1016/j.snb.2022.133109

Polkinghorne, K. R. (2006). Detection and measurement of urinary protein. *Current Opinion in Nephrology & Hypertension, 15*(6), 625-630. doi:10.1097/01.mnh.0000247502.49044.10

Porada, R., Fendrych, K., & Baś, B. (2021). Electrochemical sensor based on Ni-exchanged natural zeolite/carbon black hybrid nanocomposite for determination of vitamin B6. *Microchimica Acta, 188*(10). doi:10.1007/s00604-021-04992-x

Primpray, V., Chailapakul, O., Tokeshi, M., Rojanarata, T., & Laiwattanapaisal, W. (2019). A paper-based analytical device coupled with electrochemical detection for the determination of dexamethasone and prednisolone in adulterated traditional medicines. *Analytica Chimica Acta, 1078*, 16-23. doi:10.1016/j.aca.2019.05.072

Puangjan, A., Chaiyasith, S., Taweeporngitgul, W., & Keawtep, J. (2017). Application of functionalized multi-walled carbon nanotubes supporting cuprous oxide and silver oxide composite catalyst on copper substrate for simultaneous detection of vitamin B2, vitamin B6 and ascorbic acid. *Materials Science and Engineering: C, 76*, 383-397. doi:10.1016/j.msec.2017.03.040

Pushpanjali, P. A., Manjunatha, J. G., & Srinivas, M. T. (2020). Highly sensitive platform utilizing poly(l-methionine) layered carbon nanotube paste sensor for the determination of voltaren. *FlatChem, 24*. doi:10.1016/j.flatc.2020.100207

Puska, M., Yli-Urpo, A., Vallittu, P., & Airola, K. (2016). Synthesis and Characterization of Polyamide of Trans-4-hydroxy-L-proline used as Porogen Filler in Acrylic Bone

Cement. *Journal of Biomaterials Applications, 19*(4), 287-301. doi:10.1177/0885328205048044

Roe, J. H., & Hall, J. M. (1939). The Vitamin C Content of Human Urine and Its Determination through the 2,4-Dinitrophenylhydrazine Derivative of Dehydroascorbic Acid. *Journal of Biological Chemistry, 128*(1), 329-337. doi:10.1016/s0021-9258(18)73757-5

Sá, É. S., da Silva, P. S., Jost, C. L., & Spinelli, A. (2015). Electrochemical sensor based on bismuth-film electrode for voltammetric studies on vitamin B2 (riboflavin). *Sensors and Actuators B: Chemical, 209*, 423-430. doi:10.1016/j.snb.2014.11.136

Sahni, S., Zoltick, E. S., McLean, R. R., & Hannan, M. T. (2010). Non-D vitamins and bone health in adults. *IBMS BoneKEy, 7*(12), 431-446. doi:10.1138/20100478

Sakamoto, H., Watanabe, K., Koto, A., Koizumi, G., Satomura, T., Watanabe, S., & Suye, S.-i. (2015). A bienzyme electrochemical biosensor for the detection of collagen l-hydroxyproline. *Sensing and Bio-Sensing Research, 4*, 37-39. doi:10.1016/j.sbsr.2015.03.002

Sang, S., Li, Y., Guo, X., Zhang, B., Xue, X., Zhuo, K., . . . Yuan, Z. (2019). A Portable Device for Rapid Detection of Human Serum Albumin using an immunoglobulin-coating-based Magnetoelastic Biosensor. *Biosensors and Bioelectronics, 141*. doi:10.1016/j.bios.2019.111399

Seibel, M. J. (2005). Biochemical markers of bone turnover: part I: biochemistry and variability. *Clin Biochem Rev, 26*(4), 97-122.

Shah, N., Arain, M. B., & Soylak, M. (2020). Historical background: milestones in the field of development of analytical instrumentation. In *New Generation Green Solvents for Separation and Preconcentration of Organic and Inorganic Species* (pp. 45-73).

Simões, F. R., & Xavier, M. G. (2017). Electrochemical Sensors. In *Nanoscience and its Applications* (pp. 155-178).

Songchitsomboon, S., Komindr, S., Kulapongse, S., Puchaiwatananon, O., & Udomsubpayakul, U. (1998). Thiamin and riboflavin status of medical inpatients. *J Med Assoc Thai, 81*(12), 931-937.

Souza, D. d., Machado, S. A. S., & Avaca, L. A. (2003). Voltametria de onda quadrada. Primeira parte: aspectos teóricos. *Química Nova, 26*(1), 81-89. doi:10.1590/s0100-40422003000100015

Srithongkul, T., & Ungprasert, P. (2020). Coffee Consumption is Associated with a Decreased Risk of Incident Chronic Kidney Disease: A Systematic Review and Meta-analysis of Cohort Studies. *European Journal of Internal Medicine, 77*, 111-116. doi:10.1016/j.ejim.2020.04.018

Sugio, S., Kashima, A., Mochizuki, S., Noda, M., & Kobayashi, K. (1999). Crystal structure of human serum albumin at 2.5 Å resolution. *Protein Engineering, Design and Selection, 12*(6), 439-446. doi:10.1093/protein/12.6.439

Sun, J., & Liu, Y. (2019). Unique Constant Phase Element Behavior of the Electrolyte–Graphene Interface. *Nanomaterials, 9*(7). doi:10.3390/nano9070923

Swain, M. (2012). chemicalize.org. *Journal of Chemical Information and Modeling, 52*(2), 613-615. doi:10.1021/ci300046g

Syedmoradi, L., Daneshpour, M., Alvandipour, M., Gomez, F. A., Hajghassem, H., & Omidfar, K. (2017). Point of care testing: The impact of nanotechnology. *Biosensors and Bioelectronics, 87*, 373-387. doi:10.1016/j.bios.2016.08.084

Tesfaye, G., Negash, N., & Tessema, M. (2022). Sensitive and selective determination of vitamin B2 in non-alcoholic beverage and milk samples at poly (glutamic acid)/zinc oxide nanoparticles modified carbon paste electrode. *BMC Chemistry, 16*(1). doi:10.1186/s13065-022-00863-5

Thanh, C. T., Duoc, P. N. D., Huyen, N. T., Thu, V. T., Nghia, N. X., Binh, N. H., . . . Van Chuc, N. (2022). Development of electrochemical sensor based on polyalanine/CuCl-Gr/DWCNTs for highly sensitive detection of glyphosate. *Diamond and Related Materials, 128*. doi:10.1016/j.diamond.2022.109312

Thomas, T., Mascarenhas, R. J., D' Souza, O. J., Detriche, S., Mekhalif, Z., & Martis, P. (2014). Pristine multi-walled carbon nanotubes/SDS modified carbon paste electrode as an amperometric sensor for epinephrine. *Talanta, 125*, 352-360. doi:10.1016/j.talanta.2014.03.027

Tojo, A., & Kinugasa, S. (2012). Mechanisms of Glomerular Albumin Filtration and Tubular Reabsorption. *International Journal of Nephrology, 2012*, 1-9. doi:10.1155/2012/481520

Tortolini, C., Tasca, F., Venneri, M. A., Marchese, C., & Antiochia, R. (2021). Gold Nanoparticles/Carbon Nanotubes and Gold Nanoporous as Novel Electrochemical Platforms for L-Ascorbic Acid Detection: Comparative Performance and Application. *Chemosensors, 9*(8). doi:10.3390/chemosensors9080229

Tsai, J.-Z., Chen, C.-J., Settu, K., Lin, Y.-F., Chen, C.-L., & Liu, J.-T. (2016). Screen-printed carbon electrode-based electrochemical immunosensor for rapid detection of microalbuminuria. *Biosensors and Bioelectronics, 77*, 1175-1182. doi:10.1016/j.bios.2015.11.002

Tseng, C.-C., Ko, C.-H., Lu, S.-Y., Yang, C.-E., Fu, L.-M., & Li, C.-Y. (2021). Rapid electrochemical-biosensor microchip platform for determination of microalbuminuria in CKD patients. *Analytica Chimica Acta, 1146*, 70-76. doi:10.1016/j.aca.2020.12.029

Tsibris, J. C. M., McCormick, D. B., & Wright, L. D. (1966). Studies on the Binding and Function of Flavin Phosphates with Flavin Mononucleotide-dependent Enzymes. *Journal of Biological Chemistry, 241*(5), 1138-1143. doi:10.1016/s0021-9258(18)96813-4

Vállez-Gomis, V., Peris-Pastor, G., Benedé, J. L., Chisvert, A., & Salvador, A. (2021). Green determination of eight water-soluble B vitamins in cosmetic products by liquid chromatography with ultraviolet detection. *Journal of Pharmaceutical and Biomedical Analysis, 205*. doi:10.1016/j.jpba.2021.114308

Veis, A., & Anesey, J. (1965). Modes of Intermolecular Cross-linking in Mature Insoluble Collagen. *Journal of Biological Chemistry, 240*(10), 3899-3908. doi:10.1016/s0021-9258(18)97127-9

Vincent, J.-L. (2009). Relevance of albumin in modern critical care medicine. *Best Practice & Research Clinical Anaesthesiology, 23*(2), 183-191. doi:10.1016/j.bpa.2008.11.004

Vlasova, I. M., & Saletsky, A. M. (2009). Study of the denaturation of human serum albumin by sodium dodecyl sulfate using the intrinsic fluorescence of albumin. *Journal of Applied Spectroscopy, 76*(4), 536-541. doi:10.1007/s10812-009-9227-6

Wan, Y.-c., Liu, Y.-j., Liu, C., Ma, H.-t., Yu, H.-f., Kang, J.-w., . . . Lu, B. (2018). Rapid determination of neomycin in biological samples using fluorescent sensor based on quantum dots with doubly selective binding sites. *Journal of Pharmaceutical and Biomedical Analysis, 154*, 75-84. doi:10.1016/j.jpba.2018.02.028

Wang, S., Zhang, J., Gharbi, O., Vivier, V., Gao, M., & Orazem, M. E. (2021). Electrochemical impedance spectroscopy. *Nature Reviews Methods Primers, 1*(1). doi:10.1038/s43586-021-00039-w

Weast, R. C. (1988). *CRC handbook of chemistry and physics* (1st Student ed.). Boca Raton, FL: CRC Press.

Woessner, J. F. (1961). The determination of hydroxyproline in tissue and protein samples containing small proportions of this imino acid. *Archives of Biochemistry and Biophysics, 93*(2), 440-447. doi:10.1016/0003-9861(61)90291-0

Yang, C.-W., Harris, D. C. H., Luyckx, V. A., Nangaku, M., Hou, F. F., Garcia Garcia, G., . . . Tonelli, M. (2020). Global case studies for chronic kidney disease/end-stage kidney disease care. *Kidney International Supplements, 10*(1), e24-e48. doi:10.1016/j.kisu.2019.11.010

Yang, Y., Hu, N., Deng, J., & Yang, J. (2022). Electrochemical Sensing for Vitamins. *Chemosensors, 10*(11). doi:10.3390/chemosensors10110494

Yavarinasab, A., Abedini, M., Tahmooressi, H., Janfaza, S., Tasnim, N., & Hoorfar, M. (2021). Potentiodynamic Electrochemical Impedance Spectroscopy of Polyaniline-

Modified Pencil Graphite Electrodes for Selective Detection of Biochemical Trace Elements. *Polymers, 14*(1). doi:10.3390/polym14010031

Yomthiangthae, P., Chailapakul, O., & Siangproh, W. (2022). Rapid urinary albumin detection using a simple redox cycling process coupled with a paper-based device. *Journal of Electroanalytical Chemistry, 911*. doi:10.1016/j.jelechem.2022.116230

Yomthiangthae, P., Kondo, T., Chailapakul, O., & Siangproh, W. (2020). The effects of the supporting electrolyte on the simultaneous determination of vitamin B2, vitamin B6, and vitamin C using a modification-free screen-printed carbon electrode. *New Journal of Chemistry, 44*(29), 12603-12612. doi:10.1039/d0nj02175j

Yu, A. M., & Chen, H. Y. (2006). Electrocatalytic Oxidation of Hydrazine at the Poly(Glutamic Acid) Chemically Modified Electrode and Its Amperometric Determination. *Analytical Letters, 30*(3), 599-607. doi:10.1080/00032719708001804

Zempleni, J., Suttie, J. W., Gregory Iii, J. F., & Stover, P. J. (2013). *Handbook of Vitamins*.

Zensor R&D co., L. (2016). Screen-printed carbon electrode. Retrieved from https://www.zensorrd.com/Article13.html

Zhang, W., Liu, L., Li, Y., Wang, D., Ma, H., Ren, H., . . . Ye, B.-C. (2018). Electrochemical sensing platform based on the biomass-derived microporous carbons for simultaneous determination of ascorbic acid, dopamine, and uric acid. *Biosensors and Bioelectronics, 121*, 96-103. doi:10.1016/j.bios.2018.08.043

Zhang, W., Wang, R., Luo, F., Wang, P., & Lin, Z. (2020). Miniaturized electrochemical sensors and their point-of-care applications. *Chinese Chemical Letters, 31*(3), 589-600. doi:10.1016/j.cclet.2019.09.022

Zheng, J. P., Goonetilleke, P. C., Pettit, C. M., & Roy, D. (2010). Probing the electrochemical double layer of an ionic liquid using voltammetry and impedance spectroscopy: A comparative study of carbon nanotube and glassy carbon electrodes in [EMIM]+[EtSO4]−. *Talanta, 81*(3), 1045-1055. doi:10.1016/j.talanta.2010.01.059

Appendix

Appendix 1

NJC

ROYAL SOCIETY OF CHEMISTRY

PAPER

View Article Online
View Journal | View Issue

Cite this: *New J. Chem.*, 2020, **44**, 12603

The effects of the supporting electrolyte on the simultaneous determination of vitamin B_2, vitamin B_6, and vitamin C using a modification-free screen-printed carbon electrode†

Phanumas Yomthiangthae,[a] Takeshi Kondo,[b] Orawon Chailapakul[c] and Weena Siangproh*[a]

Received 30th April 2020,
Accepted 22nd June 2020

DOI: 10.1039/d0nj02175j

rsc.li/njc

To provide new choices and to replace the complicated steps of synthesizing modified electrodes, this research reports the systematic investigation of the effects of different supporting electrolytes on the electrochemical behavior of vitamin B_2 (VB_2), vitamin B_6 (VB_6), and vitamin C (VC) using a common screen-printed carbon electrode (SPCE) to achieve simultaneous detection. The roles of various well-known supporting electrolytes, including Britton–Robinson buffer solution (BRBS), acetate buffer solution (ABS), and phosphate buffer solution (PBS), in the electrochemical oxidation of VB_2, VB_6, and VC were carefully evaluated by square wave voltammetry (SWV). From a successive investigation based on the ionic conductivity of the species contained in the supporting electrolytes, PBS at pH 3.5 was selected as a suitable supporting electrolyte for the simultaneous detection of VB_2, VB_6, and VC. Under the optimized conditions, the simultaneous detection of VB_2, VB_6, and VC provided satisfactory sensitivity, selectivity, and reproducibility even when using a common electrode. To demonstrate the practicality and reliability of the proposed analytical procedure, the simultaneous detection of VB_2, VB_6, and VC was performed in mixed vegetable and fruit juice samples and urine samples by SWV, and the results were compared with those obtained by chromatographic detection. Therefore, this method was found to be simple and may be a new alternative for the simultaneous determination of VB_2, VB_6, and VC in practical applications.

1. Introduction

A supporting electrolyte (inert electrolyte or inactive electrolyte) is a necessary solution to preserve the conductivity and ionic strength of an electrochemical system. Chemical species containing a supporting electrolyte are required to have non-electroactive properties within the applied potential window, and their conductivities are considerably larger than those of the electroactive species or analytes.[1] The essential roles of a supporting electrolyte are to minimize the resistance of an electrochemical cell to eradicate the transportation of electrochemical species caused by migration effects in the electric field and to constrain the interfacial potential difference to the closest distance of approach of solvated ions to the electrode.[2,3] These phenomena will diminish the uncompensated iR drop, which causes potential-control errors, and the ohmic heating of a solution to enable the acquisition of factual potential measurements.[4]

Normally, the concentration of ionic species in a supporting electrolyte is at least 50–100 times that of the electroactive species and is the most significant source of electrically conducting ionic species.[5] These electrolytes can be an inorganic or organic salt, an acid or a base, or a buffer solution such as acetate, carbonate, or phosphate. Among these supporting electrolytes, buffer solutions are greatly used in electrochemical systems because of the ability to preserve the pH at a virtually constant value. Due to the advantageous properties of buffer solutions, in numerous reports of electroanalytical applications, buffer solutions are selected to serve as supporting electrolytes for the detection of interesting electroactive species, especially for vitamin detection.[6–8]

Vitamins are a disparate group of compounds which are essential nutrients for humans.[9] They are classified into 2 groups by their solubilities, namely water-soluble vitamins

[a] *Department of Chemistry, Faculty of Science, Srinakharinwirot University, Sukhumvit, Wattana, Bangkok 10110, Thailand. E-mail: weena@g.swu.ac.th, weenasi@hotmail.com; Fax: +66 2259 2098; Tel: +66 2 640 5000, ext. 18208*
[b] *Department of Pure and Applied Chemistry, Faculty of Science and Technology, Tokyo University of Science, 2641 Yamazaki, Noda, Chiba, 278-8510, Japan*
[c] *Electrochemistry and Optical Spectroscopy Center of Excellence (EOSCE), Department of Chemistry, Faculty of Science, Chulalongkorn University, 254 Phayathai Road, Pathumwan, Bangkok 10330, Thailand*

† Electronic supplementary information (ESI) available. See DOI: 10.1039/d0nj02175j

(vitamin B and vitamin C) and fat-soluble vitamins (vitamin A, vitamin D, vitamin E, and vitamin K). Vitamins play important roles in various biological functions. Vitamin B_2 (VB_2) is an important component of a flavoenzyme that catalyzes a variety of biochemical reactions of carbohydrates, proteins, and fats in the human body. VB_2 promotes the growth process and the reproductive system; strengthens visibility and relieves eye fatigue; and prevents inflammation of the mouth, lips, and tongue.[10] Vitamin B_6 (VB_6) is involved in many aspects of macronutrient metabolism, histamine synthesis, hemoglobin synthesis, and gene expression. It participates in the activities of many enzymes and maintenance of skin as well as of the nervous and immune systems.[11] Vitamin C (VC) is an antioxidant that is necessary for the growth, development, and repair of all tissues. It is involved in many functions of the human body, including the formation of collagen, the absorption of iron, the immune system, wound healing, and the maintenance of cartilage, bones, and teeth.[12] These mentioned water-soluble vitamins must be obtained daily from food. Moreover, they are not stored in the human body because of urinary excretion. Therefore, the determination of vitamins in real samples is important for various applications to monitor the quantities of vitamins in consumer products and to indicate abnormalities or diseases.

Due to the importance of the mentioned vitamins, various analytical methods have been developed and proposed for the determination of VB_2, VB_6, and VC in both individual and simultaneous measurements, including high-performance liquid chromatography,[13] spectrophotometry,[14] chemiluminescence,[15] and electrophoresis.[16] Unfortunately, these techniques have some limitations despite their high sensitivity and selectivity for detection. For example, they are time-consuming, expensive to maintain, complicated to operate, require large volumes of solution and have several pre-concentration steps. Consequently, other novel methodologies must be developed for VB_2, VB_6, and VC detection to achieve the objective of simple practicality in various field analysis applications.

For twenty-first-century analytical experimentation, the electrochemical method is another choice for the simultaneous determination of VB_2, VB_6, and VC due to its simplicity of operation, rapid results, direct measurement, and high sensitivity and selectivity. In previous electrochemical research,[17–27] the detection of VB_2, VB_6, and VC was achieved principally by various modified electrodes which provided high precision and high sensitivity. However, these electrodes are not suitable for some applications because of disadvantages such as high cost, long modification times with complicated steps, and large solution volumes required for analysis. The most important factor is that it is difficult to meet the requirements of field analysis by performing surface modification of electrodes. Therefore, the selection of a suitable, simple, and inexpensive electrode platform is currently significant for application in real sample analysis to increase the performance of analytical methods.

Currently, the advancement of screen-printing technology for the fabrication of screen-printed electrodes (SPEs) is attracting enormous attention due to the advantageous properties of SPEs compared to conventional electrodes,[28] such as cost-effectiveness, disposability, simplicity, versatility, availability of materials and patterns, elimination of electrode maintenance, requirement for low volumes of solution, and appropriateness for outside laboratory measurement. For these reasons, these devices have been widely applied in electrochemical analysis for environmental monitoring,[29] clinical diagnoses,[30] and food safety assessment.[31] Various reports demonstrated that these electrochemical devices are generally fabricated on paper as a substrate;[32–34] these are called electrochemical paper-based analytical devices (ePADs). The main advantages of ePADs are that they are simple, cost-effective, portable, and disposable.[35] However, in addition to paper, other substrates are additionally consumed as platforms for the fabrication of SPEs, such as acrylic, ceramic, and PVC sheets. To provide a different platform for the development of electrochemical devices, commercial plastic sheets (OHP films) have recently been employed to fabricate electrode platforms named transparent film-based analytical devices (TFADs).[36] Because of their compatibility with screen-printing technology, ready availability in local stationery stores and low cost, OHP films have received considerable attention for the fabrication of screen-printed electrodes.

Herein, the main objective of this research was to focus on the effect of supporting electrolyte on the simultaneous detection of VB_2, VB_6, and VC using a common screen-printed carbon electrode (SPCE) to obtain a simple detection method and to overcome the cost of analysis as well as the need for complex modifications using various modern materials. Also, we propose the manual fabrication of an SPCE, named an electrochemical transparent-film based analytical device (eTFAD), using a transparent film substrate that is commercially available in a local stationery store. Under the optimal conditions, the overall electrochemical experiment was rapid, convenient, and uncomplicated in comparison to those described in previous studies. Additionally, the proposed procedure was sensitive and selective for the determination of the amounts of selected vitamins in real samples. For various practical applications, the developed electrochemical electrode was successfully applied for the determination of mentioned vitamins in a mixed vegetable and fruit juice sample and an artificial urine sample to demonstrate the reliability of the proposed analytical system. The results obtained show the effectiveness of the method for monitoring the quantities of vitamins in consumer products or for indicating abnormalities and diseases. This finding provides an alternative method and a new vision to achieve applications using basic concepts and may encourage researchers to perform novel work using basic instruments to overcome experimental limitations.

2. Experimental

2.1. Chemicals and reagents

All chemicals were used as received without further purification. Carbon paste (C2130307D1) and silver/silver chloride paste (C2130809D5) were purchased from Gwent Group (Torfaen, United Kingdom). Riboflavin (vitamin B_2, VB_2) and L-ascorbic acid (vitamin C, VC) were purchased from Sigma-Aldrich

(St. Louis, MO, USA). Pyridoxine hydrochloride (vitamin B_6, VB_6) was purchased from Hi-Media Laboratories Pvt., Ltd (India). Sodium dihydrogen orthophosphate ($NaH_2PO_4{\cdot}2H_2O$) and disodium hydrogen orthophosphate ($Na_2HPO_4{\cdot}2H_2O$) were acquired from Ajax Finechem Pty., Ltd (New South Wales, Australia). Ethanol and *ortho*-phosphoric acid (H_3PO_4, 85% purity) were acquired from Merck (Darmstadt, Germany). Acetone (commercial grade) was purchased from CaHC (Thailand) Co., Ltd (Bangkok, Thailand).

All solutions were prepared using Milli-Q water obtained from a Millipore water purification system (R = 18.2 MΩ cm at 25 °C). All stock standard solutions (1 mM) were prepared weekly in water and maintained in the dark at −20 °C. To prepare the working standard solutions, the stock standard solution was diluted with supporting electrolyte and mixed using a vortex mixer. Phosphate buffer solution (PBS), which served as a supporting electrolyte, was prepared by mixing 0.1 M NaH_2PO_4 and 0.1 M Na_2HPO_4 and was adjusted to the desired pH with 0.1 M H_3PO_4. Britton–Robinson buffer solution (BRBS) was prepared by mixing equal volumes of 0.04 M CH_3COOH, 0.04 M H_3BO_3 and 0.04 M H_3PO_4 and was adjusted to the desired pH with 0.2 M NaOH. Acetate buffer solution (ABS) was also prepared by mixing 0.1 M CH_3COOH and 0.1 M CH_3COONa and was adjusted to the desired pH with 0.1 M HCl or 0.1 M NaOH.

2.2. Fabrication of the electrochemical transparent film-based analytical device (eTFAD)

The electrode pattern was designed using Adobe Illustrator CC 2018. To obtain the electrode blocks for screening, the designed patterns were built by Chaiyaboon Brothers Co., Ltd (Bangkok, Thailand). Screen-printed electrodes were fabricated using a manual screen-printing method on a transparent sheet as a substrate as described in a previous report.[37] Briefly, the clean transparent sheet was screen-printed with carbon paste to obtain the working electrodes and counter electrodes. Then, these electrodes were placed in an oven at a temperature of 55 °C for 30 min to remove the solvent and to dry the electrodes. Next, silver/silver chloride (Ag/AgCl) paste was screen-printed on the same transparent sheet to obtain the reference electrodes and the conductive pads. After that, the electrodes were placed in an oven at a temperature of 55 °C for 30 min. Finally, the common screen-printed carbon electrodes (SPCE) were obtained and ready to use for an experiment. A photograph of the obtained eTFAD is shown in Fig. 1.

2.3. Electrochemical measurements

The electrochemical experiments were performed using a PGSTAT128N potentiostat galvanostat from Metrohm-Autolab (Switzerland) with NOVA 1.10 software (Kanaalweg 29-G 3526 KM Utrecht, The Netherlands). A three-electrode system was fabricated on transparent sheets and was employed throughout the experiment. The geometric area of the working electrode was 0.126 cm^2 (calculated from circular area = πr^2; r = 0.2 cm). For the electrochemical measurements, a 100 μL aliquot of a standard or sample solution was thoroughly dropped onto the detection zone, covering all three electrodes. After that, electrochemical techniques were performed, including cyclic voltammetry (CV) or square wave voltammetry (SWV). For the CV measurements, the potential was applied over the range from −1.1 V to 1.3 V with a scan rate of 100 mV s^{-1}. Similarly, SWV measurements were performed for the simultaneous quantitative determination by applying potentials from −1.0 V to 1.3 V with a step potential of 5 mV, an amplitude of 25 mV, and a frequency of 5 Hz.

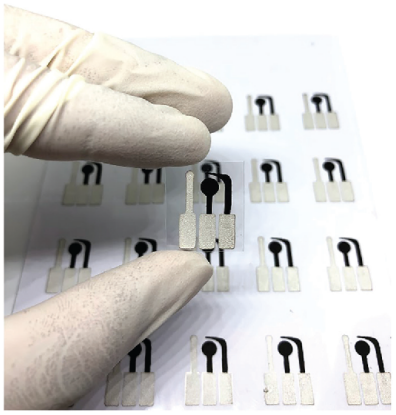

Fig. 1 Photograph of the electrochemical transparent film-based analytical device (eTFAD) consisting of screen-printed working (middle), reference (left), and counter (right) electrodes.

2.4. Sample preparation

To demonstrate the application potential of the proposed electrode, two types of samples, including mixed vegetable and fruit juice and artificial urine, were investigated for the simultaneous determination of water-soluble vitamins.

The mixed vegetable and fruit juice was purchased from a convenience store in Thailand. 5 mL of juice sample was added to a test tube. Then, the sample was centrifuged for 15 minutes at 2500 rpm, followed by filtration through a filter paper, and maintained in a dark container at 4 °C. After that, samples were spiked at various concentrations of standard vitamins, and the spiked solution was diluted 10-fold with PBS pH 3.5 (a suitable dilution order); the quantities were then measured using the SWV technique as described in Section 2.3. Then, the average recovery percentage was calculated.

Artificial urine was purchased from Carolina Biological Supply Company (Burlington, USA). For the sample preparation, the artificial urine and spiked artificial urine were simply diluted 1000-fold with PBS pH 3.5, which is a suitable dilution order for this sample. After that, the samples and spiked samples were quantitatively measured using the same procedure used for the mixed vegetable and fruit juice.

3. Results and discussion

3.1. Electrochemical behavior for the simultaneous detection of VB_2, VB_6, and VC

Cyclic voltammetry was initially used to investigate the electrochemical properties of the system and the possibility of

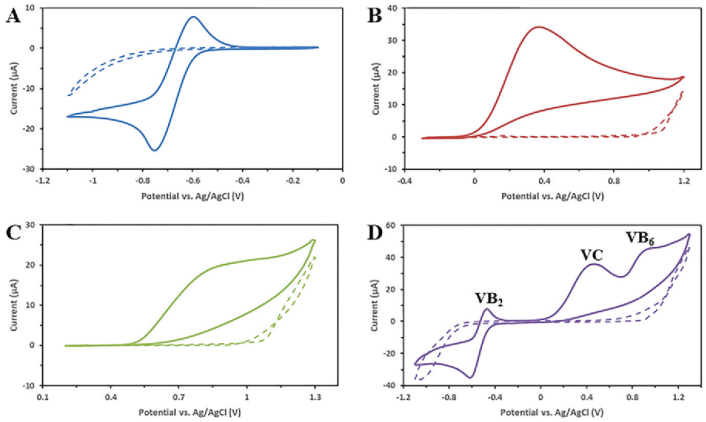

Fig. 2 Cyclic voltammograms obtained from the common SPCE in the absence (dashed line) and presence (solid line) of 1 mM VB_2 (A), 1 mM VC (B), 1 mM VB_6 (C), and the mixture solution of 1 mM VB_2, 1 mM VC, and 1 mM VB_6 (D). BRBS pH 7 served as the supporting electrolyte. All cyclic voltammograms were recorded at a scan rate of 100 mV s^{-1}.

simultaneous detection of VB_2, VB_6, and VC. To examine the oxidation or reduction mechanism of selected vitamins on a common SPCE surface, cyclic voltammograms of VB_2, VB_6, and VC in Britton–Robinson buffer solution (BRBS) at pH 7 were preliminarily recorded at a scan rate of 100 mV s^{-1}. The obtained voltammograms from both individual and simultaneous detection are shown in Fig. 2. The cyclic voltammogram of VB_2 shown in Fig. 2A exhibits a pair of sharp and well-behaved redox peaks at −0.60 V and −0.75 V for the anodic and cathodic peaks, respectively. This result reveals that VB_2 can display reversible properties because the ratio between the anodic and cathodic current is around 1.0. However, the separation of the anodic and cathodic peak potential is around 0.15 V, which is greater than that in the reversible process (0.059/n V, where n is the number of electrons transferred). This result can be attributed to the fact that the electron transfer reaction of VB_2 proceeds at a slow rate.[38] The cyclic voltammogram of VC depicted in Fig. 2B displays a sharp and strong oxidation peak at 0.35 V with a peak current of 27.65 μA. This result indicates that the oxidation of VC at the electrode surface is an irreversible process. Similarly, the oxidation of VB_6 was found to be an irreversible process due to the presence of a small and broad oxidation peak at 0.82 V, as demonstrated in Fig. 2C. From these results, it can be concluded that simultaneous detection of VB_2, VB_6, and VC can be performed on the proposed analytical electrode because of the explicit distinction of their peak potential positions.

Subsequently, the simultaneous detection of VB_2, VC, and VB_6 was investigated, as shown in Fig. 2D. From the voltammogram, VB_2 exhibited a pair of outstanding redox peaks at −0.48 V and −0.61 V for the anodic and cathodic peaks, respectively. Meanwhile, VC and VB_6 provided broad anodic peaks at 0.41 V and 0.90 V, respectively. The obtained voltammogram confirmed that simultaneous detection of VB_2, VC, and VB_6 in the oxidative direction is possible due to the distinction of the peak potential positions; as anticipated, the results are the same as those obtained from the individual detection. The discovered results are in good agreement with a previous critical review of all vitamins;[39] therefore, the simultaneous detection of VB_2, VC, and VB_6 can be performed using a common SPCE.

3.2. Influences of pH and the supporting electrolyte on the electrooxidation of VB_2, VC, and VB_6

The effects of adjusting the pH value of the supporting electrolyte on the oxidative behavior of VB_2, VC, and VB_6 disclose significant information about the mechanisms of the electrochemical reactions at a common SPCE. Therefore, the influences of pH and the supporting electrolyte on the electrooxidation of VB_2, VC, and VB_6 were carefully investigated by square wave voltammetry. The suitable pH conditions were preliminarily studied using BRBS at pH 5, 7, and 9 as representatives of acidic, neutral, and basic buffer electrolytes, respectively. The obtained voltammograms from the simultaneous detection are shown in Fig. 3A. With increasing pH value, the anodic currents of VB_2, VC, and VB_6 decreased obviously. We believe that in our case, an acidic supporting electrolyte would strongly increase the current. By considering the pK_a values of each vitamin, the results can be attributed to the fact that the ionic forms of the target analytes affect the electrooxidation processes at the electrode surface. According to data obtained from the literature,[40] the pK_a values of each vitamin are as follows: VB_2 = −0.2 and 6.0, VC = 4.2, and VB_6 = 5.6 and 9.4. These values indicate that the three compounds can exist in their ionic forms in aqueous solutions. Fig. S1 (ESI†) shows the charge *versus* pH curves (CurTiPot software)[41] for the VB_2, VC, and VB_6 molecules. As can be observed, VB_2 and VB_6 are amphoteric molecules (pI = 2.9 and 7.5, respectively) which can exist in cationic, anionic, and neutral forms. In contrast, VC presents weak acid character and is predominantly negatively charged in solutions with pH values higher than 6.5. As shown in Fig. 3A, the vitamins

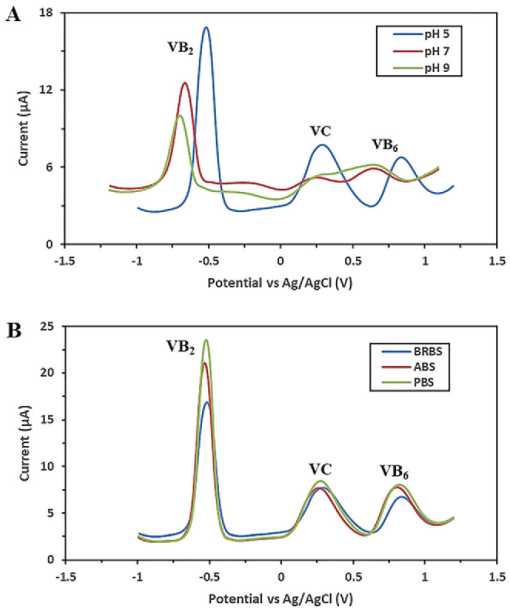

Fig. 3 Square wave voltammograms of the mixture solution of vitamins (0.1 mM VB_2, 0.4 mM VC, and 0.4 mM VB_6) in BRBS at pH 5, 7, and 9 (A) and in BRBS, ABS, and PBS at pH 5 (B) obtained from a common SPCE. All square wave voltammograms were recorded at a step potential of 5 mV, an amplitude of 25 mV, and a frequency of 5 Hz.

provided the highest anodic currents in BRBS pH 5, which is in the acidic range. It can be reasoned that VB_2, VC, and VB_6 exist predominantly in neutral, anionic, and cationic forms, respectively. We assumed that these ionic forms readily transfer electrons at the electrode surface. On the other hand, the anodic currents decreased when the vitamins were dissolved in BRBS pH 7 and 9, which are in neutral and alkaline ranges, respectively, because VB_2 and VB_6 exist predominantly in cationic and neutral forms, respectively. Meanwhile, VC exists completely in anionic form. These ionic forms in neutral and basic supporting electrolytes transfer almost no electrons at the electrode surface. From these results, it can be concluded that an acidic supporting electrolyte is suitable for the detection of VB_2, VC, and VB_6.

Afterward, the type of supporting electrolyte was investigated at a fixed pH value of 5 corresponding to the previous step to determine the most appropriate electrolyte for the detection of VB_2, VC, and VB_6. As mentioned previously, based on electrochemical research, buffer systems are universally used as supporting electrolytes due to their pH regulation ability. In this research, buffer systems at pH 5 consisting of Britton–Robinson buffer solution (BRBS), acetate buffer solution (ABS), and phosphate buffer solution (PBS) were studied by square wave voltammetry for the selection of an appropriate supporting electrolyte. Fig. 3B shows square wave voltammograms of a mixture solution in various buffer systems at pH 5. By considering the anodic currents, PBS at pH 5 provided the highest responses. We believe that in our case, the properties of the buffers, particularly their electrical conductivity, are involved in the electrooxidation of these vitamins. Consequently, the electrical conductivity of the species contained in the proposed buffer systems is discussed, as reported in ref. 42 and 43. In detail, PBS at pH 5 contains H_3PO_4, NaH_2PO_4, and Na_2HPO_4, which provided specific conductances (20 °C) of 5.5, 2.2, and 4.6 mS cm ^{1}, respectively. These values are higher than those of the other species contained in the other buffer systems. For example, ABS at pH 5 contains CH_3COOH and CH_3COONa, which provided specific conductances (20 °C) of 0.3 and 3.9 mS cm ^{1}, respectively. Similarly, BRBS at pH 5, which contains H_3PO_4, CH_3COOH, and H_3BO_3, provided the specific conductance (25 °C) of boric acid of 0.008 mS cm ^{1}. It has been found that a higher specific conductance affords better electrical conductivity. As a result, the resistance of the electrochemical cell can decrease and eliminate electromigration effects, which is desirable in controlled-potential experiments. Accordingly, it can be concluded that PBS with an acidic pH value is a suitable electrolyte for the detection of VB_2, VC, and VB_6.

To confirm the effects of the acidic electrolyte, the influence of solution pH on the electrochemical behavior of VB_2, VC, and VB_6 in PBS using a common SPCE was studied at specific pH values ranging from 3.5 to 6.5. Fig. 4A shows the anodic peak potentials (E_{pa}) for these vitamins and their linear regression equations: E_{pa} (V) = −0.0533pH − 0.295 (r^2 = 0.9929) for VB_2; E_{pa} (V) = 0.0556pH + 0.0334 (r^2 = 0.9901) for VC; and E_{pa} (V) = −0.054pH + 1.0377 (r^2 = 0.9925) for VB_6. The Nernst equation (eqn (1)) explains the relationship between E_{pa} and pH, where n and m represent the numbers of electrons and protons involved in the reaction, and a and b are the coefficients of the oxidant and reductant in the reaction:[44]

$$E_{pa} = E^0 + \left(\frac{0.0591}{n}\right)\log\left[\frac{(OX)^a}{(R)^b}\right] - \left(0.0591\frac{m}{n}\right)pH \qquad (1)$$

All the slopes between E_{pa} and pH of each vitamin were very close to 59 mV pH ^{1} at 25 °C; this indicates that the overall electrochemical process at the proposed electrode is proton-dependent, while the electron transfer is regulated by the transfer of an equal number of protons and electrons.

Furthermore, the anodic peak currents (I_{pa}) as a function of pH were investigated, as presented in Fig. 4B. The anodic currents of VB_2, VC, and VB_6 do not present significant distinction with increasing pH until the value reaches 6.5. Consequently, the difference between the anodic peak potentials of VC and VB_6 is the primary consideration to select the appropriate pH value. The difference of anodic peak potential between these two vitamins decreases with increasing pH value, leading to overlapping of the anodic peaks. PBS at pH 3.5 provided the highest difference in the anodic peak potentials; therefore, it was chosen as an appropriate pH value for the simultaneous detection of VB_2, VC, and VB_6. We suppose this is due to the dissolution of these vitamins in acidic solution (pH 3.5), in which VB_2 and VC predominantly exist in neutral forms; meanwhile, VB_6 is positively charged because of the protonation of the nitrogen in the pyridine ring. These molecules and their ionized forms can be oxidized at different applied potentials using a common SPCE.

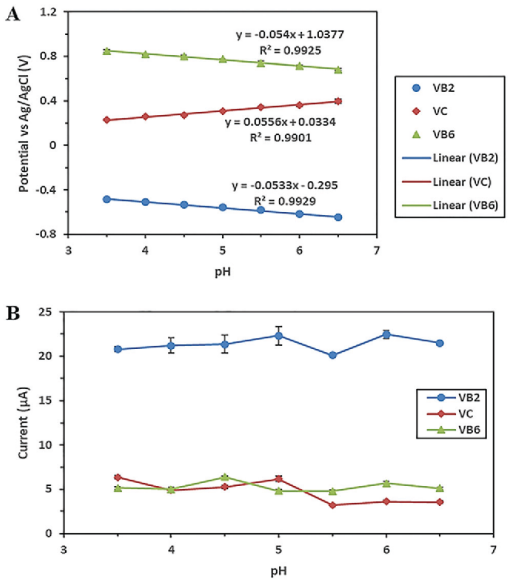

Fig. 4 Influences of solution pH on the anodic peak potentials (A) and peak currents (B) in the oxidation of 100 μM VB_2, 400 μM VC, and 400 μM VB_6 in PBS at a common SPCE.

3.3. The effects of scan rate on the electrooxidation of VB_2, VC, and VB_6

To elucidate whether the mass transfer of the analyte toward the electrode surface is diffusion- or adsorption-controlled, the effects of the scan rate on the electrooxidation of VB_2, VC, and VB_6 were investigated by cyclic voltammetry. Fig. 5A shows cyclic voltammograms of VB_2, VC, and VB_6 at a common SPCE using different scan rates. The results show that the redox peak currents for VB_2 increased with increasing scan rate while their redox peak potentials retained the same values; this suggests that the electron transfer process is reversible. On the other hand, the anodic peak currents for VC and VB_6 increased with increasing scan rate; however, their anodic peak potentials gradually shifted to positive values, indicating that the electron transfer processes were irreversible. Linear dependence of the anodic peak current of all three vitamins *versus* the square root of the scan rate was observed, as displayed in Fig. 5B. These behaviors demonstrate that the electrochemical oxidations of all three vitamins at the common SPCE are diffusion-controlled processes.[45]

Using the information received from the linear regression of the relationship between the anodic peak currents (I_{pa}) and the square root of the scan rates ($\nu^{1/2}$), the relationship shown in eqn (2) was applied to estimate the diffusion coefficients (D_0) of all three vitamins.[46]

$$I_{pa} = 0.496FAC_sD_0^{1/2}\left(\frac{F}{RT}\right)^{1/2}\nu^{1/2} \quad (2)$$

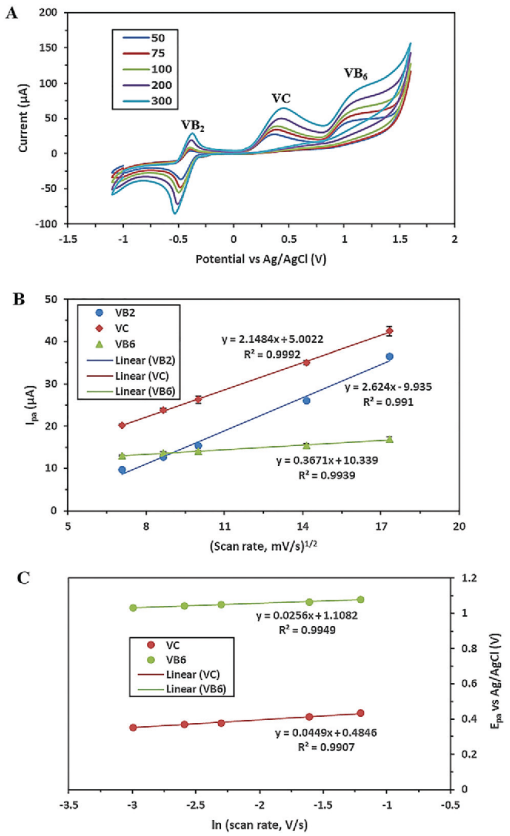

Fig. 5 (A) Cyclic voltammograms of 1 mM VB_2, 1 mM VC, and 1 mM VB_6 in PBS pH 3.5 at the common SPCE using a series of scan rates (50, 75, 100, 200, and 300 mV s^{-1}). (B) The relationships between the anodic peak current (I_{pa}) and the square root of the scan rate. (C) The variations of the anodic peak potential (E_{pa}) and the natural logarithm of the scan rate ($\ln \nu$) from 50 to 300 mV s^{-1}.

where F is the Faraday constant, A is the geometric area of the working electrode (0.126 cm^2), C_s is the concentration of the vitamin (1×10^{-6} mol cm^{-3}), D_0 is the diffusion coefficient of the vitamin, R is a gas constant (8.31447 J mol^{-1} K^{-1}), and T is the temperature (298 K). The calculated D_0 values of VB_2, VC, and VB_6 were found to be 8.07×10^{-6}, 5.32×10^{-6}, and 1.57×10^{-7} cm^2 s^{-1}, respectively. Then, the number of electrons (n) involved in the electrooxidation of VB_2 was determined by the Randles–Sevcík relationship for a reversible process (eqn (3)):

$$I_{pa} = (2.69 \times 10^5)n^{3/2}AC_sD_0^{1/2}\nu^{1/2} \quad (3)$$

Using eqn (3) and the previously estimated D_0 of VB_2, the number of electrons involved in the electrooxidation of VB_2 was calculated and was found to be $n = 1.07$ ($n \sim 1$). Next, the number of electrons involved in the electrooxidation of VC and

VB6 was determined by the Randles–Sevcík relationship for the irreversible process (eqn (4)):

$$I_{pa} = (2.99 \times 10^5)n[(1-\alpha)n]^{1/2}AC_s{D_0}^{1/2}\nu^{1/2} \qquad (4)$$

To calculate the n value, it is unavoidable to initially solve the factor of $(1-\alpha)n$. Using the Laviron theory for oxidative reactions (eqn (5)),[47] the calculation was based on the linear relationship between the anodic peak potential (E_{pa}) and the natural logarithm of the scan rate ($\ln \nu$), as shown in Fig. 5C. Based on eqn (5) and the slopes obtained from the linear relationship between E_{pa} and $\ln \nu$, the factors of $(1-\alpha)n$ for VC and VB_6 were found to be 0.572 and 1.00, respectively.

$$E_{pa} = E^0 + \frac{RT}{(1-\alpha)nF}\ln\frac{RTk_s}{(1-\alpha)nF} + \frac{RT}{(1-\alpha)nF}\ln\nu \qquad (5)$$

After calculating the factors of $(1-\alpha)n$ using eqn (4) and the previously estimated D_0 values of VC and VB_6, the numbers of electrons involved in the electrooxidation of VC and VB_6 could be calculated and were found to be $n = 1.32$ ($n \sim 2$) and $n = 0.998$ ($n \sim 1$), respectively.

3.4. Analytical performance

Square wave voltammetry was selected for the simultaneous determination of VB_2, VC, and VB_6 in mixture solutions due to its better resolution and higher sensitivity than cyclic voltammetry. Under the optimized experimental conditions (a step potential of 5 mV, an amplitude of 25 mV, and a frequency of 5 Hz), square wave voltammograms were obtained for the electrooxidation of different concentrations of the mixture of VB_2, VC, and VB_6 at a common SPCE, as shown in Fig. 6A. The results present that the well-defined anodic peaks of all three vitamins are sufficiently separated to discriminate and measure the current. Additionally, increments in the peak currents of all three vitamins can be observed simultaneously as their concentrations increase. Fig. 6B displays the calibration curves of all three vitamins, indicating that the anodic peak currents for the electrooxidation of all three vitamins increased proportionally with their corresponding concentrations. From these results, the linear ranges for the simultaneous determination of VB_2, VC, and VB_6 were found to be 1–60 μM, 10–400 μM, and 10–400 μM, with detection limits (calculated as the 3σ value of the blank) of 0.37 μM, 5.07 μM, and 3.32 μM, respectively. A comparison of the analytical performance in this work to previous work is shown in Table 1. The detection limits and linear ranges of the proposed system are not as low as those obtained for other modified electrodes. However, we first proposed the simultaneous determination of VB_2, VC, and VB_6 using a common SPCE by systematically studying all experimental parameters that affect the peak separation and sensitivity. Our proposed methodology provides various advantages, such as a low-cost, modification-free electrode and the requirement of a small sample volume for analysis. Moreover, this proposed system is easy to apply for commercialization of the electrode in the future.

To investigate the practicality of the common SPCE for the simultaneous determination of VB_2, VC, and VB_6, the individual determination of each vitamin was performed by varying the concentration of one analyte while those of the others remained constant. The results in Fig. S2A (ESI†) display that the anodic peak currents of VB_2 increased with concentration; meanwhile, the anodic peak currents of VC and VB_6 were equally unaltered at these concentrations, as shown in Fig. S2B (ESI†). In the same way, as can be seen in Fig. S2C and D (ESI†), the anodic peak currents of VC increased linearly with increasing concentration. Similarly, Fig. S2E and F (ESI†) show that the anodic peak current signals for VB_6 also increased with increasing concentration. By comparison between the anodic peak currents and concentrations from the individual and simultaneous determinations, the slope of each vitamin was virtually unchanged. This emphasizes that the electrooxidation process of each vitamin is independent; therefore, the simultaneous determination of these vitamins is feasible without any interference from each other's presence.

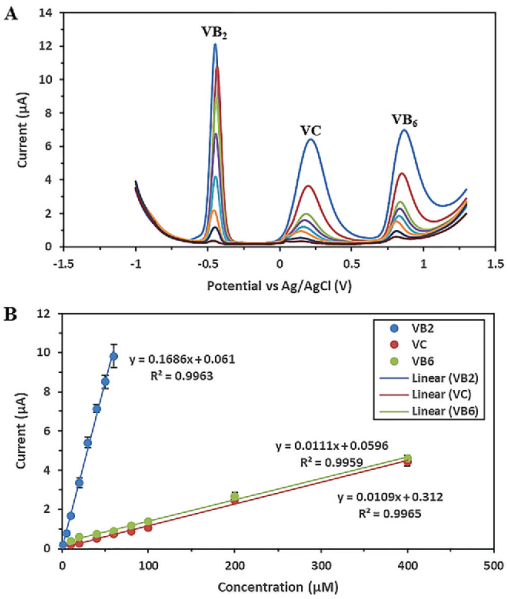

Fig. 6 (A) Square wave voltammograms of VB_2, VC, and VB_6 in concentration ranges of 1–60 μM, 10–400 μM, and 10–400 μM, respectively, in PBS pH 3.5 at the common SPCE. (B) Calibration plots of the anodic peak current of each vitamin *versus* the concentration.

The reproducibility of the determination of all three vitamins at various concentrations was calculated in terms of relative standard deviation (RSD) by using seven different electrodes ($n = 7$). The value was lower than 6.5%, which can be acceptable.[48] As shown in Table S1 (ESI†), this indicates that this electrode can be successfully employed for the simultaneous determination of water-soluble vitamins with excellent reproducibility.

3.5. Interference study

To investigate the selectivity of the proposed electrode and the developed method, the influence of various foreign species on the simultaneous determination of 20 μM VB_2, 60 μM VC, and

Table 1 Comparison of the analytical performance of this work with previous work for the simultaneous determination of VB_2, VC, and VB_6

Working electrode	Modification time[a]	Technique	Detection limit (μM)			Linear range (μM)			Ref.
			VB_2	VC	VB_6	VB_2	VC	VB_6	
PGCE	15 min	DPV	0.001	—	0.8	0.005–100	75–75 000	2.5–7500	17
MWCNT/GCE	—	CV	0.7	5	10	1–100	50–2000	50–2000	18
PEDOT/Fc^-/GCE	5 min	DPV	0.5	0.7	0.1	0.1–300	1.5–2000	0.5–1500	19
PEDOT/$Fe(CN)_6^{4-}$/GCE			0.02	0.5	0.3	0.04–200	1–2000	0.7–1500	
PEDOT/ZrO_2NPs/GCE	10 min	DPV	0.012	0.45	0.2	0.05–300	1–1500	0.5–1000	20
Ag-PLA/GCE	10 min	LSV	0.08	3	5	0.1–23	5–4000	10–3000	21
f-MWCNT-Cu_2O–Ag_2O composite/copper substrate	>1 day	DPV	0.014	0.011	0.008	0.05–1752	0.05–1628	0.02–1056	22
Modification-free SPCE	No	SWV	0.37	5.07	3.32	1–60	10–400	10–400	This work

PGCE: pretreated glassy carbon electrode; MWCNT: multi-walled carbon nanotubes; PEDOT: poly(3,4-ethylenedioxythiophene); Fc: ferrocenecarboxylic acid; $Fe(CN)_6^{4-}$: ferricyanide; ZrO_2NPs: zirconia nanoparticles; Ag-PLA: silver-doped poly(L-arginine); f-MWCNT-Cu_2O–Ag_2O: functionalized multi-walled carbon nanotubes supporting Cu_2O and Ag_2O composite; DPV: differential pulse voltammetry; LSV: linear sweep voltammetry. [a] Estimated modification time (1 electrode). All modification steps were included.

Table 2 Tolerance ratios of foreign species in the simultaneous determination of 20 μM VB_2, 60 μM VC, and 60 μM VB_6 on the common SPCEs

Foreign species	Tolerance ratio ($C_{species}/C_{target\ vitamins}$)		
	VB_2	VC	VB_6
Na^+, K^+, Mg^{2+}, Ca^{2+}, Al^{3+}, Cl^-, HCO_3^-, SO_4^{2-}, PO_4^{3-}	3000	1000	1000
VB_1, VB_3, VB_5, glucose, fructose, citrate, L-lysine, L-cysteine, L-methionine	300	100	100
Fe^{2+}, Cu^{2+}, VB_9, oxalate	30	10	10
VB_{12}, uric acid	15	5	5
Albumin, globulin	5	5	5

60 μM VB_6 in PBS pH 3.5 was evaluated. The tolerance limit was calculated to be lower than 5% of the relative error. The results revealed that 3000-fold and 1000-fold concentration ratios of Na^+, K^+, Mg^{2+}, Ca^{2+}, Al^{3+}, Cl^-, HCO_3^-, SO_4^{2-}, and PO_4^{3-}; 300-fold and 100-fold concentration ratios of VB_1, VB_3, VB_5, glucose, fructose, citrate, L-lysine, L-cysteine, and L-methionine; 30-fold and 10-fold concentration ratios of Fe^{2+}, Cu^{2+}, VB_9, and oxalate; 15-fold and 5-fold concentration ratios of VB_{12} and uric acid; and 5-fold concentration ratios of albumin and globulin did not interfere with the measurement of VB_2, VC, and VB_6 (Table 2). No significant changes in the current signals were observed. Thus, the proposed electrodes show good selectivity towards the simultaneous determination of these three vitamins.

3.6. Application in real samples

To examine the practicality and reliability of the proposed method, the simultaneous determination of VB_2, VC, and VB_6 at the common SPCE was performed in mixed vegetable and fruit juice and artificial urine samples. The concentrations of the vitamins were determined by square wave voltammetry using the standard addition method to prevent any matrix influence. Recovery studies were carried out by spiking VB_2, VC, and VB_6 into the samples at various concentration levels. The experimental results revealed in Tables S2 and S3 (ESI†) display that the recovery values were in the range of 83.91–109.10%, which is acceptable. Furthermore, to confirm the accuracy of the proposed method, the concentrations of VB_2, VC, and VB_6 in these samples were also determined by HPLC-DAD. The paired *t*-test between the two methods disclosed that the results were in good agreement because the calculated *t*-value (2.15) was less than the critical value (2.31) for a two-tailed comparison. Therefore, a common SPCE can be successfully used for the simultaneous determination of VB_2, VC, and VB_6 in real applications.

4. Conclusions

In summary, a simple and cost-effective modification-free SPCE was developed for the simultaneous determination of VB_2, VC, and VB_6. To the best of our knowledge, the measurement of these water-soluble vitamins at a common SPCE was performed for the first time. While continuously maintaining high efficiency, the proposed electrode still provided many advantages over previous conventional modified-electrodes, such as disposability, simple fabrication procedure, elimination of electrode maintenance, and low solution volume requirement. The effects of various typical supporting electrolytes were successively studied to investigate the electrochemical behavior of VB_2, VC, and VB_6. Under the optimal conditions, using PBS pH 3.5 as a suitable supporting electrolyte, a common SPCE exhibited good sensitivity, selectivity, and reproducibility towards the simultaneous determination of VB_2, VC, and VB_6 in the oxidative direction without any surface modification of the working electrode. Finally, the proposed procedure was applied for the simultaneous determination of these vitamins in mixed vegetable and fruit juice and in artificial urine with satisfactory results. Therefore, this proposed assay can be selected as a good and attractive choice for the simultaneous determination of water-soluble vitamins in food and clinical samples.

Conflicts of interest

There are no conflicts to declare.

Acknowledgements

PY would like to acknowledge the National Research Council of Thailand (NRCT) through the Royal Golden Jubilee PhD program (Grant number PHD/0179/2560). WS is thankful for partial financial support from the Thailand Research Fund *via* the Research Grant (Grant number RSA6080060). Laboratory facilities were supported by the Department of Chemistry, Faculty of Science, Srinakharinwirot University.

Notes and references

1 S. J. Chalk, *IUPAC Compendium of Chemical Terminology*, supporting electrolyte, 2019.
2 J. Wang, *Analytical Electrochemistry*, VCH Publishers, Inc., New York, 1994.
3 C. M. A. Brett and A. M. O. Brett, *Electrochemistry: Principles, Methods And Applications*, Oxford University Press, Oxford, 1993.
4 D. T. Sawyer and J. R. Roberts, *Experimental for Chemists*, Wiley, New York, 1974.
5 Z. Zainal, C. Y. Lee, M. Z. Hussein, A. Kassim and N. A. Yusof, *J. Photochem. Photobiol., A*, 2005, **172**, 316–321.
6 J. Lu, Y. Kou, X. Jiang, M. Wang, Y. Xue, B. Tian and L. Tan, *Colloids Surf., A*, 2019, **530**, 123652.
7 P. S. Prasad, S. P. Kumar, K. Bharathi and V. Narayanan, *Mater. Today*, 2018, **5**, 9026–9032.
8 T. Sha, J. Liu, M. Sun, L. Li, J. Bai, Z. Hou and M. Zhou, *Talanta*, 2019, **200**, 300–306.
9 D. A. Bender, *Nutritional Biochemistry of the Vitamins*, Cambridge University Press, New York, 2nd edn, 2003.
10 W. T. Penberthy, Niacin, riboflavin, and thiamine, in *Biochemical, Physiological, and Molecular Aspects of Human Nutrition*, ed. M. H. Stipanuk and M. A. Caudill, Elsevier Saunders, Missouri, 2000.
11 D. Kuzmanović, M. Khan, E. Mehmeti, R. Nazir, N. R. R. Amaizah and D. M. Stanković, *Diamond Relat. Mater.*, 2016, **64**, 184–189.
12 N. Lavanya, E. Fazio, F. Neri, A. Bonavita, S. G. Leonardi, G. Neri and C. Sekar, *J. Electroanal. Chem.*, 2016, **770**, 23–32.
13 F. L. Russell, Quantitative determination of water-soluble vitamins, in *Food Analysis by HPLC*, ed. L. M. N. Nollet, Marcel Dekker Inc, New York, 2000.
14 S. P. Arya, M. Mahajan and P. Jain, *Anal. Chim. Acta*, 2001, **427**(2), 245–251.
15 M. J. Chaichi and S. O. Alijanpour, *J. Lumin.*, 2013, **134**, 195–200.
16 D. Abd El-Hady and H. M. Albishri, *Talanta*, 2015, **139**, 150–158.
17 H. Y. Gu, A. M. Yu and H. Y. Chen, *Anal. Lett.*, 2001, **34**(13), 2361–2374.
18 W. Xiang, J. Y. Li and Z. Y. Ma, *J. Anal. Sci. Technol.*, 2007, **23**(4), 437–440.
19 T. Nie, J.-K. Xu, L.-M. Lu, K.-X. Zhang, L. Bai and Y.-P. Wen, *Biosens. Bioelectron.*, 2013, **50**, 244–250.
20 T. Nie, K. Zhang, J. Xu, L. Lu and L. Bai, *J. Electroanal. Chem.*, 2014, **717-718**, 1–9.
21 G. Liu, Y. M. Wang and D. M. Sun, *J. Anal. Chem.*, 2016, **71**, 102–109.
22 A. Puangjan, S. Chaiyasith, W. Taweeporngitgul and J. Kaewtep, *Mater. Sci. Eng., C*, 2017, **76**, 383–397.
23 B. Bas, M. Jakubowska and L. Górski, *Talanta*, 2011, **84**, 1032–1037.
24 S. B. Revin and S. A. John, *Electrochim. Acta*, 2012, **75**, 35–41.
25 N. Shadjou, M. Hasanzadeh and A. Omari, *Anal. Biochem.*, 2017, **539**, 70–80.
26 P. K. Sonkar, V. Ganesan, S. K. S. Gupta, D. K. Yadav, R. Gupta and M. Yadav, *J. Electroanal. Chem.*, 2017, **807**, 235–243.
27 K. L. Westmacott, A. Crew, O. Doran and J. P. Hart, *Talanta*, 2018, **181**, 13–18.
28 Z. Taleat, A. Khoshroo and M. M. Ardakani, *Microchim. Acta*, 2014, **181**(9–10), 865–891.
29 K. Pungjunun, S. Chaiyo, N. Praphairaksit, W. Siangproh, A. Ortner, K. Kalcher, O. Chailapakul and E. Mehmeti, *Biosens. Bioelectron.*, 2019, **143**, 111606.
30 S. Nantaphol, A. A. Kava, R. B. Channon, T. Kondo, W. Siangproh, O. Chailapakul and C. S. Henry, *Anal. Chim. Acta*, 2019, **1056**, 88–95.
31 F. Arduini, S. Cinti, V. Caratelli, L. Amendola, G. Palleschi and D. Moscone, *Biosens. Bioelectron.*, 2019, **126**, 346–354.
32 L. M. Fu and Y. N. Wang, *Trends Anal. Chem.*, 2018, **107**, 196–211.
33 V. Primpray, O. Chailapakul, M. Tokeshi, T. Rojanarata and W. Laiwattanapaisal, *Anal. Chim. Acta*, 2019, **1078**, 16–23.
34 T. R. de Oliveira, W. T. Fonseca, G. de, O. Setti and R. C. Faria, *Talanta*, 2019, **105**, 480–489.
35 S. Chaiyo, E. Mehmeti, W. Siangproh, T. L. Hoang, H. P. Nguyen, O. Chailapakul and K. Kalcher, *Biosens. Bioelectron.*, 2018, **102**, 113–120.
36 S. Fujisaki, H. Shibata, K. Yamada, K. Suzuki and D. Citterio, *Analyst*, 2019, **144**, 2746–2754.
37 S. Nantaphol, W. Jesadabundit, O. Chailapakul and W. Siangproh, *J. Electroanal. Chem.*, 2019, **832**, 480–485.
38 E. S. Sá, P. S. da Silva, C. L. Jost and A. Spinelli, *Sens. Actuators, B*, 2015, **209**, 423–430.
39 M. D. Lovander, J. D. Lyon, D. L. Parr IV, J. Wang, B. Parke and J. Leddy, *J. Electrochem. Soc.*, 2018, **165**(2), G18–G49.
40 M. Swain, *J. Chem. Inf. Model.*, 2012, **52**, 613–615.
41 I. G. R. Gutz, CurTiPot pH and Acid–Base Titration, 2012, Available from: http://www2.iq.usp.br/docente/gutz/Curtipot.html.

42 D. R. Lide, *CRC Handbook of Chemistry and Physics*, 2005, Internet Version, Available from: http://www.hbcpnetbase.com.
43 P. C. Ho and D. A. Palmer, *Electrical conductivity measurements of aqueous boric acid at 25–350 °C at saturation vapor pressure*, 1995.
44 T. Thomas, R. J. Mascarenhas, O. J. D Souza, S. Detriche, Z. Mekhalif and P. Martis, *Talanta*, 2014, **125**, 352–360.
45 G. Jiang, X. Gu, G. Jiang, T. Chen, W. Zhan and S. Tian, *Sens. Actuators, B*, 2015, **209**, 122–130.
46 A. C. Boni, A. Wong, R. A. F. Dutra and M. D. P. T. Sotomayor, *Talanta*, 2011, **85**, 2067–2073.
47 E. Laviron, *J. Electroanal. Chem.*, 1979, **101**, 19–28.
48 G. W. Latimer, *Official Methods of Analysis of AOAC International*, AOAC International, 20th edn, 2016.

Appendix 2

Journal of Electroanalytical Chemistry 911 (2022) 116230

Contents lists available at ScienceDirect

Journal of Electroanalytical Chemistry

journal homepage: www.elsevier.com/locate/jelechem

Rapid urinary albumin detection using a simple redox cycling process coupled with a paper-based device

Phanumas Yomthiangthae [a], Orawon Chailapakul [b], Weena Siangproh [a,*]

[a] Department of Chemistry, Faculty of Science, Srinakharinwirot University, Wattana, Bangkok 10110, Thailand
[b] Department of Chemistry, Faculty of Science, Chulalongkorn University, Phayathai, Bangkok 10330, Thailand

ARTICLE INFO

Keywords:
Albumin
Electrochemical detection
Paper-based device
Redox cycling process
Ferricyanide
Methylene blue

ABSTRACT

A novel electrochemical-chemical (EC) redox cycling process was proposed for the sensitive, simple, and rapid detection of urinary albumin. This system employs a unique detection scheme based on the combination of ferricyanide ($[Fe(CN)_6]^{3-}$) and methylene blue (MB) for signal amplification without the need for any electrode surface modifications. Measurements of bovine serum albumin (BSA) were performed as proof of concept using disposable electrochemical paper-based analytical devices (ePADs) as detection platforms. The quantification of albumin is accomplished by using an indirect detection strategy. In the absence of BSA, electron transfer via EC redox cycling process occurs readily between the redox species and the electrode surface, resulting in a large electrochemical signal. The redox species solution containing BSA, on the other hand, provides a low signal current due to the hindrance of BSA on the electrode surface, which impedes the electron transfer of the proposed redox probe. Under the optimized conditions, the linear range was 1–500 mg dL^{-1} with a detection limit of 0.072 mg dL^{-1}. This finding leads to the development of a powerful method for the direct detection of albumin at a low concentration and no requirement for correction by creatinine. The proposed devices were successfully used to detect albumin in real urine samples with satisfactory results, demonstrating good agreement with the standard method and the reliability. Aside from the ease and rapidity, the proposed method is inexpensive, sensitive, and a promising tool for clinical diagnosis of chronic kidney disease and suitable for point-of-care testing in developing countries.

1. Introduction

Chronic kidney disease (CKD) is one of the major global health issues associated with the gradual loss of kidney function, which leads to premature death, decreased quality of life, and high healthcare costs [1]. The high-risk factor of diabetes mellitus, cardiovascular disease, and other adverse health outcomes, including end-stage renal disease (ESRD), are all increased by CKD. According to the previous reports, the prevalence of CKD at the 3rd and 4th stages in Thai population over the age of 18 was estimated to be 9.3%, representing 4.8 million patients [2], whereas 4.6 million of Thai people also suffer from CKD at the 1st and 2nd stages. To prevent the progression of CKD, the accessibility of albumin level screening is highly required for a person who is at risk of kidney disease.

A 24-h urine collection has long been the "gold standard" method in clinical diagnostic tests for the accurate detection of urinary albumin excretion [3]. This urinalysis takes into account albumin fluctuations during the day and day-to-day readings caused by factors, such as activities of the patient, emotional state, amount of protein consumed, blood pressure, and body temperature [4]. Albumin concentrations in urine should typically be less than 30 mg/24 h [5]. The higher albumin concentration in a range of 30–300 mg/24 h indicates microalbuminuria status, which is the earliest stage of diabetic nephropathy [6]. Furthermore, this stage may progress to irreversible macroalbuminuria [7], in which albumin will be found at more than 300 mg/24 h in the urine. This severe status increases the risk of future CKD. The main difficulty of a 24-h urine collection is that the results probably take at least 1 week to be obtained, resulting in a delay in report. However, it is still an accurate diagnosis because of the low false-positive results obtained in elderly patients, making it a good predictor of quantitative albumin excretion. Consequently, a 24-h urine collection strategy was selected as a suitable tool for albumin measurement to accurately indicate a risk of renal failure.

Conventional spectroscopy and colorimetry have been widely used in clinical analysis for albumin quantification [8]. The major disadvantages of these methods are the large volumes of reagents required and

* Corresponding author.
E-mail address: weena@g.swu.ac.th (W. Siangproh).

https://doi.org/10.1016/j.jelechem.2022.116230
Received 5 October 2021; Received in revised form 12 March 2022; Accepted 15 March 2022
Available online 18 March 2022

the incompatibility with detergents, which can interfere with the ability of dye to bind the protein. To overcome these limitations, other techniques were developed, such as enzyme-linked immunosorbent assay (ELISA) [9], chromatography [10], flow injection analysis [11], surface plasmon resonance [12], and fluorescence emission spectroscopy [13]. Each method is well-known in terms of high sensitivity and selectivity. However, the vast majority of such protein detection systems have time-consuming procedures and use expensive instruments. Therefore, the development of alternative techniques that are simple and rapid for the albumin detection is greatly interesting.

The electroanalytical method is a powerful tool that is effectively used in a variety of clinical diagnostic applications owing to its high sensitivity, low-cost instrument, portability, and ease of operation [14]. Several previous studies demonstrated that using an electrochemical technique provided a broad linear concentration range with a low detection limit, indicating its capability to detect albumin at the trace level [15–17]. Moreover, a variety of unique nanomaterials, including silicon nanowires (SiNWs) [18], CdSe/ZnS quantum dots [19], and MoS_2 nanoflakes [20], as well as molecularly imprinted polymers (MIPs) [21] were used for electrode modification, resulting in high sensitivity and selectivity. The use of large-scale conventional electrode systems and the complicated modification steps are the main problems of these works, limiting their applications for rapid albumin screening in developing countries. As a result, the strategy of improving sensitivity by using unmodified electrodes promptly motivated interest in overcoming these drawbacks.

Recently, a label-free electrochemical immunoassay for rapid protein measurements of malaria biomarkers that uses electrochemical-chemical (EC) redox cycling process to amplify the signal was presented [22]. In this immunoassay, hexaammineruthenium (III) ($[Ru(NH_3)_6]^{3+}$) and methylene blue (MB) were used as an electron mediator and a mediator substrate, respectively. $[Ru(NH_3)_6]^{3+}$ was firstly reduced to $[Ru(NH_3)_6]^{2+}$ via an electrochemical reaction on the electrode surface. Subsequently, MB was used to re-oxidize $[Ru(NH_3)_6]^{2+}$ back to $[Ru(NH_3)_6]^{3+}$ via a chemical reaction. This process occurs continuously, resulting in the generation of a large electrochemical signal. The results indicated that the EC redox cycling process was effective in amplifying the detection signal without the need for additional electrode modification. As a result, the EC redox cycling system has a potential for use in point-of-care testing in resource-constrained settings.

The primary aim of this research was to develop a simple and rapid electrochemical detection of albumin using a non-modified electrode fabricated on a disposable paper substrate called an electrochemical paper-based analytical device (ePAD). Graphene was used as a core material for the fabrication of ePADs, which provided high surface area, electrical conductivity, and biocompatibility. The sensor measures albumin using the EC redox cycling process, which combines a mixed redox probe of two electroactive species, ferricyanide ($[Fe(CN)_6]^{3-}$) and MB, for signal amplification without requiring any modifications to the working electrode. Unlike previous electrochemical sensors, our devices provide a sensitive and selective assay for accurate albumin detection at low concentrations without the need for creatinine correction. This platform also demonstrates the feasibility of detecting albumin in real urine samples without any interference effects, making it is suitable for use as an alternative tool for a 24-h urine collection to predict the early stages of kidney disease.

2. Experimental section

2.1. Chemicals and reagents

The details of chemicals and reagents are presented in the Supplementary Information.

2.2. Manufacturing process of the ePAD

With a variety of paper designs, a foldable ePAD was specifically designed to propose an alternative style for a simple detection of urinary albumin. Fig. 1 presents the pattern of paper devices created using Adobe Illustrator CC 2018. The ePAD had two main components, namely, a gray side (left) serving as a counter electrode (CE) and a reference electrode (RE) on the hydrophilic area and an orange side (right) serving as a working electrode (WE) (1.5 cm × 3.0 cm in size) on the hydrophobic area. To fabricate the ePAD, the device pattern was first printed on filter paper (Whatman no. 4) employing the wax-printing technique using Fuji Xerox ColorQube 8580. The printed device was then placed on a hot plate at 175 °C for 50 s to allow the wax to dissolve into the paper. At this point, the ePAD was made up of both hydrophobic and hydrophilic areas in the same device. Subsequently, a three-electrode system was created on the patterned paper using the manual screen-printing method described in the previous report [23]. In brief, graphene paste (ZP-1838) was directly screen-printed onto a paper device to produce both WE and CE. WE had a geometric area of 0.126 cm^2 (calculated using circular area = πr^2; r = 0.2 cm). Then, to create RE and conductive pads, Ag/AgCl paste (C2130809D5) was screen-printed onto the same device. Following each screen-printing process, the device was heated in an oven at 55 °C for 30 min to allow the solvent in the pastes to evaporate and the electrodes to dry. After that, a transparent tape was applied on the back side of the orange paper to prevent solution leakage during electrochemical measurement. Before use, the middle hydrophilic area of the gray side was punctured to create a sample reservoir (5 mm in diameter). A double-sided adhesive tape was used to attach the upper and lower parts of the paper device on the gray side. Then, the paper device was folded by folding a gray side attached to an orange side, which allowed the solution to flow directly to cover electrode surfaces. Besides, after connecting the paper device with electrical wires from a potentiostat, a transparent tape was used to attach the paper device to the smooth surface of a lab bench, making both sides of the paper attach more firmly with no leaking of solution. The ePAD is now ready to be used for the detection of albumin in the next step.

2.3. Electrochemical measurements

The ECAS100 potentiostat from Zensor Research & Development Corporation (Taiwan) was used for the electrochemical experiments. As a redox cycling process, the mixture solution containing 4 mM of $[Fe(CN)_6]^{3-}$ and 0.05 mM of MB in PBS (pH 7.4) was used for this study, and a blue-green color solution was obtained. This solution was prepared in a microcentrifuge tube and labeled as in the absence of albumin. In the presence of albumin, a redox cycling solution and BSA standard solution were mixed in the same tube. For detection, 100 μL of a pure redox cycling solution or that mixed with BSA standard solution was thoroughly dropped onto an ePAD sample reservoir, covering all three electrodes. Subsequently, electrochemical techniques, such as cyclic voltammetry (CV) and differential pulse voltammetry (DPV), were performed. The potential was applied over a range of +0.6 to −0.6 V, with a scan rate of 100 mV s^{-1} for CV measurements. DPV measurements were used for quantitative analysis using potentials ranging from +0.5 to −0.2 V, with an increment potential of 10 mV, an amplitude of 50 mV, a pulse width of 200 ms, a sample width of 100 ms, and a pulse period of 500 ms. To quantify albumin concentration, the signal current of the redox cycling solution with BSA standard solution was measured and compared with the signal current of the redox cycling solution without BSA standard solution. The analysis can be conducted for 1 min, as presented in Scheme 1.

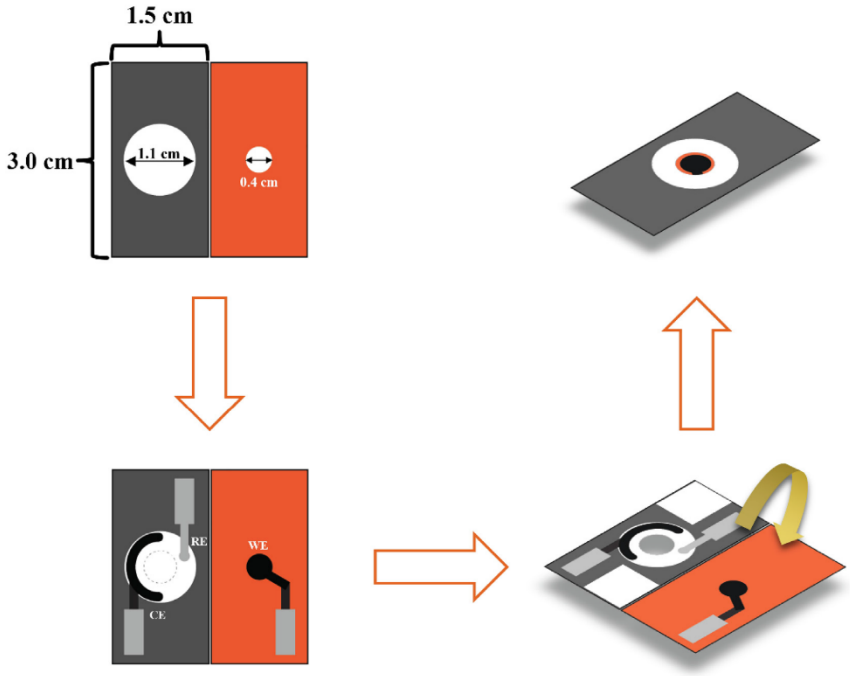

Fig. 1. The design and composition of ePAD used in this work.

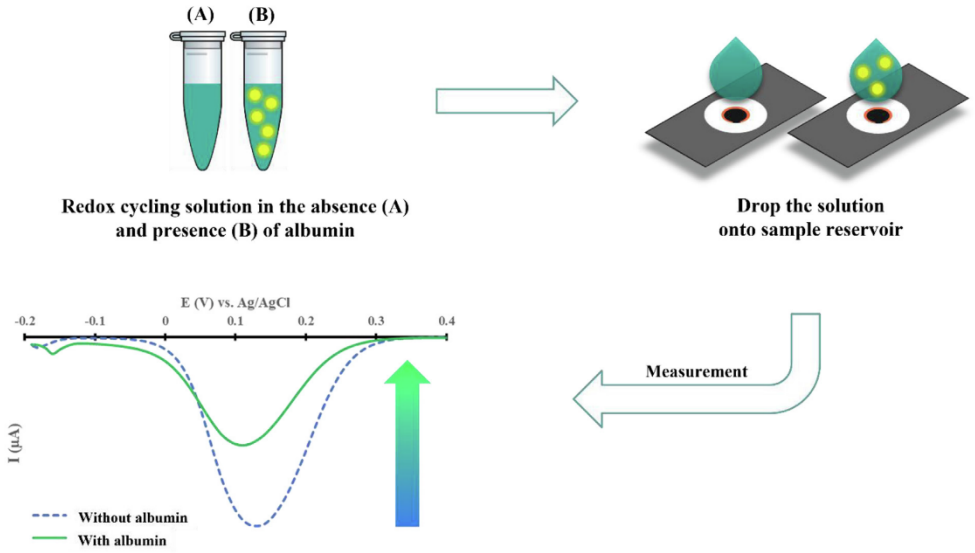

Scheme 1. Schematic illustration of the overall detection process for the measurement of albumin by mixing BSA standard solution with a redox cycling solution.

2.4. Sample preparation

Urine samples were examined for albumin detection to demonstrate the real-world application of the proposed method. Urine samples were collected from healthy human volunteers in our laboratory and immediately refrigerated at 4 °C. We informed all volunteers about what would happen to the human subjects in a trial. The details of urine preparation are presented in the Supplementary Information. The Bradford assay [24] was employed to confirm the accuracy of the proposed method.

3. Results and discussion

3.1. Preliminary study of EC redox cycling process

Prior to performing the albumin detection, an electrochemical investigation of EC redox cycling system was first performed to demonstrate the potential of each proposed process to support the expected results. Cyclic voltammograms of buffer solutions containing only $[Fe(CN)_6]^{3-}$, MB, and the mixture of $[Fe(CN)_6]^{3-}$ and MB were obtained using ePADs, as presented in Fig. 2A. The CV curve of a solution containing only $[Fe(CN)_6]^{3-}$ revealed a pair of redox peaks at +0.36 and −0.15 V, with anodic and cathodic peak currents of +10.64 and −10.67 μA, respectively. Because of the high peak separation (0.51 V) and low peak currents, the electrochemical reaction of $[Fe(CN)_6]^{3-}$ proceeds at a slow rate. Similarly, the solution containing only MB produced a pair of redox peaks at −0.21 and −0.30 V, with anodic and cathodic peak currents of +6.21 and −4.05 μA, respectively. We assumed that MB (MB_{ox}) directly obtains two electrons and one proton to form leucomethylene blue (LMB, MB_{red}), and that LMB is then oxidized back to MB by losing two electrons and one proton [25]. According to the findings, MB can also provide a reversible process at the bare graphene electrode surface. On the other hand, the CV curve of a solution containing both $[Fe(CN)_6]^{3-}$ and MB showed high peak currents for $[Fe(CN)_6]^{3-/4-}$ redox couple of +30.90 and −29.01 μA at peak potentials of +0.21 and +0.05 V (peak separation of 0.16 V) for anodic and cathodic directions, respectively. Another pair of redox peaks for $MB_{ox/red}$ was observed at −0.23 and −0.31 V, with anodic and cathodic peak currents of +4.97 and −2.61 μA, respectively. In comparison with a solution containing only $[Fe(CN)_6]^{3-}$, the $[Fe(CN)_6]^{3-/4-}$ redox couple in mixture solution generated 3 times higher peak currents and 3.2 times lower peak separation. The findings indicated that the EC redox cycling process can increase electron transfer efficiency across the interface. In contrast, the anodic-cathodic peak current of MB obtained from the mixture solution was lower than that obtained from the solution containing only MB. We suspected that it was the signal of MB molecules that remained after the redox cycling system proceeded, and thus, a low electrochemical signal was obtained. To explain a unique EC redox cycling process, $[Fe(CN)_6]^{3-}$ is reduced to $[Fe(CN)_6]^{4-}$ via an electrochemical reaction at the bare graphene electrode, which is then re-oxidized by MB via a chemical reaction, as presented in Fig. 2B. Due to the simultaneous regeneration of $[Fe(CN)_6]^{3-}$, this redox cycling process continuously occurs, resulting in a large electrochemical signal. Based on these findings, it can be concluded that the EC redox cycling process between $[Fe(CN)_6]^{3-}$ and MB was effective for amplifying the detection signal when using an unmodified electrode.

Furthermore, the DPV technique was used to confirm this EC redox cycling process. In this work, we chose the electrochemical measurement in the reductive direction to avoid some interferences observed in the sample, such as ascorbic acid, uric acid, and dopamine, which provide the signal in the oxidative direction [26]. As a result, DPV measurements were performed using potentials ranging from +0.5 to −0.5 V. The solution containing only $[Fe(CN)_6]^{3-}$ exhibited a broad voltammogram at a cathodic potential of +0.01 V with a cathodic current of −3.76 μA, as presented in Fig. S1. Meanwhile, the DPV curve of a solution containing only MB revealed a well-defined cathodic peak at −0.23 V with a current of −11.30 μA. The mixture solution of $[Fe(CN)_6]^{3-}$ and MB, on the other hand, generated a sharp and symmetrical peak of $[Fe(CN)_6]^{3-}$ at a cathodic potential of +0.14 V with a cathodic current of −34.90 μA. Another peak was a cathodic peak of MB at a potential of −0.25 V with a current of −8.76 μA. The signal of $[Fe(CN)_6]^{3-}$ obtained from a mixture solution generated 9.3-fold higher cathodic current with a higher positive potential than the signal obtained from a solution containing only $[Fe(CN)_6]^{3-}$. For the MB peak, the signal current of MB obtained from the mixture solution was lower than that of the MB single solution. The results of this additional investigation were in good agreement with those of the CV study, indicating that the proposed EC redox cycling process has a high catalytic capability for the electrochemical reduction of $[Fe(CN)_6]^{3-}$. As a result, without any modifications to the working electrode, a high sensitivity for albumin detection can be obtained.

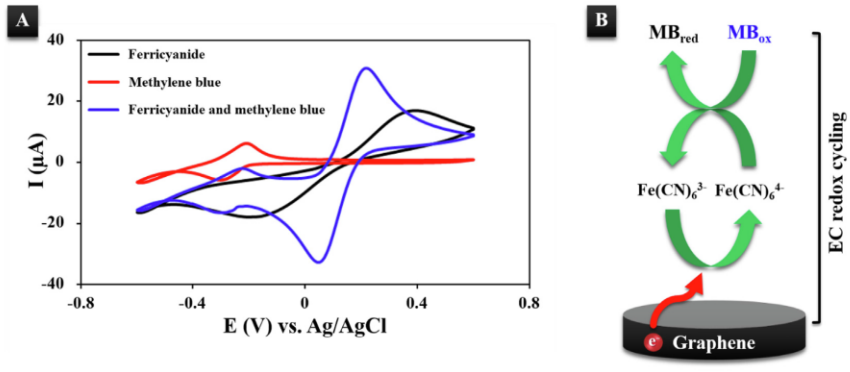

Fig. 2. (A) Cyclic voltammograms of PBS (pH 7.4) containing only 1 mM $[Fe(CN)_6]^{3-}$ (black line), 0.05 mM MB (red line), and the mixture of 1 mM $[Fe(CN)_6]^{3-}$ and 0.05 mM MB (blue line). (B) Schematic illustration of EC redox cycling process using $[Fe(CN)_6]^{3-}$ and methylene blue (MB).

3.2. Optimization of EC redox cycling process

The effects of $[Fe(CN)_6]^{3-}$ and MB concentrations on the EC redox cycling process are presented in the Supplementary Information and Fig. S2.

3.3. Albumin detection using EC redox cycling process

The albumin detection was performed using the DPV technique under optimized experimental conditions, as presented in Fig. 3A. A differential pulse voltammogram of a buffer solution containing only 400 mg dL^{-1} BSA standard solution revealed no cathodic peak, indicating that BSA is a non-electroactive macromolecule that cannot occur in the reduction process on an unmodified graphene electrode. As a result, the EC redox cycling process was applied to provide the high current response. A cathodic peak of $[Fe(CN)_6]^{3-}$ at +0.13 V with a peak current of −79.17 μA was observed on the DPV curve of a redox solution containing 4 mM $[Fe(CN)_6]^{3-}$ and 0.05 mM MB. The results indicated that the EC redox cycling process produced a high signal current of $[Fe(CN)_6]^{3-}$, expecting a high sensitivity for albumin detection without further electrode modification. Subsequently, a cathodic peak of $[Fe(CN)_6]^{3-}$ at +0.11 V with a peak current of −43.73 μA was observed in a mixture solution of 4 mM $[Fe(CN)_6]^{3-}$, 0.05 mM MB, and 400 mg dL^{-1} BSA standard solution. In comparison with a redox solution containing both $[Fe(CN)_6]^{3-}$ and MB, the lower cathodic peak potential was obtained, and the difference in the cathodic peak current (ΔI_{pc}) was equal to −35.44 μA, indicating that BSA hinders the electron-transfer process of the EC redox cycling system, as shown in Fig. 3B. We strongly believe that this behavior may be the obstruction of negatively charged BSA (pI = 4.7) [27] at the electrode surface, leading to the blocking of the reduction process for $[Fe(CN)_6]^{3-}$ to accept electrons from a working electrode. This circumstance resulted in a diminishing current response because $[Fe(CN)_6]^{3-}$ is hardly reduced to $[Fe(CN)_6]^{4-}$, which is then slightly re-oxidized by MB. Aside from detecting albumin by mixing a BSA standard with a redox cycling solution, we discovered another method, which is the dropping and drying of the BSA standard solution on the working electrode as shown in Scheme S1. The cathodic peak of $[Fe(CN)_6]^{3-}$ at +0.13 V with a peak current of −79.17 μA obtained from a redox cycling solution on a bare working electrode is presented in Fig. S3. In contrast, a redox cycling solution on a working electrode covered with BSA, labeled as BSA/Graphene, generated a cathodic peak of $[Fe(CN)_6]^{3-}$ at +0.11 V with a peak current of −48.10 μA. The lower cathodic peak potential was obtained, and the ΔI_{pc} was equal to −31.07 μA when compared with the signal current in the absence of BSA. The results indicated that the BSA molecule blocks the electroactive sites on the graphene surface, resulting in a lower cathodic response of a redox cycling solution. This finding was compatible with albumin detection by mixing a BSA standard solution with a redox cycling solution; however, it was not suitable for a rapid detection, which was our ultimate goal, due to the time-consuming process of drying BSA on the working electrode. Based on these findings, we decided to mix all solutions in the same microcentrifuge tube to detect albumin simply and rapidly. As a result, in the following investigation, BSA will be quantified using a mixture of BSA standard solution and a redox cycling solution.

3.4. Analytical performance

Following the presentation of the albumin detection strategy in Section 3.3, the analytical performance of albumin was evaluated by combining the optimal redox cycling solution (4 mM $[Fe(CN)_6]^{3-}$ and 0.05 mM MB) with various concentrations of BSA standard solution. As presented in Fig. 4A, the peak currents decreased as a function of BSA concentration. Fig. 4B presents the relationship between different BSA concentrations and ΔI_{pc} values. The results indicated that the change in the ΔI_{pc} responses has a non-linear relationship with the BSA concentrations. The logarithmic value of the BSA concentrations was plotted against the ΔI_{pc} values to obtain the linear relationship, as presented in the inset of Fig. 4B. This discovery revealed that the calibration curve was obtained in the range of 1–500 mg dL^{-1} ($y = -20.199x + 0.7704$ with a correlation coefficient (R^2) of 0.9904). The limit of detection ($3SD_{blank}$/slope) and the limit of quantification ($10SD_{blank}$/slope) from a calculation were found to be 0.072 and 0.24 mg dL^{-1}, respectively. These findings demonstrated that the EC redox cycling process can achieve highly sensitive and quantitative detection of BSA over a wide linear range. Table 1 presents the comparison of the analytical performance between the proposed method and those of some previous reports for albumin detection found in the literature. According to this information, our assay proposed the detection of BSA using non-modified graphene electrodes fabricated on a paper substrate for the first time, which have the advantages of cost-effectiveness, simple disposability, and uncomplicated operation. Furthermore, the proposed method was very compelling for rapid

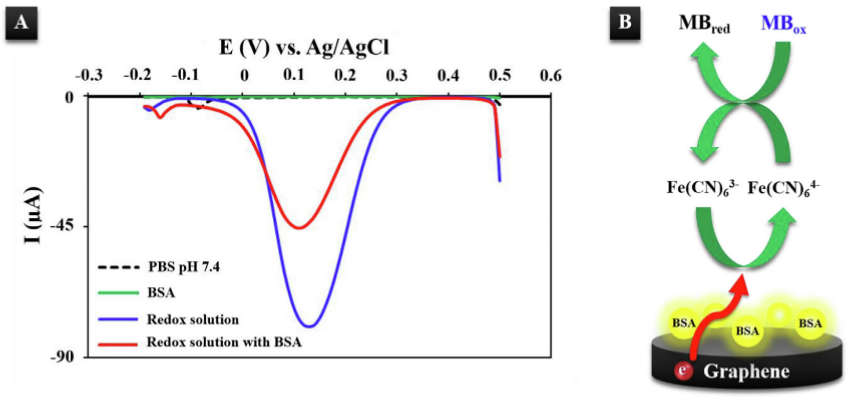

Fig. 3. (A) Differential pulse voltammograms of PBS (pH 7.4) (black dash line) containing only 400 mg dL^{-1} BSA standard solution (green line), the mixture of 4 mM $[Fe(CN)_6]^{3-}$ and 0.05 mM MB (blue line), and the mixture of 4 mM $[Fe(CN)_6]^{3-}$, 0.05 mM MB, and 400 mg dL^{-1} BSA standard solution (red line). (B) Schematic illustration of the EC redox cycling process in the presence of BSA.

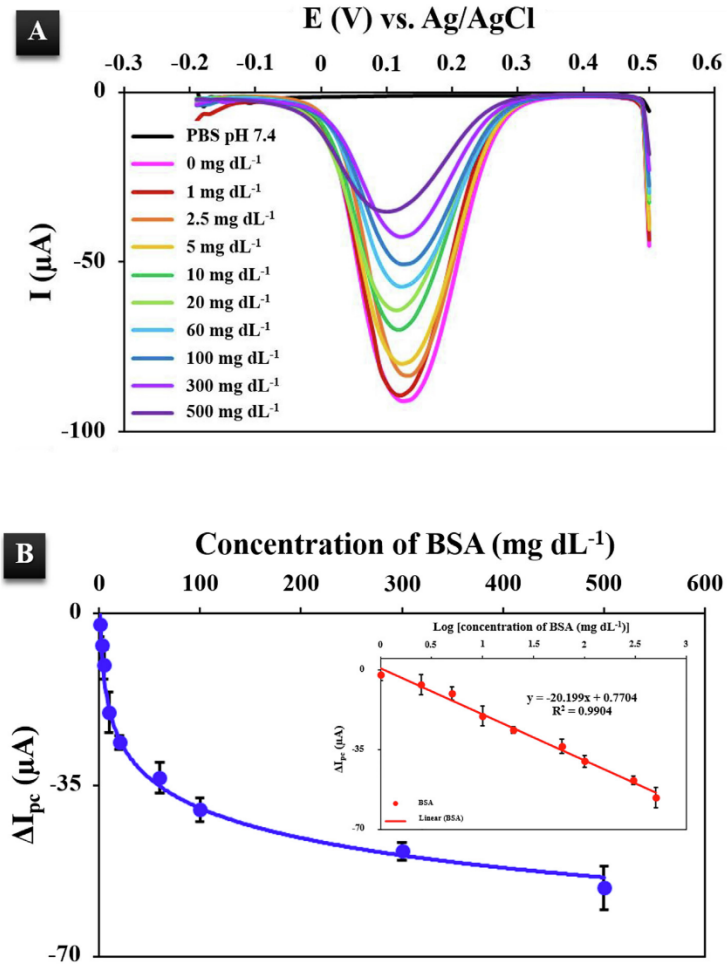

Fig. 4. (A) DPVs for different BSA concentrations mixed with 4 mM $[Fe(CN)_6]^{3-}$ and 0.05 mM MB in PBS (pH 7.4). BSA concentrations: 1, 2.5, 5, 10, 20, 60, 100, 300, and 500 mg dL^{-1}. (B) The ΔI_{pc} of BSA on ePADs at different concentrations (1 to 500 mg dL^{-1}). Inset: Calibration curve plotted on a logarithmic scale.

Table 1
Comparison of the analytical performance between the proposed method and other reports based on electrochemical technique for the detection of BSA.

Biosensor/Substrate	Detection strategy	Technique	Limit of detection (mg dL^{-1})	Linear range (mg dL^{-1})	Ref.
BDDE	Direct	CV	5	5–3000	[28]
SWCNTs/Au	Direct	CV	–	0.67–8	[29]
GCE	Indirect	DPV	0.76	1–8	[30]
$[Ru(bpy)_2(tatp)]^{2+}$-SWCNTs/ITO	Indirect	DPV	0.3	0.6–5	[31]
HCNT-PtNFs/GCE	Indirect	DPV	0.01	1.7–17	[32]
Graphene/PAD	Indirect	DPV	0.072	1–500	This work

detection in clinical applications, so we anticipated that the performance of this proposed sensor would be sufficient for the detection of BSA in real urine samples.

The reproducibility of this device was also investigated using three different concentrations of BSA standard solution (10, 80, and 400 mg dL^{-1}) mixed with 4 mM $[Fe(CN)_6]^{3-}$ and 0.05 mM MB in PBS (pH 7.4). For each mixture solution, nine sensors (n = 9) were examined, and the electrochemical measurements were then performed using the DPV technique. The relative standard deviations were found to be in the range of 3.38% – 6.26%, indicating that good device-to-device reproducibility with low variation was obtained for BSA detection.

3.5. Interference study

The influence of some possible interfering substances found in urine samples on the detection of BSA using the EC redox cycling process was investigated using the DPV technique under optimal conditions to elucidate the selectivity of the proposed assay. The redox cycling solution (4 mM $[Fe(CN)_6]^{3-}$and 0.05 mM MB) containing 50 mg dL^{-1} BSA standard solution was detected via DPV measurement using ePADs, in which the signal current was set to 100%. The freshly prepared mixture solutions containing the redox cycling solution, 50 mg dL^{-1} BSA standard solution, and some foreign substances were successively detected under the same DPV conditions. The interfering substances used for this study were 400 μg dL^{-1} dopamine, 30 mg dL^{-1} ascorbic acid, 85 mg dL^{-1} uric acid, 500 mg dL^{-1} Na^+, K^+, NH_4^+, Mg^{2+}, Ca^{2+}, SO_4^{2-}, glucose, creatinine, and 2000 mg dL^{-1} urea, which are the maximum concentrations found in the samples [33–35]. The cathodic response of solution in the absence of foreign species was used to normalize the signal currents of solutions containing interferences. Fig. 5 shows that the changes in the cathodic current of BSA containing interferences were less than ± 5%, indicating that foreign species had no significant effect on the signal current of the redox cycling solution containing BSA. These findings confirmed the good selectivity of developed redox probes for albumin detection in the presence of various possibly interfering substances.

3.6. Dilution effect

Because urine contains a highly variable matrix that may affect albumin detection, the influence of dilution effect was investigated to ensure accurate quantification. Various dilution ratios of a real urine sample containing 50 mg dL^{-1} BSA standard solution with redox cycling solution (4 mM $[Fe(CN)_6]^{3-}$and 0.05 mM MB) were examined for recovery tests. We selected PBS (pH 7.4) as a diluent solution for BSA detection in this experiment. Table S1 presents that a dilution of at least 50-fold resulted in a good recovery, indicating that interferences in urine would be eliminated during albumin detection. This discovery suggested that a 50-fold dilution using PBS (pH 7.4) could avoid a variety of interferences and dilution effects in urine samples. As a result, urine samples are diluted at 50-fold with PBS (pH 7.4) before analysis.

3.7. Matrix effect

A matrix-matched calibration was performed using a 50-fold diluted urine sample (where no albumins were present by precipitation with 0.1 M $CuSO_4$) to assess the matrix effect for this proposed method. The matrix effect was calculated by the following equation [36]:.

$$Matrixeffect = \left(\frac{A}{B} - 1\right) \times 100\%$$

Where A denoted the slope of calibration curve in matrix and B denoted the slope of calibration curve in solvent (PBS pH 7.4).

In this study, BSA concentrations ranging from 1 to 500 mg dL^{-1} were spiked directly into diluted urine samples. The solutions were then mixed with 4 mM $[Fe(CN)_6]^{3-}$ and 0.05 mM MB. DPV measurements were used to detect the signal currents of these mixture solutions. Because of the different batch of fabricated ePADs, normalized currents ($I_{normalized}$) of cathodic responses were then calculated using the following equation:.

$$I_{normalized} = \frac{I - I_{min}}{I_{max} - I_{min}}$$

Where I was the cathodic peak current of a solution containing different concentrations of BSA. The maximum and minimum cathodic peak currents obtained from each calibration data set were denoted by I_{max} and I_{min}, respectively.

Subsequently, $I_{normalized}$ values were plotted against the same logarithmic value of BSA concentrations as used for the external calibration curve. As presented in Fig. 6, the matrix effect was found to be −15.17%, indicating that the proposed sample dilution is capable of removing interferences in urine due to a matrix effect value of approximately |15%| [37]. This finding demonstrated that the matrix effect was negligible, implying that the matrix-matched calibration would not be required because the 50-fold dilution of urine not only eliminated interfering substances but also decreased the matrix in the sample. A sample matrix had no significant effect on the detection of BSA in a real sample; thus, the redox cycling solution can be used to accurately detect albumin in complex biological samples.

3.8. Application in real urine samples

The detection of albumin in 13 urine samples obtained from healthy volunteers was evaluated to demonstrate the practical application of this developed assay. All samples were diluted 50-fold in PBS (pH 7.4) before being mixed with 4 mM $[Fe(CN)_6]^{3-}$and 0.05 mM MB. These solutions were then performed by DPV measurement using ePADs, and the amount of albumin in the samples was calculated using the linear equation of the standard calibration curve. The

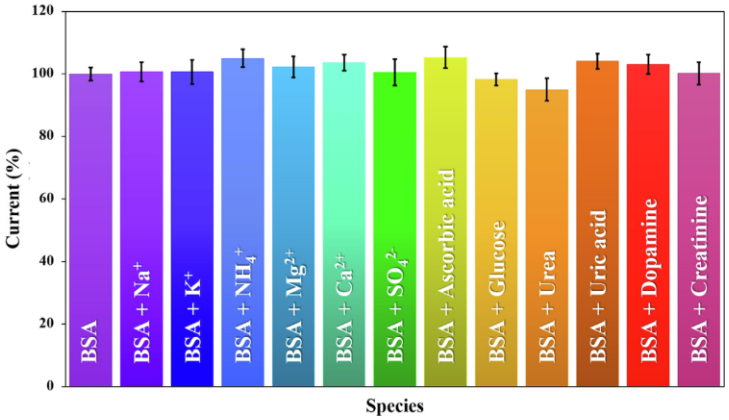

Fig. 5. Effect of some interfering substances on the detection of 50 mg dL^{-1} BSA standard solution mixed with $[Fe(CN)_6]^{3-}$ and MB (n = 3).

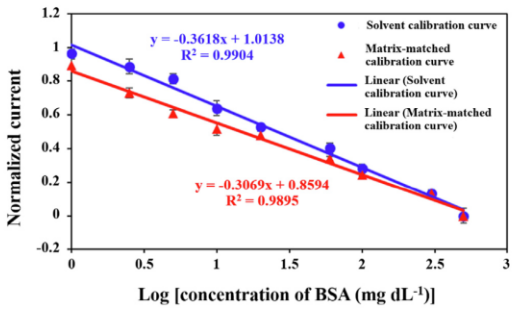

Fig. 6. Comparison of a solvent calibration curve with a matrix-matched calibration curve for BSA detection (n = 3).

recovery study was investigated to verify the accuracy and reliability by adding the known concentration of 50 mg dL^{-1} BSA standard solution into diluted samples. The results summarized in Table S2 indicate that good recovery values were obtained in the range of 96.04% – 104.60%. Moreover, the results obtained using the proposed method were validated by comparing them with the standard Bradford assay. The calculated *t*-value (0.86) was less than the critical *t*-value (2.18) for a two-tailed comparison; the results revealed that the albumin concentrations obtained using this method and those using the standard method were not significantly different. These results indicated the accuracy and reliability of albumin detection in urine samples without creatinine correction. As a result, albumin detection using a mixture solution of $[Fe(CN)_6]^{3-}$ and MB as a redox probe could be a powerful alternative tool for point-of-care testing of urinary albumin in the early stages of kidney disease.

4. Conclusions

For the first time, a powerful EC redox cycling process for albumin detection based on a disposable paper-based device was successfully developed. The process can be simply performed using a mixture of two electroactive species, namely, $[Fe(CN)_6]^{3-}$ and MB. This system generates a large electrochemical signal without requiring any modification for working electrode. The indirect detection strategy was employed for albumin detection due to an obvious decrement of cathodic current in the presence of target analyte. Under optimized conditions, the calibration curve demonstrated a linear relationship between the difference in the cathodic peak current (ΔI_{pc}) and the logarithmic concentration of BSA standard solution in the wide range of 1 to 500 mg dL^{-1}. The detection and quantification limits were found to be 0.072 and 0.24 mg dL^{-1}, respectively. A good reproducibility for the detection was obtained, with RSD lower than 6.3%. Furthermore, the developed method demonstrated a good selectivity for albumin detection in an environment of interferences; thus, this proposed assay has been successfully applied to detect albumin in real urine samples without creatinine correction, yielding desirable results. The major advantages of this procedure are the simplicity of operation, the cost-effectiveness of paper-based devices, and short measurement time of 1 min. Therefore, this redox cycling process offers a promising system for point-of-care testing and can be adapted in the future for simple and highly sensitive detection of other biomolecules.

Declaration of Competing Interest

The authors declare that they have no known competing financial interests or personal relationships that could have appeared to influence the work reported in this paper.

Acknowledgements

PY would like to acknowledge the National Research Council of Thailand (NRCT) through the Royal Golden Jubilee Ph.D. program (Grant number PHD/0179/2560). WS would like to thank partially support by Srinakharinwirot University through the grant number 032/2565 (Fundamental Fund for Basic Research) and the National Research Council of Thailand (NRCT) through the grant number N41A640073.

Appendix A. Supplementary data

Supplementary data to this article can be found online at https://doi.org/10.1016/j.jelechem.2022.116230.

References

[1] T. Srithongkul, P. Ungprasert, Coffee Consumption is Associated with a Decreased Risk of Incident Chronic Kidney Disease: A Systematic Review and Meta-analysis of Cohort Studies, Eur. J. Intern. Med. 77 (2020) 111–116.
[2] C.-W. Yang, D.C.H. Harris, V.A. Luyckx, M. Nangaku, F.F. Hou, G. Garcia Garcia, H. Abu-Aisha, A. Niang, L. Sola, S. Bunnag, S. Eiam-Ong, K. Tungsanga, M. Richards, N. Richards, B.L. Goh, G. Dreyer, R. Evans, H. Mzingajira, A. Twahir, M.I. McCulloch, C. Ahn, C. Osafo, H.-H. Hsu, L. Barnieh, J.-A. Donner, M. Tonelli, Global case studies for chronic kidney disease/end-stage kidney disease care, Kidney International Supplements 10 (1) (2020) e24–e48.
[3] K.R. Polkinghorne, Detection and measurement of urinary protein, Curr. Opin. Nephrol. Hypertens. 15 (2006) 625–630.
[4] J. Kamińska, V. Dymicka-Piekarska, J. Tomaszewska, J. Matowicka-Karna, O.M. Koper-Lenkiewicz, Diagnostic utility of protein to creatinine ratio (P/C ratio) in spot urine sample within routine clinical practice, Crit. Rev. Clin. Lab. Sci. 57 (5) (2020) 345–364.
[5] H.J. Lambers Heerspink, A.H. Brantsma, D. de Zeeuw, S.J.L. Bakker, P.E. de Jong, R.T. Gansevoort, Albuminuria Assessed From First-Morning-Void Urine Samples Versus 24-Hour Urine Collections as a Predictor of Cardiovascular Morbidity and Mortality, American Journal of Epidemiology, 168(2008) 897-905.
[6] C.E. Mogensen, Microalbuminuria Predicts Clinical Proteinuria and Early Mortality in Maturity-Onset Diabetes, New England Journal of Medicine 310 (6) (1984) 356–360.
[7] M.M. Ansar, R. ShahrokhiRad, M.K. Lebady, Risk Factors of Microalbuminuria and Macroalbuminuria in Type 2 Diabetic Patients in North of Iran – Rasht, Nephro-Urology Monthly 9 (2016).
[8] A. Jahanban-Esfahlan, L. Roufegarinejad, R. Jahanban-Esfahlan, M. Tabibiazar, R. Amarowicz, Latest developments in the detection and separation of bovine serum albumin using molecularly imprinted polymers, Talanta 207 (2020) 120317.
[9] C. Guoning, G. Pengqi, W. Yan, W. Lu, S. Hua, L.i. Yunzhe, J. Wanghui, C. Chun, F. u. Qiang, Preparation of molecularly imprinted polymers and application in a biomimetic biotin-avidin-ELISA for the detection of bovine serum albumin, Talanta 198 (2019) 55–62.
[10] M. Hamidi, N. Zarei, A reversed-phase high-performance liquid chromatography method for bovine serum albumin assay in pharmaceutical dosage forms and protein/antigen delivery systems, Drug Test Anal 1 (5) (2009) 214–218.
[11] N. Ratanawimarnwong, K. Ponhong, N. Teshima, D. Nacapricha, K. Grudpan, T. Sakai, S. Motomizu, Simultaneous injection effective mixing flow analysis of urinary albumin using dye-binding reaction, Talanta 96 (2012) 50–54.
[12] L.L. Zhang, F.F. Ma, Y.F. Kuang, S. Cheng, Y.F. Long, Q.G. Xiao, Highly sensitive detection of bovine serum albumin based on the aggregation of triangular silver nanoplates, Spectrochim. Acta A Mol. Biomol. Spectrosc. 154 (2016) 98–102.
[13] H. Lu, K. Wang, B. Liu, M. Wang, M. Huang, Y. Zhang, et al, Systematic oligoaniline-based derivatives: ACQ–AIE conversion with a tunable insertion effect and quantitative fluorescence "turn-on" detection of BSA, Mater. Chem. Front. 3 (2019) 331–338.
[14] Ö.B. Ünlüer, F. Ghorbani-Bidkorbeh, R. Keçili, C.M. Hussain, Future of the modern age of analytical chemistry: Nanominiaturization, Handbook on Miniaturization in Analytical Chemistry (2020) 277–296.
[15] L. Bhavani Devi, S. Berchmans, A.B. Mandal, Highly sensitive detection of proteins using voltammetric assay in the presence of silver nanostructures, Journal of Electroanalytical Chemistry 665 (2012) 20–25.
[16] H.-J. Chen, Z.-H. Zhang, L.-J. Luo, S.-Z. Yao, Surface-imprinted chitosan-coated magnetic nanoparticles modified multi-walled carbon nanotubes biosensor for detection of bovine serum albumin, Sens. Actuators B Chem. 163 (1) (2012) 76–83.
[17] B.B. Prasad, A. Prasad, M.P. Tiwari, Multiwalled carbon nanotubes-ceramic electrode modified with substrate-selective imprinted polymer for ultra-trace detection of bovine serum albumin, Biosens. Bioelectron. 39 (1) (2013) 236–243.
[18] M.-W. Shao, H. Yao, M.-L. Zhang, N.-B. Wong, Y.-Y. Shan, S.-T. Lee, Fabrication and application of long strands of silicon nanowires as sensors for bovine serum albumin detection, Appl. Phys. Lett. 87 (18) (2005) 183106.
[19] K. Pinwattana, J. Wang, C.-T. Lin, H. Wu, D. Du, Y. Lin, O. Chailapakul, CdSe/ZnS quantum dots based electrochemical immunoassay for the detection of

phosphorylated bovine serum albumin, Biosens. Bioelectron. 26 (3) (2010) 1109 1113.
[20] M. Kukkar, A. Sharma, P. Kumar, K.-H. Kim, A. Deep, Application of MoS_2 modified screen-printed electrodes for highly sensitive detection of bovine serum albumin, Anal. Chim. Acta 939 (2016) 101 107.
[21] D. Duan, H. Yang, Y. Ding, D. Ye, L. Li, G. Ma, Three-dimensional molecularly imprinted electrochemical sensor based on AuNPs@Ti-based metal-organic frameworks for ultra-trace detection of bovine serum albumin, Electrochim. Acta 261 (2018) 160 166.
[22] G. Dutta, P.B. Lillehoj, Wash-free, label-free immunoassay for rapid electrochemical detection of PfHRP2 in whole blood samples, Sci. Rep. 8 (1) (2018).
[23] S. Boonkaew, P. Teengam, S. Jampasa, S. Rengpipat, W. Siangproh, O. Chailapakul, Cost-effective paper-based electrochemical immunosensor using a label-free assay for sensitive detection of ferritin, Analyst 145 (14) (2020) 5019 5026.
[24] M.M. Bradford, A rapid and sensitive method for the quantitation of microgram quantities of protein utilizing the principle of protein-dye binding, Anal. Biochem. 72 (1-2) (1976) 248 254.
[25] H. Ju, J. Zhou, C. Cai, H. Chen, The electrochemical behavior of methylene blue at a microcylinder carbon fiber electrode, Electroanalysis 7 (12) (1995) 1165 1170.
[26] W. Zhang, L. Liu, Y. Li, D. Wang, H. Ma, H. Ren, Y. Shi, Y. Han, B.-C. Ye, Electrochemical sensing platform based on the biomass-derived microporous carbons for simultaneous determination of ascorbic acid, dopamine, and uric acid, Biosens. Bioelectron. 121 (2018) 96 103.
[27] I.M. Vlasova, A.M. Saletsky, Study of the denaturation of human serum albumin by sodium dodecyl sulfate using the intrinsic fluorescence of albumin, J. Appl. Spectrosc. 76 (4) (2009) 536 541.
[28] M. Chiku, T.A. Ivandini, A. Kamiya, A. Fujishima, Y. Einaga, Direct electrochemical oxidation of proteins at conductive diamond electrodes, J. Electroanal. Chem. 612 (2) (2008) 201 207.
[29] Y.-S. Chen, J.-H. Huang, Electrochemical sensing of bovine serum albumin at self-assembled SWCNTs on gold, Diam. Relat. Mater. 18 (2-3) (2009) 516 519.
[30] L. Fotouhi, S. Banafsheh, M.M. Heravi, Electrochemistry of the interaction of furazolidone and bovine serum albumin, Bioelectrochemistry 77 (1) (2009) 26 30.
[31] S.-B. Ji, Z.-H. Yan, J.-W. Wu, L.-L. Chen, H. Li, One-step electrochemically co-assembled redox-active $[Ru(bpy)_2(tatp)]^{2+}$ BSA SWCNTs hybrid film for non-redox protein biosensors, Biosens. Bioelectron. 39 (1) (2013) 106 111.
[32] M. Cui, Q.i. Zhang, M. Fu, X. Fan, H. Lu, H. Wang, Y. Zhang, H. Wang, Template-Free Controllable Electrochemical Synthesis of Hierarchical Flower-Like Platinum Nanoparticles/Nitrogen Doped Helical Carbon Nanotubes for Label-Free Biosensing of Bovine Serum Albumin, J. Electrochem. Soc. 166 (2) (2019) B117 B124.
[33] M. Krieg, K.J. Gunßer, E. Steinhagen-Thiessen, H. Becker, Vergleichende quantitative Analytik klinisch-chemischer Kenngrößen im 24-Stunden-Urin und Morgenurin, Clin. Chem. Lab. Med. 24 (1986).
[34] J.H. Roe, J.M. Hall, The Vitamin C Content of Human Urine and Its Determination through the 2,4-Dinitrophenylhydrazine Derivative of Dehydroascorbic Acid, J. Biol. Chem. 128 (1) (1939) 329 337.
[35] K. Pagana, Mosby's diagnostic and laboratory test reference, St louis, Elsevier, MI, 2018.
[36] S. Sang, Y. Li, X. Guo, B.o. Zhang, X. Xue, K. Zhuo, C. Zhao, W. Zhang, Z. Yuan, A Portable Device for Rapid Detection of Human Serum Albumin using an immunoglobulin-coating-based Magnetoelastic Biosensor, Biosens. Bioelectron. 141 (2019) 111399.
[37] Y.-C. Wan, Y.-J. Liu, C. Liu, H.-T. Ma, H.-F. Yu, J.-W. Kang, C.-L. Gao, Z.-Q. Wu, D. Zheng, B. Lu, Rapid determination of neomycin in biological samples using fluorescent sensor based on quantum dots with doubly selective binding sites, J. Pharm. Biomed. Anal. 154 (2018) 75 84.

VITA